2022

# Unearthing The Effects Of European-American Settlement On A Northeast Ohio Kettle Lake Through Diatom Stratigraphy

Justine Paul A. Berina
*The College of Wooster*, jberina22@wooster.edu

# Unearthing the effects of European-American settlement on a northeast Ohio kettle lake through diatom stratigraphy

by

Justine Paul A. Berina

Submitted in partial fulfillment of the requirements of Senior Independent Study at

The College of Wooster

March 28, 2022

# Abstract

Recently, wetland conservation has highlighted the necessity for assessing limnological changes following European-American settlement. A prior study at Brown's Lake (northeast Ohio) identified a stratigraphic sequence that shows an abrupt transition from organic-rich muds to several centimeters of a bright loess layer, then a recovery to organic-rich sediments near the top. Based on $^{210}$Pb dates, the loess deposition occurred before 1846 CE, when a growing population cleared trees and farmed intensively. Likewise, organics had recovered after 1950 CE, when people abandoned farmland and practiced conservation tillage. However, the effects of settlement on limnology are poorly known. Diatoms (microscopic algae; class Bacillariophyceae) respond to modifications in water quality and habitat parameters, and siliceous cell walls enable preservation in sediments as fossils. Therefore, a diatom stratigraphy can record the lake's limnological history. A 1-m sediment core was extracted using a modified-Livingstone sampler and dated using AMS radiocarbon dating. A total of 380 cells from the core were analyzed. The data reveal shifting relative abundances that coincide with settlement activities. Before 880 CE, *Thalassiosira* sp., a non-motile genus, is dominant, making up 22.1% of diatoms. Between 880 CE and 1950 CE, *Achnanthidium* sp., a motile genus, is abundant, making up 25.0% of diatoms. It has been noted that the replacement of planktonic genera by diatoms capable of moving through fine sediments suggests a time of excess siltation. From 1950 CE to the present-day, *Cyclotella* sp., a non-motile genus, is dominant, making up 30% of diatoms. Despite these associations, the data cannot provide evidence of a cause-and-effect relationship due to confounding variables (e.g., climate, habitat availability, and structures), errors, and limitations. This study offers the first catalog of historical and modern diatom assemblages at Brown's Lake to support conservation initiatives.

# Acknowledgments

First and foremost, I would like to thank my thesis advisors—Dr. Gregory C. Wiles and Dr. Mark A. Wilson—for the opportunity to contribute to this project, funding, and guidance.

Furthermore, I am thankful for the generosity of the College of Wooster's alumni, friends, and community; together, their investments have helped me become successful.

I would also like to thank Nicholas C. Wiesenberg for his incredible help with coring, sampling, and slide preparation, Dr. Seth Kelly for introducing me to oil immersion microscopy, and Dr. Shreeram P. Inamdar from the University of Delaware for offering me a diatom collection summer internship and years of experience in water science.

Special thanks to Dr. Thomas V. Lowell, Dr. Aaron F. Diefendorf, Megan C. Corcoran, and Dietrich Watts from the University of Cincinnati for their sustained collaboration and communication; and the Earth Sciences, Biology, and Chemistry Departments for laboratory access.

Finally, I would like to thank my parents, sisters Lesley and Claudette, aunt Cecile, cousin Lyn, and partner Nathan for their unwavering encouragement, support, and trust.

This list only captures a small portion of people who supported me in this endeavor. I send my deepest gratitude to all who contributed to this thesis.

# List of Figures

# List of Tables

# Table of Contents

# Introduction

The unique sediment sequence at Brown's Lake has the potential to deepen understanding of the link between European-American settlement and limnological changes and guide people in conserving wetlands. In 2015, the College of Wooster's Department of Earth Sciences, alongside a team from the University of Cincinnati's Department of Geology, extracted a 1-m sediment core from Brown's Lake. The core shows an abrupt transition from organic-rich muds to several centimeters of a bright loess layer, then a recovery to organic-rich sediments near the top. $^{210}$Pb radiometric dating established that at about 45 cm depth, the loess dates back to 1846 CE, a year marked by intensive land clearing and population boom. Analysis of the core's magnetics, grain size, and mineralogy suggests this layer is windblown sediment from land clearing and agriculture. The loess layer's upper section (30 cm depth where organics begin to recover) dates back to 1950 CE, a time of newfound emphasis on sustainable farming and conservation. The loess layer's appearance and disappearance at Brown's Lake coincide with anthropogenic activities in Wayne County. However, limnological changes associated with human settlement are not well understood. Diatoms respond to modifications in water quality and habitat parameters, and siliceous cell walls enable preservation in sediments as fossils. Hence, the objective of this study is to construct the first diatom stratigraphy of Brown's Lake and interpret changes in its limnology through time.

# Site Description

## Location

Brown's Lake Bog (BLB) is a peat-filled kettle hole situated 4.2 km west of Shreve in Wayne County, Ohio. The Nature Conservancy, the current site manager, acquired the kettle hole in 1966 CE. In 1968 CE, the Ohio Department of Natural Resources designated BLB a Natural Landmark and State Nature Preserve for its distinctive plant assemblage (Sanger and Crowl, 1979). Today, the site contains a lake (Brown's Lake) and a bog (Brown's Lake Bog; Fig. 1).

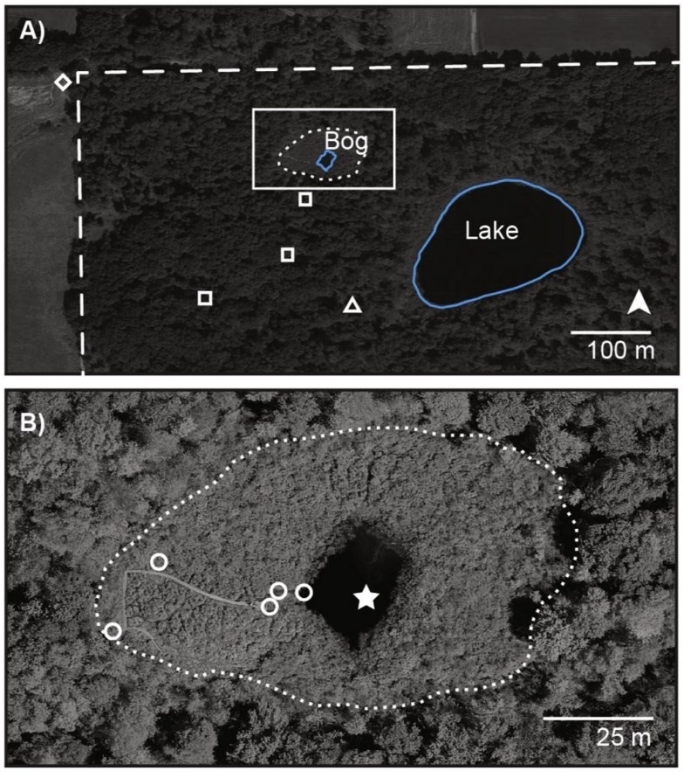


Fig 1. Maps of Brown's Lake Bog (BLB) State Nature Preserve. Panel A shows Brown's Lake (blue lines), Brown's Lake Bog (blue lines), and the park's northwestern boundary (dashed line). The two southernmost squares (farthest from the bog) show the location of oak-dominated kames while the triangle mark a precipitation gauge's location. Panel B provides more detail of the

region within the white box in panel A, such as the bog's shoreline vegetation zone (dotted line). The circles show the shoreline vegetation sampling sites, and the star marks the sediment collection point (Freimuth et al., 2019, Fig. 1).

## History

Researchers have reconstructed Brown's Lake Bog's history from the latest glacial interval into the Holocene using limnetic sediments and palynological records. When the Laurentide ice sheet retreated from northeast Ohio about 14,660± 60 $^{14}$C yr BP, dead-ice from the retreating glacier became buried by outwash plain sediments (Sanger and Crowl, 1979; Shane and Anderson, 1993; Bailey, 2003, Lutz et al., 2007; Glover et al., 2011). As the buried ice melted, it formed depressions called kettle holes across the terrain. The kettle hole west of Shreve filled with rainwater and groundwater, creating Brown's Lake and an adjacent small kettle wetland, Brown's Lake Bog (Fig. 1). The modern-day Brown's Lake is highly oligotrophic and hypoxic (Lutz et al., 2007); thus, it permits organic matter to accumulate and be preserved in part. According to Bailey (2003), sediment cores from Brown's Lake Bog indicate peat began to accumulate in the kettle hole about 10,254± 60 $^{14}$C yr BP (Table 1).

Table 1. Uncalibrated radiocarbon ages from Brown's Lake Bog (Bailey, 2003, Table 1.)

| Sample depth (cm) | $^{14}$C yr BP | Material |
|---|---|---|
| 856-858 | 9,004± 83 | branch fragments |
| 923-926 | 10,254± 60 | aquatic plant material |
| 1235-1237 | 14,660± 60 | aquatic plant material |

Meanwhile, the kettle wetland's open water (288 m$^2$) had further acidified due to decomposing organic plant matter and poor drainage, forming a kettle bog (Freimuth et al., 2019). Freimuth et al. (2019) observed that a *Sphagnum* moss mat (4,329 m$^2$) covers the bog's shrub-dominated

shoreline vegetation zone (Fig. 2). Additionally, the bog and its shoreline vegetation zone are part of a more extensive forest (0.370 $km^2$) transitioning from a lowland deciduous fen closest to the bog into well-drained oak-dominated kames farthest from the bog (Fig. 1). Freimuth et al. (2019) noted that Brown's Lake Bog is hydrologically closed; precipitation and groundwater recharge it.

Fig. 2. Brown's Lake Bog, its *Sphagnum* moss mat, and shoreline vegetation zone in the summer.

Glacial landforms are present around Brown's Lake Bog (BLB). A few hundred meters north and east of the kettle hole, several kames—some adjacent to valley walls—rise over the peatland plain (Fig. 3). A kame is an irregularly shaped hill or mound composed of sand, gravel, and till that previously accumulated in a depression on a retreating glacier and deposited on the land surface with further melting of the glacier. Additionally, the upland and nearby hills are mantled by undifferentiated end moraine and ground moraine from Hayesville till. The site rests within the Killbuck lobe boundaries of the Woodfordian ice advance (White, 1967). Several hundred meters south and west of BLB are preglacial valleys that extensive postglacial lakes once occupied. These preglacial valleys, often greater than 4 m deep, contain shallow peatland.

Brown’s Lake and one adjacent miniature bog, Brown’s Lake Bog, are remainders of the kettle hole's past open-water conditions.

Fig. 3. A plowed kame at the head of Brown’s Lake Bog’s access trail. Photo courtesy of Dr. Mark Wilson.

Brown’s Lake is currently dystrophic since it is located within a peatland and holds brownish, tea-colored water rich in dissolved organic matter (Fig. 4). A dystrophic lake refers to a lake with brown acidic water low in oxygen and supports little life due to high dissolved humic material (Tundisi and Tundisi, 2011). More than 40 years ago, thermal stratification was observed to set in by May, and oxygen rapidly reduces to zero in the hypolimnion (Sanger and Crowl, 1979). Brown’s Lake remains stratified throughout the summer until the fall overturn. Sanger and Crowl (1979) reported that oxygen levels are replenished in the bottom waters by October, but the high sedimentary biochemical oxygen demand keeps concentrations regularly below 5.0 mg/L. For most of the winter, the hypolimnion remains anoxic (Sanger and Crowl, 1979).

Fig. 4. Brown's Lake and its brownish, tea-colored water in the summer. Photo courtesy of Dr. Gregory Wiles.

## Flora

Brown's Lake Bog is one of the few relict wetlands remaining in Ohio, and it boasts a rare plant assemblage (Aughanbaugh and Diller, 1968; Sanger and Crowl, 1979). According to Sanger and Crowl (1979), the wetland surrounding Brown's Lake is a nutrient-rich, marginal fen forest (Fig. 5). A fen is a minerotrophic peatland; it typically receives moisture and nutrients from mineral-rich groundwater and surface water. A constant groundwater supply and stable water table give a fen its distinguishing characteristics: a near-neutral pH and relatively higher nutrient levels than a bog. Swamp loosestrife (*Decodon verticillatu*s) forms a dense zone at the lake's water edge followed landward by a band of alder (*Alnus serrulata*) (Sanger and Crowl, 1979). Vast areas of poison sumac (*Rhus vernix*), willow (*Salix* sp.), and *Sphagnum* mosses sometimes exist in the semi-aquatic zone. The drier fen forest, 10 m to 20 m from the lake's shoreline, is comprised mostly of river maple (*Acer saccharinum*), black cherry (*Prunus serotina*), willow, and a rich array of shrubs, herbs, and ferns (Sanger and Crowl, 1979). Other known tree species in Brown's Lake

Bog's forested area include northern white oak (*Quercus alba*), northern red oak (*Quercus rubra*), and American elm (*Ulmus americana*) (Freimuth et al., 2019).

Fig. 5. Images of the fen forest's flora. The fen forest that surrounds Brown's Lake supports a diverse plant community, including many species of ferns (left) and trees (right).

On the other hand, Sanger and Crowl (1979) mentioned Brown's Lake Bog's water edge as the most nutrient-poor in the kettle hole, approaching ombrotrophic bog conditions. An ombrotrophic bog receives moisture and nutrients from precipitation only, rather than a combination of groundwater and rain (Charman, 2002). Rainwater has a low pH and contains insignificant amounts of essential plant nutrients. Thus, plants tolerant of acidic, nutrient-poor soils make their home in Brown's Lake Bog's shoreline (Fig. 6). These include bog mosses along with cranberry (*Vaccinium oxycoccus*), bog rosemary (*Andromeda glaucophylla*), pitcher plant (*Serracenia purpurea*), sundew (*Drosera rotundifolia*), woody shrubs (*Toxicodendron vernix*, *Vaccinium corymbosum),* woody groundcover (*Salix petiolaris*, *Vaccinium macrocarpon*), herbaceous plants, graminoids, and other common bog species (Sanger and Crowl, 1979; Freimuth et al., 2019). Aughanbaugh and Diller (1968) wrote a catalog of 469 species representing 98 families found in Brown's Lake Bog, highlighting the site's plant diversity.

Fig. 6. Images of the bog's flora. Unlike the fen forest, the Brown's Lake Bog's shoreline is near ombrotrophic. Therefore, it supports an exclusive plant community adapted to acidic, nutrient-poor environments. This community includes carnivorous plants like pitcher plants (left) and sundews (right). Photos courtesy of Dr. Mark Wilson.

In 1967 CE, the Advisory Board on National Parks and History Sites endorsed Brown's Lake Bog's inclusion on the National Registry of National Landmarks. The Registry, founded in 1964 CE, promotes the preservation and protection of selected natural sites (Aughanbaugh and Diller, 1968). Brown's Lake Bog (BLB) is one of the few well-preserved boreal acidic bogs left in a region where most wetlands have been drained for agricultural use, filled by siltation, polluted by industrial or other uses, or otherwise changed in character by human-caused alterations. Moreover, BLB is a valuable field station for paleobotany, glaciology, and ecology education and research. Ecological succession states may be traced from the kettle hole's well-drained upland forest through swamp woodland and the bog zone to open water, according to Aughanbaugh and Diller (1968). For these reasons, the Ohio Department of Natural Resources added BLB to the National Registry of Natural Landmarks in 1968 CE.

## Water conditions

In 2020, the College of Wooster's Earth Sciences Department installed a pedant logger (Onset HOBO MX2201) at the center of Brown's Lake (40.68071°, -82.06250°). Beginning July 20, 2020, the logger has been taking hourly water temperature measurements at the following depths: 1 m, 2 m, 3 m, 4 m, 5 m, and 6 m. Brown's Lake was highly stratified from July 20 through July 28, 2020 (Fig. 7). The top layer (epilimnion) had the highest temperature since solar radiation warms water on the lake's surface more rapidly than in deeper waters. Meanwhile, the bottom layer (hypolimnion) had the lowest temperature. Sunlight usually penetrates a few meters into the lake, thus heating only the top few meters. As the water warms up and loses density, it stays on the lake's surface and floats above the cooler, denser water below. Water temperatures decreased by depth in the summer when thermal stratification peaked. By August 4, 2020, the epilimnion started to cool steadily due to decreasing solar insolation. As the water cools down and gains density, it sinks and mixes with the cooler, more dense water below. Around September 15, 2020, the epilimnion mixed with water at 2 m depth, indicated by near-identical, subsequent temperatures. About October 20, the epilimnion mixed with water at 2 m and 3 m depths. Around November 1, 2020, the epilimnion mixed with water at 2 m, 3 m, and 4 m depths. By November 4, 2020, the epilimnion mixed with water at 2 m, 3 m, 4 m, and 5 m depths (Fig. 7). On December 21, 2021, the lake mixed thoroughly at the start of winter from top to bottom. The epilimnion cooled to a temperature equal to the hypolimnion, about 4°C, and was ice-free. The lake maintained this temperature until March 7, 2021, when the epilimnion started to warm steadily due to increasing solar exposure. On June 21, 2021, the lake became strongly stratified at the beginning of summer (Fig. 7).

The measurements show a mixing pattern of a warm monomictic lake. A warm monomictic lake mixes once a year in the winter at or above 4°C, never freezes, and is stratified for the rest of the year. More data are needed to confirm that Brown's Lake undergoes only a single winter overturn instead of a fall and spring overturn, as Sanger and Crowl (1979) described over 40 years ago.

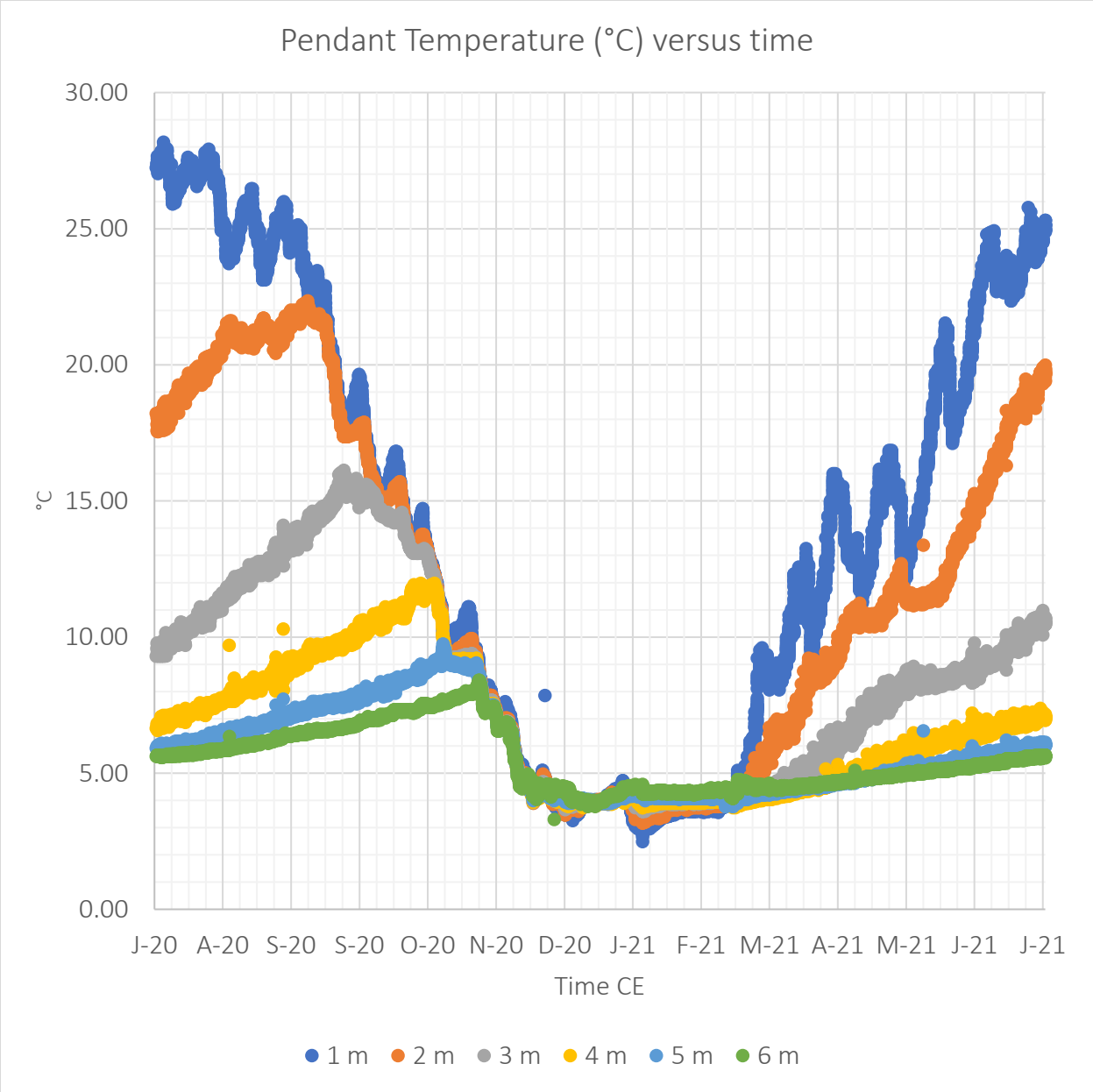


Fig. 7. Thermal profile of Brown's Lake, from July 2020 through July 2021. The diagram shows a profile from the hypolimnion (6 m depth) to epilimnion (1 m depth). The density difference between warmer and colder bottom waters keeps the lake stratified throughout the year except in the winter when the top and bottom waters mix and reach the same temperature at or above 4°C.

## Tree ring records

In 2018, the College of Wooster's Department of Earth Sciences built a ring-width chronology using 53 tree cores from 26 white oak trees (*Quercus alba*) collected over decades from Brown's Lake Bog's forested area to study past climate and environmental change. The ring-width chronology was standardized with the ARSTAN software and a horizontal line through the mean to exclude low-frequency variations like growth trends due to age, size, and biological persistence (Fritts, 1976; Cook, 1985). Then the standardized chronology was correlated to temperature, precipitation, and drought records from the OARDC climate station in Wooster, Ohio, using the KNMI Climate Explorer tool (Trouet and Oldenborgh, 2013).

The chronology shows increasing ring widths over time, conflicting with the typical growth of trees (Fig. 8). Trees usually produce thinner rings as they age and grow in circumference. Trees produce the same amount of wood annually; therefore, as their diameters increase, the wood spreads over a larger area and causes the rings to decrease in width (Cook, 1987). The Brown' Lake regional chronology displays an atypical growth pattern, likely due to environmental change brought by European-American settlement. Additionally, it reveals a growth release that started in 1820 CE and ended in 1850 CE. Although European-American settlers moved to Ohio during the 1700s, most arrived during the early to mid-1800s, after Ohio's statehood was granted in 1803 CE (Galbreath, 1925). In 1796 CE, Wayne County was established. Its population multiplied from 3,206 in 1800 CE to 11,933 in 1820 CE. By 1850 CE, when the ring widths stopped increasing, the county's population was 32,981 and remained relatively constant (Galbreath, 1925). At this time, people constructed roads, logged trees, and cleared lands for farms and homes at unprecedented levels.

Land clearing and selective logging have reduced resource competition for trees that remained uncut. White oaks regenerated quickly in gaps but were poor competitors under closed canopies (Abrams, 2003). Cutting down trees has cleared canopy space, allowing the white oak trees to

grow larger rings (Cook, 1987). After the growth release, ring width does not go back down but remains constant through the present-day. The ring width's plateauing coincides with Wayne County's population's plateauing in 1850 CE. Factors that stabilize ring width growth include a low-frequency rise in precipitation due to climate change, increased carbon dioxide and nitrogen from fossil fuel burning, or windblown sediment matter from farms that could contain phosphorus or nitrogen. However, rising atmospheric carbon dioxide levels due to anthropogenic activities are unlikely to significantly affect the doubling of tree ring width (Jacoby and D'Arrigo, 1997).

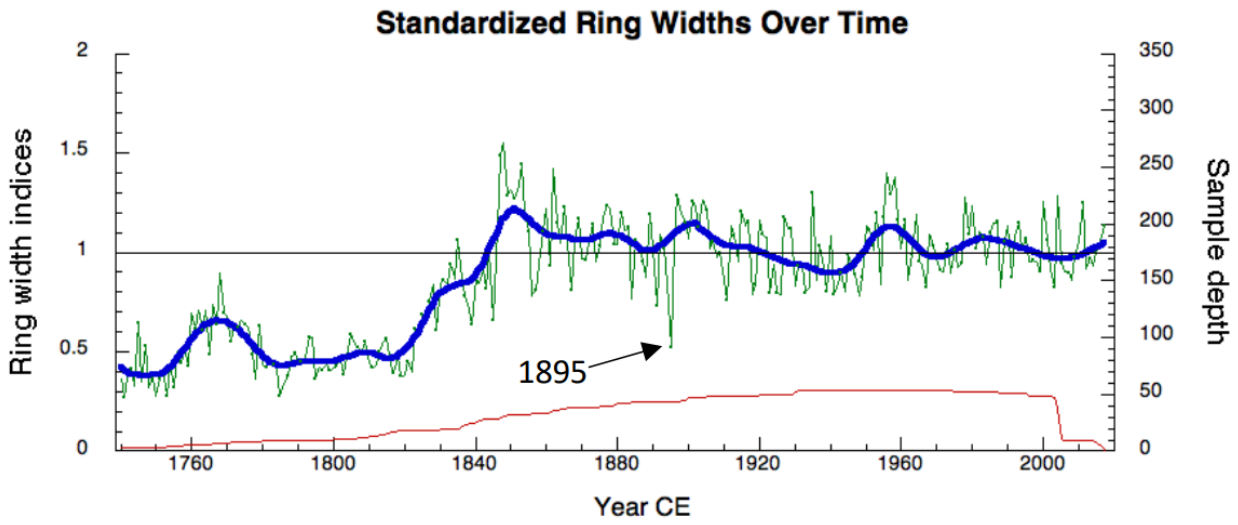


Fig. 8. The standardized ring-width chronology from 1740 to 2017. A drought in 1895 is indicated by the black arrow. The number of cores (sample depth) is designated by the red line (Devereux, 2018, Fig. 3).

Ring width correlates positively with precipitation but negatively with temperature. The positive correlation with precipitation is highest in July ($\rho = 0.31$) because it is the hottest time of the year (Fig. 9). The trees experience more stress in hotter months; hence, their growth is more sensitive to moisture (Tardif et al., 2006). White oak trees are sensitive to water balance in the early growing season, as indicated by the strong correlations in May ($\rho = 0.22$) and June ($\rho = 0.26$). The

stress that trees experience during the hotter months also explains the strong negative correlation with June mean temperature (ρ = -0.40) in Fig. 10 and the strong positive correlation (ρ = 0.40) with the Palmer Drought Severity Index (PDSI) in Fig. 11.

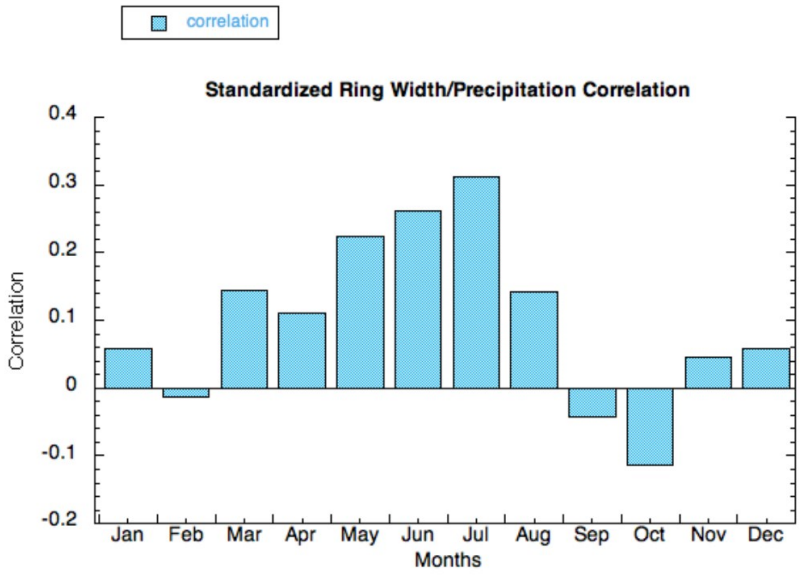


Fig. 9. Histogram of standardized ring-width and precipitation correlation. July has the strongest correlation of 0.31 (Devereux, 2018, Fig. 5).

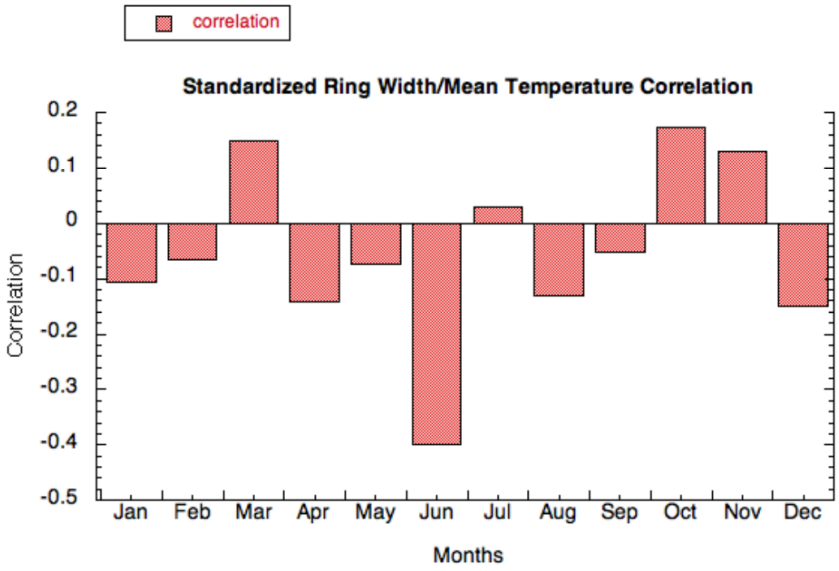


Fig. 10. Histogram of standardized ring-width and mean monthly temperature correlation. June has the strongest correlation of -0.40 (Devereux, 2018, Fig. 4).

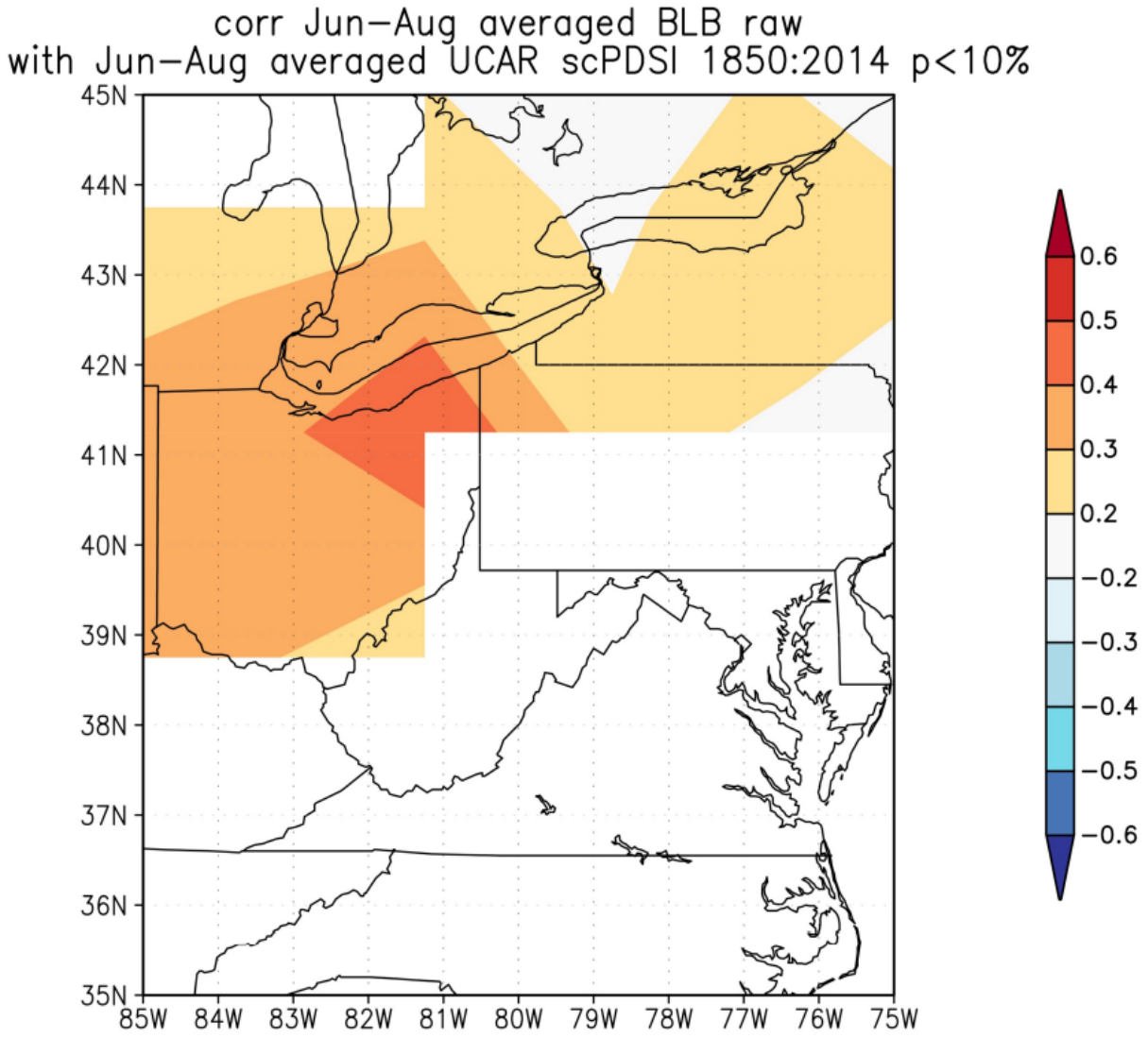


Fig. 11. Map of standardized ring-width and Palmer Drought Severity Index (PDSI) correlation. Darker colors indicate stronger correlations. Northeast Ohio, where Brown's Lake Bog is located, has a correlation of 0.40 (Devereux, 2018, Fig. 6).

The Palmer Drought Severity Index (PDSI) measures relative dryness based on available temperature and precipitation data (Cook and Krusic, 2004). Positive values signify wetter conditions, while negative values represent drier conditions. Tree rings are thinner during drier conditions (negative PDSI values). For instance, there was a drought in 1895 CE (Fig. 8). Thus, the

ring-width for 1895 CE was narrower than the rings around it (from rainier years), and the PDSI value is -4 (Fig. 12). Conversely, tree rings are wider during wetter conditions (positive PDSI values).

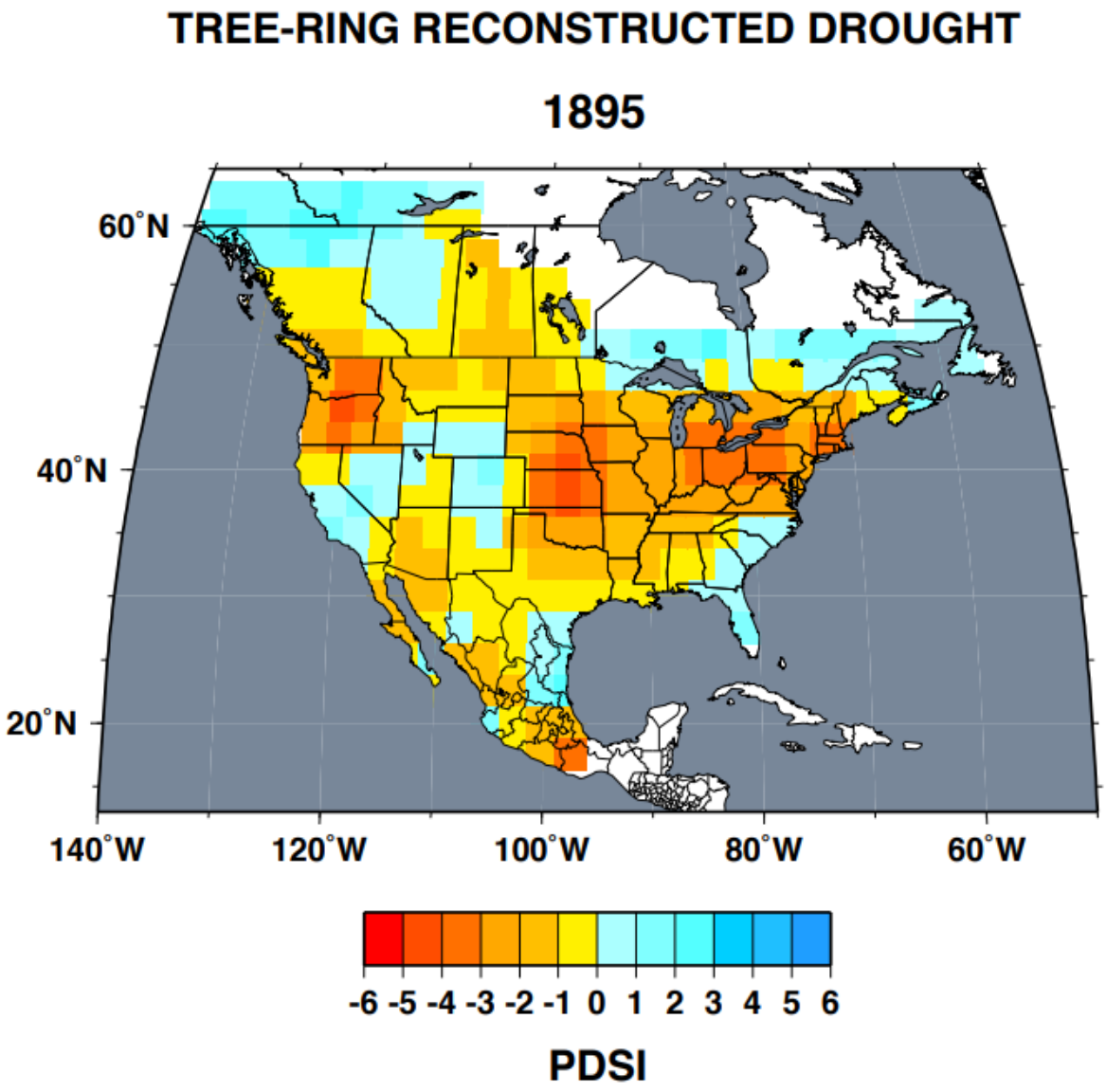


Fig. 12. Map of PDSI measurements of drought in 1895 CE. Warmer colors symbolize drier conditions. That year drought was severe in Ohio, resulting in a PDSI value of -4 (Devereux, 2018, Fig. 7).

## Anthropogenic layer

In 2015, the College of Wooster's Department of Earth Sciences, alongside a team from the University of Cincinnati's Department of Geology, extracted a 1-m sediment core from Brown's Lake (Fig. 13). The core shows an abrupt transition from organic-rich muds to several centimeters of a bright loess layer, then a recovery to organic-rich sediments near the top. To understand the lake's unique stratigraphy, the team sent the whole core to the St. Lacroix Watershed Research Station in Washington County, Minnesota, for $^{210}$Pb radiometric dating. Additionally, the team conducted loss on ignition, magnetic susceptibility, x-ray diffraction, and grain-size analyses on the core.

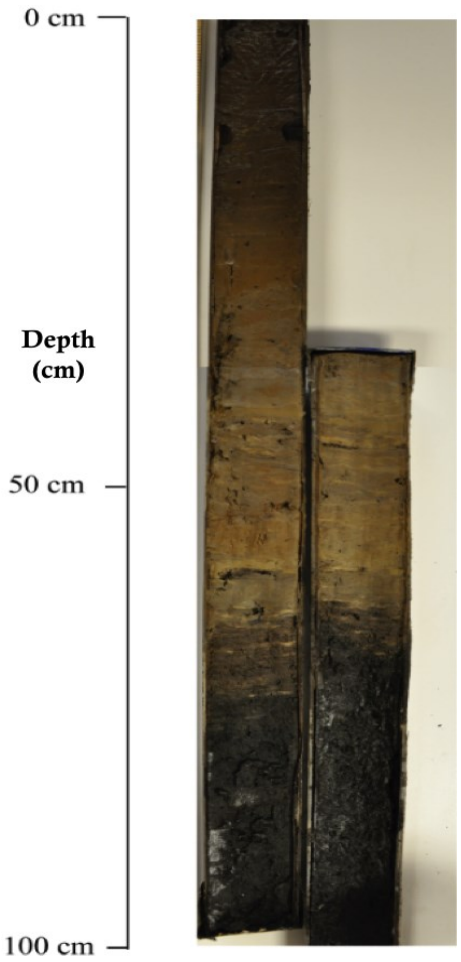


Fig. 13. 1-m sediment core from Brown's Lake, collected in 2015.

$^{210}$Pb radiometric dating established that at about 45 cm depth, the core dates back to 1846 CE (Fig. 14). Extrapolating downwards places land clearing and quartz and clay's increased flux into the lake to 1820 CE. Moreover, magnetics, grain size, and mineralogy support a wind-blown hypothesis for the sediment associated with land clearing and agriculture (Jimerson et al., 2016). The magnetics are inverse to the organic content determined from loss on ignition (Fig. 15). The loess layer is high on magnetics but low in organics. However, magnetics decreased in the upper 30 cm of the core, while organics recovered gradually.

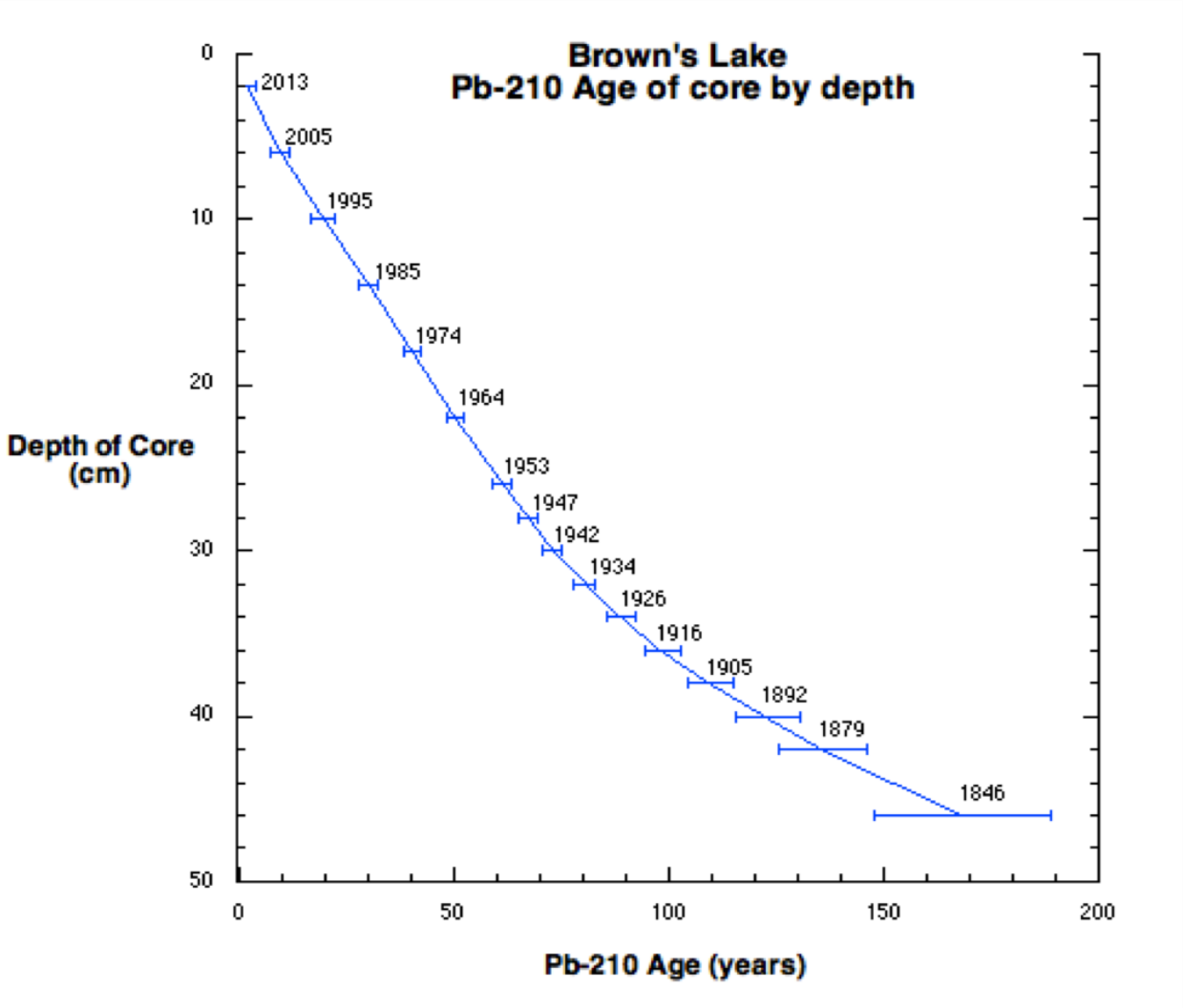


Fig. 14. Age of sediments by depth using $^{210}$Pb radiometric dating. The middle section of the loess layer (45 cm depth) dates back to 1846 CE.

According to Jimerson et al. (2016), the return to organic-rich sediments is consistent with the abandonment of farmland, changes in agriculture, including conservation tillage and a wetter climate, less windblown flux, and more organics. Additionally, ring-width chronology and observational climate records suggest that the early land clearing may have occurred during a relatively dry and cool period, while the return to organic-rich sediment—which started in 1950 CE—is associated with wetter and warmer weather conditions.

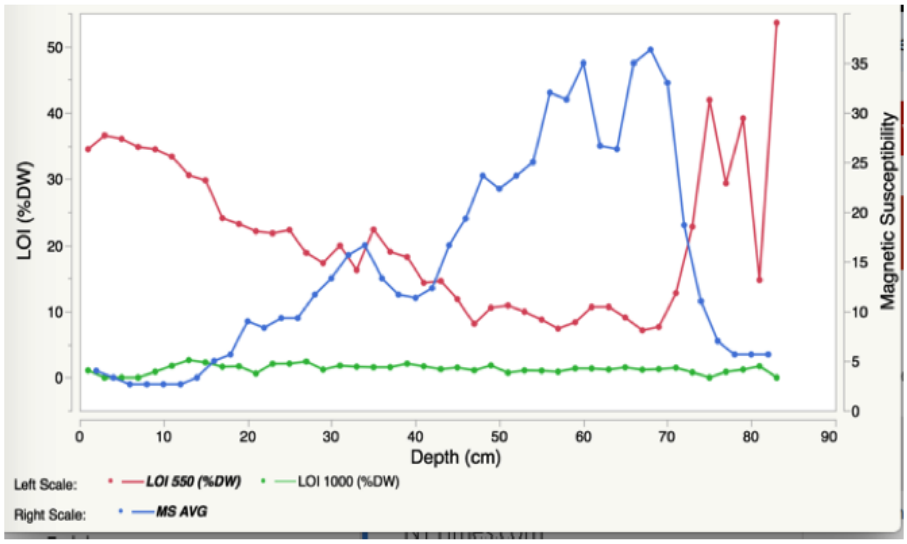


Fig. 15. Percent organics and magnetics by depth. The magnetics are inverse to the organic content calculated from loss on ignition.

Overall, the loess layer at Brown's Lake coincides with anthropogenic activities in Wayne County. The middle section of the loess layer (45 cm depth) dates back to 1846 CE, a year marked by intensive land clearing and population boom. Meanwhile, the loess layer's upper section (30 cm depth) dates back to 1950 CE, a time of newfound emphasis on sustainable farming and conservation. However, limnological changes caused directly or indirectly by human settlement are not well understood. Diatoms respond to modifications in water quality and habitat parameters, and siliceous cell walls enable preservation in sediments as fossils. Thus, diatom stratigraphy can record the history of limnological changes.

# Diatoms

Diatoms are a diverse group of single-celled algae (of the class Bacillariophyceae) known for their intricate cell walls composed of transparent, opaline silica (Bradley, 2014). They thrive within the photic zone of seas, freshwater, and even in damp environments or soils globally. Diatoms make up a substantial part of Earth's biomass, producing 20–50% of the planet's oxygen through photosynthesis, absorbing tons of carbon dioxide and silicon in their habitats, and forming the bulk of siliceous, biogenic sediment deposits in the ocean, lake, or wetland bottoms. Furthermore, diatoms make long-chain fatty acids within their cells, thus serving as the base energy source for many food webs (Diatoms.org). Lastly, diatoms' exceptional preservation, abundance, and predictable distribution patterns due to water and habitat conditions make them useful paleoenvironmental indicators (Cohen, 2003; Bradley, 2014).

## Size

All diatoms are unicellular, and the majority are microscopic. Individual cells range in size from 2 µm to 500 µm (Diatoms.org). Thus, phycologists use a combination of light microscopes and scanning electron microscopes (SEM) to view diatoms (Taylor et al., 2007; Fig. 16). When observed through a light microscope, diatoms are transparent because light passes through their silica-based cell walls. Living diatoms often appear tinted with yellowish-brown spots due to their chloroplasts. Chloroplasts are photosynthesizing organelles containing pigments like chlorophyll and the carotenoid fucoxanthin (Hasle et al., 1996; Cohen, 2003). When observed with an SEM, diatoms look opaque because electrons bounce off their cell walls' surface.

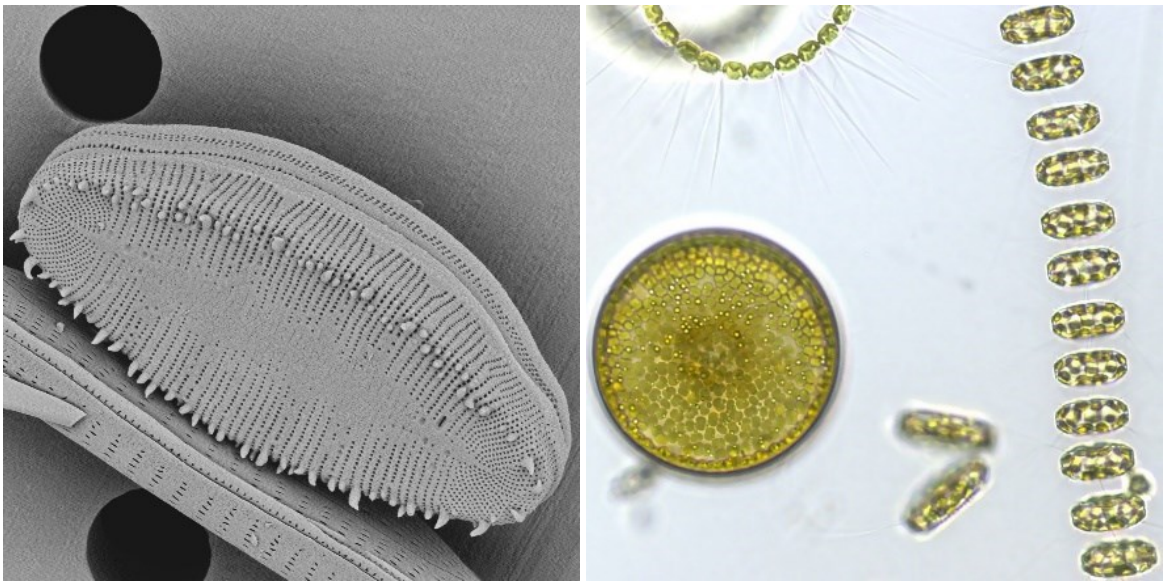

Fig. 16. Diatoms as seen through an SEM (left) and light microscope (right). A single diatom cell ranges in size from 2 µm to 500 µm. Photos from Diatoms.org.

## Life Modes

While some diatoms live as solitary cells, other diatoms exist in groups. Planktonic species have adaptations enabling them to be buoyant, like building star-shaped, zigzag, and chain-like colonies connected by silica spines (Diatoms.org; Fig. 17). Meanwhile, benthic species attach themselves to the surfaces of rocks, other organisms such as algae and macrophytes (large aquatic plants), or soft substrates (Cohen, 2003). They accomplish this through adaptations like mucilage (a thick, gluey secretion) and specialized shapes or parts conducive to clinging (Taylor et al., 2007). These modifications enable benthic species to stay in place, resist waves, and collect nutrients dissolved in the water. Furthermore, benthic species have a slit-like structure called the raphe that allows them to glide over surfaces, including fine-grained sand, tidal zone mud, or other diatoms (Fig. 18). Diatoms' movement speed correlates with their raphe's development (Diatoms.org).

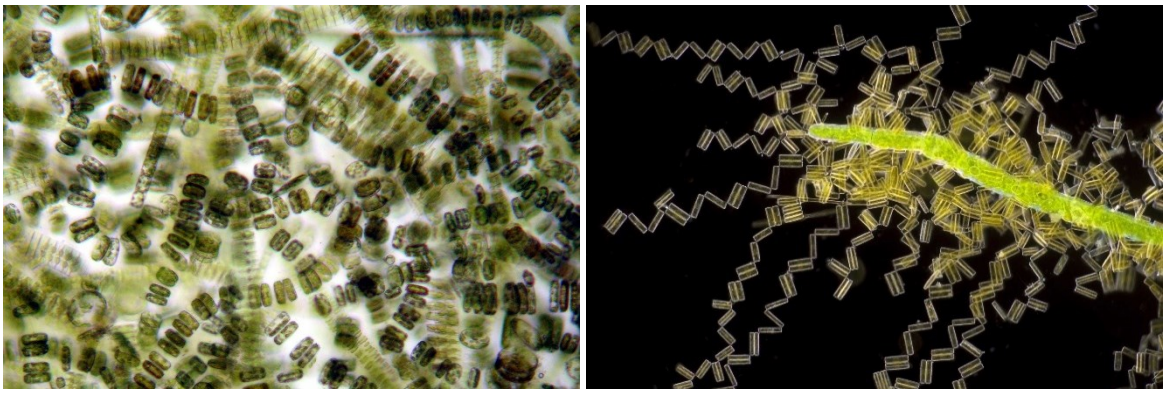

Fig. 17. Chains of living, colonial *Fragilariopsis* and *Thalassiosira* filtered from sea ice in the Bering Sea (left). Filaments of *Diatoma* attached to the green alga *Cladophora* (right). Photos from Diatoms.org.

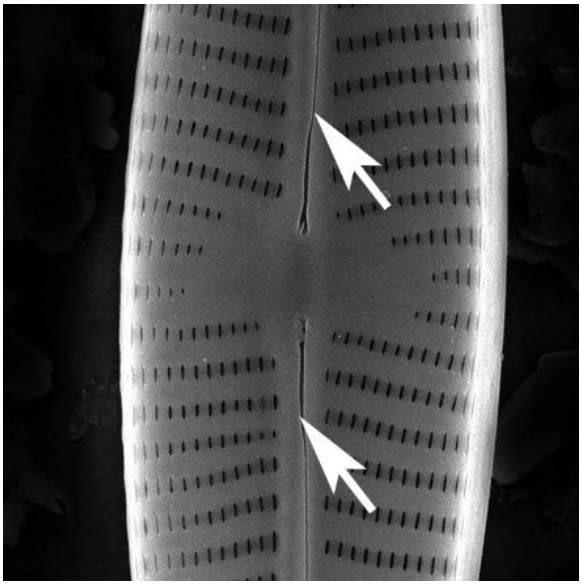

Fig. 18. SEM image of the two branches of the raphe system on a single valve of *Navicula tripunctata*, a biraphid diatom. Both valves of its frustule possess a raphe system, which enables it to glide over surfaces. Photo from Diatoms.org.

## Morphology

Phycologists use diatoms' distinctive, siliceous cell walls to describe thousands of species (Cohen, 2003). Two intersecting valves and their linking girdle bands form a frustule, the siliceous part of diatoms' cell walls. The larger valve (epitheca) overlaps, the smaller valve (hypotheca) like a Petri dish's overlapping halves (Fig. 19). Diatom taxonomy is based mainly on valves' unique morphology (Diatoms.org; Fig. 20; Fig. 21). Visible features within a frustule include the nucleus, vacuoles, lipids, chloroplasts, and photosynthetic pigments (Taylor et al., 2007; Fig. 22). There are two main types of diatoms found in freshwater bodies, namely centric (radially symmetrical) and pennate (axially symmetrical) diatoms (Cohen, 2003; Taylor et al., 2007; Fig. 19). Centric diatoms are generally circular and planktonic, while pennate diatoms are benthic but are sometimes briefly suspended in the water column (Taylor et al., 2007). A raphe (a slit-like part through which cytoplasmic structures extend and allow for gliding motion across substrates) subdivides pennate diatoms longitudinally (Van den Hoek et al., 1995; Fig. 19).

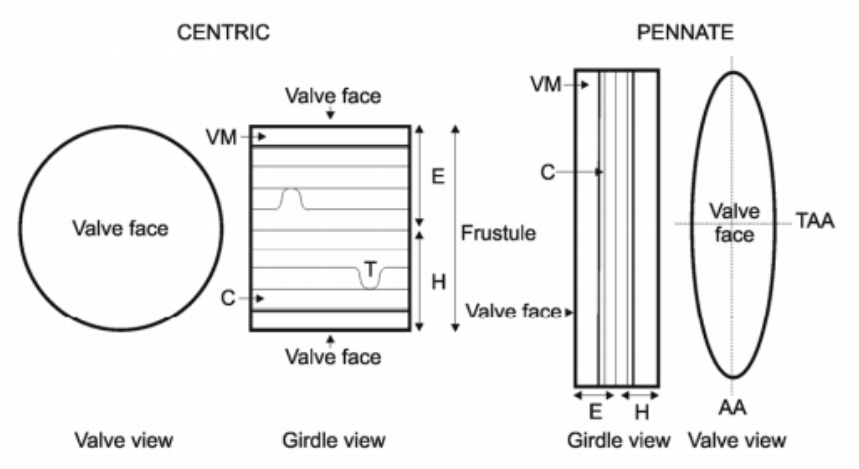


Diagram of diatom cells to show the relationships of the siliceous components.
**E** = epivalve + epicingulum; **H** = hypovalve + hypocyngulum; **C** = copulae or girdle bands;
**VM** = valve mantle. Copulae (girdle bands) may have a tongue- like extension (**T**) which inserts into any space between the ends of the adjacent split copula. **AA** = apical axis, **TAA** = transapical axis

Fig. 19. A diagram of a centric and pennate diatom showing the positions of siliceous parts (Taylor et al., 2007).

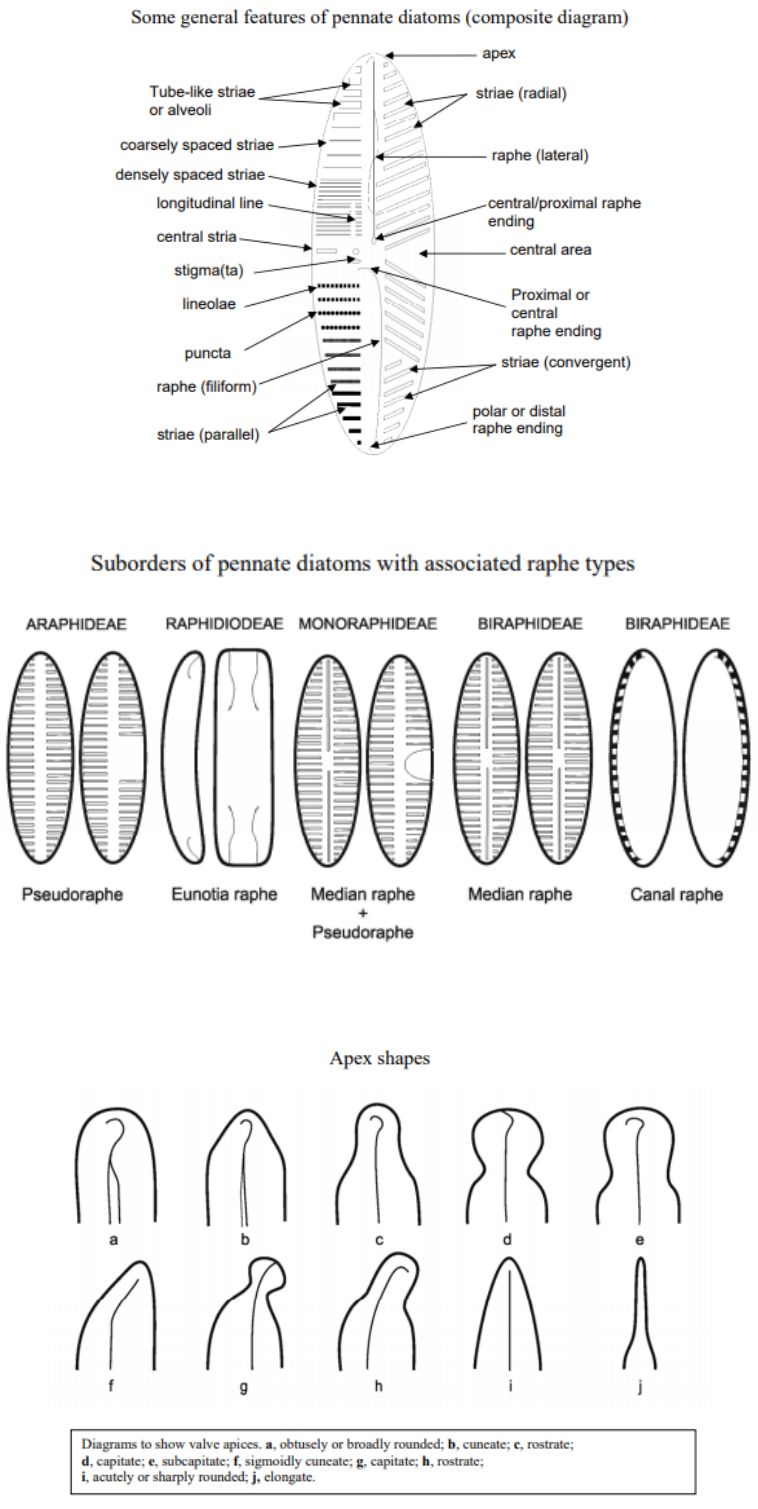


Fig. 20. Diagrams of pennate diatoms' common features (top), suborders based on raphe type (middle), and apex shapes (bottom) (Taylor et al., 2007).

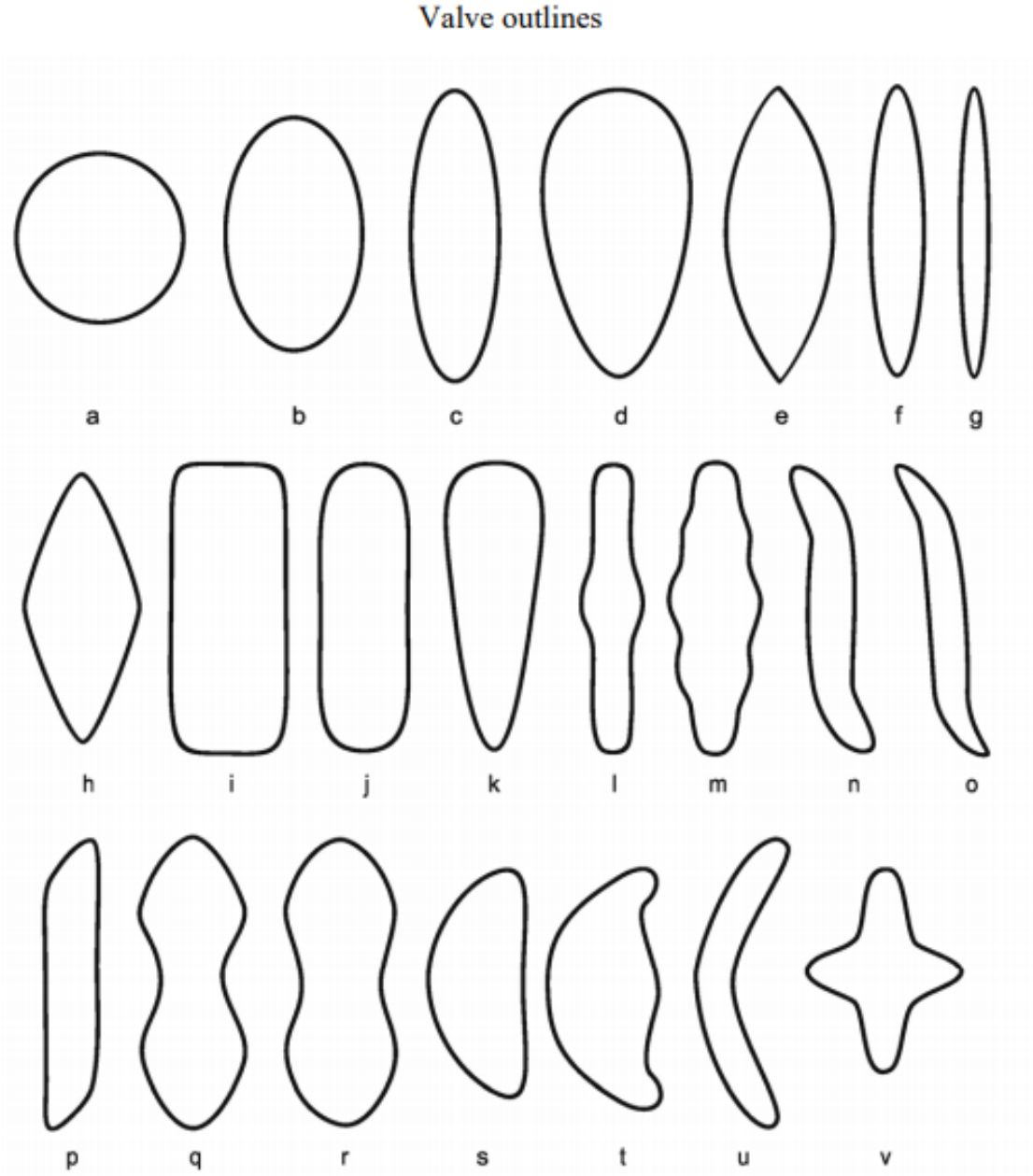


Fig. 21. Outlines of different valve and girdle shapes. Diatom taxonomy is based largely on valves' appearance (Taylor, et al., 2007).

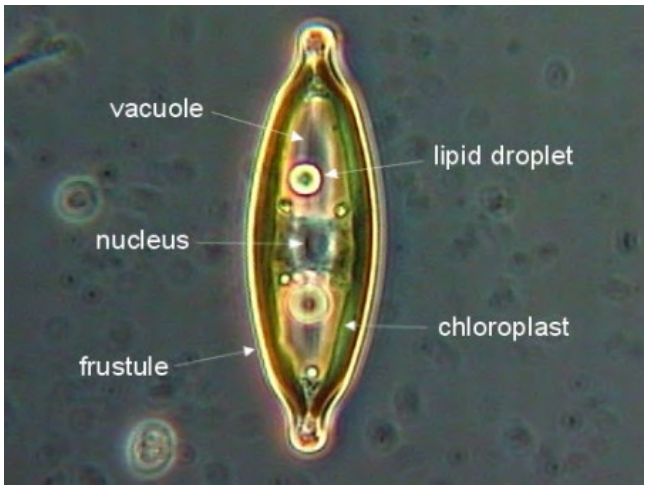


Fig. 22. Light microscope image of a living diatom showing its structures (Taylor et al., 2007).

## Paleoenvironmental applications

Paleolimnologists and geologists use diatoms in ocean, lake, and wetland sediments to interpret past and present conditions. When diatoms die, they sink and accumulate in profusion on the bottom of water bodies. Their frustules do not instantly decompose and can be preserved up to tens of millions of years (Diatoms.org). The diatoms date back to at least the Late Jurassic, and most taxa have a global or continent-wide extent (Bayer and Du Buff, 2002; Stoermer and Smol, 2010). Additionally, diatoms are sensitive to changes in water quality and habitat parameters (e.g., temperature, chemistry, pH, dissolved oxygen, salinity, and nutrient content, especially nitrogen and phosphorus) (Battarbee et al., 2001; Mackay et al., 2003; Stoermer and Smol, 2010). Furthermore, diatom taxonomy is based primarily on valve's distinct ornamentation that allows both living and fossil individuals to be identified to species level (Hasle et al., 1996; Cohen, 2003; Taylor et al., 2007; Stoermer and Smol, 2010). Therefore, diatoms' extraordinary preservation, abundance, and distribution due to water and habitat conditions enable accurate determination of environmental parameters to which particular diatoms respond—over a range of geological and human timescales (Bayer and Du Buff, 2002; Bradley, 2014).

# Methodology

## Coring and sampling

In 2021, our team used a modified-Livingstone coring instrument to obtain sediment cores, which contained pre-settlement and post-settlement diatoms and peat, near Brown's Lake's lakefront (40.681581°, -82.062323°). The approximate coring location is shown in Fig. 23. The instrument consists of a 1-m long metal steel tube, a 1-m long square rod, and a piston with a rubber washer that fits snugly inside the tube. Before coring, we augured a hole to a depth of 1-m to 3-m and inserted a PVC pipe (1-m in length and 5 cm in diameter) to maintain the hole. Then, we placed a tripod over the hole to stabilize the instrument. We lowered the instrument's barrel to a predetermined depth, with the rod inside the tube and the piston at the end of the barrel. We lifted the rod from the barrel and locked it above the tube. This process created a void filled with sediment where we lowered the barrel. The sediment's movement into the barrel moved the piston upward and created suction. The suction prevented sediment from falling from the bottom of the tube as we raised the instrument. After pulling the sediment-filled instrument from the ground, we removed residual sediment from the tube and rod before extraction. We added extension rods as we extracted sediments from greater depths. We continued coring for several meters below the anthropogenic layer's depth. We then repeated the coring process at least once within 1-m of the initial hole so that two or more cores could be correlated.

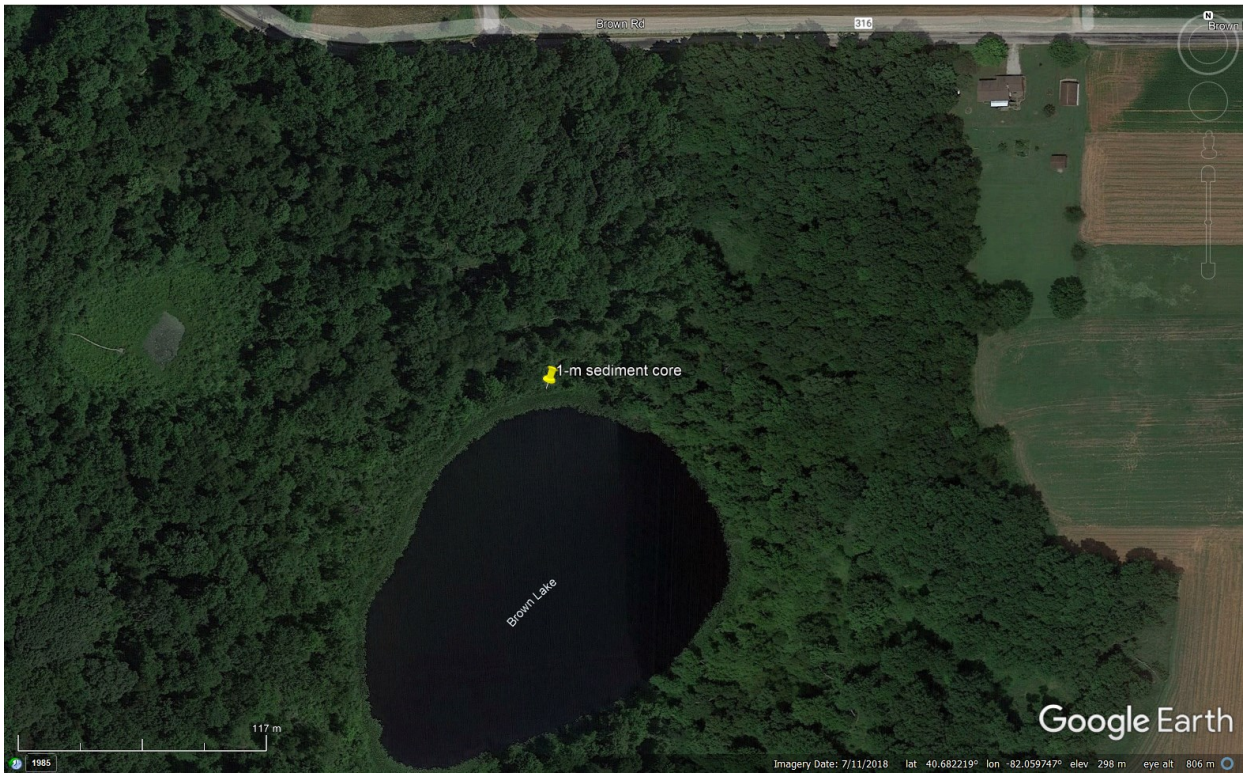


Fig. 23. Satellite view of Brown's Lake showing the approximate extraction site of the 1-m sediment core from October 2021.

While coring, we created a depth chart and initial lithologic character description for each sediment core. We covered a wooden board with a new sheet of polyvinylidene chloride "Saran" plastic wrap before each thrust to collect the extruded core. We scrapped the core with a knife and noted its color, texture, material, and other distinguishing features (Fig. 24). Then, we wrapped the core and encased it in a polyvinyl chloride "PVC" pipe. Finally, we transported the cores to our laboratory and placed them in a cold storage room.

To collect modern-day diatoms, we grabbed samples of Brown's Lake's sediment-water interface at the lake's center using a probing instrument (Fig. 25). We also cut submerged lily pads (macrophytes) at the lake's edges and stored them in zip-lock bags filled with water from

Brown's Lake. Lastly, we transferred the samples to our laboratory and kept them in a refrigerator.


Fig. 24. Describing sediment cores on-site. The modified-Livingstone corer is in the background.

Fig. 25. Sampling Brown's Lake's sediment-water interface with a probing instrument.

## AMS radiocarbon dating

Radiocarbon dating refers to determining the age of some carbonaceous material by calculating the time before the present that the material died. Radiocarbon dates are usually expressed years before present or BP. Although generally accurate, these dates come with a margin of error (+/- years) and must be corrected using calibration curves and converted to calendar age, usually quoted as Cal yr BCE/CE.

An organism exchanges carbon with its surroundings through photosynthesis and cellular respiration during its life. Plants for example, absorb $CO_2$ from the air and release $O_2$ into the atmosphere. In nature, carbon exists as three isotopes: the nonradioactive "stable" $^{12}C$ and $^{13}C$ and the radioactive "unstable" $^{14}C$. Each isotope has a different number of neutrons in its nucleus and percent abundance. $^{12}C$ is the more abundant of the two stable isotopes of carbon, amounting to 98.93% of carbon on Earth. Its nucleus comprises 6 protons and 6 neutrons. The sum of protons and neutrons in $^{12}C$ represents its atomic mass, 12. Meanwhile, $^{14}C$ occurs in trace amounts, roughly 1 atom per 1 trillion atoms of carbon in the atmosphere. The unstable $^{14}C$ undergoes beta decay into the stable isotope $^{14}N$ at a constant rate.

When a plant dies, it ceases exchanging carbon with its surroundings. The plant stops acquiring $^{14}C$, but the $^{14}C$ fixed in its biological material continues to decay. Thus, the ratio of $^{14}C$ to $^{12}C$ in its remains will decrease steadily. Because $^{14}C$ decays at a constant rate, the radiocarbon proportion can be used to determine how long it has been since a plant died. Half-life refers to the time it takes for 50% of a radioactive isotope to decay into a stable isotope. $^{14}C$ has a half-life of approximately 5,730± 40 yr.

We split the 1-m sediment core containing the anthropogenic layer into two halves: archival and sampling. We placed archival half of the core next to a meter stick, described its physical characteristics, and photographed it. Then, using a clean steel spatula, we extracted 2 g to 4 g of

moist, peat-filled sediment from 22 cm, 27 cm, 42 cm, and 62 cm downcore. Depths 27 cm, 42 cm, and 62 cm lie beneath the anthropogenic layer, providing the estimated ages of pre-settlement sediments. We washed the steel spatula with deionized water between each extraction to prevent contamination. Then, we wrapped the samples in aluminum foil separately, sealed them in individual zip-lock bags, and mailed them to the International Chemical Analysis laboratory in Damascus, Maryland, for Accelerator Mass Spectrometry (AMS) radiocarbon dating (Fig. 26). Radiocarbon ages, given in Cal yr BCE/CE, were calibrated using INTCAL20 and estimated with 2 σ calibration. Conventional ages, reported in BP (before present, 1950 CE), corrected for fractionation using the $\delta^{13}C$. After sampling the archival core, we placed it back in a cold storage room.

Fig. 26. Peat-filled sediment wrapped in aluminum foil for AMS radiocarbon dating.

## Slide preparation

We used the sampling half of the 1-m sediment core for slide preparation. We placed the core next to a meter stick and using a clean steel spatula, we removed sediment from the PVC pipe at 5 cm intervals, starting from the top of the core. We weighted each 49 $cm^3$ sample using an analytical balance. Then, we gently stirred the removed sediment with 200 mL deionized water in a glass beaker and transferred the suspension to its corresponding polypropylene bottle. (We recommend using clear, wide-mouth borosilicate glass containers instead.) We washed the steel spatula and glass beaker with deionized water between each removal and stirring to avoid contamination. Finally, we stored the bottles inside a refrigerator and allowed the suspension to settle for at least a day.

We also used the sediment-water interface samples and lily pads for slide preparation. We gently swirled the liquid contents of the zip-lock bags containing the lily pads. This process washes away diatoms attached to the lily pads, which appear as a yellow-brown slime, and suspends them in water. After swirling, we placed the zip-lock bags in the refrigerator and let liquid contents settle for 24 h. Similarly, we weighted a 49 $cm^3$ subsample of sediment-water interface samples, mixed it with 200 mL deionized water in a glass beaker, and transferred the suspension to its corresponding polypropylene bottle.

Within a day, the suspension inside the bottles separated into three distinct layers: pale yellow (top), green-brown (middle), and grey-black (bottom) (Fig. 27). We extracted 5 mL to 10 mL of water from the green-brown layer with a transfer pipette and dropped the liquid to its designated boiling tube. We used a new transfer pipette for each bottle to prevent contamination and avoid splashing liquid to the sides of the boiling tubes. Likewise, the suspension inside the zip-lock bags separated into two layers: pale yellow (top) and yellow-brown with flake-like pieces (bottom). Similar to the suspension inside the bottles, we extracted

5 mL to 10 mL of water from the yellow-brown layer with a transfer pipette and dropped the liquid to its designated boiling tube.


Fig. 27. Sediment suspension after settling for at least a day.

Next, we placed the boiling tubes inside a glass beaker, filling it with a water bath. Then, we set the beaker on a hot plate under a fume hood. At this point, we added 20 mL of 30% hydrogen peroxide ($H_2O_2$) to each boiling tube (Fig. 28). The volume of suspension water and hydrogen peroxide may be adjusted as long as a 2:1 ratio is maintained. The combined volume of suspension water and hydrogen peroxide should not exceed half of the boiling tube's capacity to avoid spilling. Finally, we turned the hot plate to 100°C or maximum setting until all organic material was oxidized, usually between 1 h and 3 h. During the boiling process, we ensured that

the water bath's level remain higher than the boiling tubes' contents by adding water to the beaker periodically. The boiling tubes' content appeared clear to slightly cloudy at this stage. After turning off the hot plate, we added a few drops of trace metals grade hydrochloric acid (HCl) into the boiling tube to remove the remaining hydrogen peroxide plus any carbonates. We also washed down the sides of each boiling tube with deionized water. Lastly, we allowed the boiling tubes' contents to cool to room temperature in the fume hood.

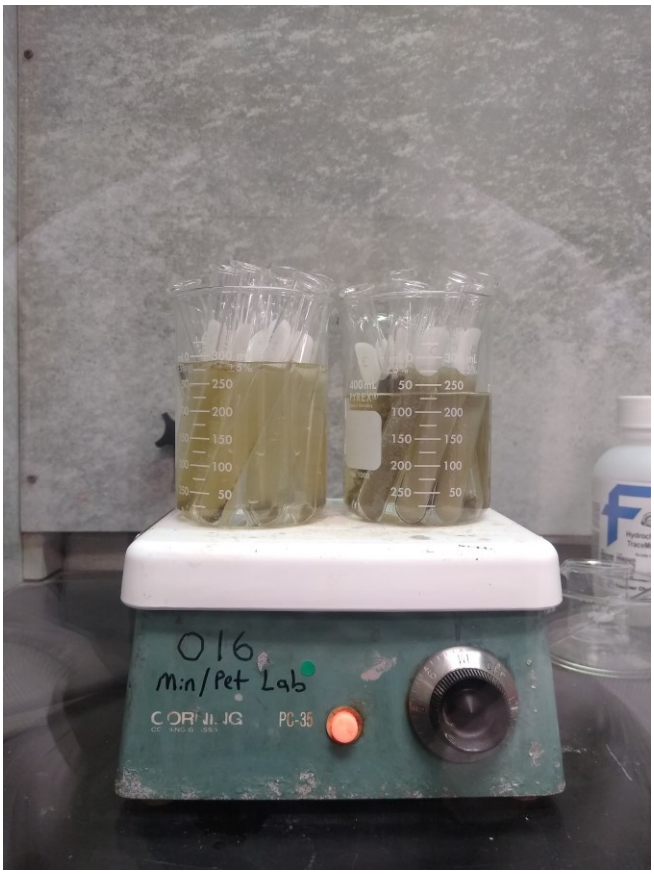


Fig. 28. Oxidizing organics with hot hydrogen peroxide.

After cooling, we used a transfer pipette to resuspend each boiling tube's contents and transferred a total of 6 mL to 4 colorless, PCR-clean 1.5 mL Eppendorf Safe-Lock centrifugation tubes. We used a new transfer pipette for each boiling tube to prevent contamination. Then, we

centrifuged the tubes for 3 min at 2,000 rpm using a Beckman Coulter Microfuge® 18 centrifuge with an F241.5P rotor. For each centrifugation tube, we decanted the supernatant, resuspended the diatom pellet with deionized water, and repeated centrifugation. We repeated the centrifugation process at least three times or until all traces of the hydrochloric acid had been removed. At this point, we mixed the diatom pellet in a small amount of deionized water and transferred the diatom suspension to a clean, small-capacity glass vial. (We recommend adding a few drops of 4% formaldehyde solution to prevent fungal growth in long-term storage.)

To make a permanent slide for each sample, we resuspended and dispensed 100 µL of the diatom suspension onto an 18 mm, rounded cover glass using a micropipette and air-dried it for at least 24 h in a dust-free room. (We caution against using a hot plate or oven to hasten the drying process as these methods cause obstructive bubbles and crusts to form.) On the leftmost side of a pre-cleaned and labeled 25 mm x 75 mm glass slide, we added a drop of the Norland Optical Adhesive 61 (NOA 61) and mounted the glass cover on top of it. We placed the glass slide 1 cm under a handheld UV lamp for a minimum of 30 min to cure the mounting medium. NOA 61 is cured by UV light with maximum absorption between 350 nm and 381 nm. The manufacturer's recommended energy for a complete cure in these wavelengths is 3 J/cm$^2$. After curing, we examined the glass slide under 400x magnification to determine diatom density. If there are approximately 5 to 20 individual frustules in any field of view, the diatom solution can be dispensed directly from the vial onto the cover glass. But if there are too many diatoms overlapping, we recommend transferring 100 µL of the diatom suspension to a new 1.5 mL centrifugation tube and diluting it with a 100 µL to 900 µL deionized water. Finally, we mounted cover glass with the ideal diatom density onto the center of the glass slide.

Contamination of samples is a serious problem. Reused glassware and spatulas must be thoroughly washed. Samples must be appropriately separated during the preparation process so that droplets from one sample will not spill into another. Pipettes used for transferring liquids and dispensing the diatom suspension should only be used for one sample and then discarded.

The polypropylene bottles, boiling tubes, centrifugation tubes, glass vials, and slides must be labeled clearly. Lastly, the permanent slides must be placed inside a microscope slide box for preservation (Fig. 29).

Fig. 29. Preserving permanent slides inside a microscope slide box.

## Microphotography

We took 10 to 20 non-overlapping photographs for each permanent slide using a Nikon Eclipse E400-POL biological microscope with a 10x eyepiece, plan-achromat 40x objective with a 0.65 numerical aperture, and Teledyne Lumenera INFINITY5-5 5.1-megapixel global shutter CMOS microscope camera (Fig. 30). We selected and identified 20 individual cells to the genus level from those sets of photographs. Identification is made by comparing diatoms with descriptions

and illustrations in the taxonomic literature. We repeated this process for all our permanent slides (20 in total), leading to the identification of 400 diatoms from Brown's Lake.

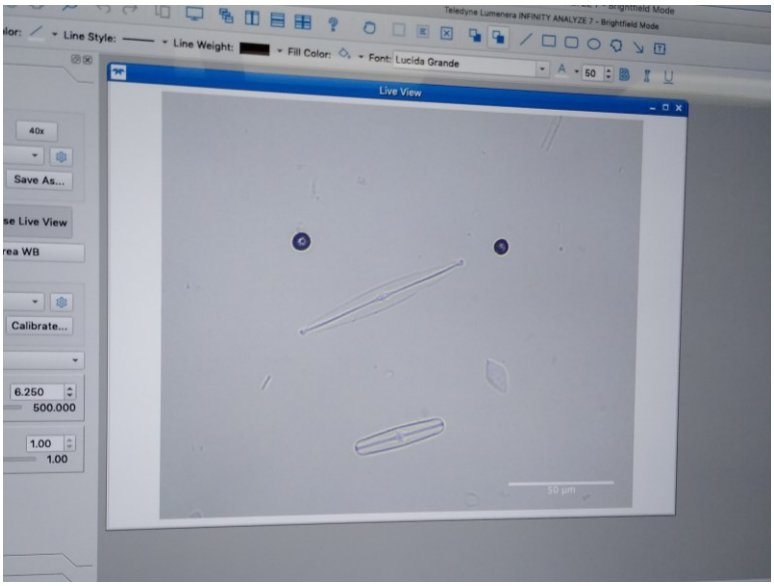


Fig. 30. Live-view of a permanent slide under a biological microscope.

## Diatom identification and analysis

We listed the genera of diatoms collected from Brown's Lake on a spreadsheet. The columns represent the permanent slide or sample name, while the rows denote the diatom identification number, which ranges from 1 to 20. We assigned the 380 diatoms from the sampling core and sediment-water interface into three age categories: modern, post-settlement, and pre-settlement. Diatoms found in the sediment-water interface and at depths 0 cm to 5 cm were labeled "modern." Those found in the anthropogenic layer that falls between 5 cm to 30 cm downcore were tagged "post-settlement." Lastly, diatoms found in depths 30 cm to 90 cm were marked "pre-settlement." Finally, we compared diatom distribution between these groups by plotting taxonomic data into a side-by-side bar chart and calculating the relative abundance (percent composition) of genera in each of the three categories.

# Data Presentation

## AMS radiocarbon dates

The AMS radiocarbon dates of 4 samples set the timing of sedimentation events in Brown's Lake (Table 2). Results reveal that sediment at 27 cm downcore, the lower part of the silt and clay unit, accumulated around 950 – 1060 CE. This age range predates the European-American settlement of northeast Ohio during the 1800s by more than 700 years. Interestingly, an age reversal is observed in the sediment record. Results indicate that sediment at 42 cm downcore deposited around 1,260 – 1,330 CE, while sediments at 62 cm downcore accumulated around 820 – 740 BCE.

Table 2. Uncalibrated and calibrated radiocarbon ages from Brown's Lake. The calibrated ages are obtained using INTCAL20 A 2 σ calibration (95% probability) is used. Conventional ages are given in BP (before present, 1950 CE), and have been corrected for fractionation using the $\delta^{13}C$.

| Sample depth (cm) | $^{14}C$ yr BP | Cal yr |
|---|---|---|
| 22 | 1,080± 40 | 880 – 1,030 CE |
| 27 | 1,020± 40 | 890 – 930 CE (3.00%)<br>950 – 1,060 CE (66.4%)<br>1,070 – 1,160 CE (25.2%) |
| 42 | 690± 40 | 1,260 – 1,330 CE (61.4%)<br>1,350 – 1400 CE (34.0%) |
| 62 | 2580± 40 | 820 – 740 BCE (65.4%)<br>700 – 660 BCE (8.20%)<br>650 – 540 BCE (21.9%) |

## Core description

The lithology of the 1-m sediment core from Brown's Lake is described below. There are three distinct lithologic units: peat, silt and clay, and peat (Fig. 31). The uppermost section, 0 cm to 5 cm downcore, is mostly peat. This unit's color gradually turns from brown to light brown downcore. The middle section, 5 cm to 27 cm, is predominantly silt and clay. This unit's color is primarily grey-brown, but it sharply becomes light brown at 22 cm downcore. The bottommost section, 27 cm to 90 cm downcore, is mostly peat. This unit's color progressively turns from brown to dark brown downcore. Besides having a darker color than the uppermost section's peat, the bottom peat unit has more fibrous material.

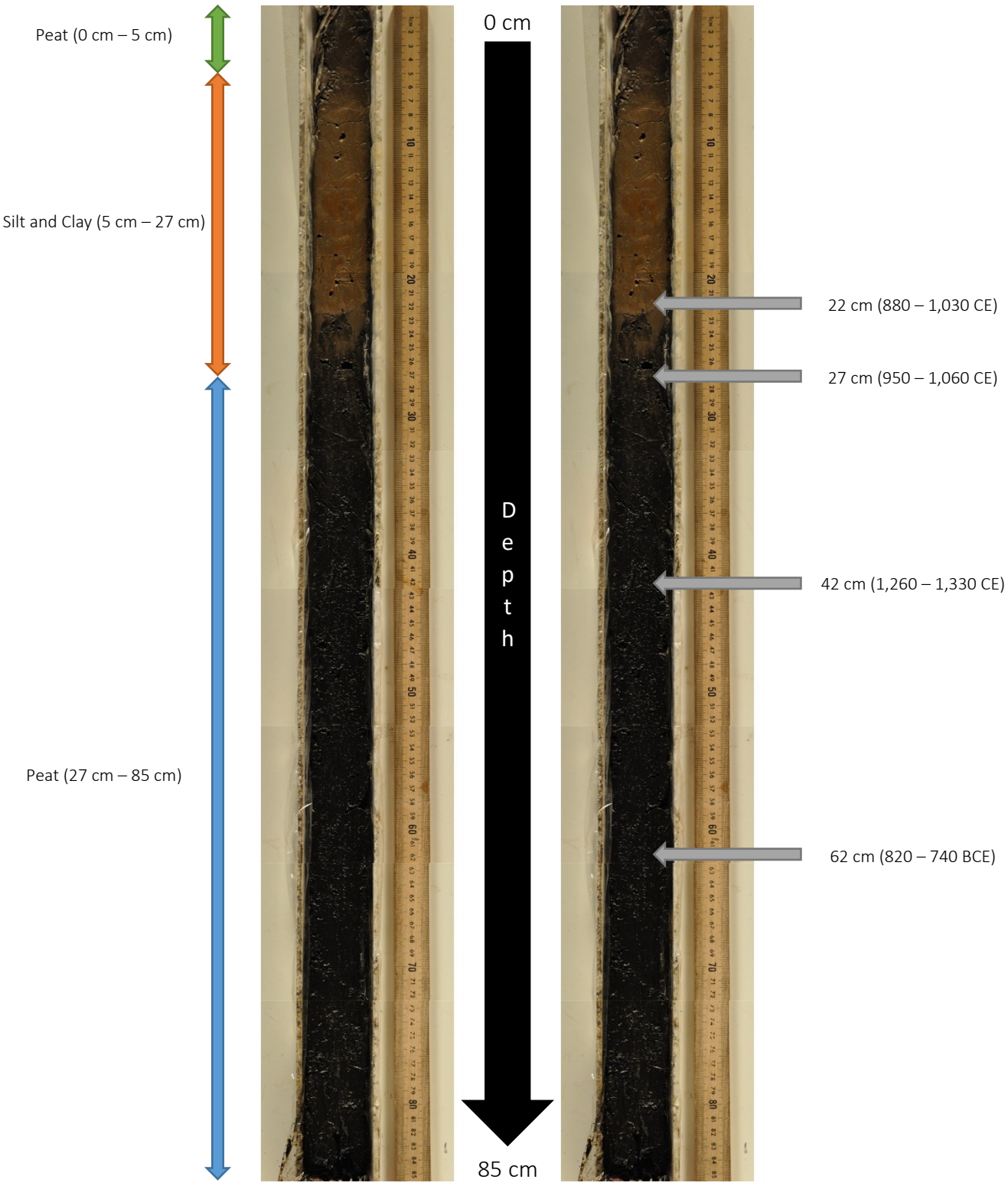


Fig. 31. The archival half of the 1-m sediment core from Brown's Lake. Green, orange, and blue arrows differentiate lithologic units (left). Gray arrows show calibrated ages of sediment (right).

## Diatom distribution

The identification of 380 diatoms from the sampling core and sediment-water interface reveals shifting distribution patterns throughout time.

In the sediment-water interface and 0 cm to 5 cm downcore, *Cyclotella* sp., a centric, planktonic, and non-motile genus, is dominant, making up to 30% of "modern" diatoms (Table 3; Fig. 32). It is followed by *Navicula* sp. (20.0%) and *Thalassiosira* sp. (17.0%) in terms of relative abundance. (Relative abundance is calculated by dividing the number of diatoms from one genus by the total number from all genera per sample set.) Overall, non-motile diatoms outnumber motile ones in a 60:40 ratio (Fig. 33). Based on the older core extracted in 2015, $^{210}$Pb radiometric dating sets the age range of modern taxa between 1950 CE to the present-day.

Table 3. Distribution of modern diatoms. Cells are sampled from the sediment-water interface and 0 cm to 5 cm downcore and estimated to have died between 1950 CE and the present-day.

| Modern Taxa | Count | Percent | Motility |
|---|---|---|---|
| *Achnanthidium* sp. | 4 | 10.0 | motile |
| *Cyclotella* sp. | 12 | 30.0 | non-motile |
| *Fragilaria* sp. | 2 | 5.0 | non-motile |
| *Gomphonema* sp. | 2 | 5.0 | motile |
| *Navicula* sp. | 8 | 20.0 | motile |
| *Nitzschia* sp. | 2 | 5.0 | motile |
| *Tabellaria* sp. | 3 | 7.5 | non-motile |
| *Thalassiosira* sp. | 7 | 17.5 | non-motile |
| TOTAL | 40 | 100.0 | |

From 5 cm to 30 cm downcore, *Achnanthidium* sp., a monoraphid, benthic, and motile genus, is dominant, making up to 25.0% of diatoms of "post-settlement" diatoms (Table 4; Fig. 32). It is followed by *Fragilaria* sp. (21.0%) and *Asterionella* sp. (18%) in terms of relative abundance. Generally, non-motile and motile diatoms in a 50:50 ratio (Fig. 33). $^{14}C$ radiometric dating sets the age range of post-settlement taxa between 880 CE and 1950 CE.

Table 4. Distribution of post-settlement diatoms. Cells are sampled from 5 cm to 30 cm downcore and estimated to have died between 880 CE and 1950 CE.

| Post-settlement Taxa | Count | Percent | Motility |
|---|---|---|---|
| *Achnanthidium* sp. | 25 | 25.0 | motile |
| *Amphipleura* sp. | 3 | 3.0 | non-motile |
| *Asterionella* sp. | 18 | 18.0 | non-motile |
| *Cocconeis* sp. | 1 | 1.0 | non-motile |
| *Cyclotella* sp. | 1 | 1.0 | non-motile |
| *Cymbella* sp. | 1 | 1.0 | motile |
| *Diatoma* sp. | 1 | 1.0 | non-motile |
| *Eunotia* sp. | 4 | 4.0 | motile |
| *Fragilaria* sp. | 21 | 21.0 | non-motile |
| *Gomphonema* sp. | 5 | 5.0 | motile |
| *Navicula* sp. | 14 | 14.0 | motile |
| *Nitzschia* sp. | 1 | 1.0 | motile |
| *Tabellaria* sp. | 1 | 1.0 | non-motile |
| *Thalassiosira* sp. | 4 | 4.0 | non-motile |
| TOTAL | 100 | 100.0 | |

From 30 cm to 90 cm downcore, *Thalassiosira* sp., a centric, planktonic, and non-motile genus, is dominant, making up to 22.1% of "pre-settlement" diatoms (Table 5; Fig. 32). It is followed by *Eunotia* sp. (17.9%) and *Tabellaria* sp. (13.3%) in terms of relative abundance. Generally, non-motile and motile diatoms are nearly equal, 49:51 ratio (Fig. 33). $^{14}C$ radiometric dating sets the age of pre-settlement taxa to before 880 CE.

Table 5. Distribution of pre-settlement diatoms. Cells are sampled from 30 cm to 90 cm downcore and estimated to have died before 880 CE.

| Pre-settlement Taxa | Count | Percent | Motility |
|---|---|---|---|
| *Achnanthidium* sp. | 12 | 5.0 | motile |
| *Asterionella* sp. | 3 | 1.3 | non-motile |
| *Cyclotella* sp. | 27 | 11.3 | non-motile |
| *Cymbella* sp. | 7 | 2.9 | motile |
| *Epithemia* sp. | 1 | 0.4 | motile |
| *Eunotia* sp. | 43 | 17.9 | motile |
| *Fragilaria* sp. | 2 | 0.8 | non-motile |
| *Gomphonema* sp. | 16 | 6.7 | motile |
| *Navicula* sp. | 29 | 12.1 | motile |
| *Nitzschia* sp. | 14 | 5.8 | motile |
| *Pinnularia* sp. | 1 | 0.4 | motile |
| *Tabellaria* sp. | 32 | 13.3 | non-motile |
| *Thalassiosira* sp. | 53 | 22.1 | non-motile |
| TOTAL | 240 | 100.0 | |

Table 6. Abundance of genera, expressed in number of diatoms per genus.

| Taxa | Modern (Count) | Post-settlement (Count) | Pre-settlement (Count) |
|---|---|---|---|
| *Achnanthidium* sp. | 4 | 25 | 12 |
| *Amphipleura* sp. | 0 | 3 | 0 |
| *Asterionella* sp. | 0 | 18 | 3 |
| *Cocconeis* sp. | 0 | 1 | 0 |
| *Cyclotella* sp. | 12 | 1 | 27 |
| *Cymbella* sp. | 0 | 1 | 7 |
| *Diatoma* sp. | 0 | 1 | 0 |
| *Epithemia* sp. | 0 | 0 | 1 |
| *Eunotia* sp. | 0 | 4 | 43 |
| *Fragilaria* sp. | 2 | 21 | 2 |
| *Gomphonema* sp. | 2 | 5 | 16 |
| *Navicula* sp. | 8 | 14 | 29 |
| *Nitzschia* sp. | 2 | 1 | 14 |
| *Pinnularia* sp. | 0 | 0 | 1 |
| *Tabellaria* sp. | 3 | 1 | 32 |
| *Thalassiosira* sp. | 7 | 4 | 53 |
| TOTAL | 40 | 100 | 240 |

Table 7. Abundance of genera, expressed in percent composition.

| Taxa | Modern (Percent) | Post-settlement (Percent) | Pre-settlement (Percent) |
|---|---|---|---|
| *Achnanthidium* sp. | 10.0 | 25.0 | 5.0 |
| *Amphipleura* sp. | 0.0 | 3.0 | 0.0 |
| *Asterionella* sp. | 0.0 | 18.0 | 1.3 |
| *Cocconeis* sp. | 0.0 | 1.0 | 0.0 |
| *Cyclotella* sp. | 30.0 | 1.0 | 11.3 |
| *Cymbella* sp. | 0.0 | 1.0 | 2.9 |
| *Diatoma* sp. | 0.0 | 1.0 | 0.0 |
| *Epithemia* sp. | 0.0 | 0.0 | 0.4 |
| *Eunotia* sp. | 0.0 | 4.0 | 17.9 |
| *Fragilaria* sp. | 5.0 | 21.0 | 0.8 |
| *Gomphonema* sp. | 5.0 | 5.0 | 6.7 |
| *Navicula* sp. | 20.0 | 14.0 | 12.1 |
| *Nitzschia* sp. | 5.0 | 1.0 | 5.8 |
| *Pinnularia* sp. | 0.0 | 0.0 | 0.4 |
| *Tabellaria* sp. | 7.5 | 1.0 | 13.3 |
| *Thalassiosira* sp. | 17.5 | 4.0 | 22.1 |
|  | 100.0 | 100.0 | 100.0 |

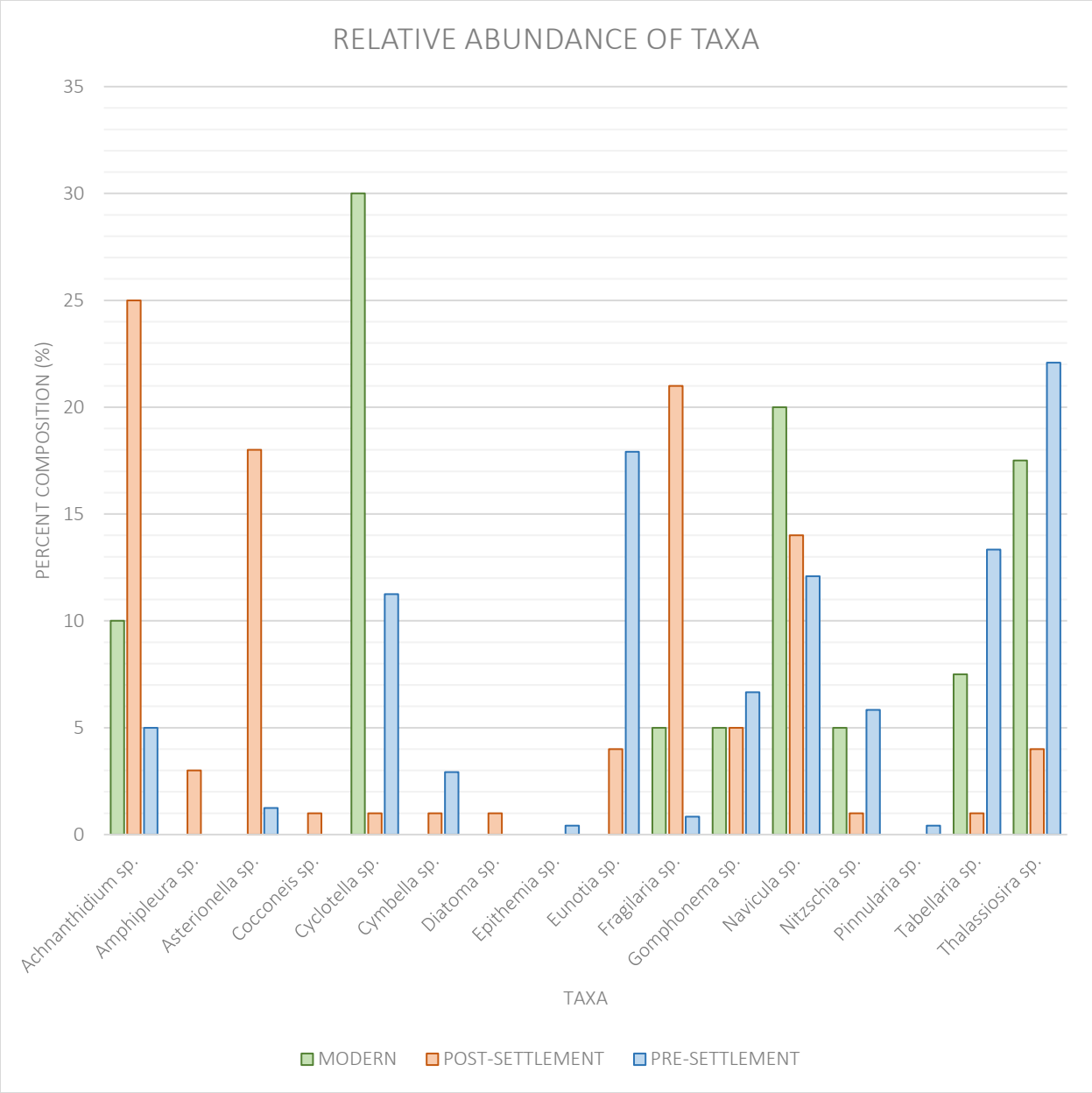


Fig. 32. Relative abundance of genera. *Cyclotella* sp., a centric, planktonic, and non-motile genus, is dominant in modern times. In post-settlement times, *Achnanthidium* sp., a monoraphid, benthic, and motile genus, is abundant. *Thalassiosira* sp., a centric, planktonic, and non-motile genus is dominant in pre-settlement times.

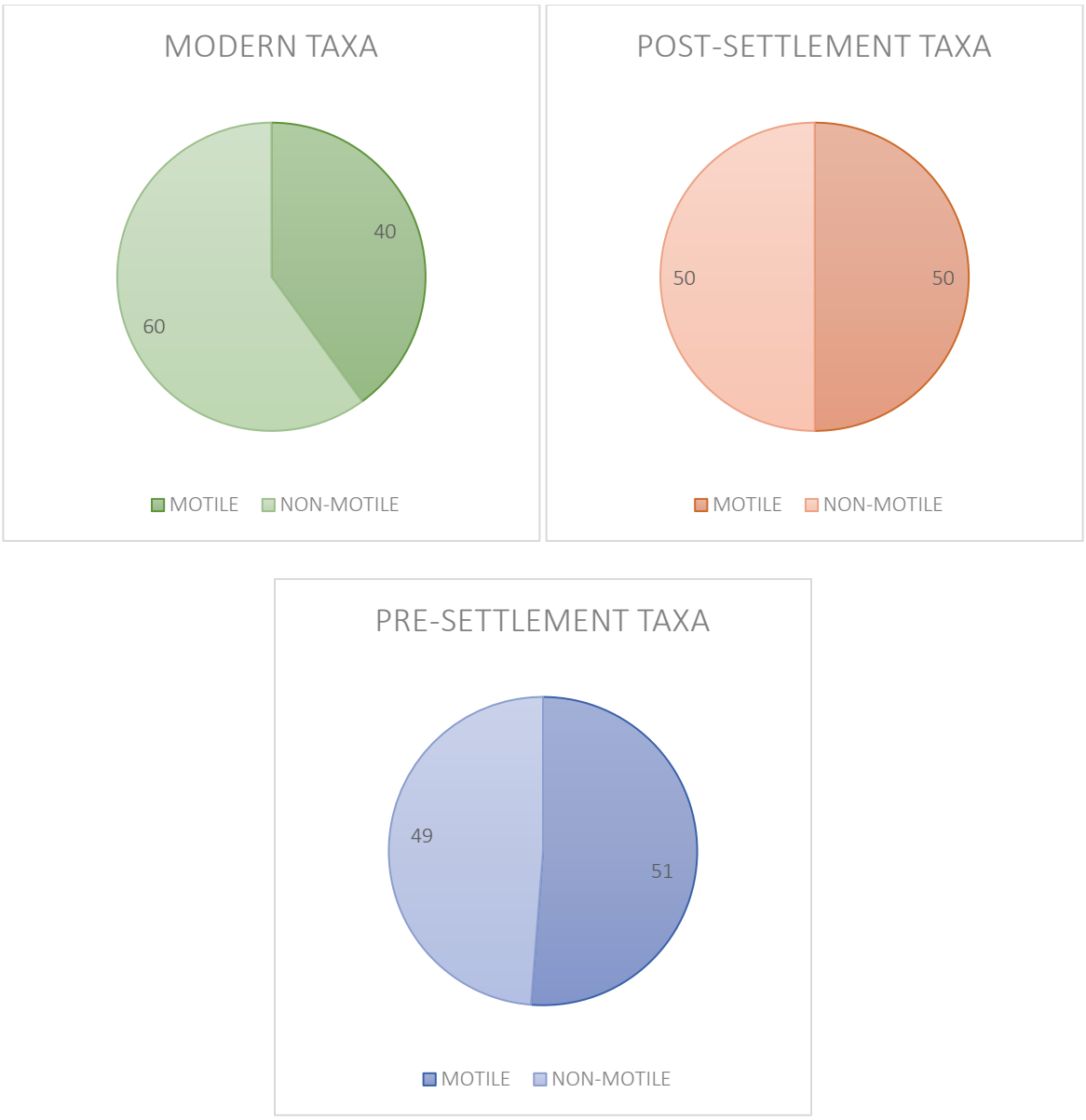


Fig. 33. Ratio between non-motile and motile diatoms through time. In modern times, non-motile genera are more abundant than motile ones. In post-settlement times, non-motile and motile genera are equal, 50:50 ratio. In pre-settlement times, non-motile and motile genera are nearly equal, 49:51 ratio.

# Interpretation and Discussion

## Interpretation

An initial assessment of the data shows some diatoms (i.e., *Achnanthidium* sp., *Cyclotella sp.*, *Fragilaria sp.*, *Gomphonema sp.*, *Navicula sp.*, *Nitzschia sp*., *Tabellaria sp*., and *Thalassiosira* sp.) are common in Brown's Lake from pre-settlement times to today. However, their relative abundances have shifted over the years. In Fig. 33, there is a near-equal ratio, 49:51, between non-motile and motile genera during pre-settlement times (before 880 CE). Sediment in this period had plenty of peat and fibrous material. But during post-settlement times (between 880 CE and 1950 CE), the ratio between non-motile and motile genera reached 50:50. In this period, sediment became silty and clayey relatively quickly. In modern times (between 1950 CE and the present-day), the ratio between non-motile and motile genera is 60:40, favoring non-motile taxa. It is worth noting that today's sediment is rich in peat, similar to pre-settlement sediment. Changes in the relative abundance of taxa based on their traits, such as motility, can be used to indicate biological or stressor conditions (Stoermer and Smol, 2010). The replacement of planktonic genera by diatoms with the morphological capability of moving through fine sediments (i.e., *Achnanthidium* sp., *Gomphonema* sp., *Navicula* sp., and *Nitzschia* sp.) during the post-settlement period, therefore, indicates a time of excess siltation (Stoermer and Smol, 2010). In the same manner, the presence of *Epithemia* sp. (a genus that can have N-fixing blue-green endosymbionts) during the pre-settlement period suggests a time of low nitrogen concentrations compared to phosphorus (DeYoe et al., 1992). Conversely, the absence of *Epithemia* sp. during the post-settlement and modern periods indicates times of high nitrogen levels compared to phosphorus. Last but not least, according to Vadeboncoeur et al. (2003), the contribution of benthic algae to overall lake production varies as a function of lake morphometry and trophic status, with estimated percentage contributions ranging from 1% to nearly 100%. It has been noted that pelagic production tends to rise with increasing nutrient load, while benthic production falls as light constrains the production of bottom-dwelling algae and submerged macrophytes (Scheffer and van Nes, 2007; Bennion et al., 2010).

## Discussion

This project is the College of Wooster Department of Earth Sciences' first attempt to construct the diatom stratigraphy of Brown's Lake and understand the effects of European-American settlement in Wayne County, in northeast Ohio, on the lake's limnology. The replacement of planktonic genera by diatoms with the morphological capability of moving through fine sediments indicates a period of excess siltation from 880 CE to 1950 CE. This change is represented stratigraphically by a bright loess layer interbedded between organic-rich muds (Fig. 13; Fig. 31). Jimerson et al. (2016) hypothesized that this layer is windblown sediment from land clearing and agriculture, based on its magnetics, grain size, and mineralogy. The middle section of the loess layer (45 cm depth) dates back to the mid-1800s when Wayne County's population peaked, and people had built roads, logged trees, and cleared lands intensively. From 1950 CE to the present-day, planktonic genera has become more abundant than motile ones. This change is marked stratigraphically by a steady return to organic-rich sediments (Fig. 13; Fig. 31). Also, from 1950 CE to the present-day, people began to abandon farmland and practice conservation tillage, and there was less windblown flux and more organics (Jimerson et al., 2016).

Generally, the diatom stratigraphy shows limnological changes associated with settlement activities. However, other factors may be at play. Ring-width chronology and observational climate records indicate that the mid-1800s were relatively dry and cool while 1950 CE and onwards were wetter and warmer (Jimerson et al., 2016). Hence, climate may have influenced diatom distribution throughout time. Also, the ratio between planktonic and non-planktonic taxa relies on habitat availability and structure, such as the presence of plants, illuminated surface sediments, and open water, which are related to nutrients; diatom-nutrient relationships are often indirect (Bennion et al., 2010). For these reasons, the diatom stratigraphy cannot provide evidence of cause and effect; it can only provide evidence of some relationship (between European-American settlement and limnological changes) that an experimental design could further explore. The diatom stratigraphy is an observational study since data were recorded as they naturally exist, and no variables were actively manipulated.

Due to the nature of the data, the diatom stratigraphy is by no means free of errors and limitations. This section begins by exploring the errors and limitations of radiometric methods. First, we used separate 1-m sediment cores, one collected in 2015 and the other in 2021, to determine the age of sediments. The core from 2015 used $^{210}$Pb 0radiometric dating, while the core from 2021 used $^{14}$C radiometric dating. Suppose the diatom stratigraphy was reproduced or revised in a future study. In that case, we recommend performing both $^{210}$Pb and $^{14}$C radiometric dating on the same core to minimize or eliminate discrepancies between sedimentary layers. Most significantly, caution must be taken when interpreting $^{14}$C dates. Radiocarbon dates from basal peat (visually defined as the boundary between peat and inorganic lake sediment) can be affected by contamination due to root penetration from above and the movement of mobile human acids. These lead to unexpected ages, mostly that are too young (Smith and Cloutman, 1988; Charman, 2002; Barber and Charman, 2003). Other biases in $^{14}$C radiometric dating include the reservoir effect (leads to ages that are too old) and carbon cycling in the sediment-water interface (Ojala et al., 2019). Charman (2002) summarizes that problems in radiocarbon dating are linked with "assumptions of the atmospheric concentration of $^{14}$C in the past and deposition and post-depositional processes." In this project, $^{14}$C radiometric dating of the 1-m sediment core from 2021 gave anomalous dates at 22 cm, 27 cm, 42 cm downcore (Table 2). The derived ages of sediments from 22 cm downcore were 300 years to 400 years older than sediments from 42 cm downcore. Comparatively, sediments from 27 cm downcore were 200 to 300 years older than those from 42 cm downcore. This 'age reversal' highlights issues in radiocarbon dating.

Recently developed techniques for higher-precision estimates of peat age could help overcome uncertainties associated with conventional radiocarbon dating. For instance, wiggle-matching, which utilizes the non-linear relationship between $^{14}$C age and calendar age to match the shape of the calibration curve with a series of closely spaced peat dates, is used to date peats from periods where there are plateaus in the calibration curve (Kilian et al., 1995; van Geel et al., 1998). Selecting pure *Sphagnum* moss peats for AMS $^{14}$C wiggle-matching may be ideal for dating peat deposits (Killian et al., 2000; Barber and Charman., 2003). Despite its advantages, Charman

(2002) states that "wiggle-matching has not been widely used in routine paleoecology because of the high costs of obtaining an adequate number of closely spaced dates." Meanwhile, $^{210}$Pb radiometric dating is best suited for recent sediments (up to 200 years old) due to $^{210}$Pb's shorter half-life of 22.26 years (Charman. 2002; Barber and Charman, 2003). Oldfield et al. (1995) compared $^{210}$Pb-dated profiles with other age estimates and suggest that "radiometric measurements alone cannot be relied on to give an accurate chronology of peat accumulation." Additional techniques should be used in conjunction with $^{210}$Pb chronologies as a cross-check (Oldfield et al., 1995; Charman, 2002; Barber and Charman, 2003).

This section ends by outlining the errors and limitations of diatom analysis. First, the inexpensive 40x objective and 5.1-megapixel camera are insufficient for accurate, species-level identification as several diatoms are smaller than 50 µm. Second, the sample size (n = 380) might be small and not accurately represent Brown's Lake's past and present diatom population. We recommend using research-grade optics and larger sample size when reproducing or revising the diatom stratigraphy. Other challenges include the physical, chemical, and biological processes that combine and affect the types and numbers of diatoms preserved in sediments. For example, although diatoms are present in wetter parts of peatlands, they may undergo dissolution in the peat column (Kingston, 1982; Bennett et al., 1991). Dissolution is also a problem in freshwater systems; cells may be partly dissolved so that identification gets more difficult or impossible (Flower, 1993). Previous investigations have reported that roughly fifty percent of diatom frustules in surface sediments suffer from dissolution in varying degrees. Only a tiny fraction of frustules may be preserved in sediments (Mackay et al., 2000; Ryves et al., 2001). On top of preservation issues, there is a suspicion that many diatom 'species' described are morphological variations of a single taxon (Bradbury, 1975). Bradbury (1975) summarizes that such variations may result from "a decrease in cell size during vegetative reproduction or a polymorphism reflecting environmental conditions" (Hostetter and Hoshaw, 1972; Schultz, 1971). Describing such variants as distinct taxa causes a multiplicity of names for the same organism in the taxonomic literature, hinders communication, and complicates the synthesis of ecological or stratigraphic information.

# Conclusions

The data highlight limnological changes in Brown's Lake associated with European-American settlement. The initial diatom stratigraphy shows that relative abundances of diatoms have shifted over the years. *Thalassiosira* sp., a centric, planktonic, and non-motile genus, is dominant, making up 22.1% of diatoms during pre-settlement times (before 880 CE). But during post-settlement times (between 880 CE and 1950 CE), *Achnanthidium* sp., a monoraphid, benthic, and motile genus, is abundant, making up 25.0% of diatoms. This transition is represented stratigraphically by a bright loess layer hypothesized as windblown sediment from land clearing and agriculture. From 1950 CE to the present-day, *Cyclotella* sp., a centric, planktonic, and non-motile genus, is dominant, making up 30% of diatoms. This transition is marked stratigraphically by a steady return to organic-rich sediments and when people started to abandon farmland and practice conservation tillage. Despite these associations, the diatom stratigraphy cannot provide evidence of a cause-and-effect relationship. Confounding variables, such as climate and habitat availability and structures, can change a lake's diatom distribution and limnology. Furthermore, one should consider the errors and limitations of radiometric dating and diatom analysis, depending on a project's objectives, budget, and indicator metrics. To conclude, this study requires further work in identifying the water quality and habitat parameters for identified taxa through literature review and experimentation. Consequently, it can deepen understanding of the link between human settlement and limnological changes and help people conserve wetlands.

# References Cited


Abrams, M.D., 2003, Where has all the white oak gone?: BioScience, v. 53, p. 927–939.

Aughanbaugh, J., and Diller, O.D., 1968, Flora of Brown's Lake Bog and vicinity: Wooster, Ohio Chapter Nature Conservancy, 23 p.

Bailey, C., 2003, Reconstruction of the late-glacial environmental history of Brown's Lake Bog, Northeast Ohio [Unpublished undergraduate thesis]: Wooster, College of Wooster, 86 p.

Barber, K., and Charman, D.J., 2003, Holocene paleoclimate records from peatlands *in* Mackay, A., Jones, V.J., Battarbee R.W., Birks, H.J.B., and Oldfield, F. eds., Global change in the Holocene (first edition): London, Routledge, p. 211–226.

Battarbee, R.W., Vivienne, J.J., Flower, R.J., Cameron, N.G., Bennion, H., Carvalho, L., and Juggins, S., 2001, Diatoms *in* Smol, J.P., Birks, H.J.B., and Last, W.M., eds., Tracking environmental change using lake sediments: Dordrecht, Kluwer Academic Publishers, v. 3, p. 155–202.

Bayer, M., and Du Buff, H., eds., 2002, Automatic diatom identification: Singapore, World Scientific, 329 p.

Bennett, P.C., Siegel, D.I., Hill, B.M., and Glaser, P.H., 1991, Fate of silicate minerals in a peat bog: Geology, v. 19, p. 328–331.

Bennion, H., Sayer, C.D., Tibby, J., and Carrick, H.R., 2010, Environmental change in shallow lakes *in* Stoermer, E.F. and Smol, J.P., eds., 2010, The diatoms: Applications for the environmental and earth sciences (second edition): New York, Cambridge University Press, p. 152–167.

Bradbury, J.P., 1975, Diatom stratigraphy and human settlement in Minnesota: Geological Society of America, Special Paper 171, 74 p.

Bradley, R.S., 2014, Paleoclimatology: Reconstructing climates of the Quaternary (third edition): Waltham, Academic Press, 696 p.

Charman, D.J., 2002, Peatlands and environmental change: West Sussex, John Wiley & Sons, 301 p.

Cohen, A.S., 2003, Paleolimnology: The history and evolution of lake systems: New York, Oxford University Press, 528 p.

Cook, E.R., 1987, The decomposition of tree-ring series for environmental studies: Tree Ring Bulletin, v. 47, p. 37–59.

Cook, E.R., and Krusic, P.J., 2004, The North American Drought Atlas: Lamont-Doherty Earth Observatory and the National Science Foundation (available at https://iridl.ldeo.columbia.edu/SOURCES/LDEO/.TRL/.NADA2004/.pdsi-atlas.html).

Devereux, K., 2018, A dendroclimatological analysis of Brown's Lake Bog Preserve, Wayne County, Ohio [Unpublished undergraduate thesis]: Wooster, College of Wooster, 14 p.

DeYoe, H.R., Lowe, R.L., and Marks, J.C., 1992, Effects of nitrogen and phosphorus on the endosymbiont load of *Rhopalodia gibba* and *Epithemia turgida* (Bacillariophyceae): Journal of Phycology, v. 28, p. 723–873.

Flower, R.J., 1993, Diatom preservation: experiments and observations on dissolution and breakage in modern and fossil material: Hydrobiologia, v. 269, p. 473–484.

Freimuth, E.J., Deifendorf, A.F., Lowell, T.V., and Wiles, G.C., 2019, Sedimentary n-alkanes and n-alkanoic acids in a temperate bog are biased toward wood plants: Organic Geochemistry, v. 128, p. 94–107.

Galbreath, C.B., 2011, History of Ohio, Volume 1: Chicago and New York, The American Historical Society, 710 p.

Glover, K.C, Lowell, T.V., Wiles, G.C., Pair, D., Applegate, P., and Hajdas, I., 2011, Deglaciation, basin formation and post-glacial climate change from a regional network of sediment core sites in Ohio and eastern Indiana: Quaternary Research, v. 76, p. 401–410.

Hasle, G.R., Syvertsen, E.E., Steidinger, K.A., Tangen, T., and Tomas, C.R., 1996, Identifying marine diatoms and dinoflagellates: Waltham, Academic Press, 613 p.

Hostetter, H.P., and Hoshaw, R.P., 1972, Asexual development patterns of the diatom *Stauroneis anceps* in culture: Journal of Phycology, v. 8, p. 289–296.

Jacoby, G.C., and D'Arrigo, R.D., 1997, Tree rings, carbon dioxide, and climate change: Proceedings of the National Academy of Sciences USA, v. 94, p. 8350–8353.

Jimerson, C.R., Freimuth, E.J., Pollock, M., and Wiles, G.C., 2016, Land use changes over the past 200 years in northeast Ohio recognized in lake cores from Brown's Lake Bog, northeast Ohio: Geological Society of America Abstracts with Programs: v. 48, p. 7.

Kilian, M.R., van der Plicht, J., and van Geel, B., 1995, Dating raised bogs: new aspects of AMS $1^4C$ wiggle-matching, a reservoir effect and climatic change, Quaternary Science Reviews, v. 14, p. 959–966.

Killian, M.R., van Geel, B., and van der Plicht, J., 2000, $^{14}C$ AMS wiggle matching of raised bog deposits and models of peat accumulation, Quaternary Science Reviews, v. 19, p. 1011–1033.

Kingston, J.C., 1982, Association and distribution of common diatoms in surface samples from northern Minnesota peatlands: Nova Hedwigia, v. 19, p. 333–345.

Lutz, B., Wiles, G.C., Lowell, T.V, and Michaels, J., 2007, The 8.2-ka abrupt climate change event in Brown's Lake, northeast Ohio: Quaternary Research, v. 67, p. 292–296.

Mackay, A., Battarbee, R.W., Flower, R.J., et al., 2000, The deposition and accumulation of endemic planktonic diatoms in the sediments of Lake Baikal and an evaluation of their potential role in climate reconstruction during the Holocene: Terra Nostra, v. 9, p. 34–48.

Mackay, A., Jones, V.J., and Battarbee, R.W., 2003, Approaches to Holocene climate reconstruction using diatoms *in* Mackay, A., Jones, V.J., Battarbee R.W., Birks, H.J.B., and Oldfield, F. eds., Global change in the Holocene (first edition): London, Routledge, p. 294–309.

Ojala, A.E.K., Saarnisto, M., Jungner, H., Snowball, I., and Muscheler, R., 2019, Biases in radiocarbon dating of organic fractions in sediments from meromictic and seasonally hypoxic lakes, Bulletin of the Geological Society of Finland, v. 91, p. 221–235.

Oldfield, F., Richardson, N., and Appleby, P.G., 1995, Radiometric dating ($^{210}Pb$, $^{137}Cs$, $^{241}Am$) of recent ombrotrophic peat accumulation and evidence for changes in mass balance: The Holocene, v. 5, p. 141–148.

Ryves, D.B., Huggins, S., Fritz, S.C., and Battarbee, R.W., 2001, Experimental diatom dissolution and the quantification of microfossil preservation in sediments: Paleogeography, Paleoclimatology, Paleoecology, v. 172, p. 99–113.

Sanger, J.S., and Crowl, G.H., 1979, Fossil pigments as a guide to the paleolimnology of Browns Lake, Ohio: Quaternary Research, v. 11, p. 342–352.

Scheffer, M., and van Ness, E.H., 2007, Shallow lakes theory revisited: Various alternative regimes driven by climate, nutrients, depth, and lake size, Hydrobiologia, v. 584, p. 455–466.

Schultz, M.E., 1971, Salinity-related polymorphism in the brackish-water diatom *Cyclotella cryptica*: Canadian Journal of Botany, v. 49, p. 1285–1289.

Shane, L.C.K., and Anderson, K.H., 1993, Intensity, gradients, and reversals in late glacial environmental change in east-central North America: Quaternary Science Reviews, v. 12, p. 307–320.

Smith, A.G., and Cloutman, E.W., 1988, Reconstruction of Holocene vegetation history in three dimensions at Waun-Fignen-Felen, an upland site in South Wales, Philosophical Transactions of the Royal Society of London, B322, p. 159–219.

Stoermer, E.F. and Smol, J.P., eds., 2010, The diatoms: Applications for the environmental and earth sciences (second edition): New York, Cambridge University Press, 667 p.

Tardif, J.C., Conciatori, F., Nantel, P., and Gagnon, D., 2006, Radial growth and climate responses of white oak (*Quercus alba*) and northern red oak (*Quercus rubra*) at the northern distributing limit of white oak in Quebec, Canada: Journal of Biogeography, v. 33, p. 1657–1669

Taylor, J.C., Harding, W.R., and Archibald, C.G.M., 2007, An illustrated guide to some common diatom species from South Africa: Water Commission Report TT 282/07, 225 p.

Trouet, V., and Oldenborgh, G. J., 2013, KNMI Climate Explorer: a web-based research tool for high-resolution paleoclimatology: Tree-Ring Research, v. 69, p. 3–13.

Tundisi, J.G., and Tundisi, T.M., 2011, Limnology: Boca Raton, Taylor & Francis Group, 870 p.

Vadeboncoeur, Y., Jeppesen, E., Vander Zanden, M.J., et al., 2003, From Greenland to green lakes: Cultural eutrophication and the loss of benthic pathways in lakes: Limnology and Oceanography, v. 48, p. 1408-1418.

Van den Hoek, C., Mann, D.G., and Jahns, H.M., 1995, Algae: An introduction to phycology: Cambridge, Cambridge University Press, 623 p.

Van Geel, B., van der Plicht, J., Kllian, M.R., et al., 1998, The sharp rise of Delta $^{14}C$ ca. 800 cal BC: Possible causes, related climatic teleconnections and the impact on human environments: Radiocarbon, v. 40, p. 535–550.

White, W.G., 1967, Glacial Geology of Wayne County, Ohio: Ohio Division of Geological Survey Report of Investigations No. 62, 39 p.

# Appendices

## Plate I: Taxa by depth *(p. 62–182)*

These photos show all the 380 diatoms used for the statistical analysis in this study, arranged by depth. (An additional 20 diatoms from the lily pads are included for reference.) The images are captured using a Nikon Eclipse E400-POL biological microscope with a 10x eyepiece, plan-achromat 40x objective with a 0.65 numerical aperture, and Teledyne Lumenera INFINITY5-5 5.1-megapixel global shutter CMOS microscope camera.

## Plate II: Alphabetical list of taxa *(p. 183–194)*

These photos illustrate some of the genera identified in Brown's Lake, sorted in alphabetical order. The images are captured using a Nikon LABOPHOT-POL polarizing microscope with a 10x eyepiece, Olympus A100PL 1,30 160/0.17 100x objective with immersion oil IMMOIL-F30CC, and Teledyne Lumenera INFINITY3-6 6.0-megapixel CCD microscope camera. This set does not include all the species or variations for each genus.

Lily pads

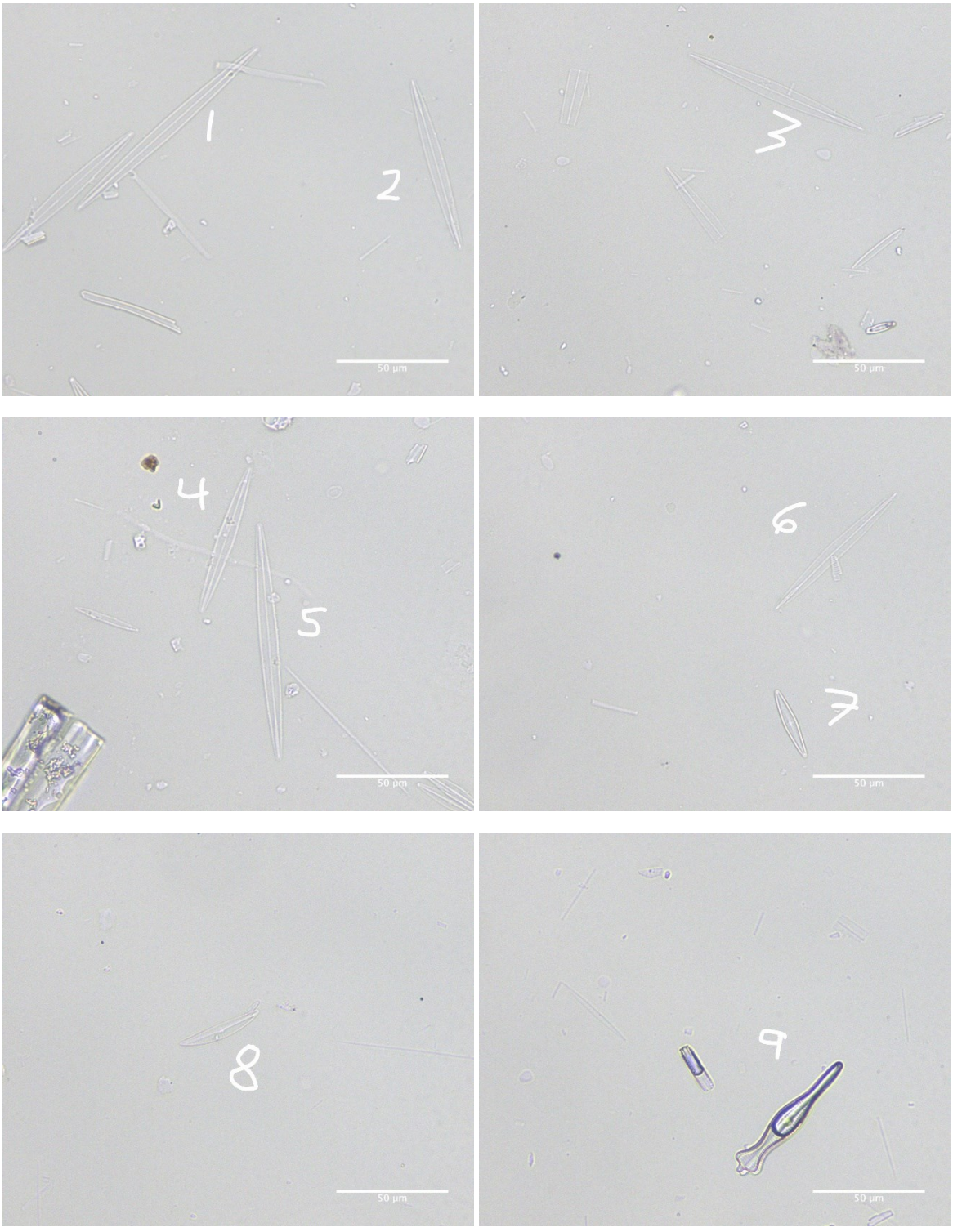

Lily pads

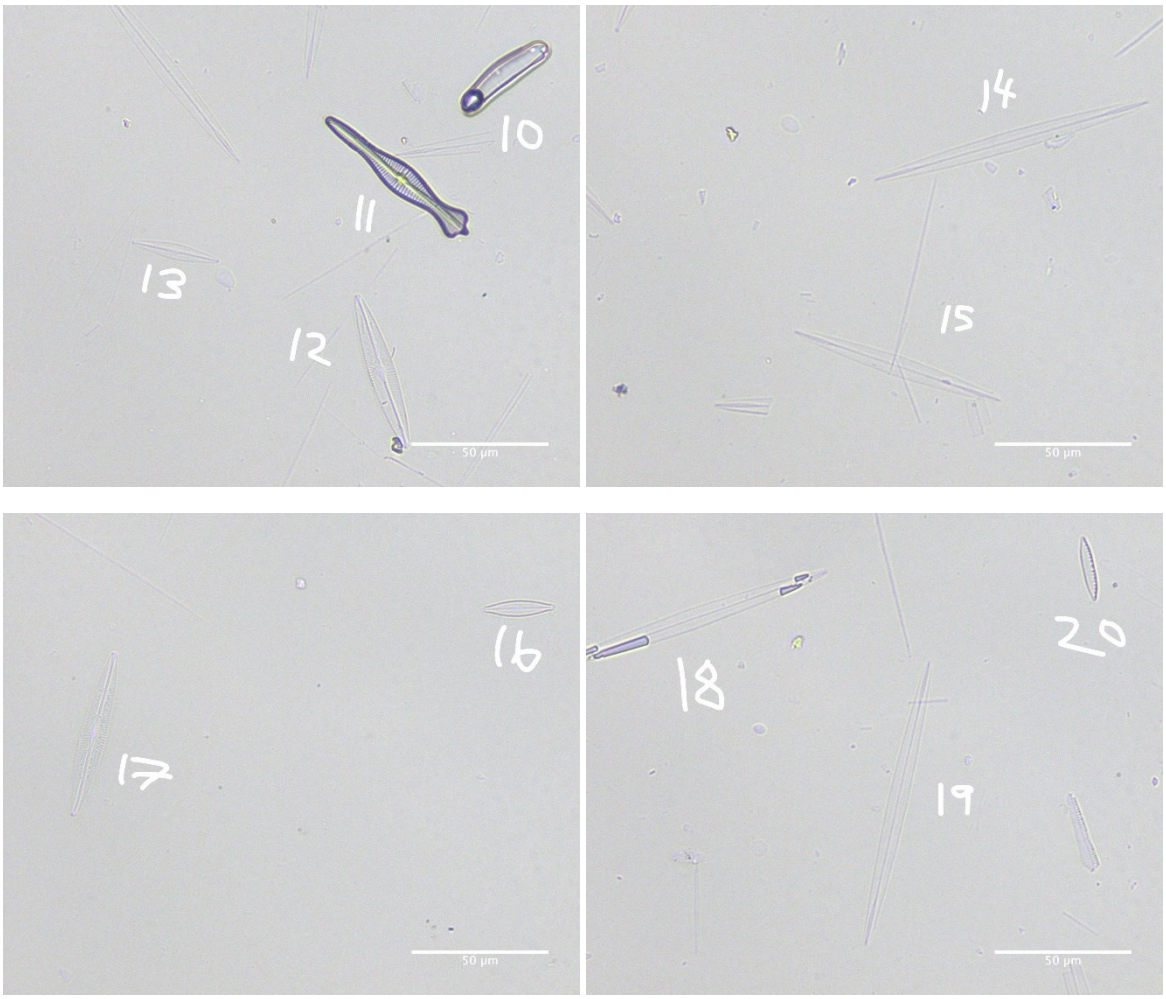


| Diatom ID | Taxon | Diatom ID | Taxon |
|---|---|---|---|
| 1 | *Amphipleura* sp. | 11 | *Gomphonema* sp. |
| 2 | *Amphipleura* sp. | 12 | *Navicula* sp. |
| 3 | *Amphipleura* sp. | 13 | *Navicula* sp. |
| 4 | *Amphipleura* sp. | 14 | *Amphipleura* sp. |
| 5 | *Amphipleura* sp. | 15 | *Amphipleura* sp. |
| 6 | *Amphipleura* sp. | 16 | *Navicula* sp. |
| 7 | *Gomphonema* sp. | 17 | *Navicula* sp. |
| 8 | *Cymbella* sp. | 18 | *Amphipleura* sp. |
| 9 | *Gomphonema* sp. | 19 | *Amphipleura* sp. |
| 10 | *Eunotia* sp. | 20 | *Nitzschia* sp. |

Sediment-water Interface

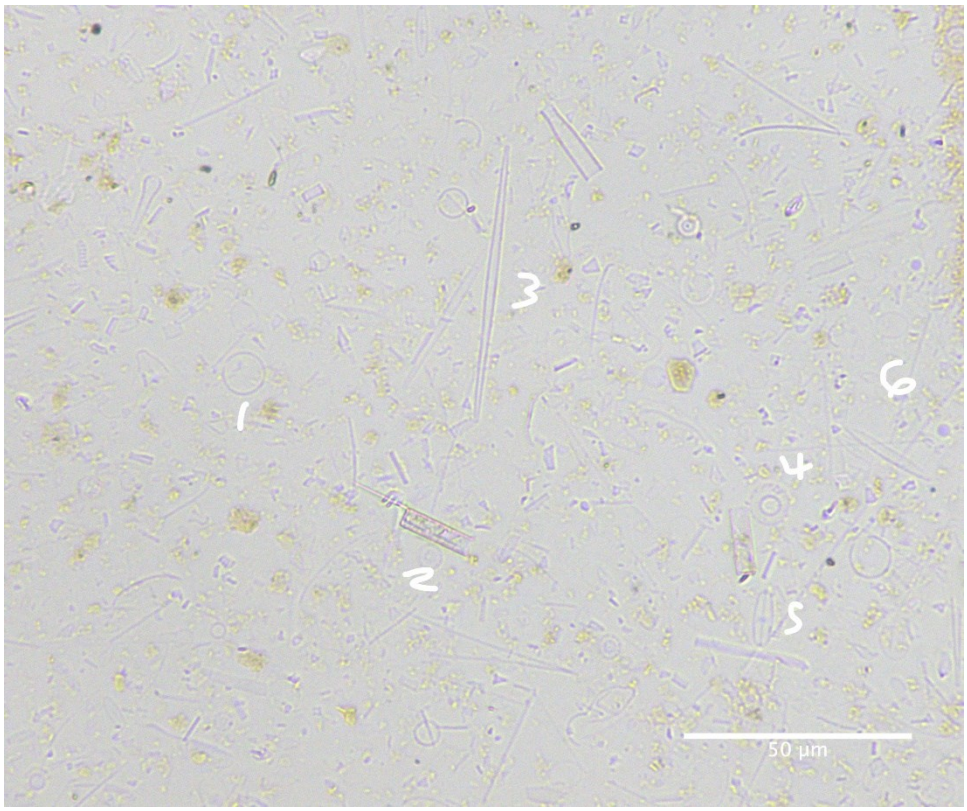


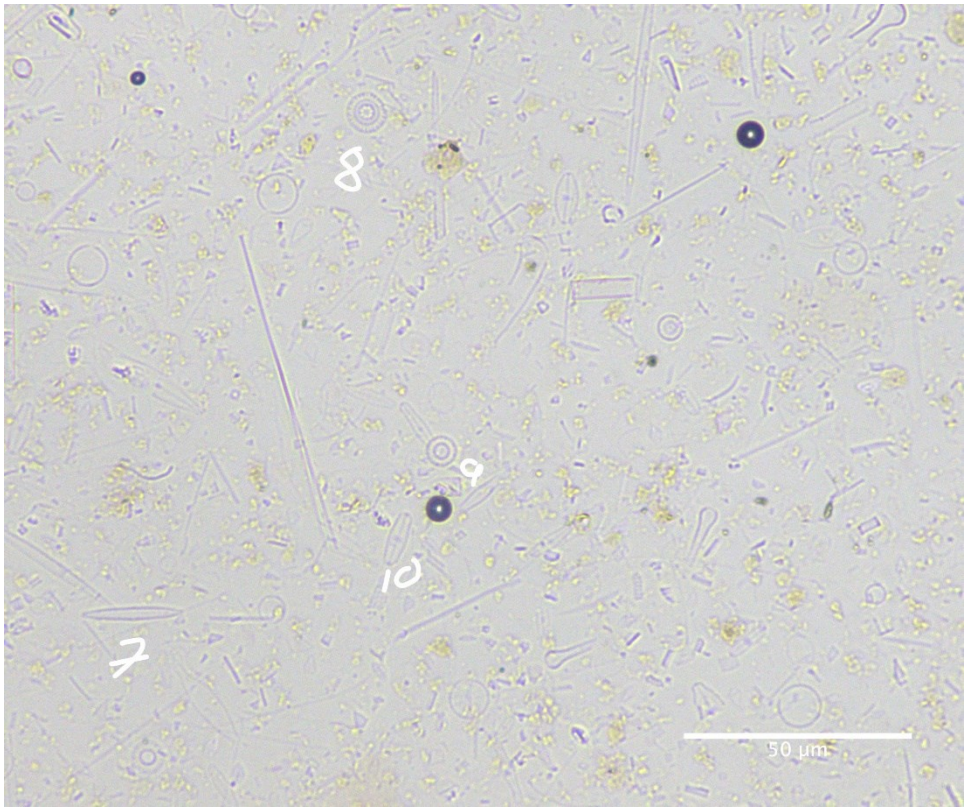

Sediment-water Interface

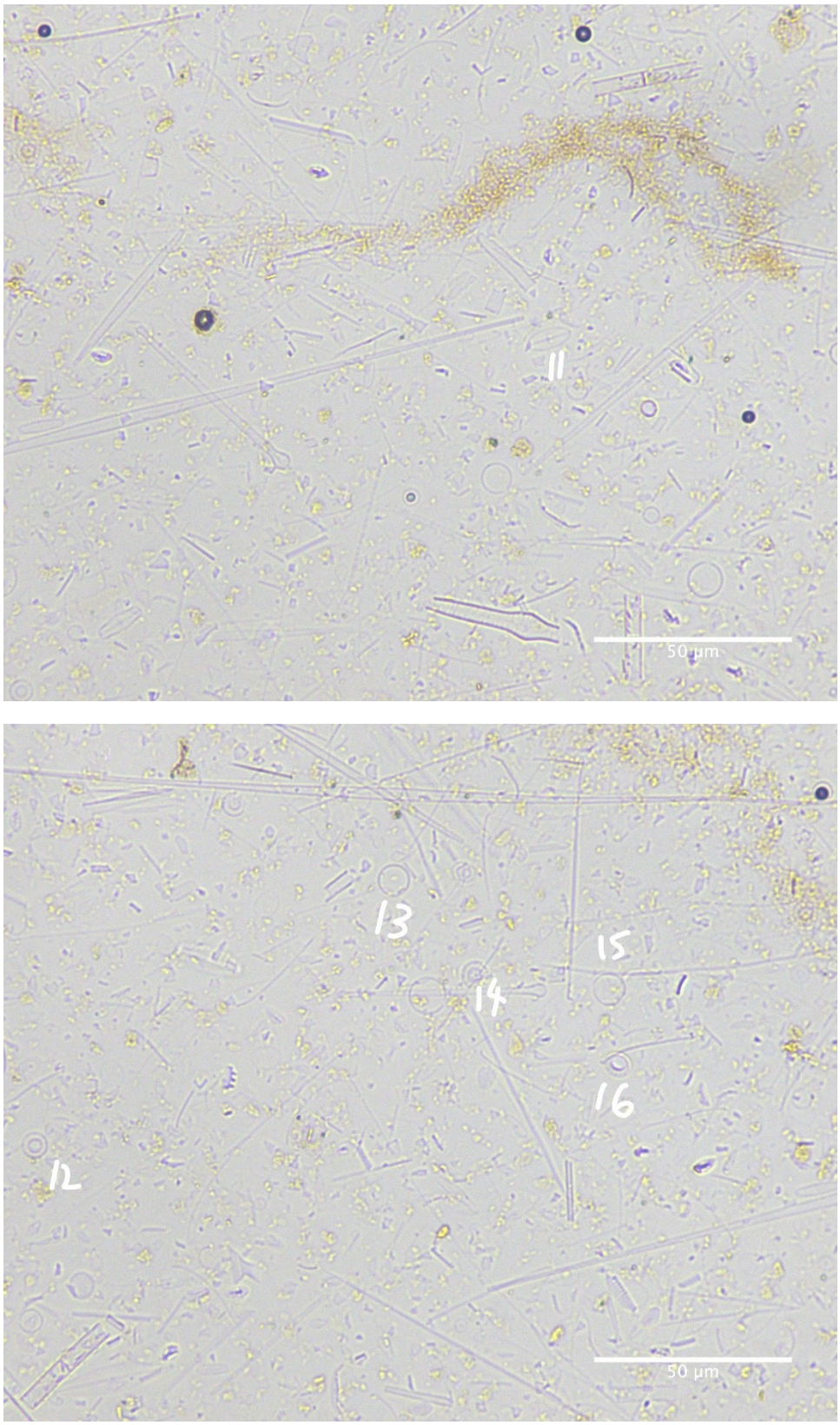

Sediment-water Interface

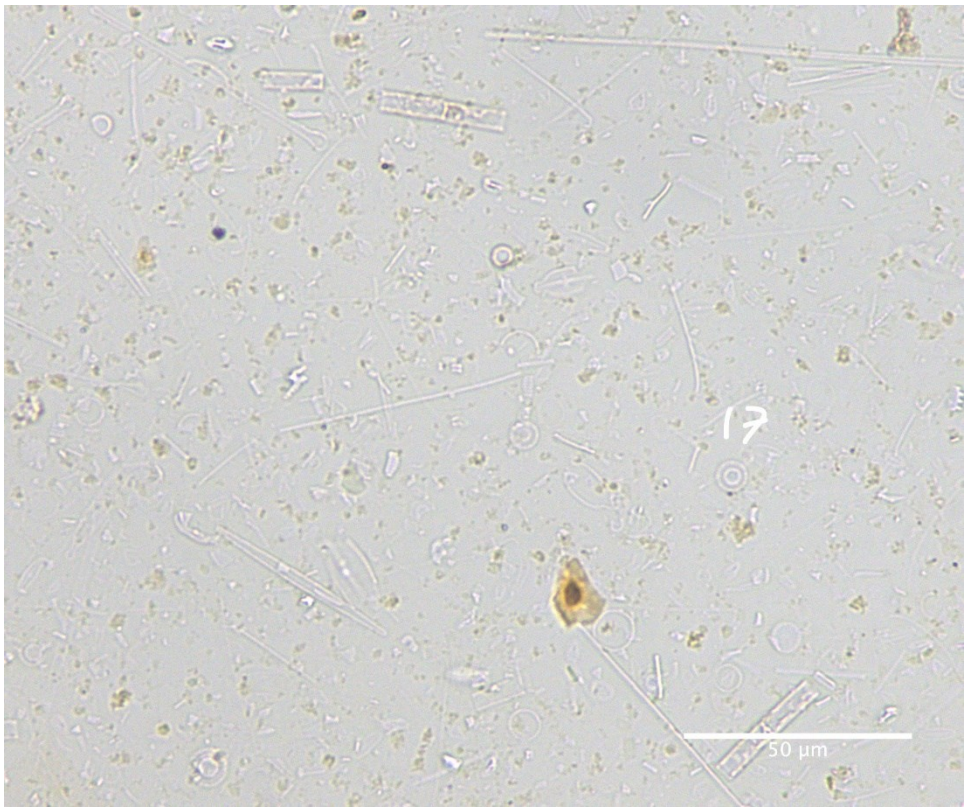


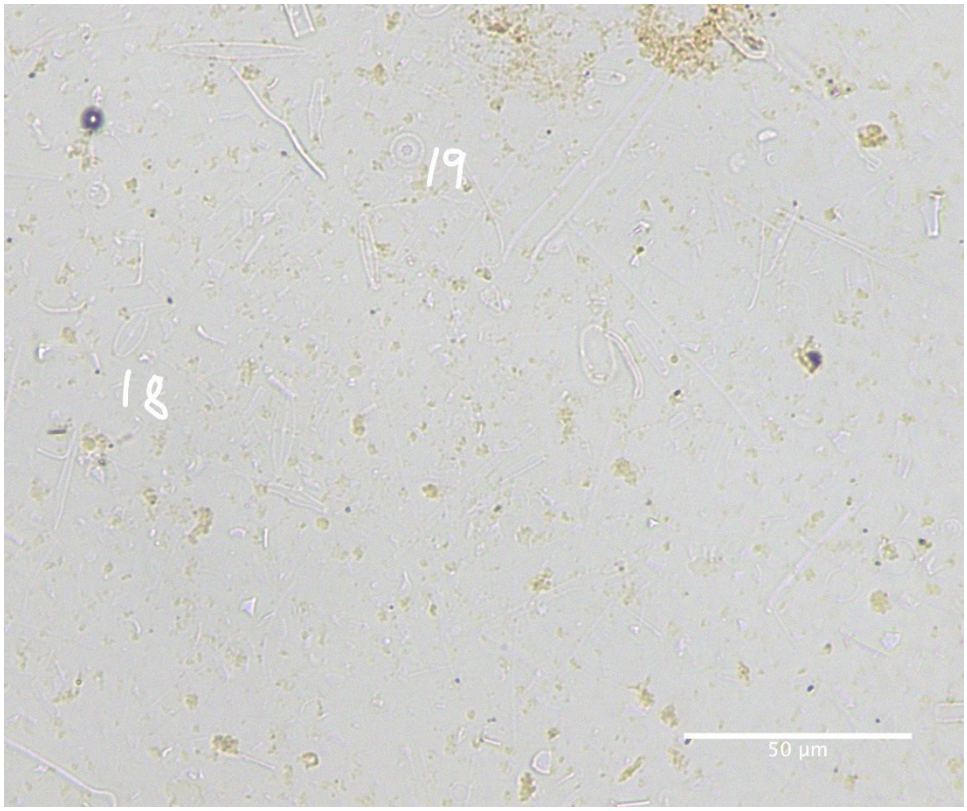

Sediment-water Interface

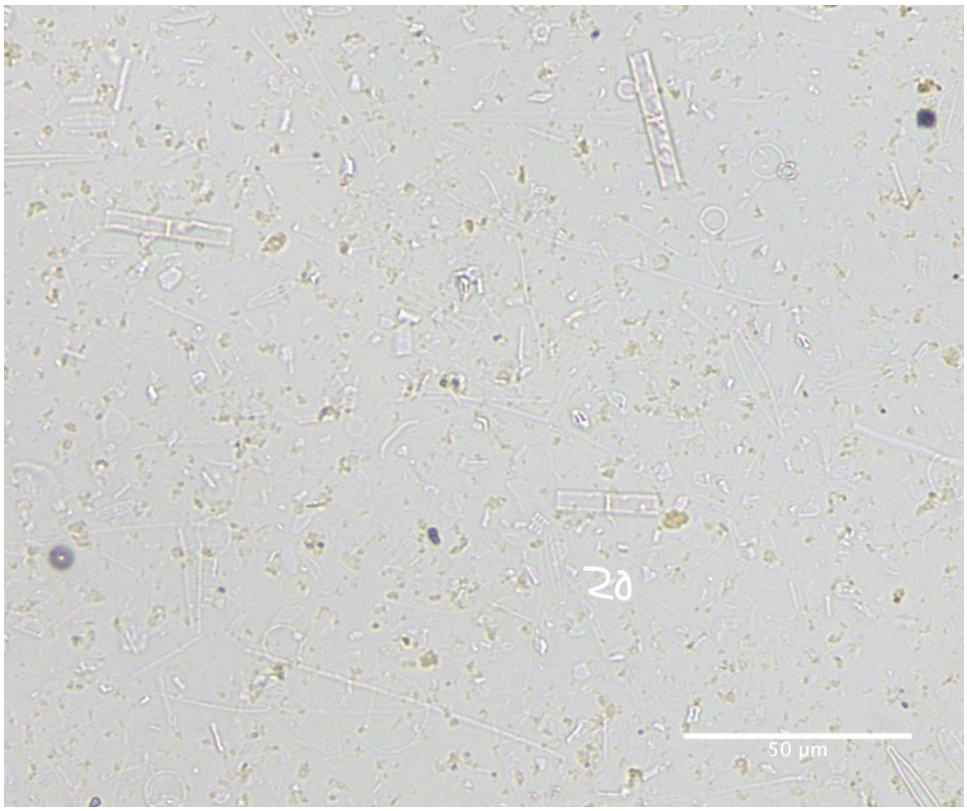


| Diatom ID | Taxon | Diatom ID | Taxon |
|---|---|---|---|
| 1 | *Thalassiosira* sp. | 11 | *Navicula* sp. |
| 2 | *Cyclotella* sp. | 12 | *Cyclotella* sp. |
| 3 | *Fragilaria* sp. | 13 | *Thalassiosira* sp. |
| 4 | *Cyclotella* sp. | 14 | *Cyclotella* sp. |
| 5 | *Navicula* sp. | 15 | *Thalassiosira* sp. |
| 6 | *Nitzschia* sp. | 16 | *Cyclotella* sp. |
| 7 | *Nitzschia* sp. | 17 | *Cyclotella* sp. |
| 8 | *Cyclotella* sp. | 18 | *Navicula* sp. |
| 9 | *Cyclotella* sp. | 19 | *Cyclotella* sp. |
| 10 | *Navicula* sp. | 20 | *Navicula* sp. |

0-5 cm downcore

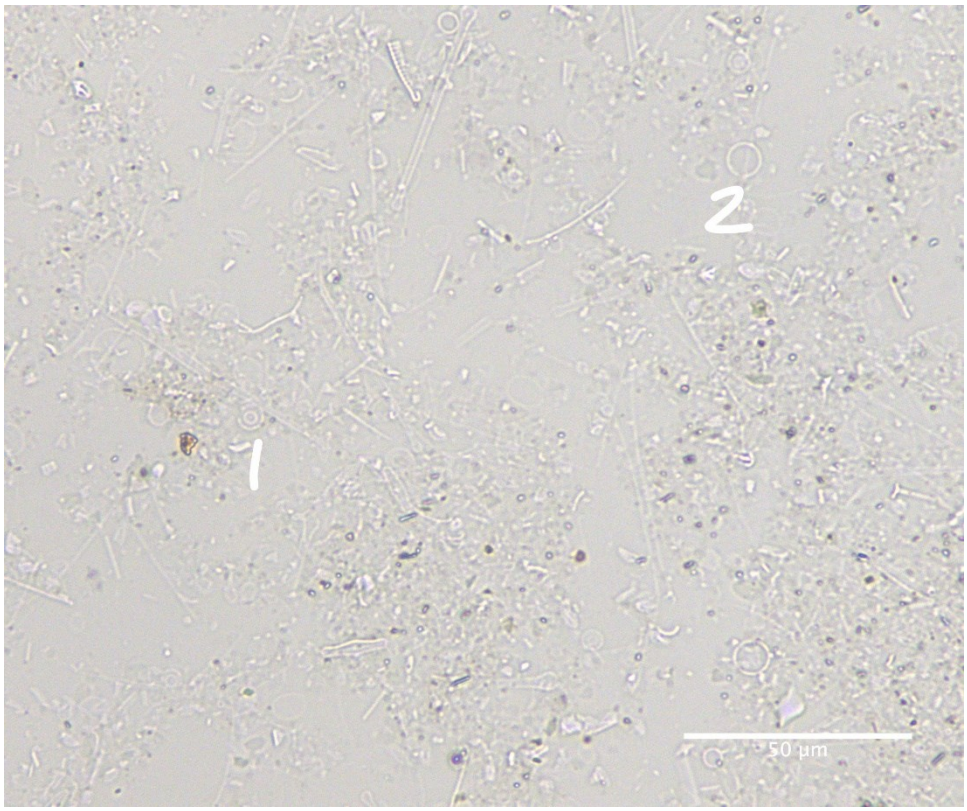


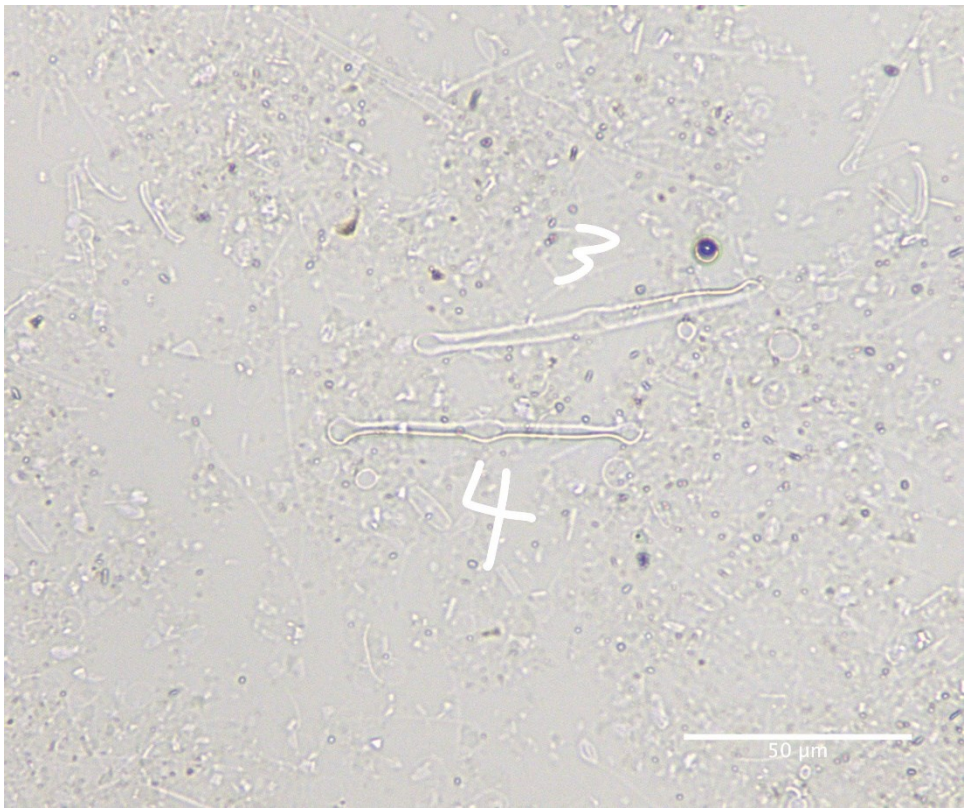

0-5 cm downcore

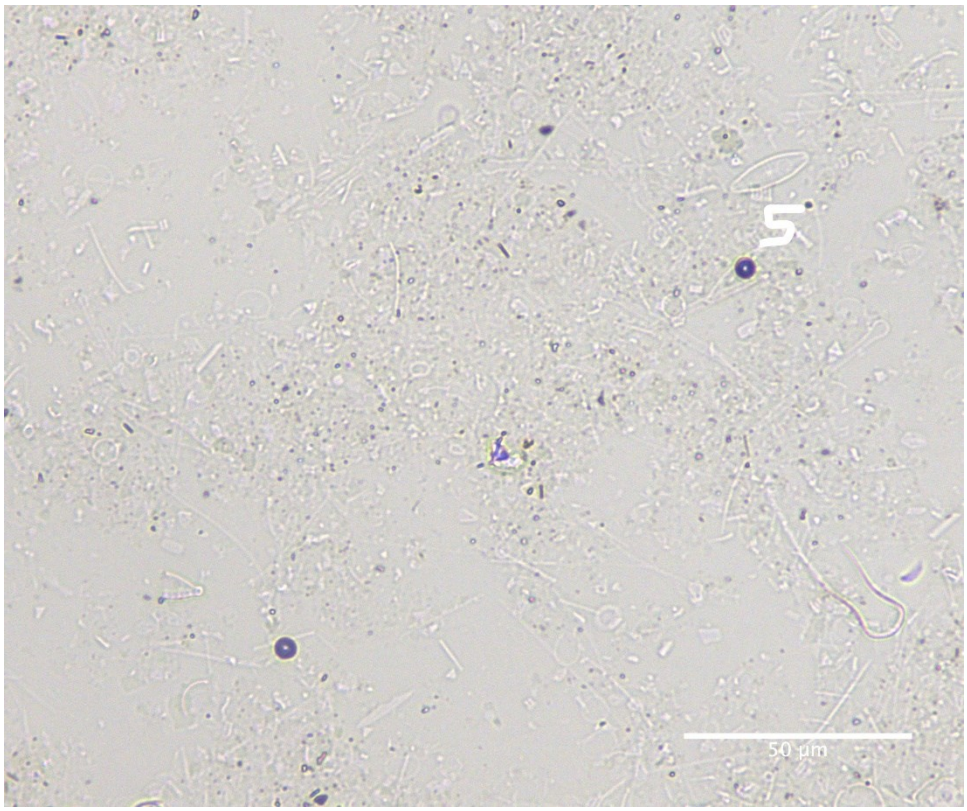


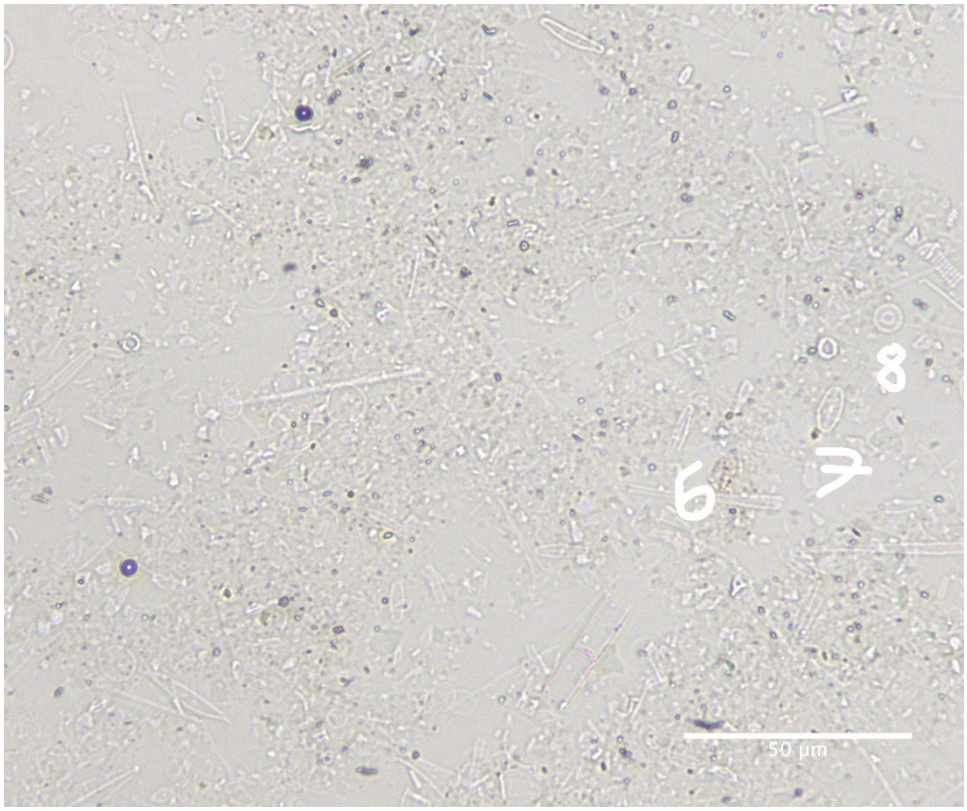

0-5 cm downcore

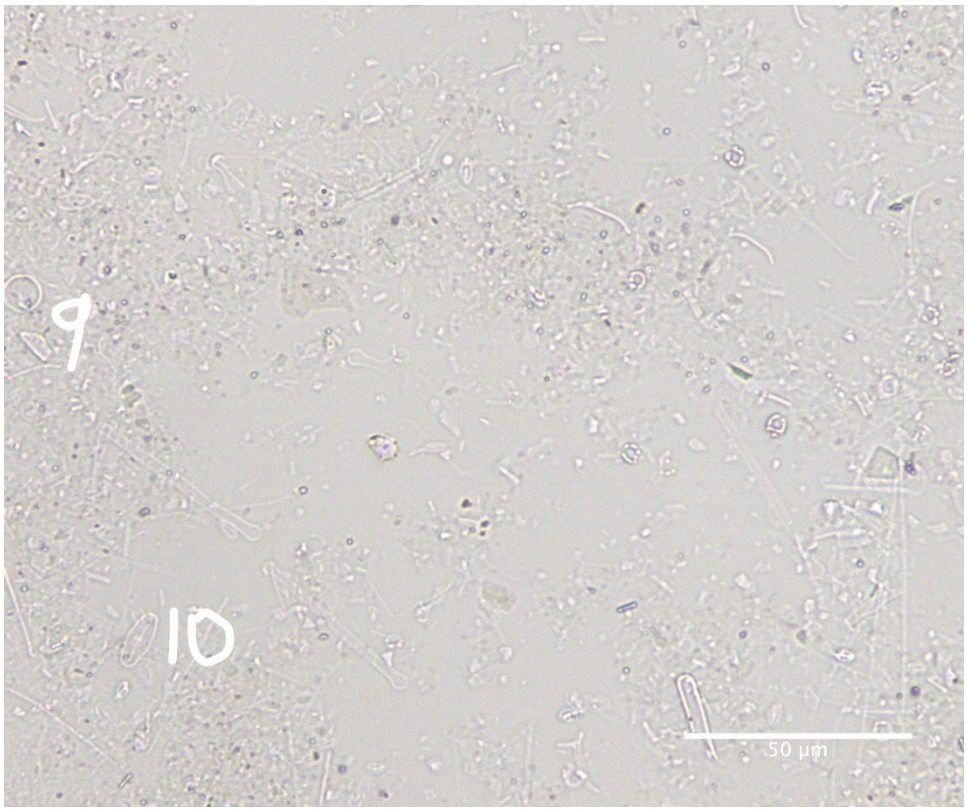


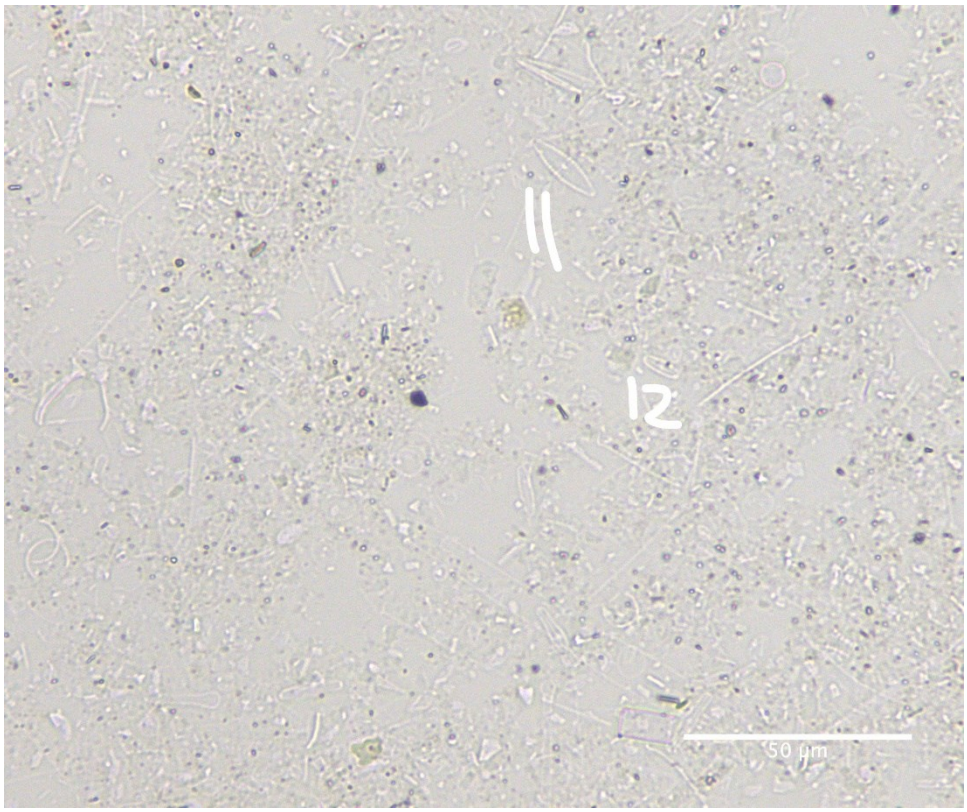

0-5 cm downcore

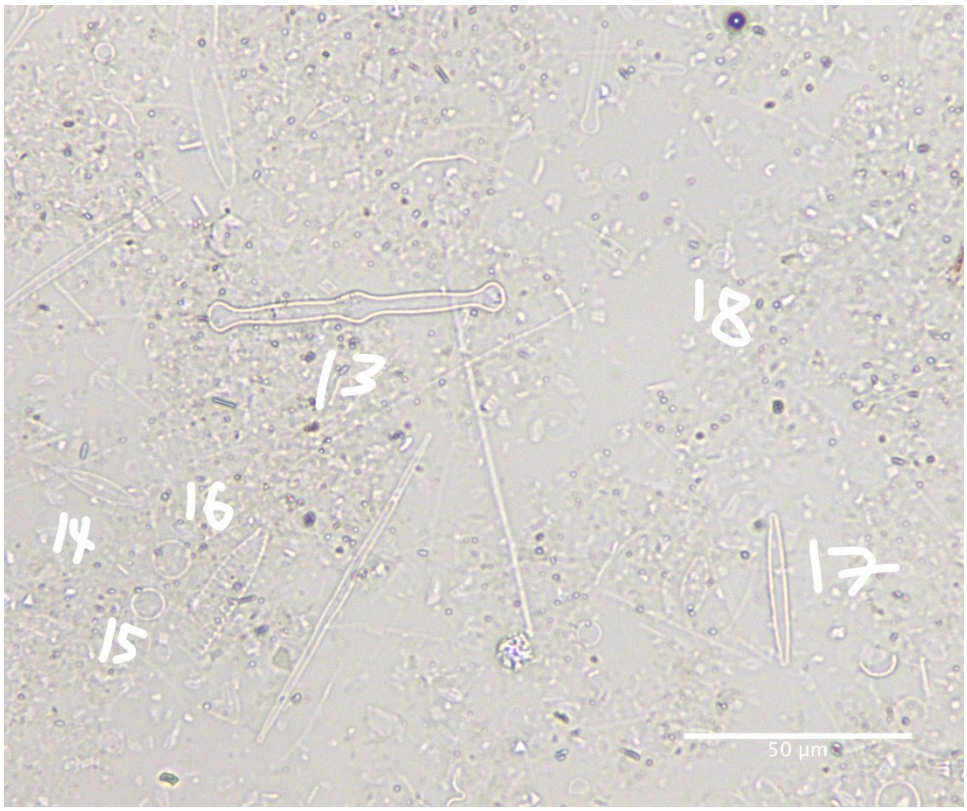


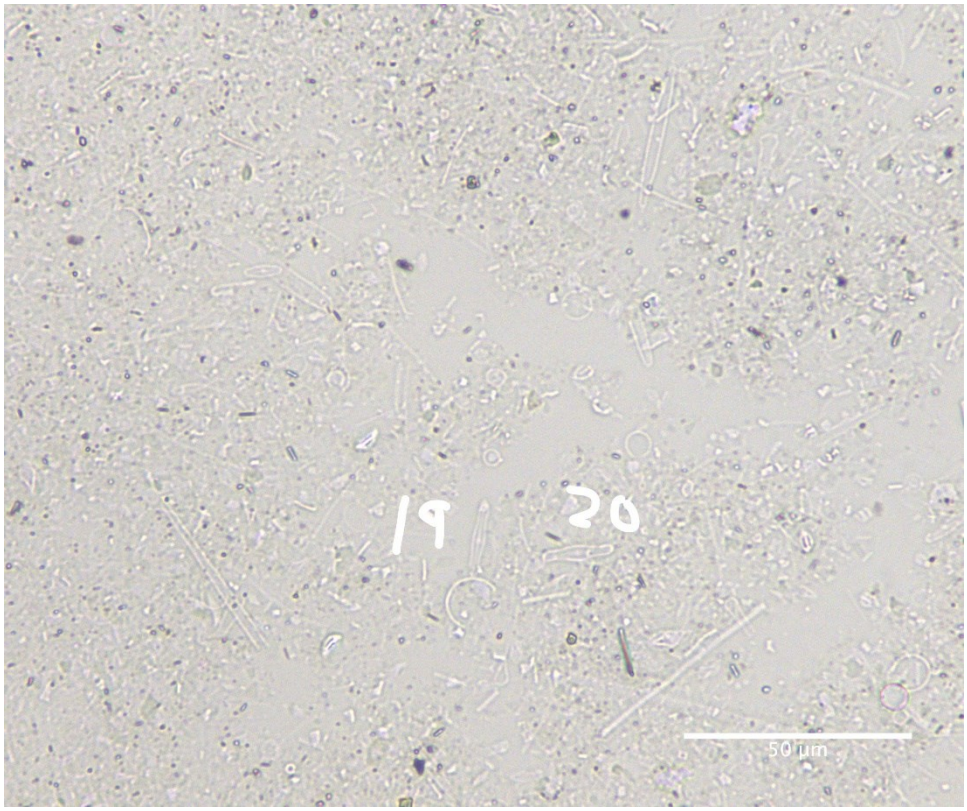

0-5 cm downcore

| Diatom ID | Taxon | Diatom ID | Taxon |
|---|---|---|---|
| 1 | *Cyclotella* sp. | 11 | *Gomphonema* sp. |
| 2 | *Thalassiosira* sp. | 12 | *Achnanthidium* sp. |
| 3 | *Tabellaria* sp. | 13 | *Tabellaria* sp. |
| 4 | *Tabellaria* sp. | 14 | *Navicula* sp. |
| 5 | *Gomphonema* sp. | 15 | *Thalassiosira* sp. |
| 6 | *Achnanthidium* sp. | 16 | *Thalassiosira* sp. |
| 7 | *Navicula* sp. | 17 | *Fragilaria* sp. |
| 8 | *Cyclotella* sp. | 18 | *Cyclotella* sp. |
| 9 | *Thalassiosira* sp. | 19 | *Achnanthidium* sp. |
| 10 | *Navicula* sp. | 20 | *Achnanthidium* sp. |

5-10 cm downcore

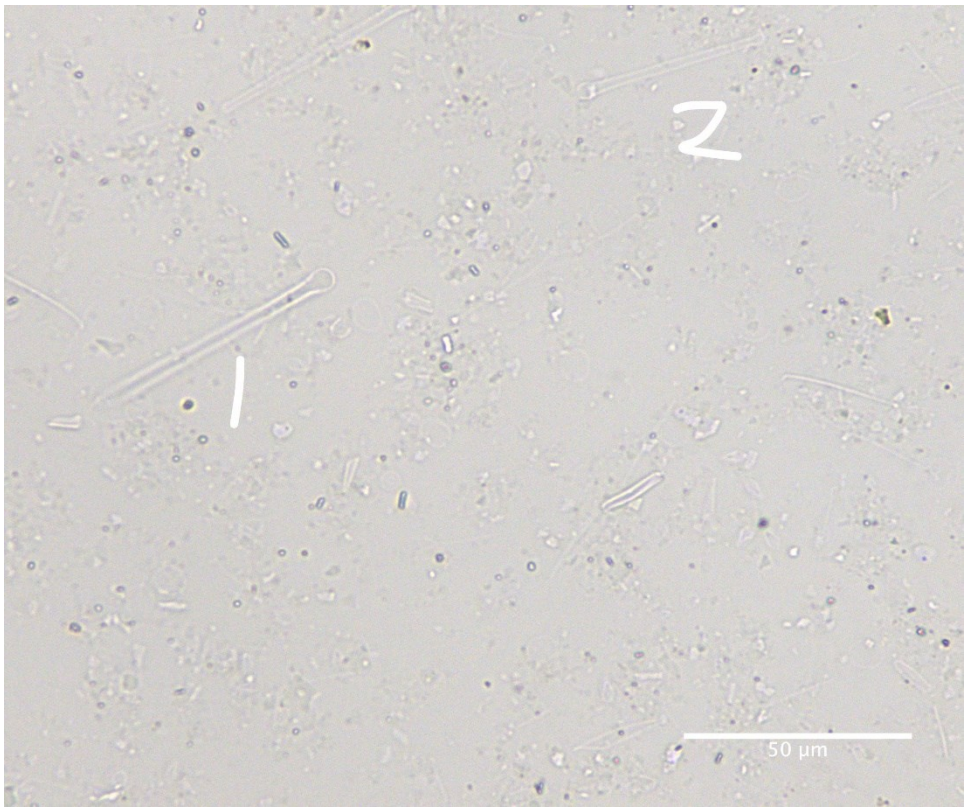


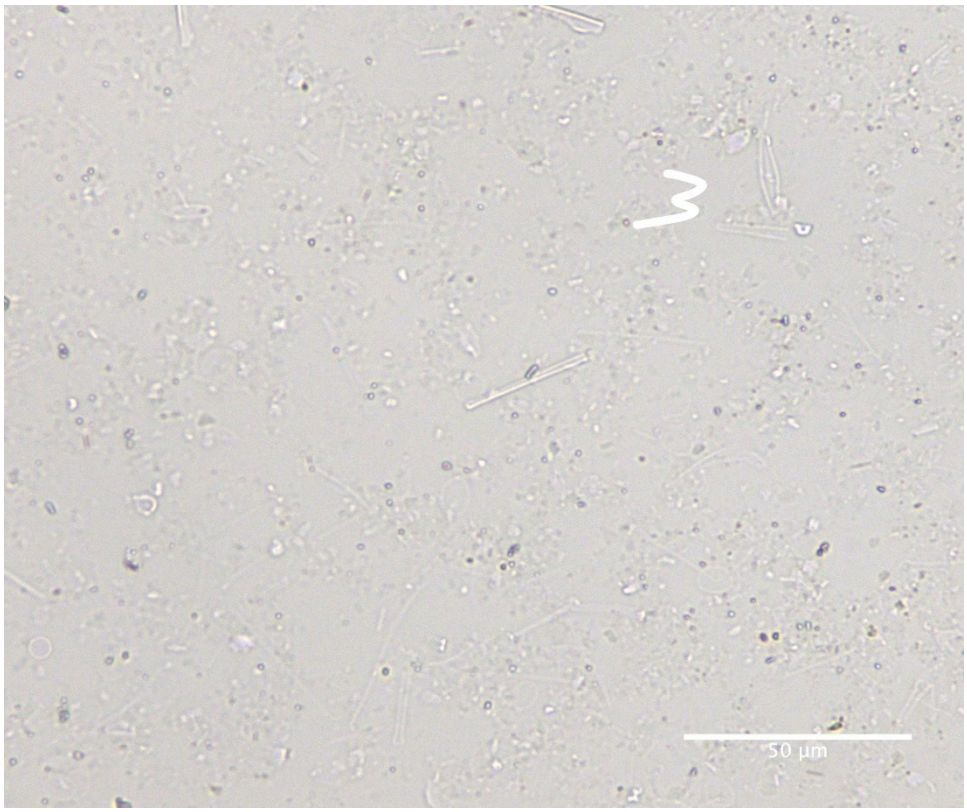

5-10 cm downcore

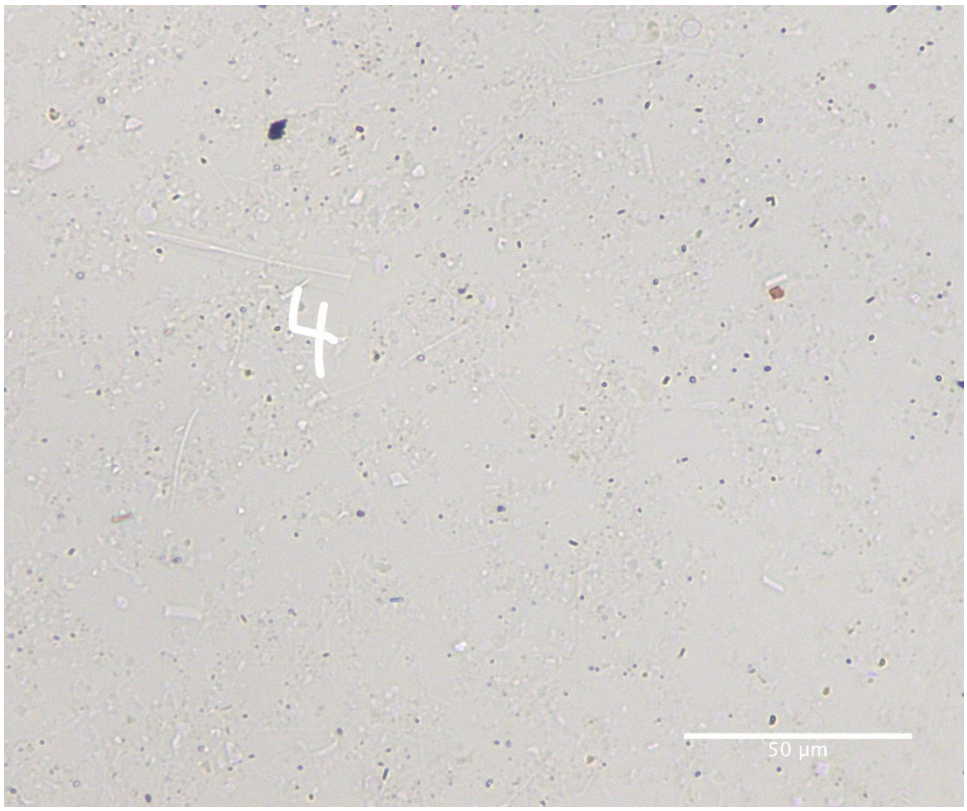


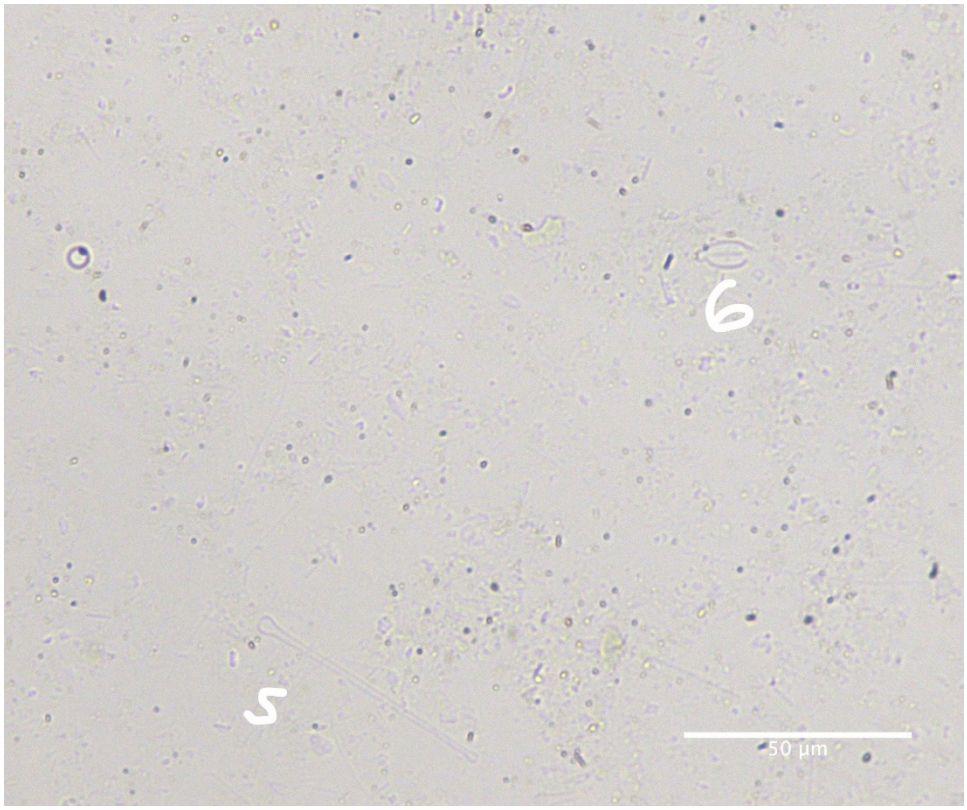

5-10 cm downcore

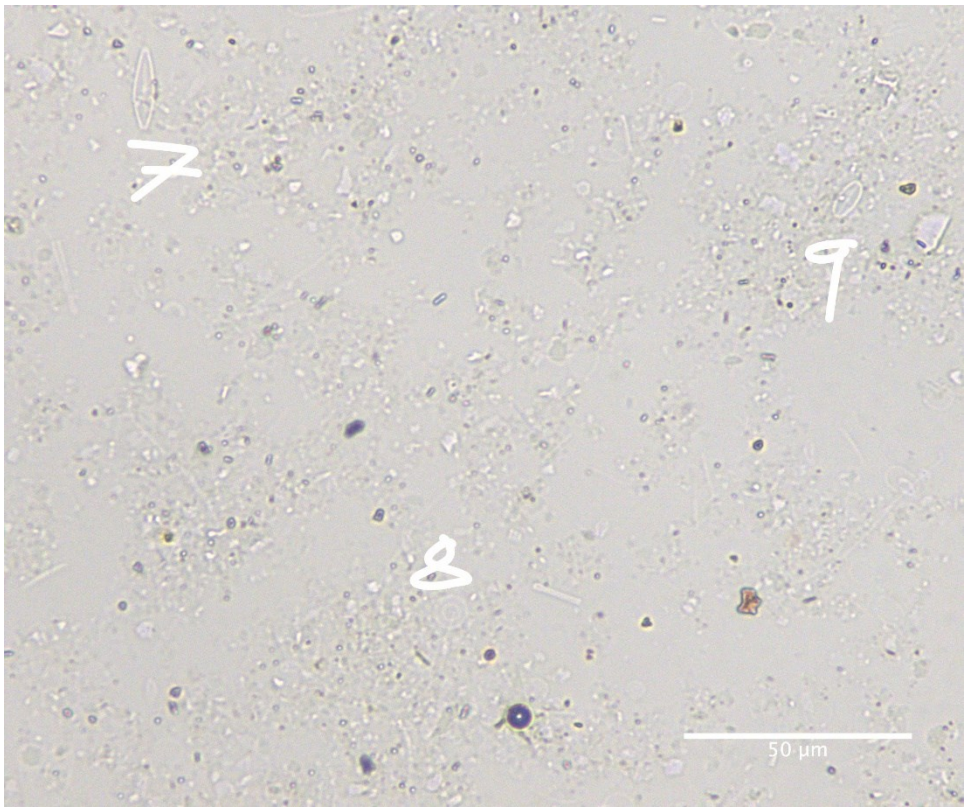


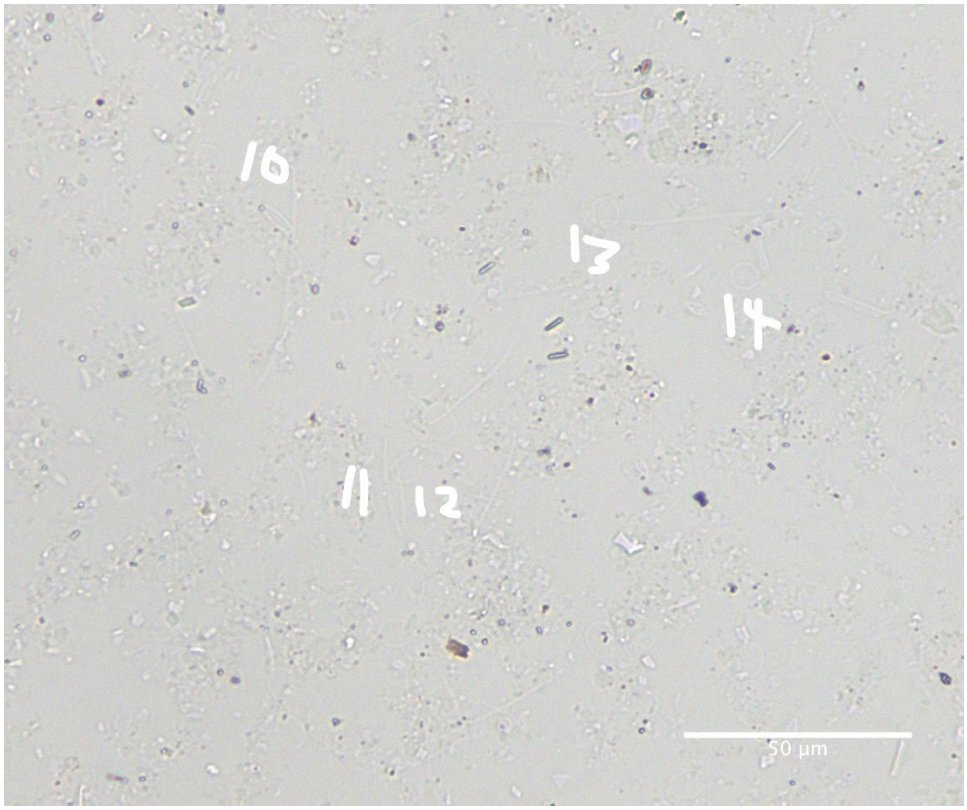

5-10 cm downcore

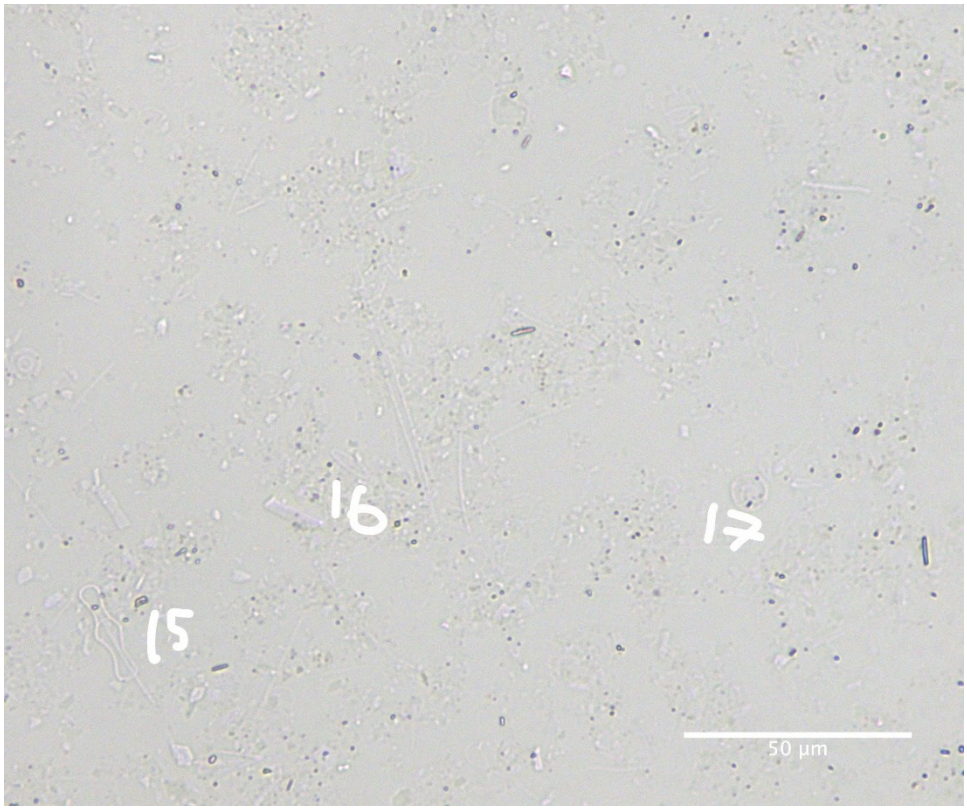


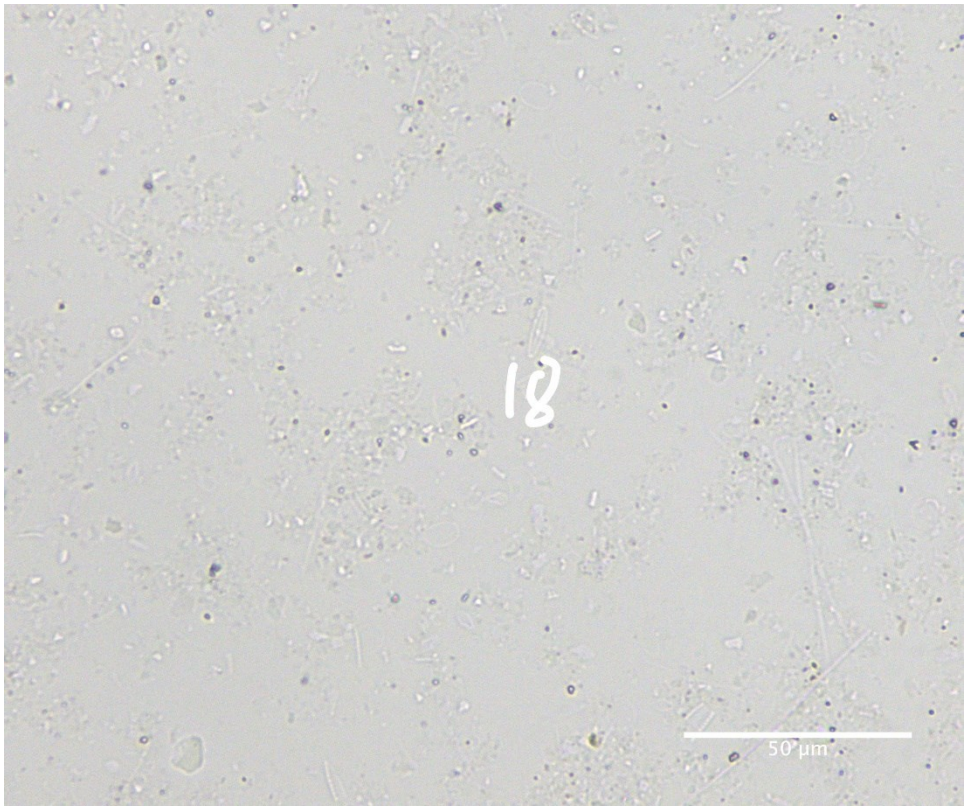

5-10 cm downcore

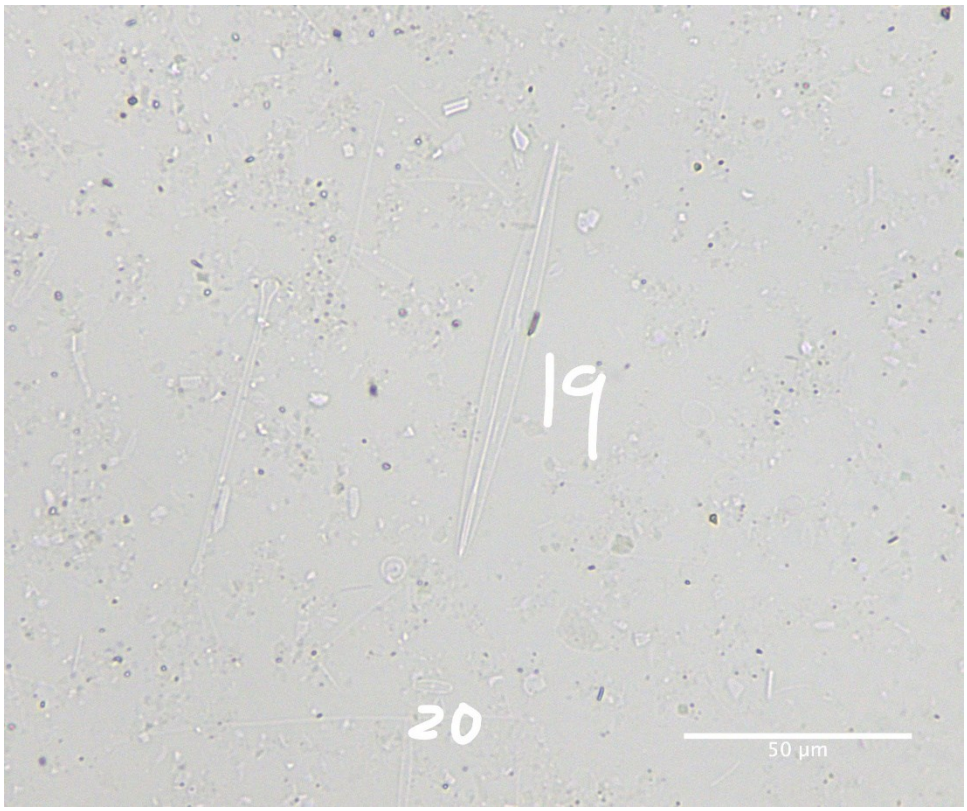


| Diatom ID | Taxon | Diatom ID | Taxon |
|---|---|---|---|
| 1 | *Asterionella* sp. | 11 | *Fragilaria* sp. |
| 2 | *Asterionella* sp. | 12 | *Thalassiosira* sp. |
| 3 | *Achnanthidium* sp. | 13 | *Thalassiosira* sp. |
| 4 | *Amphipleura* sp. | 14 | *Thalassiosira* sp. |
| 5 | *Asterionella* sp. | 15 | *Tabellaria* sp. |
| 6 | *Achnanthidium* sp. | 16 | *Achnanthidium* sp. |
| 7 | *Achnanthidium* sp. | 17 | *Thalassiosira* sp. |
| 8 | *Cyclotella* sp. | 18 | *Achnanthidium* sp. |
| 9 | *Achnanthidium* sp. | 19 | *Amphipleura* sp. |
| 10 | *Achnanthidium* sp. | 20 | *Achnanthidium* sp. |

10-15 cm downcore

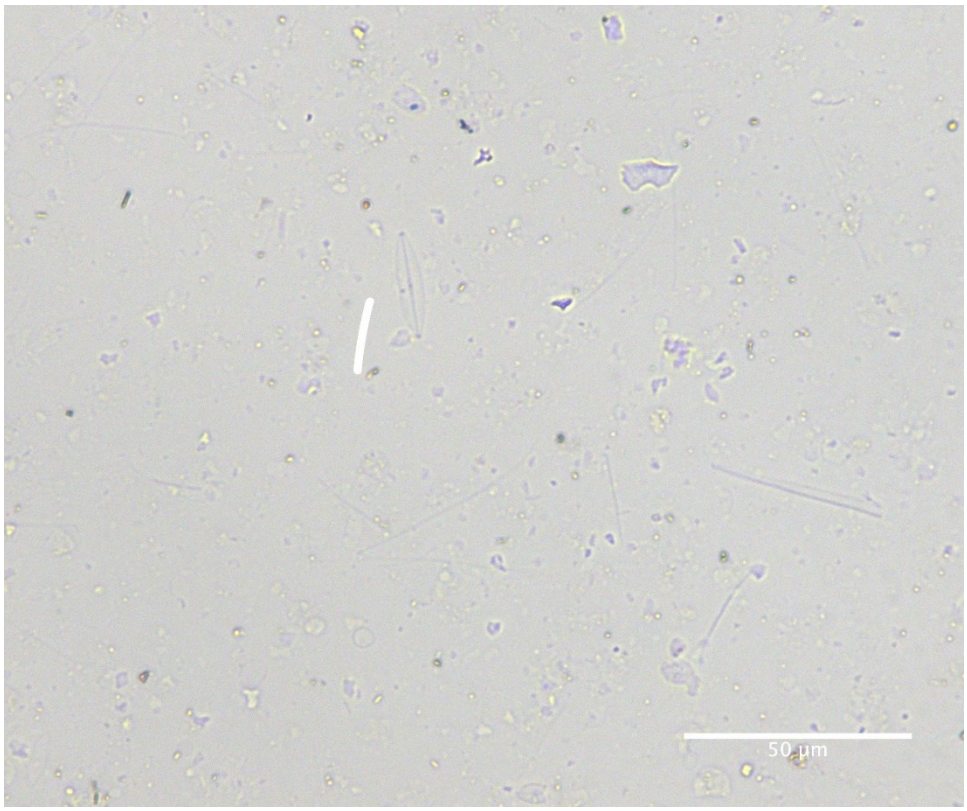


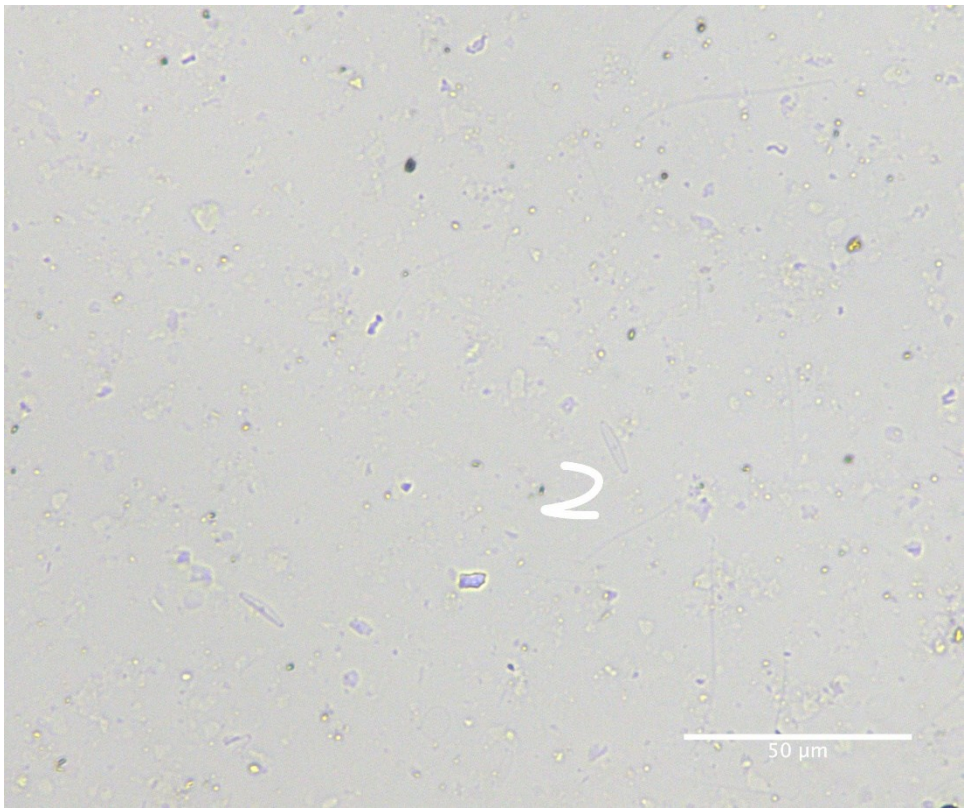

10-15 cm downcore

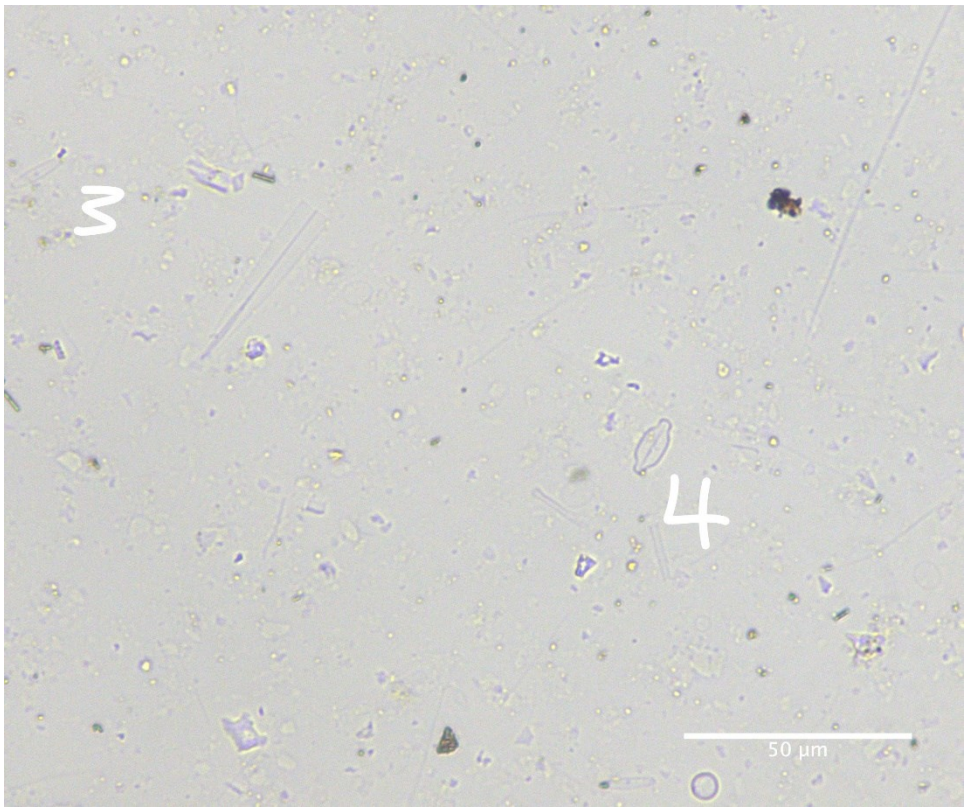


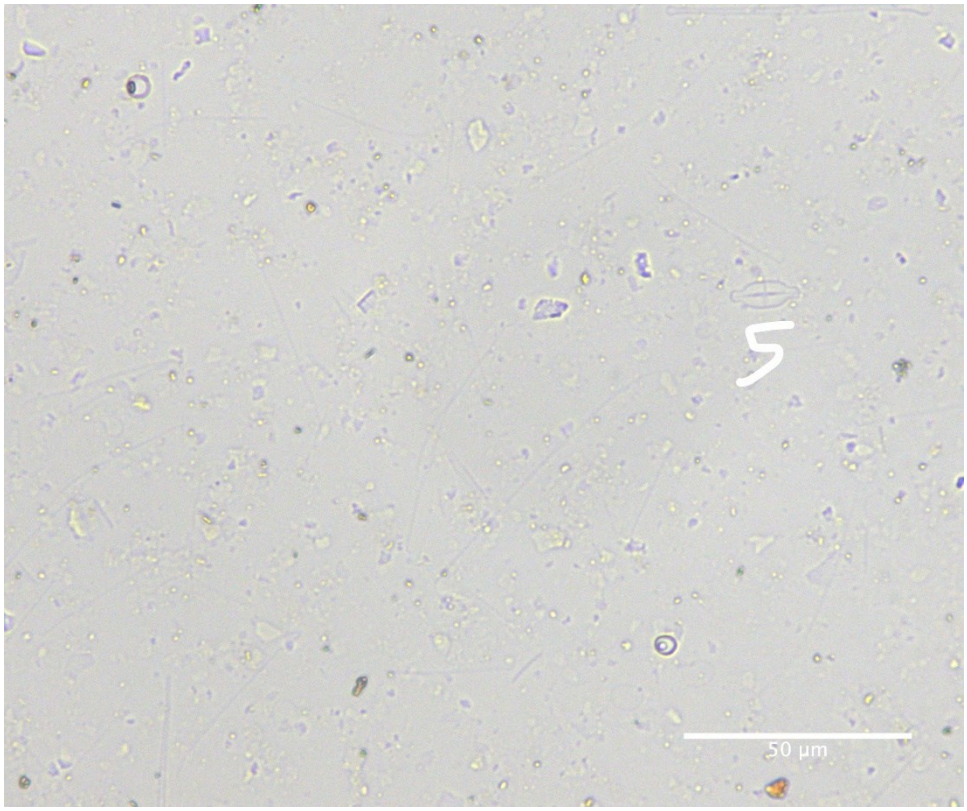

10-15 cm downcore

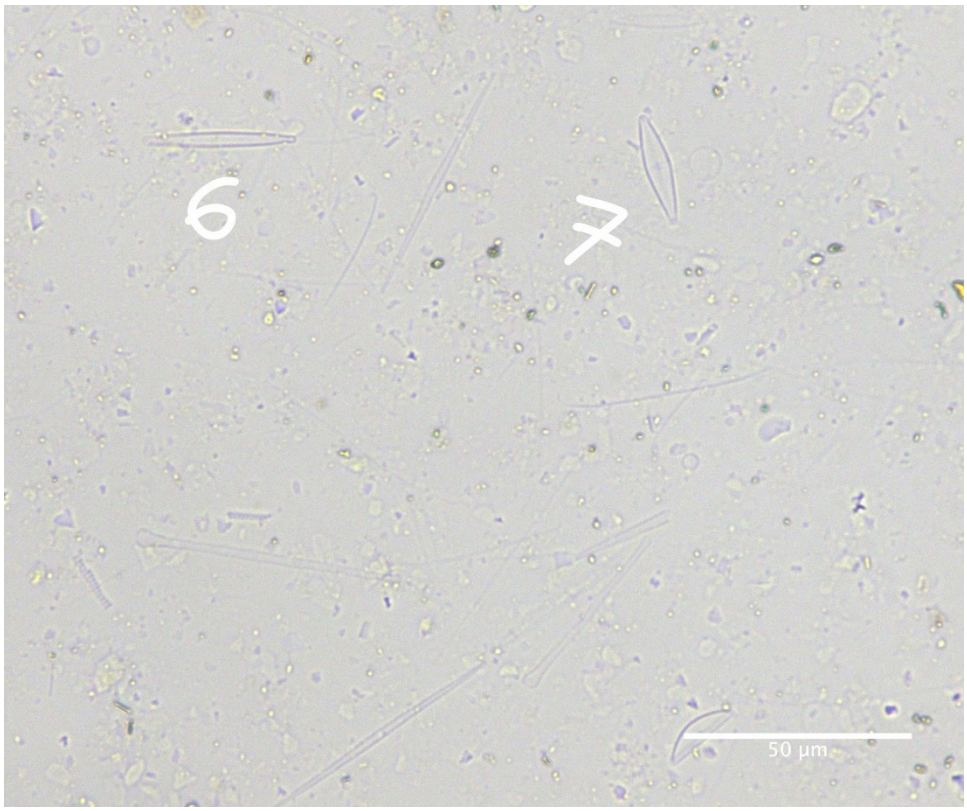


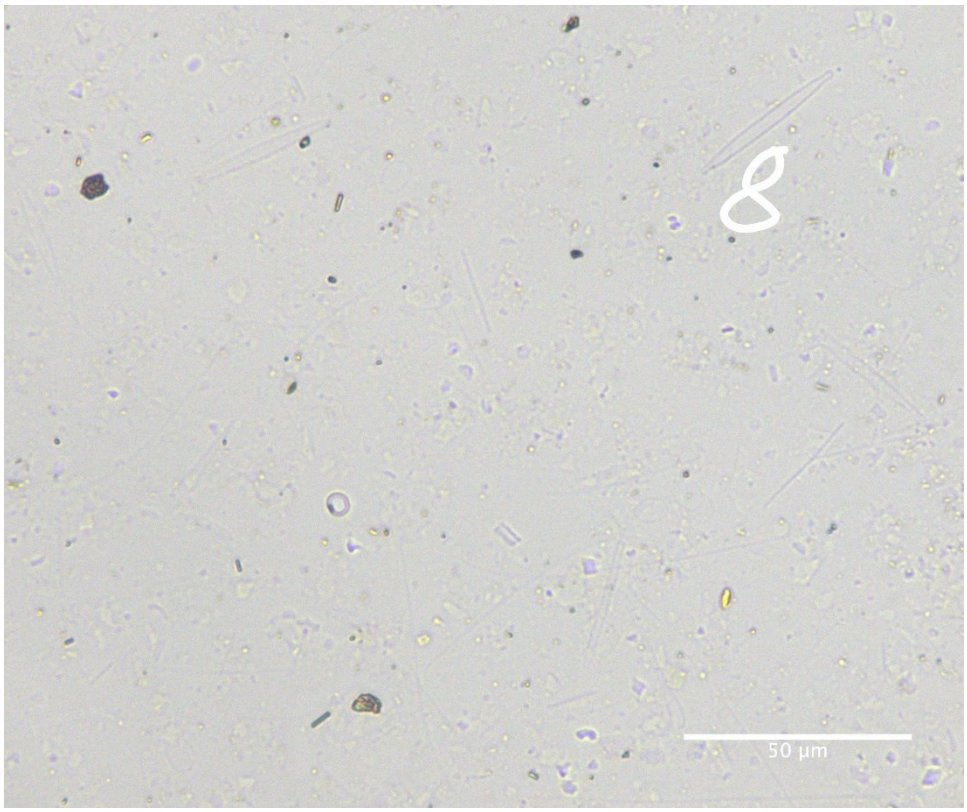

10-15 cm downcore

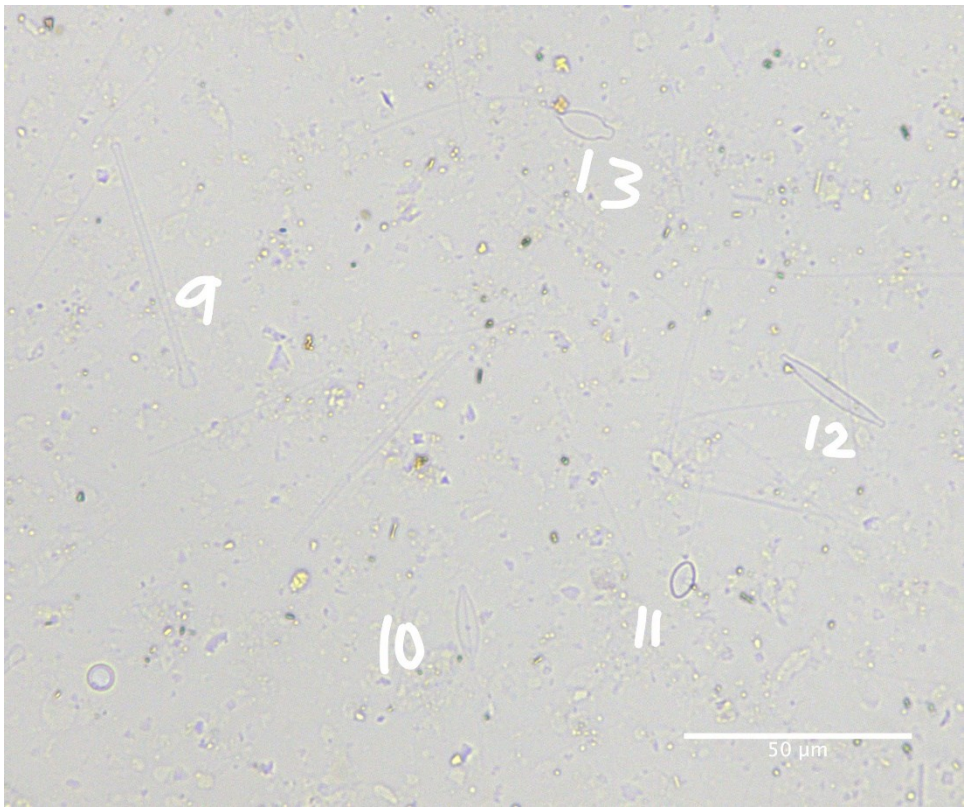


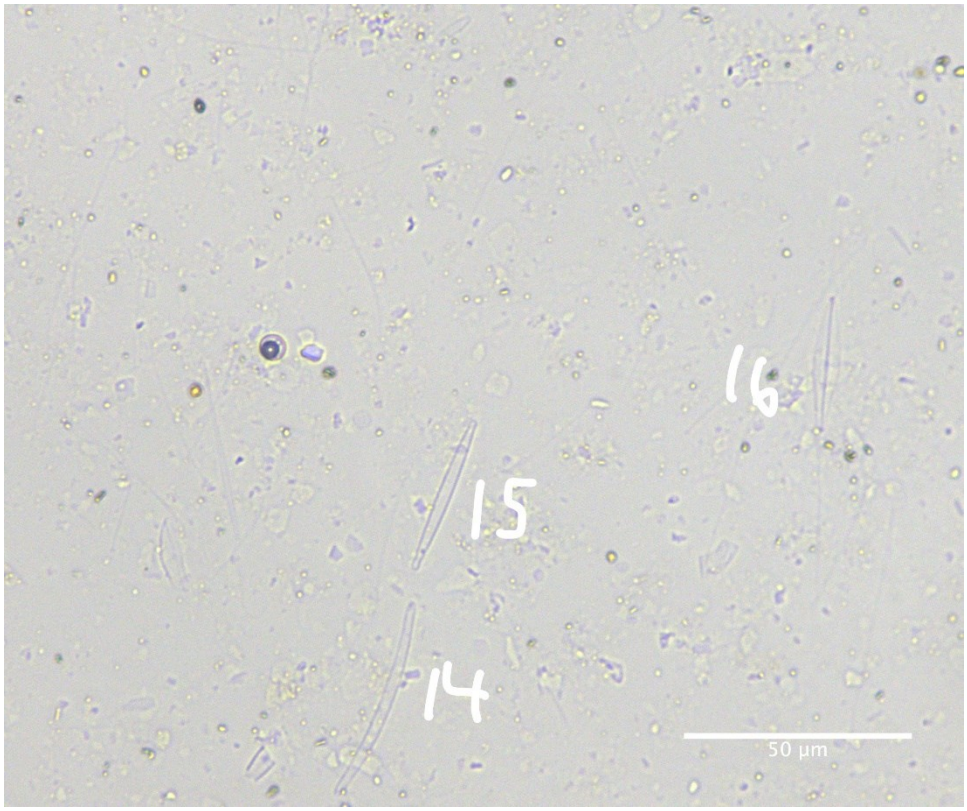

10-15 cm downcore

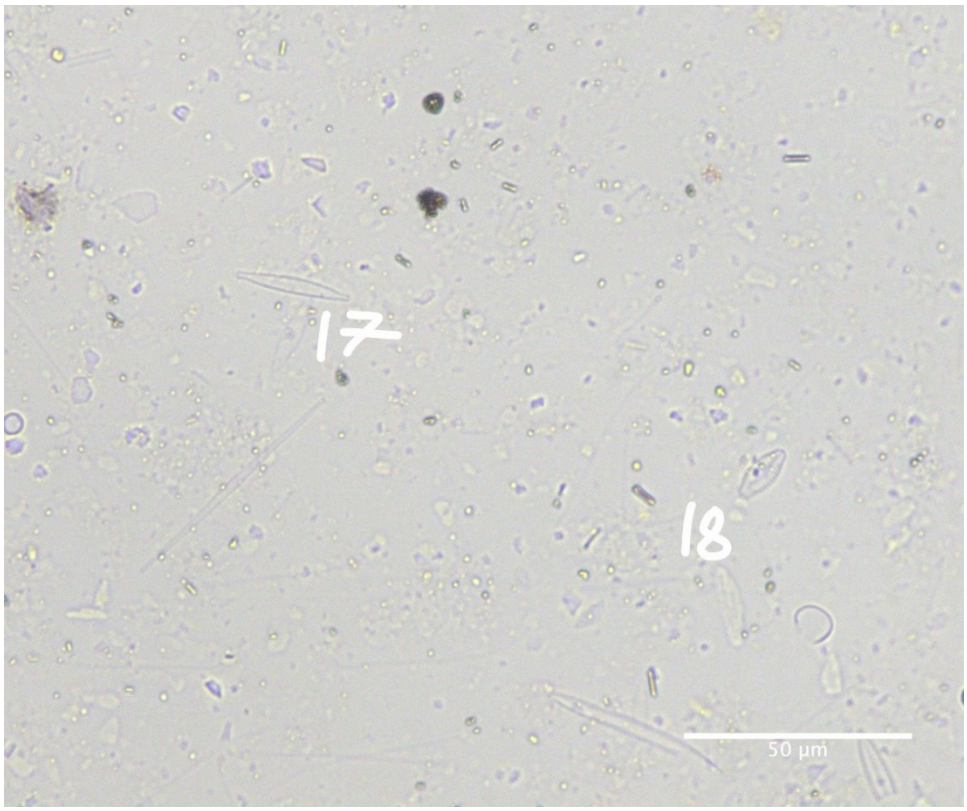


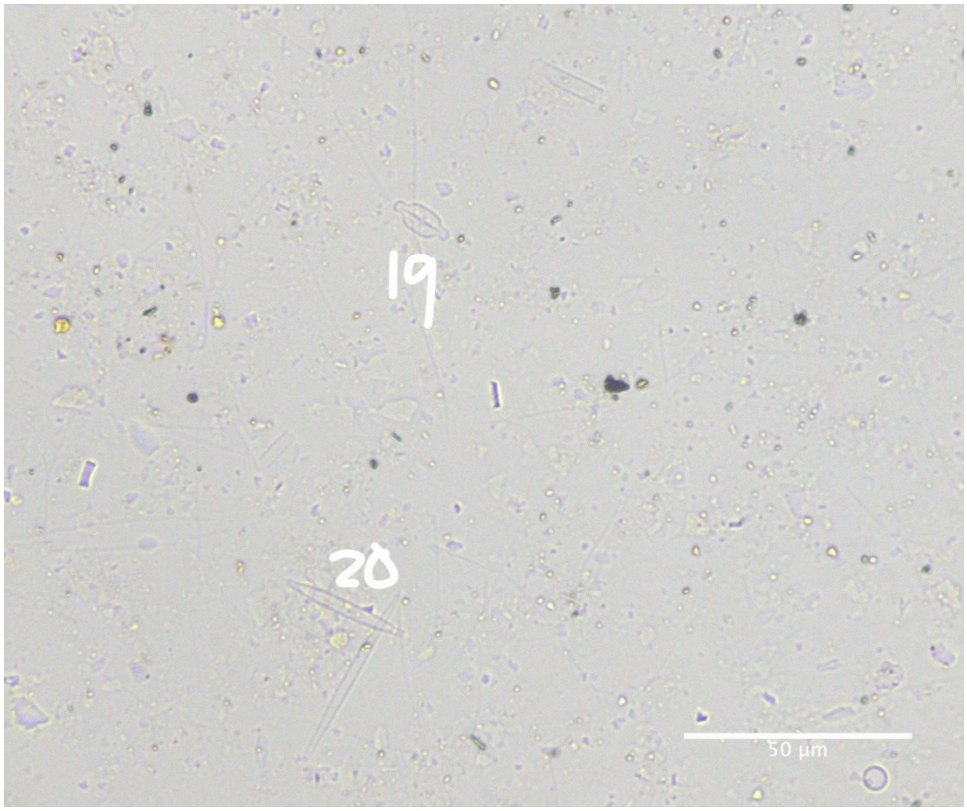

10-15 cm downcore

| Diatom ID | Taxon | Diatom ID | Taxon |
|---|---|---|---|
| 1 | *Navicula* sp. | 11 | *Achnanthidium* sp. |
| 2 | *Achnanthidium* sp. | 12 | *Fragilaria* sp. |
| 3 | *Achnanthidium* sp. | 13 | *Achnanthidium* sp. |
| 4 | *Achnanthidium* sp. | 14 | *Eunotia* sp. |
| 5 | *Achnanthidium* sp. | 15 | *Fragilaria* sp. |
| 6 | *Fragilaria* sp. | 16 | *Navicula* sp. |
| 7 | *Gomphonema* sp. | 17 | *Fragilaria* sp. |
| 8 | *Fragilaria* sp. | 18 | *Achnanthidium* sp. |
| 9 | *Asterionella* sp. | 19 | *Achnanthidium* sp. |
| 10 | *Navicula* sp. | 20 | *Fragilaria* sp. |

15-20 cm downcore

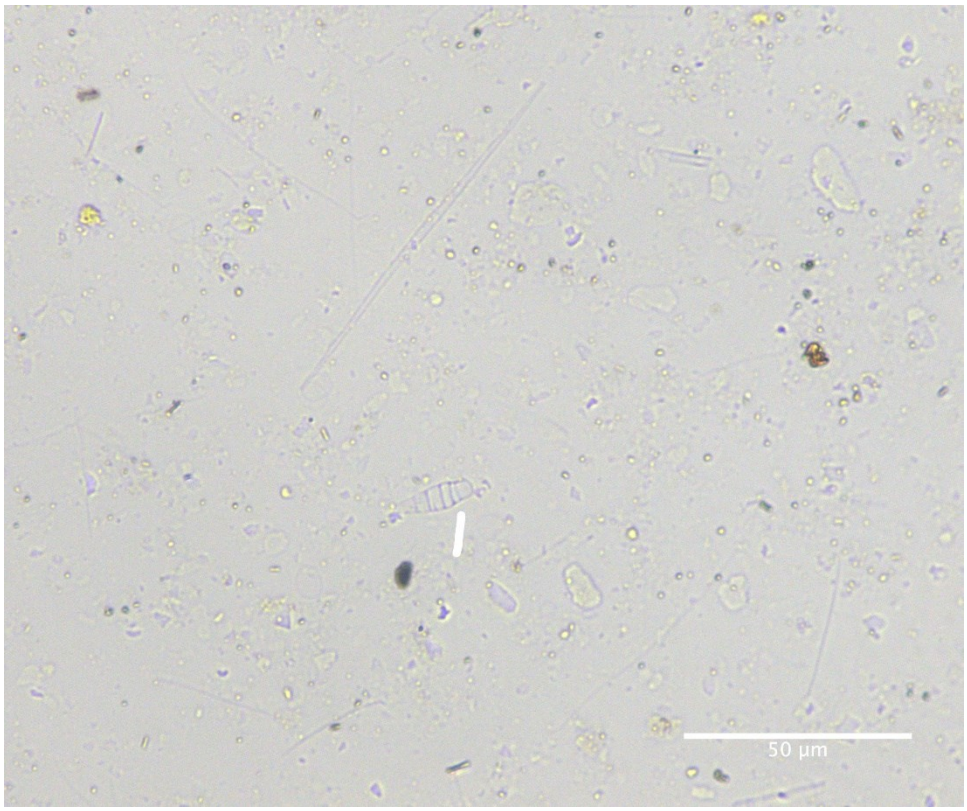


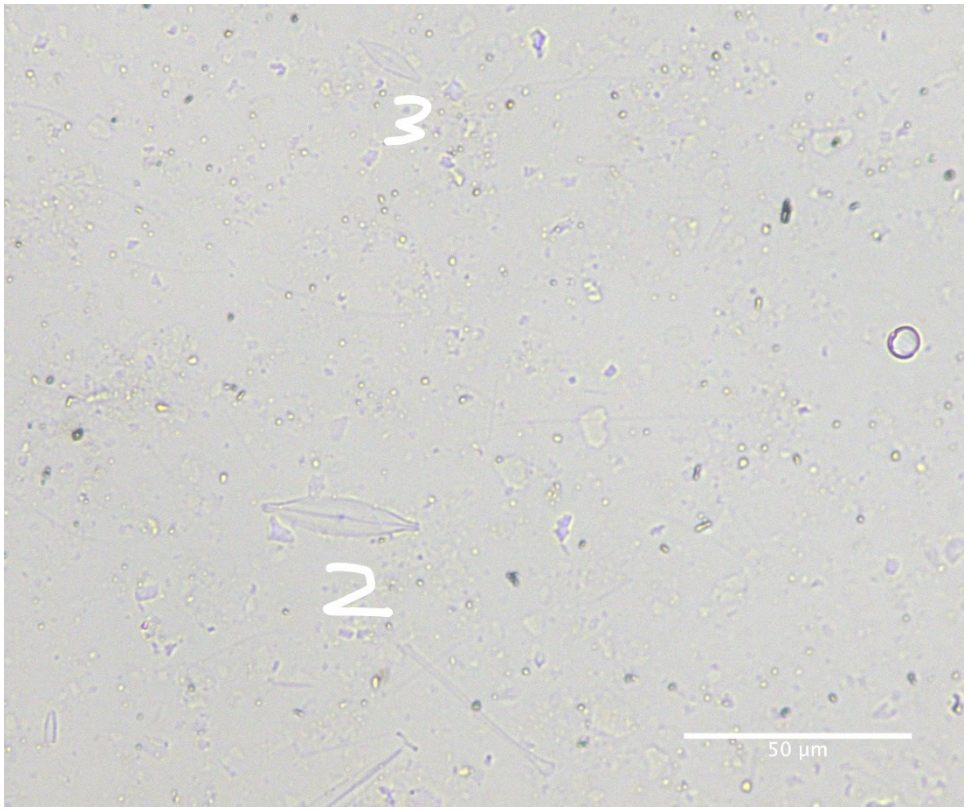

15-20 cm downcore

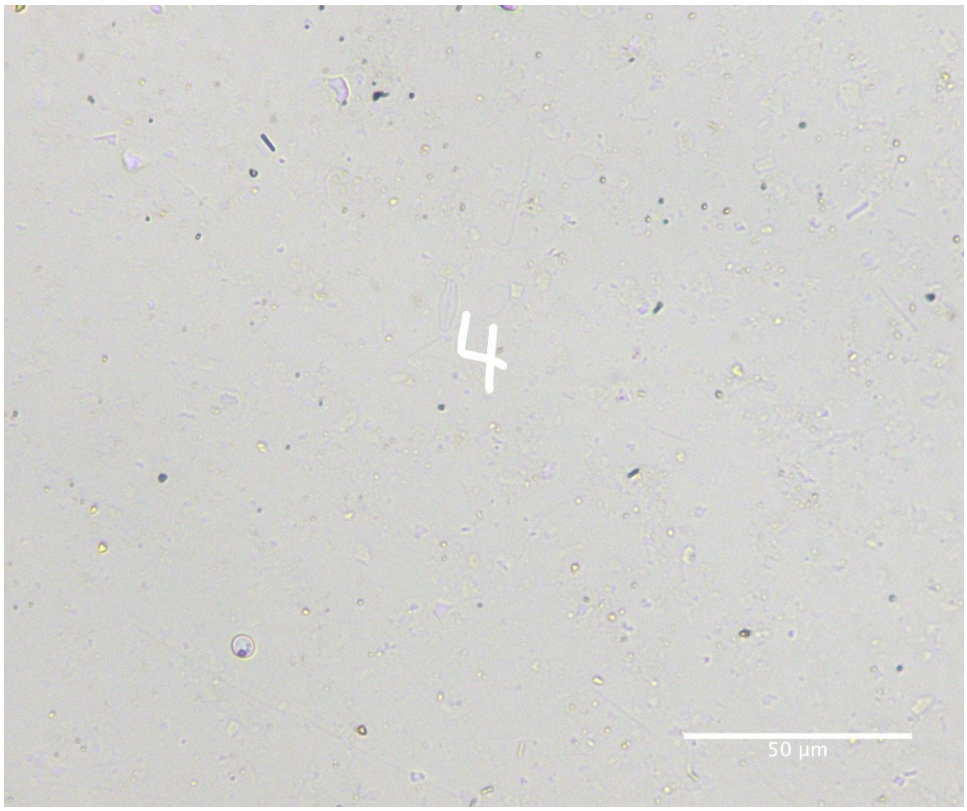


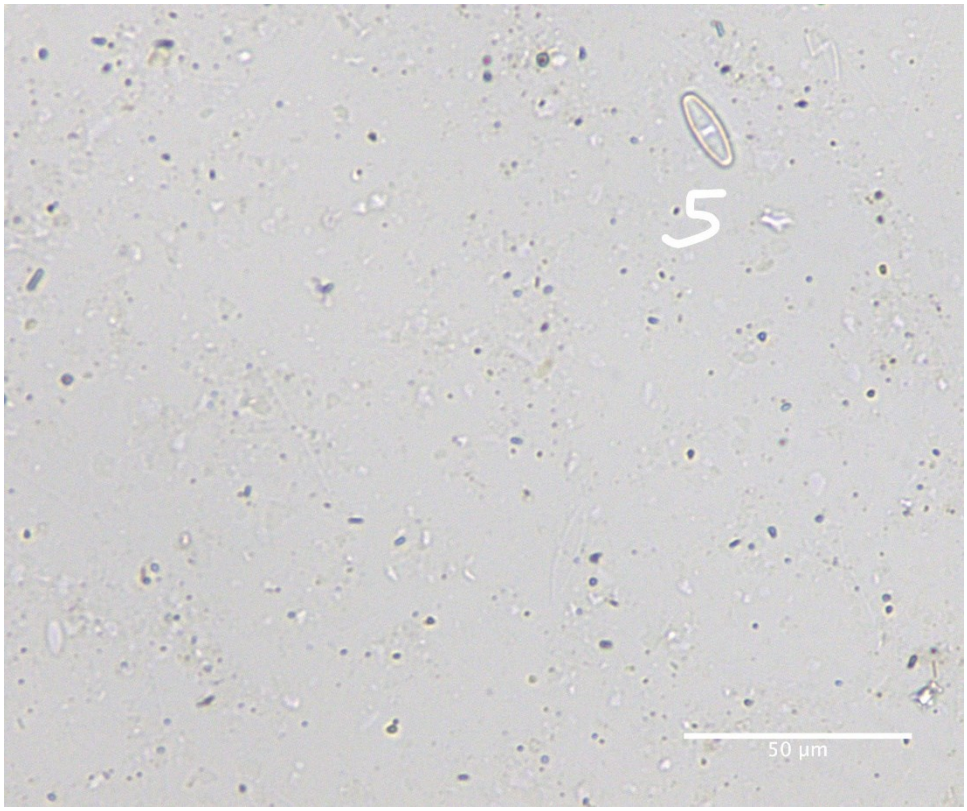

15-20 cm downcore

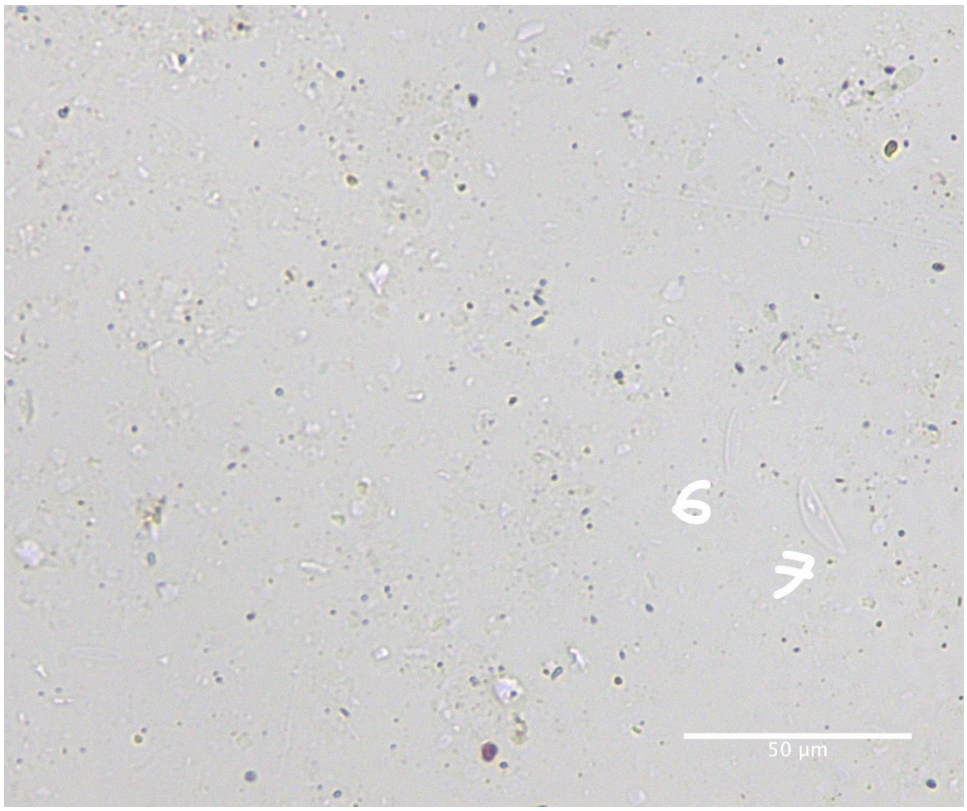


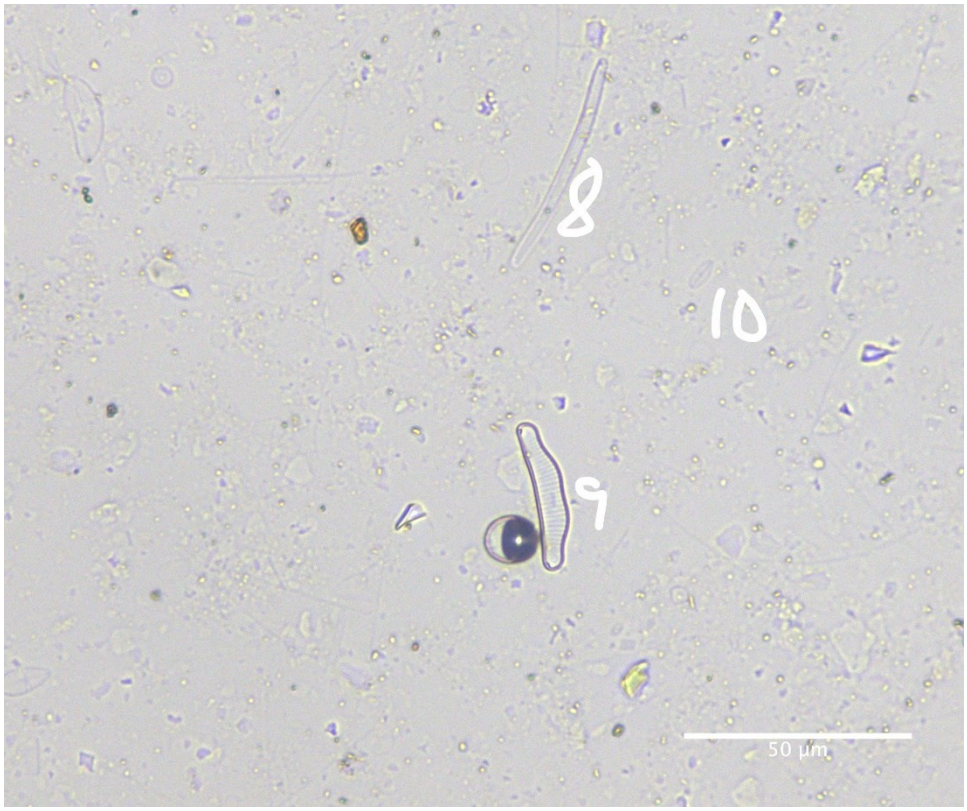

15-20 cm downcore

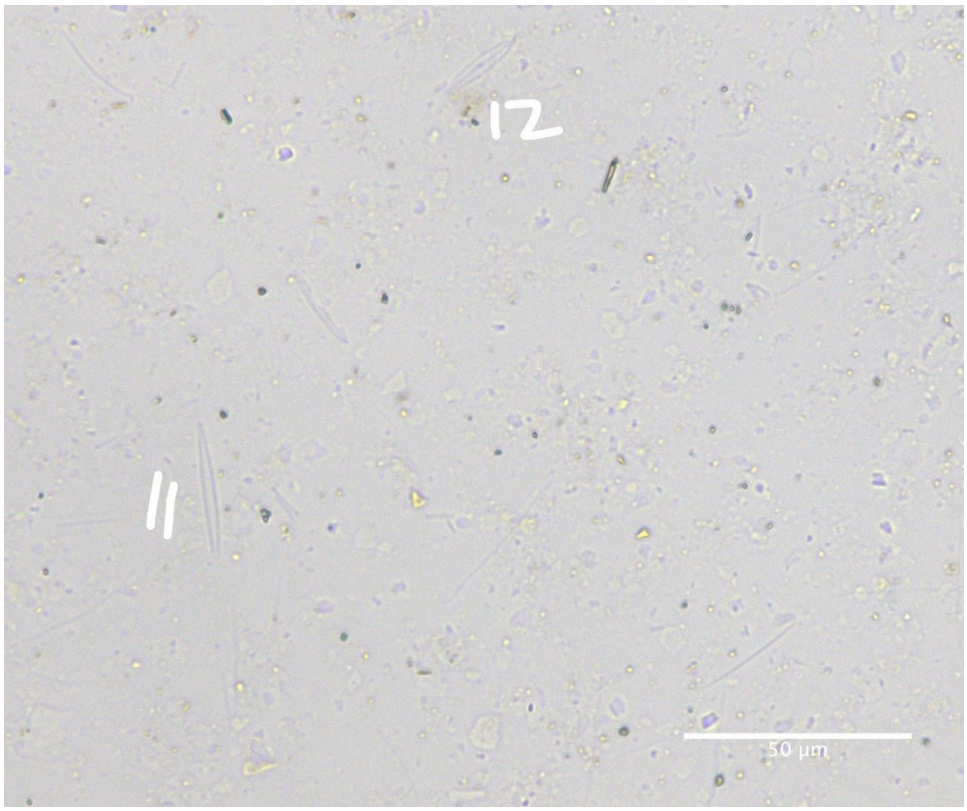


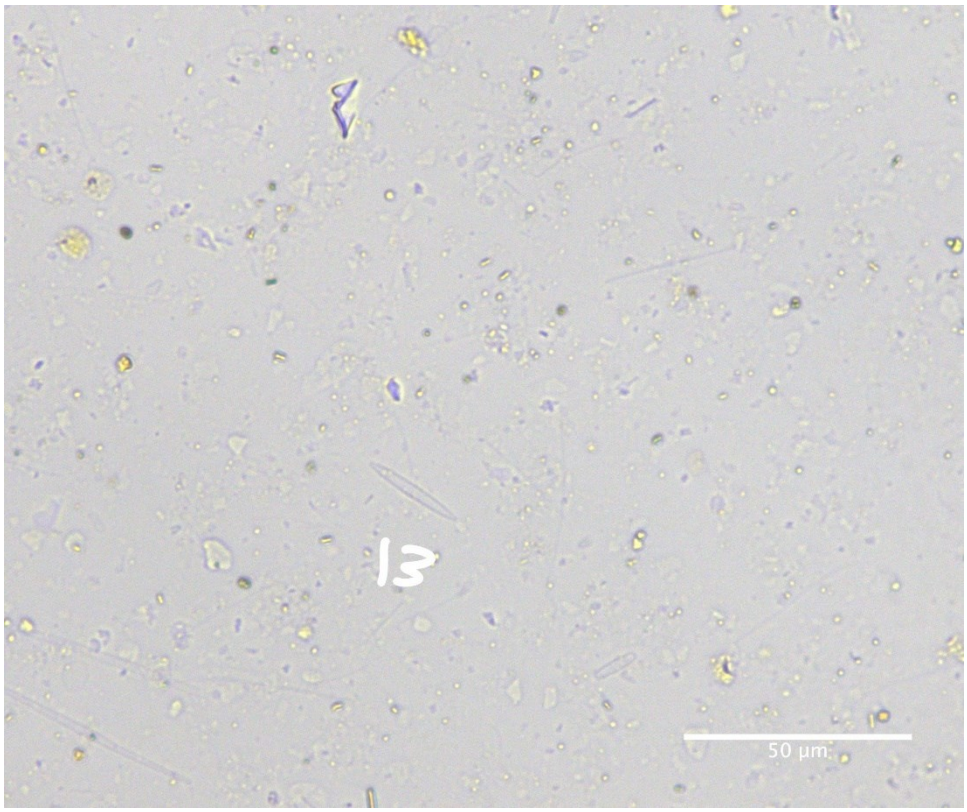

15-20 cm downcore

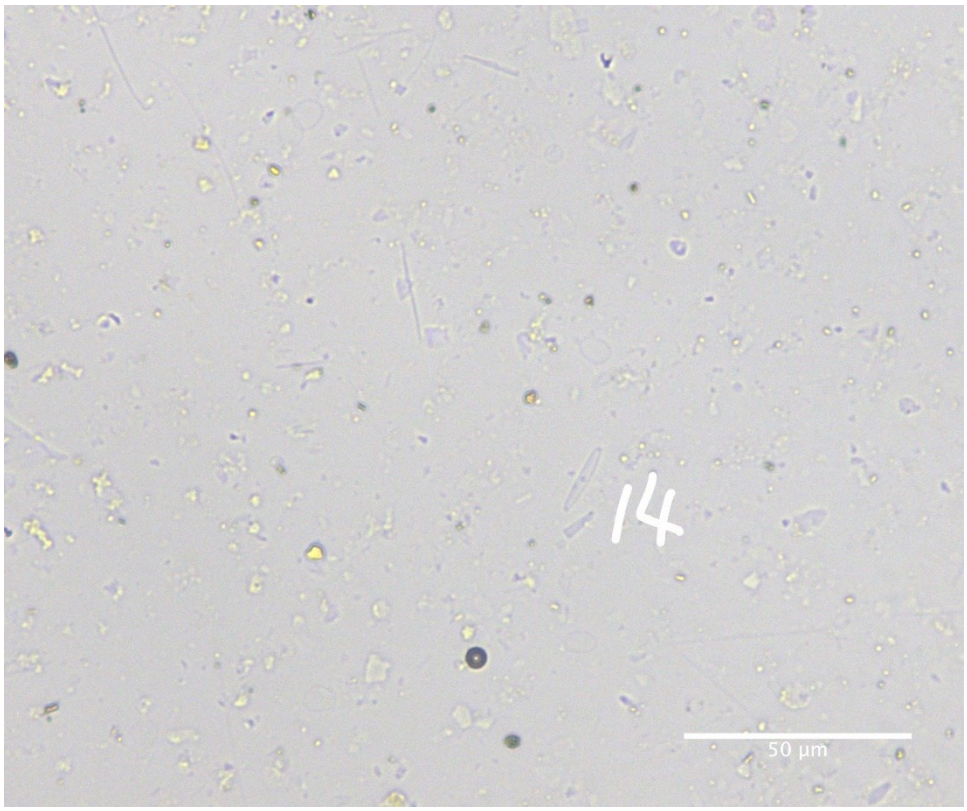


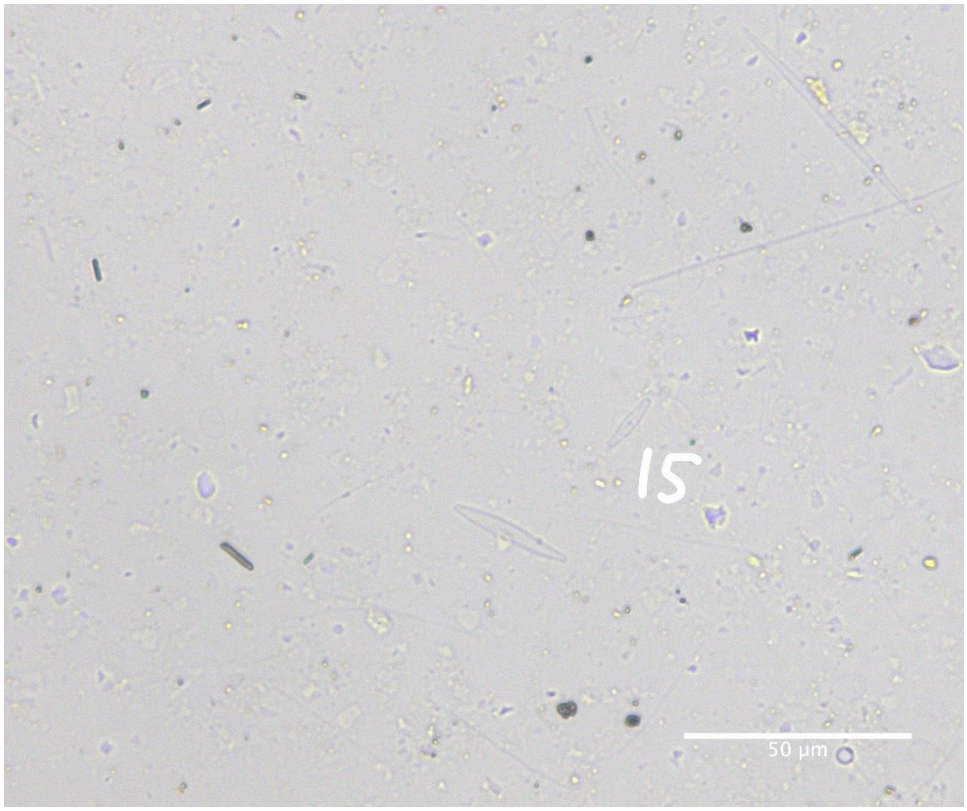

15-20 cm downcore

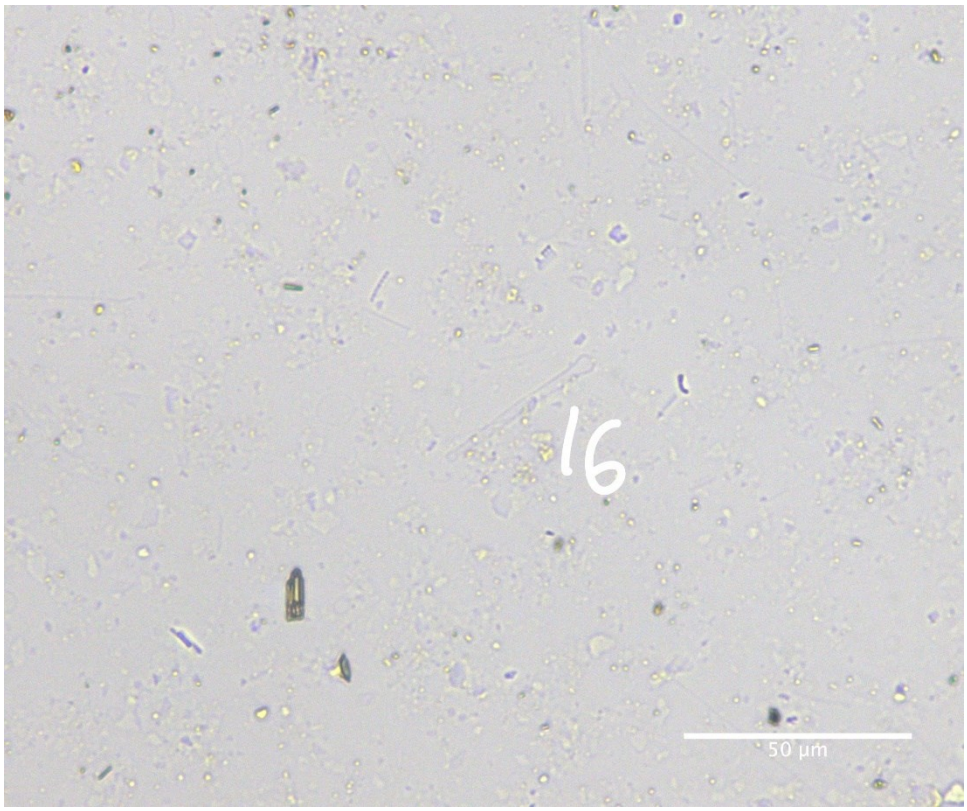


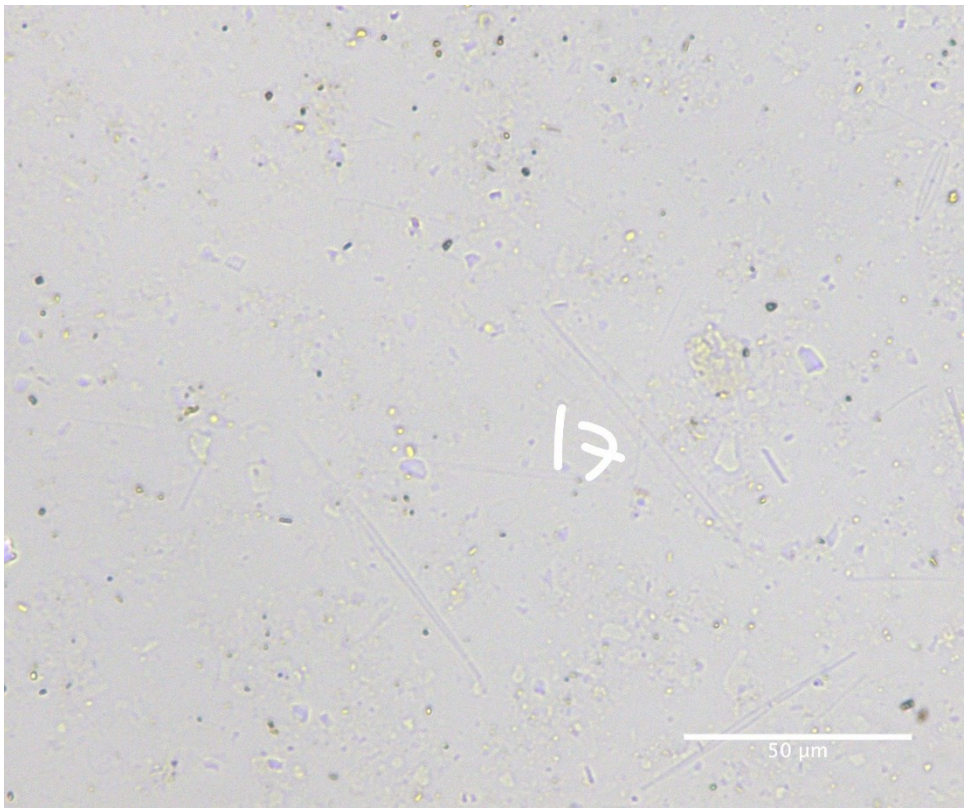

15-20 cm downcore

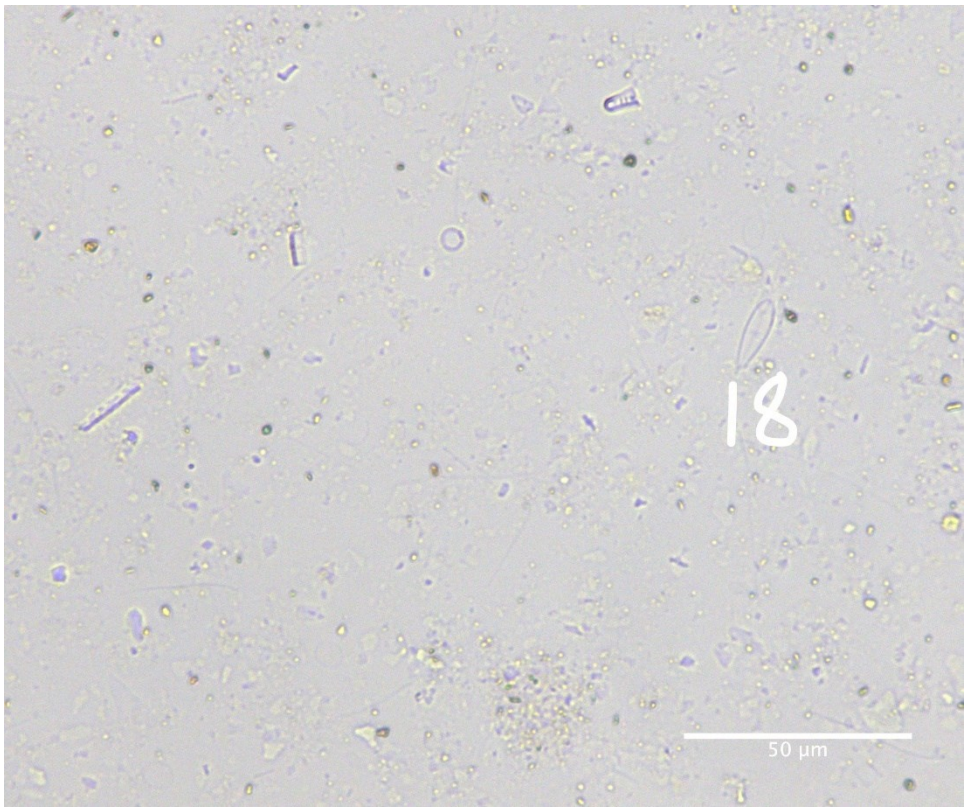


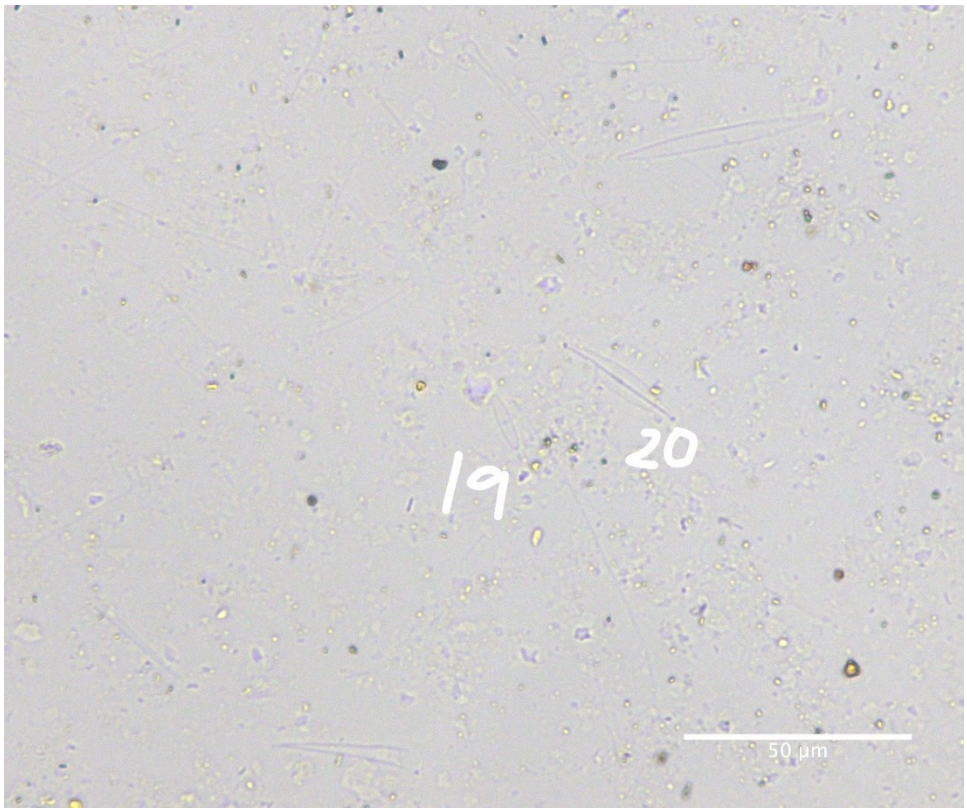

15-20 cm downcore

| Diatom ID | Taxon | Diatom ID | Taxon |
|---|---|---|---|
| 1 | *Diatoma* sp. | 11 | *Fragilaria* sp. |
| 2 | *Navicula* sp. | 12 | *Achnanthidium* sp. |
| 3 | *Navicula* sp. | 13 | *Fragilaria* sp. |
| 4 | *Achnanthidium* sp. | 14 | *Achnanthidium* sp. |
| 5 | *Achnanthidium* sp. | 15 | *Achnanthidium* sp. |
| 6 | *Nitzschia* sp. | 16 | *Asterionella* sp. |
| 7 | *Cymbella* sp. | 17 | *Amphipleura* sp. |
| 8 | *Eunotia* sp. | 18 | *Gomphonema* sp. |
| 9 | *Eunotia* sp. | 19 | *Achnanthidium* sp. |
| 10 | *Achnanthidium* sp. | 20 | *Navicula* sp. |

20-25 cm downcore

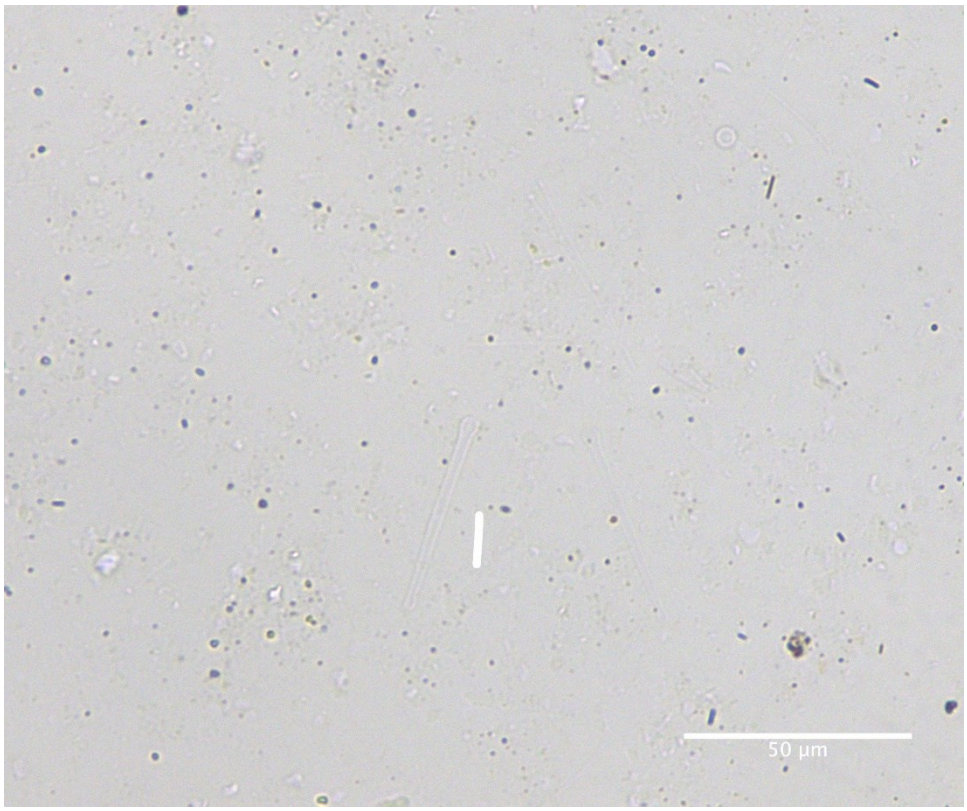


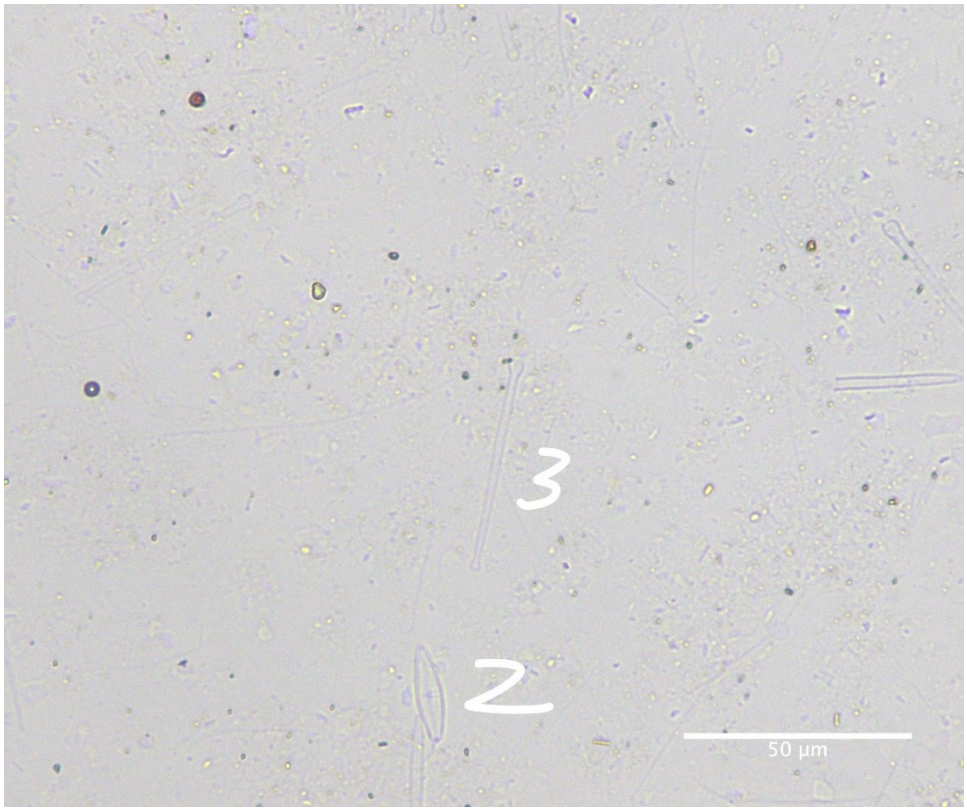

20-25 cm downcore

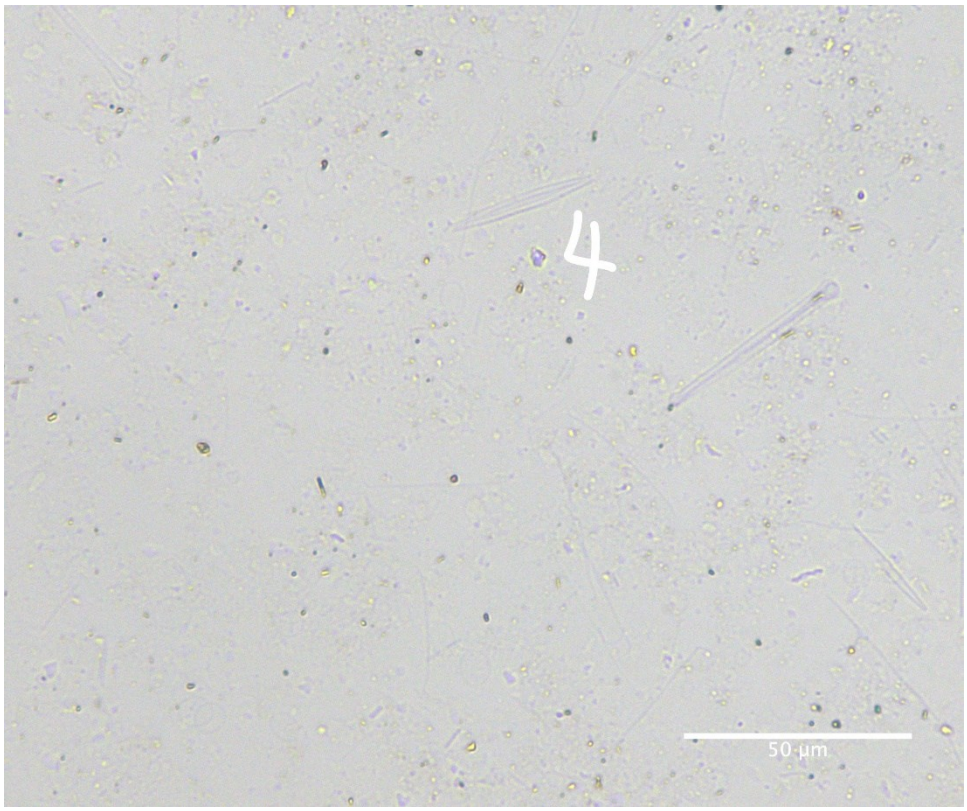


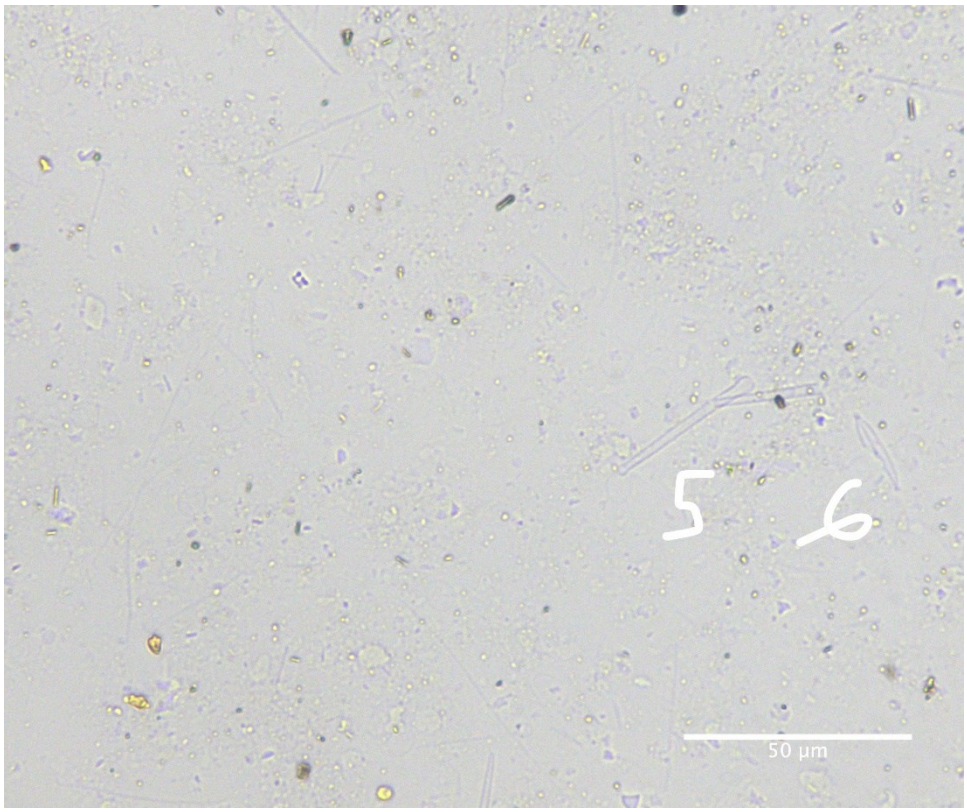

20-25 cm downcore

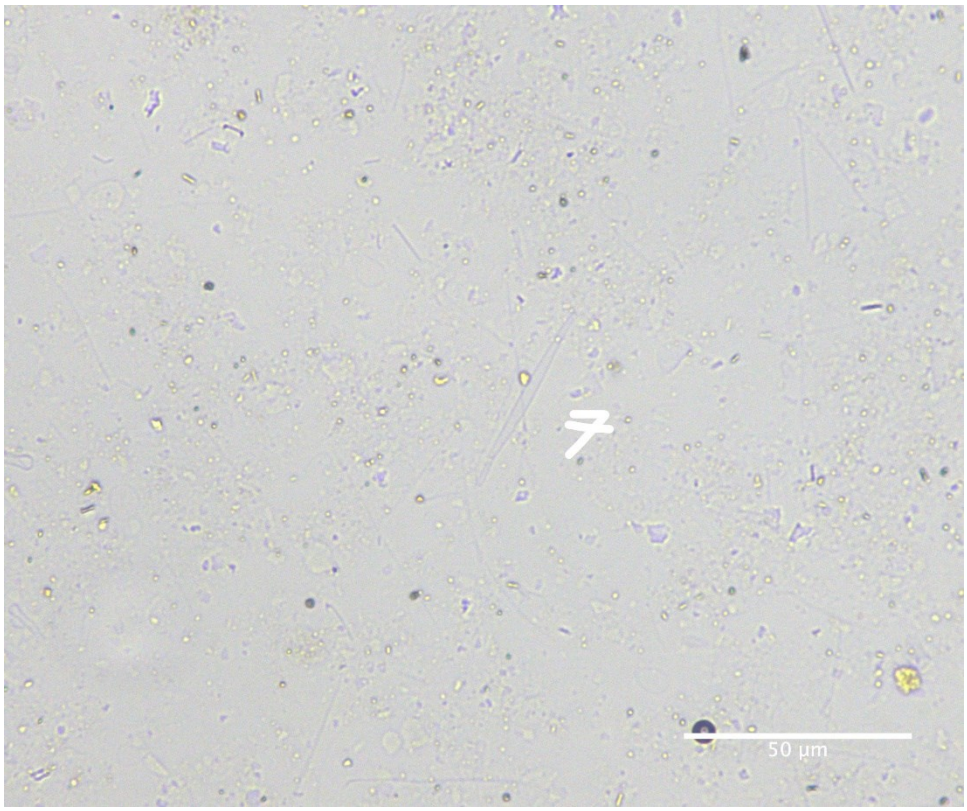


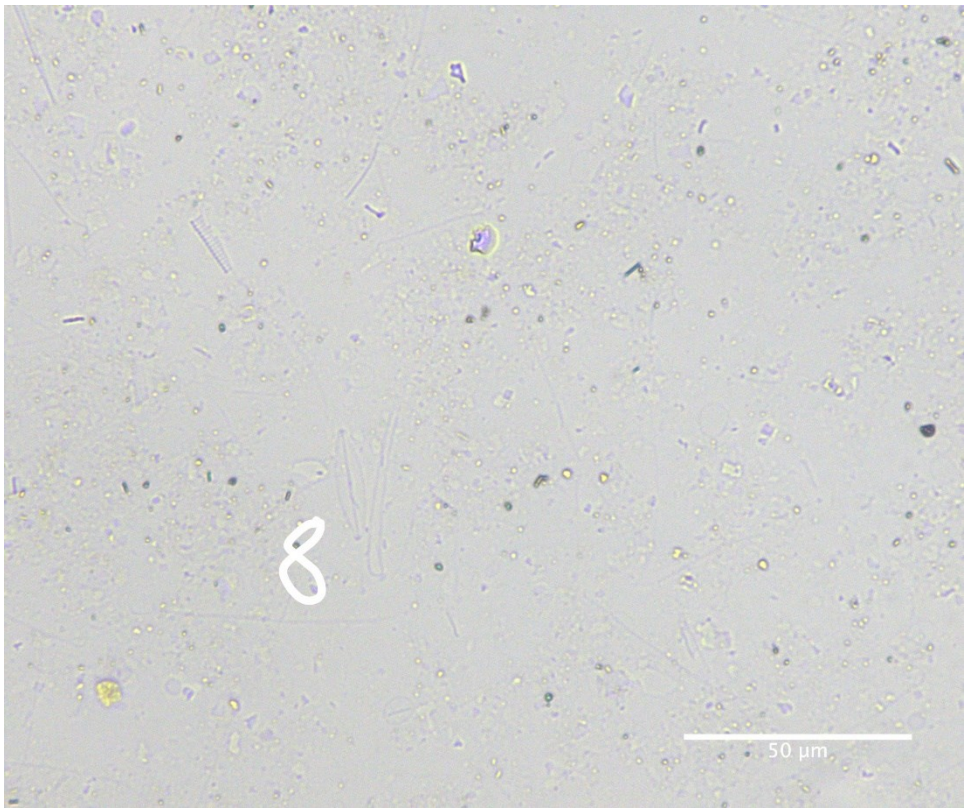

20-25 cm downcore

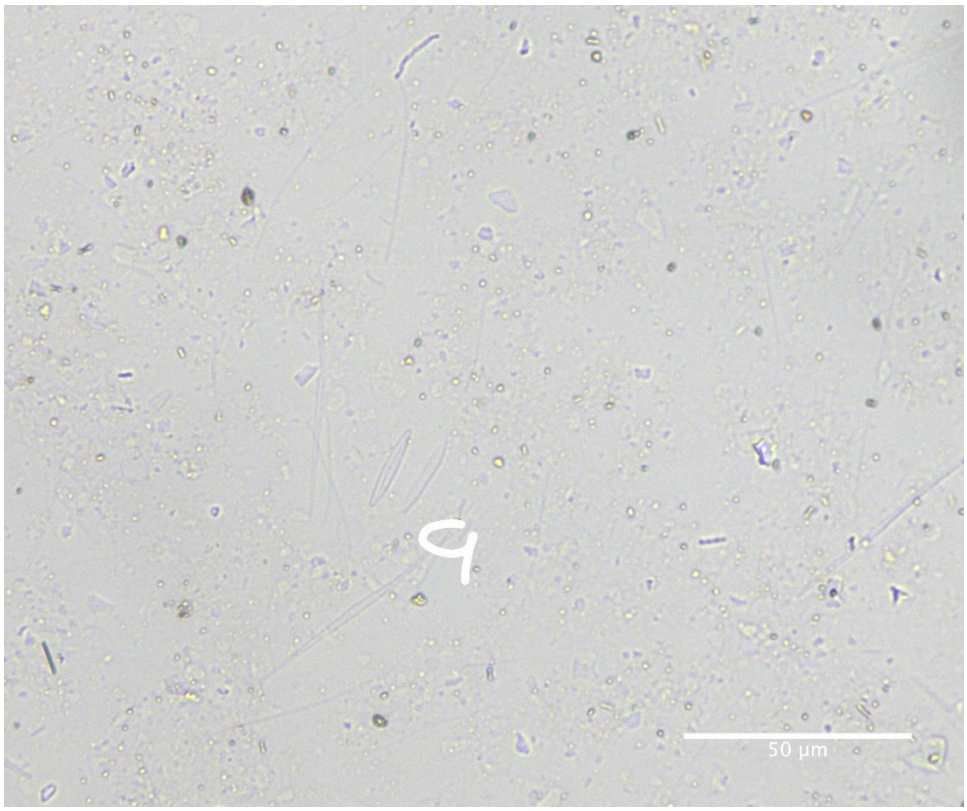


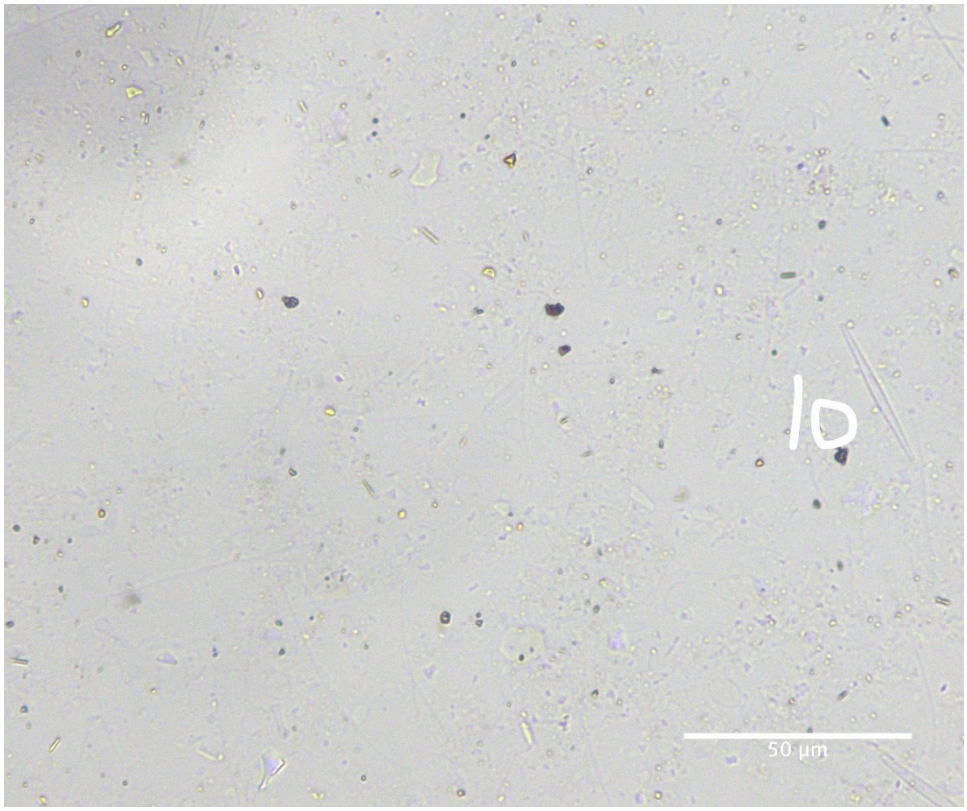

20-25 cm downcore

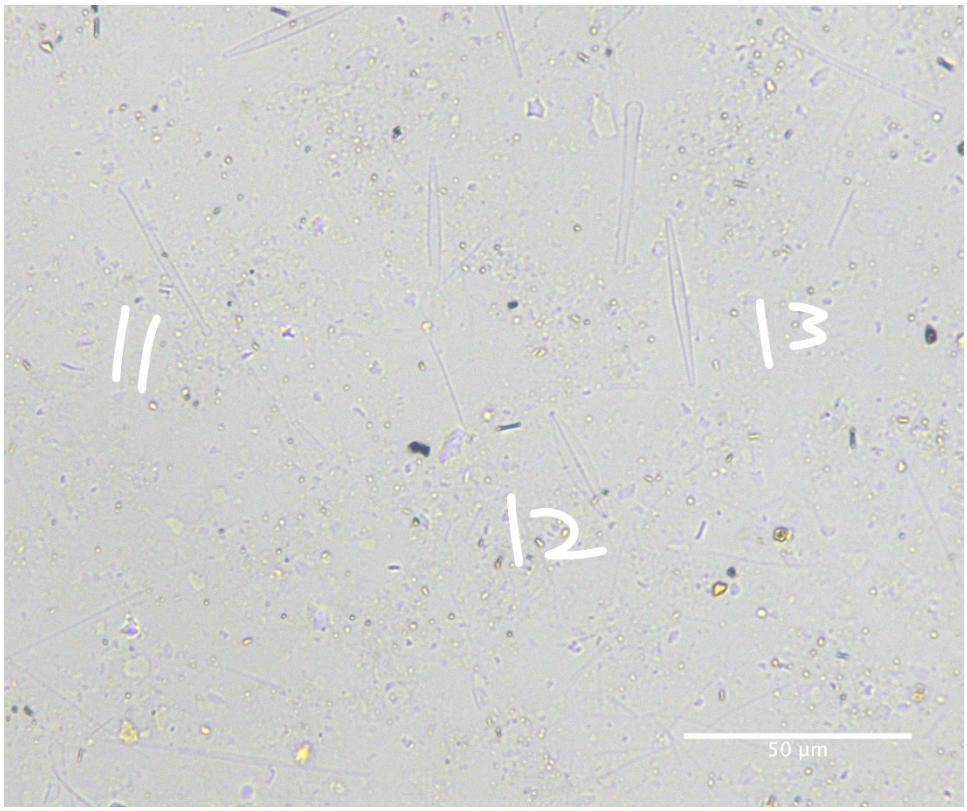


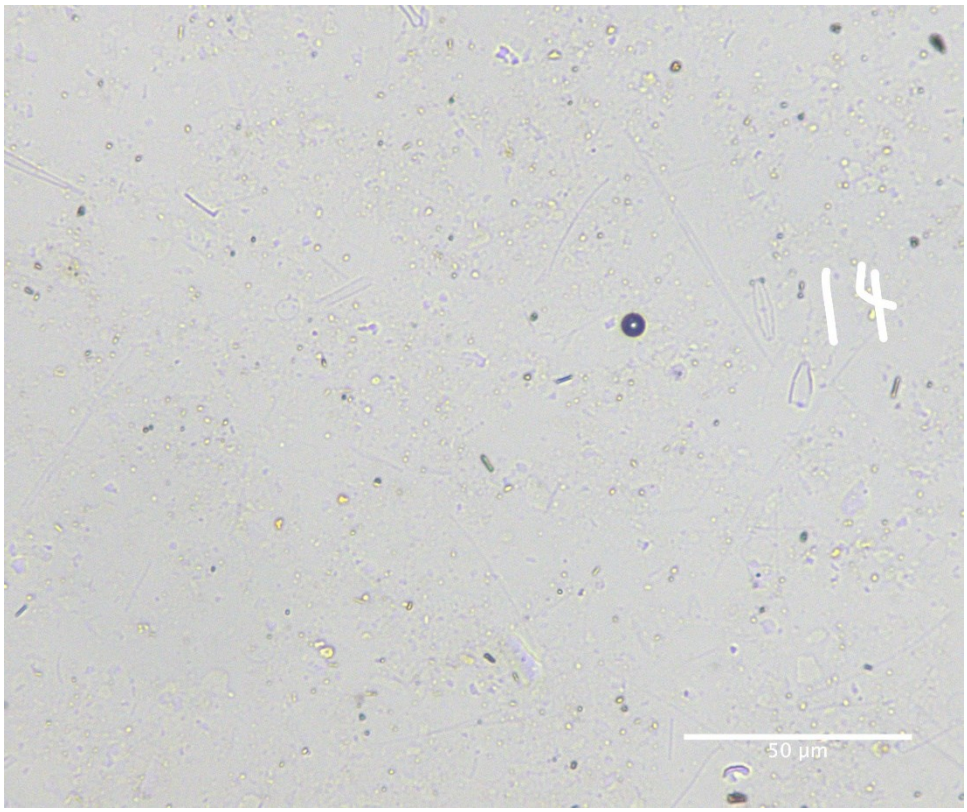

20-25 cm downcore

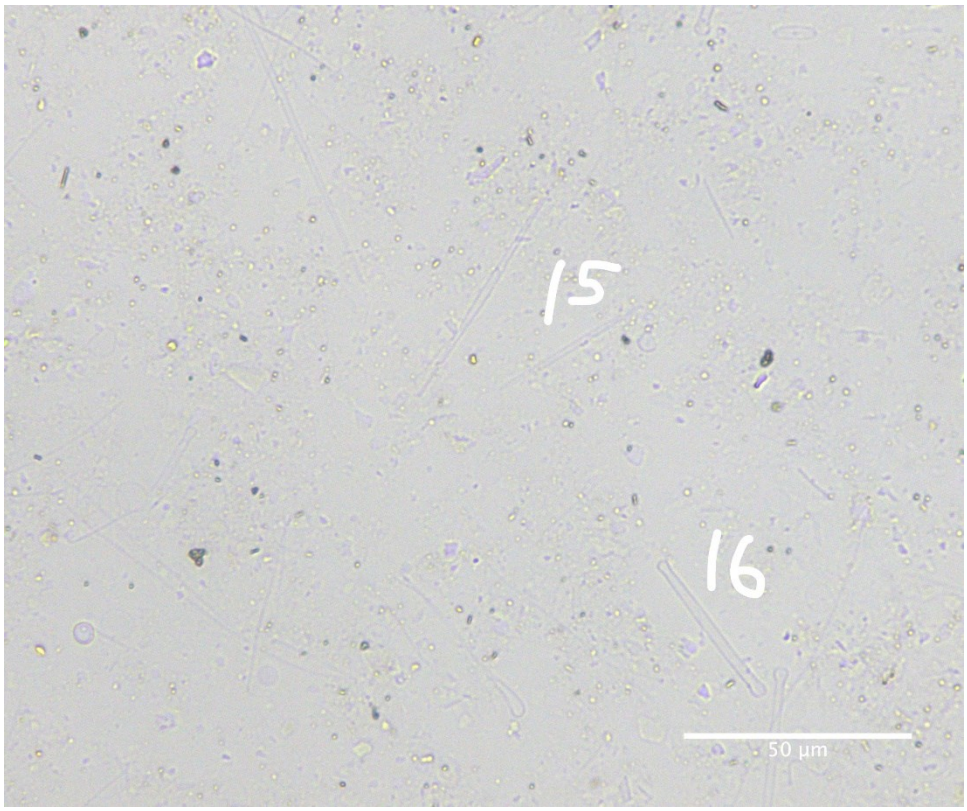


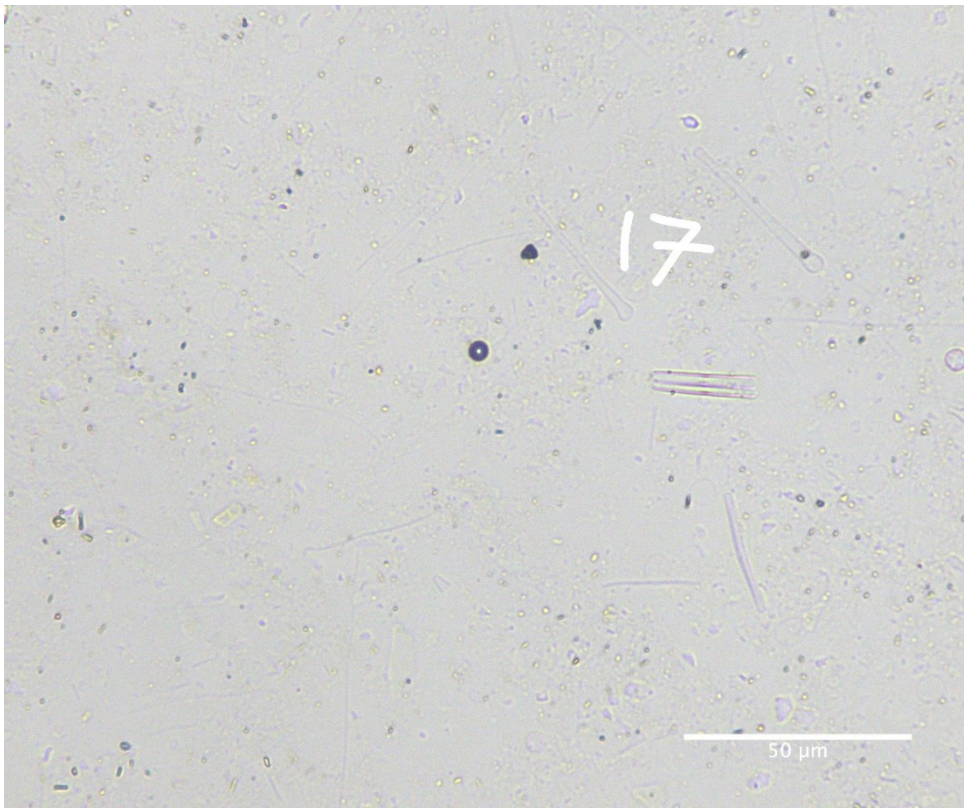

20-25 cm downcore

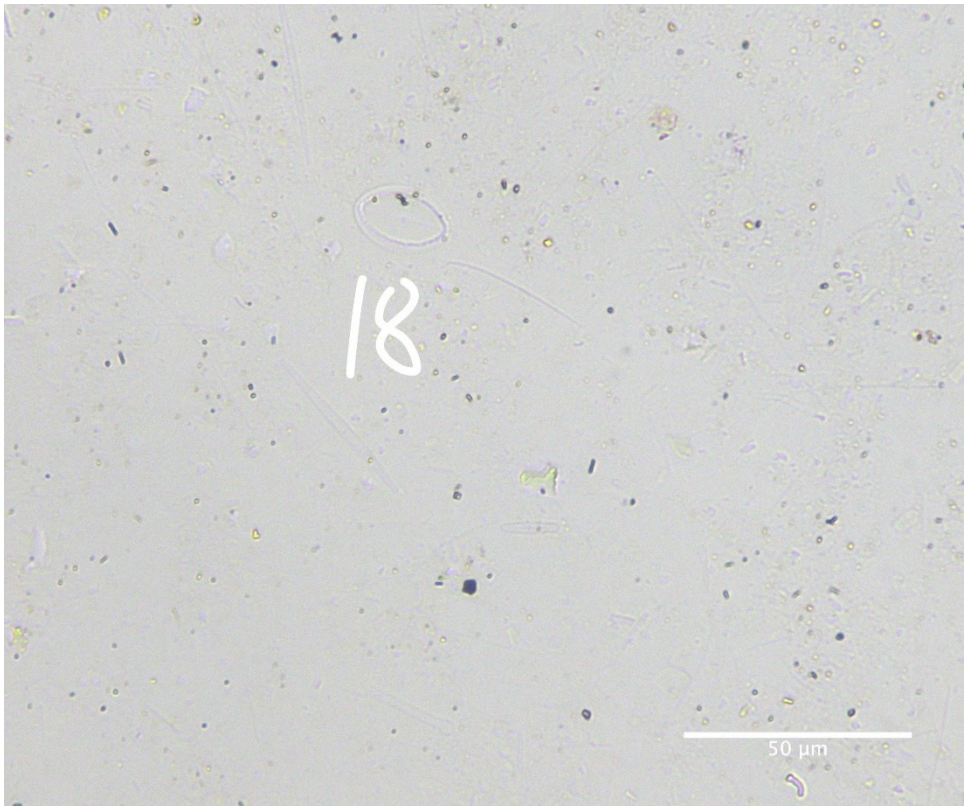


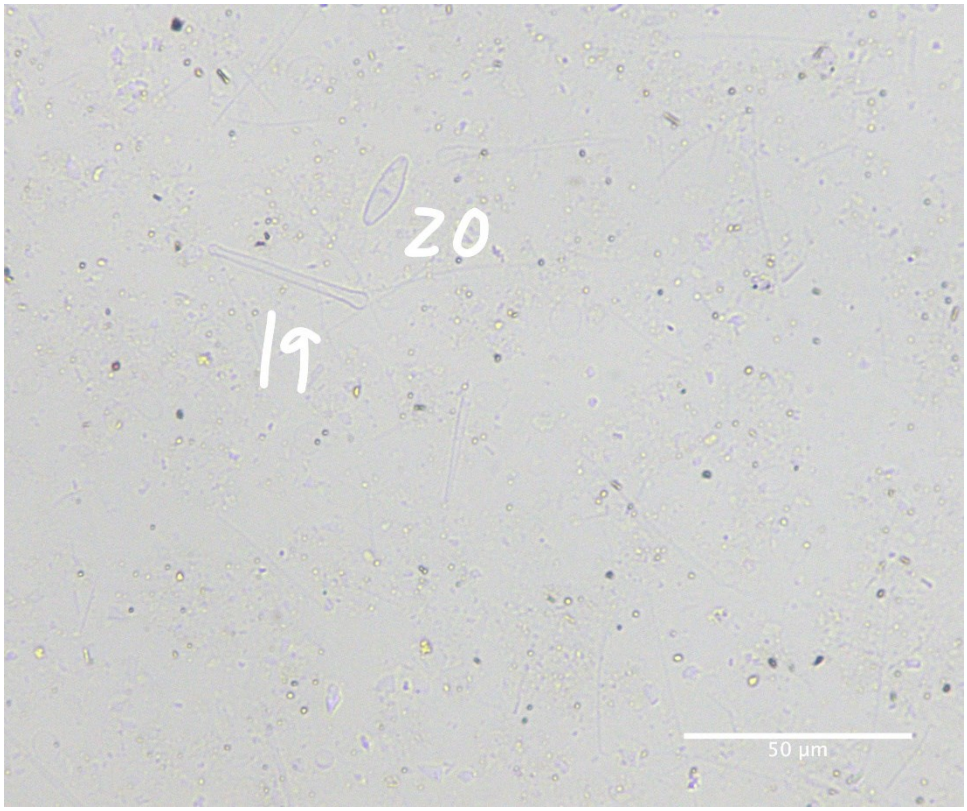

20-25 cm downcore

| Diatom ID | Taxon | Diatom ID | Taxon |
|---|---|---|---|
| 1 | *Asterionella* sp. | 11 | *Asterionella* sp. |
| 2 | *Gomphonema* sp. | 12 | *Navicula* sp. |
| 3 | *Asterionella* sp. | 13 | *Fragilaria* sp. |
| 4 | *Navicula* sp. | 14 | *Achnanthidium* sp. |
| 5 | *Asterionella* sp. | 15 | *Fragilaria* sp. |
| 6 | *Navicula* sp. | 16 | *Asterionella* sp. |
| 7 | *Fragilaria* sp. | 17 | *Asterionella* sp. |
| 8 | *Navicula* sp. | 18 | *Cocconeis* sp. |
| 9 | *Fragilaria* sp. | 19 | *Asterionella* sp. |
| 10 | *Fragilaria* sp. | 20 | *Achnanthidium* sp. |

25-30 cm downcore

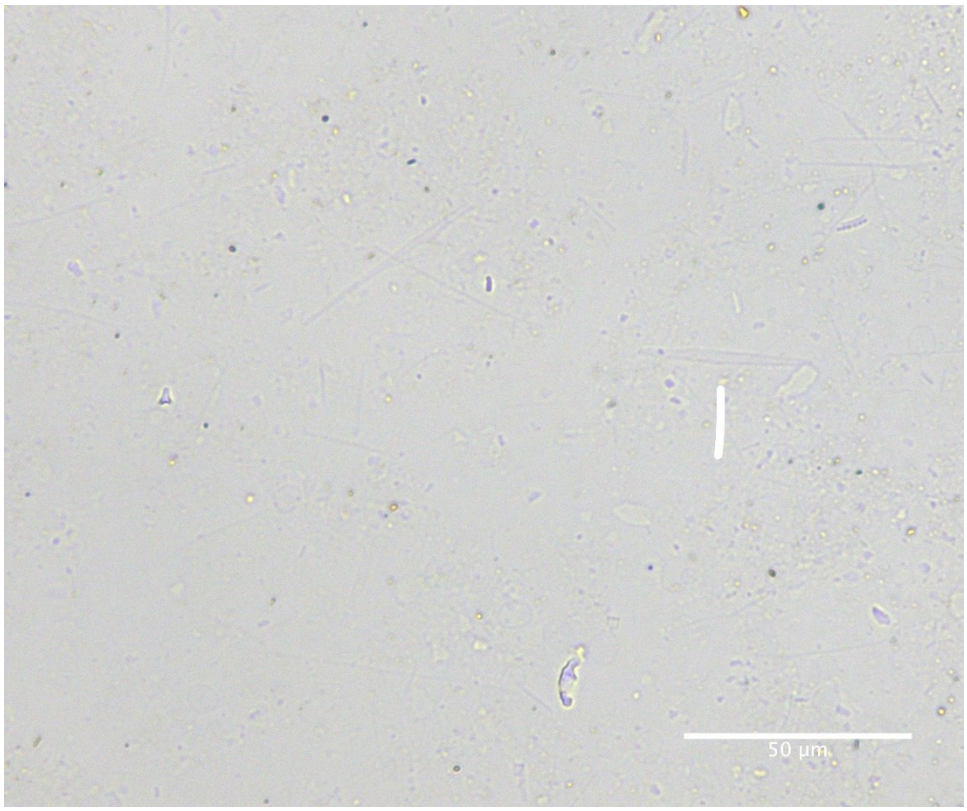


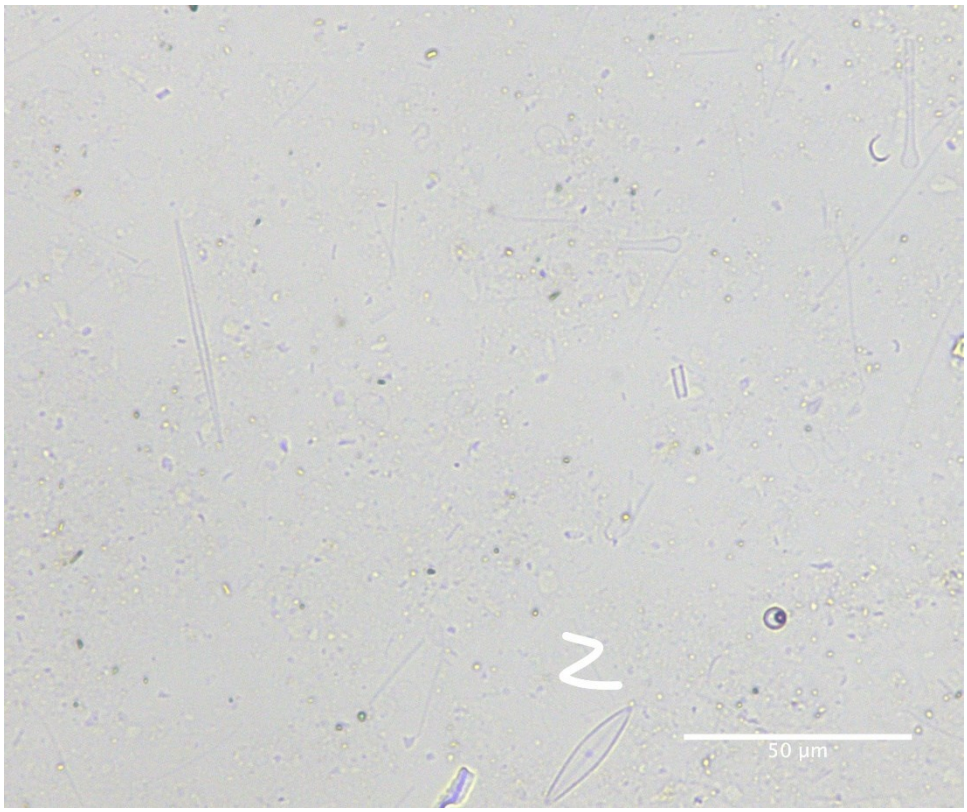

25-30 cm downcore

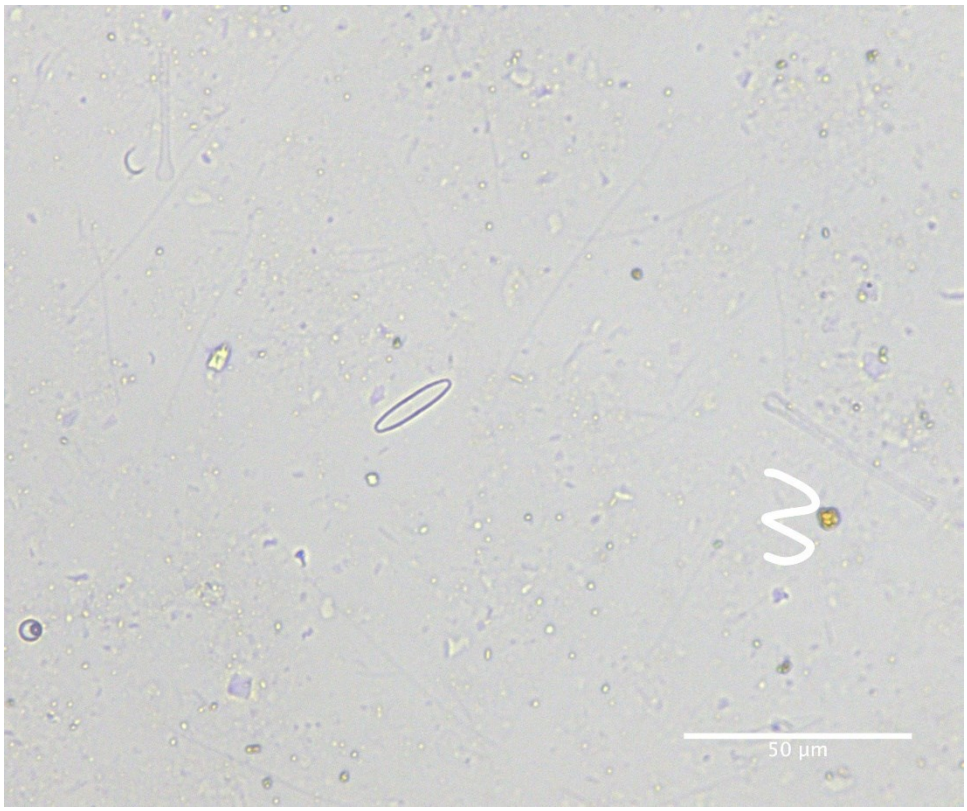


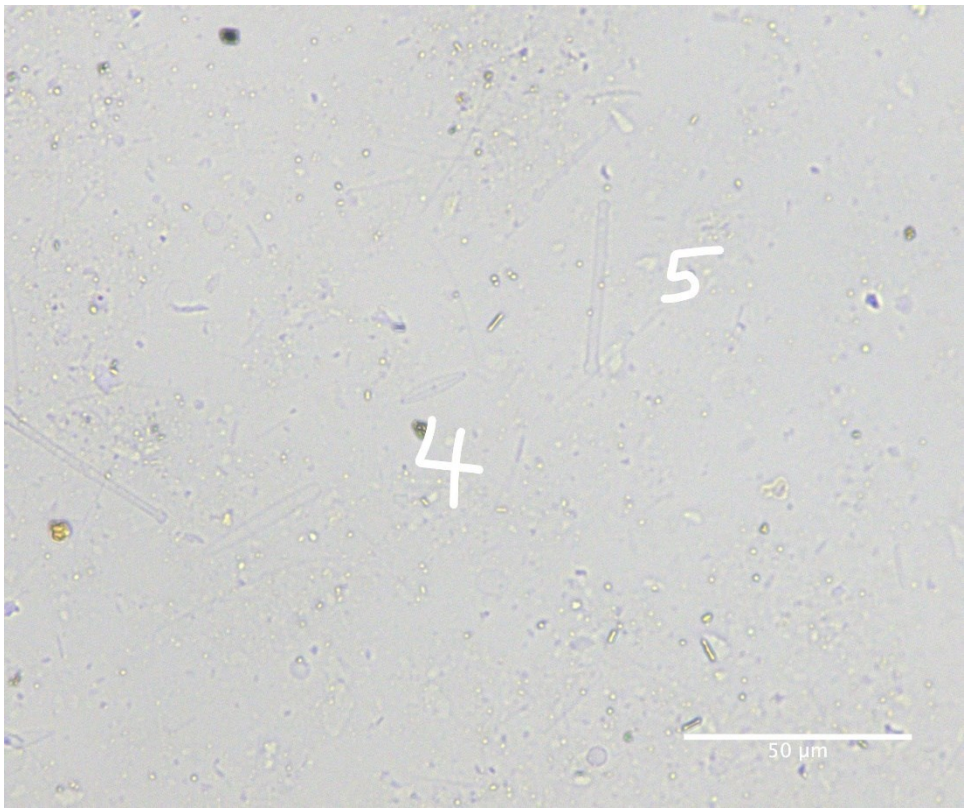

25-30 cm downcore

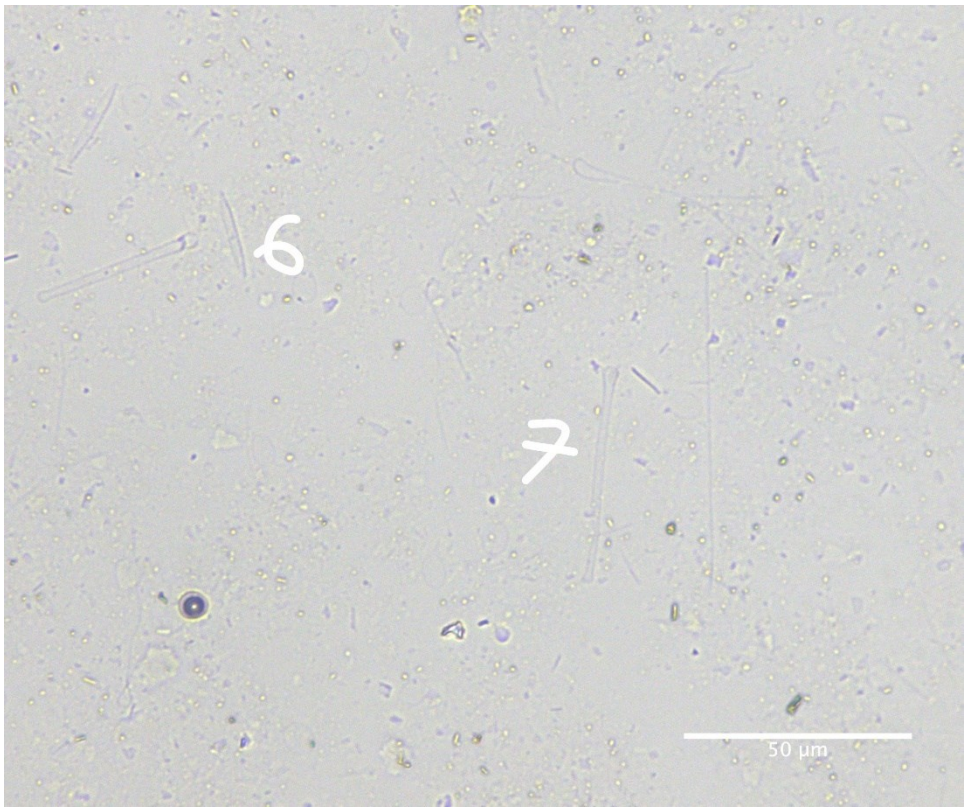


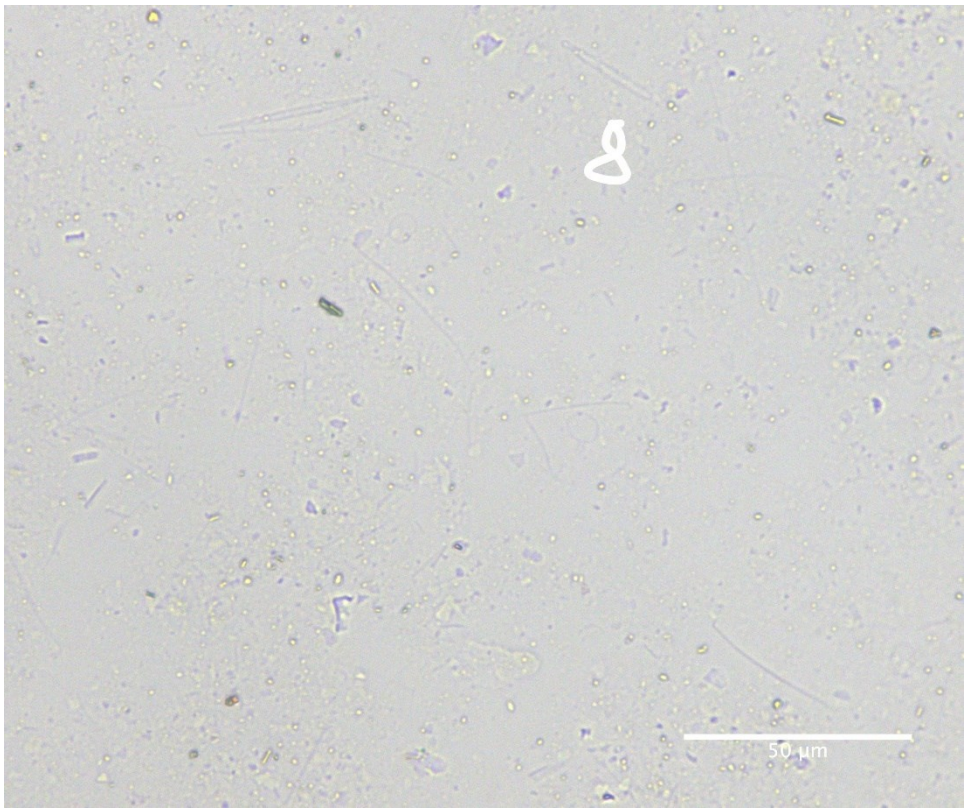

25-30 cm downcore

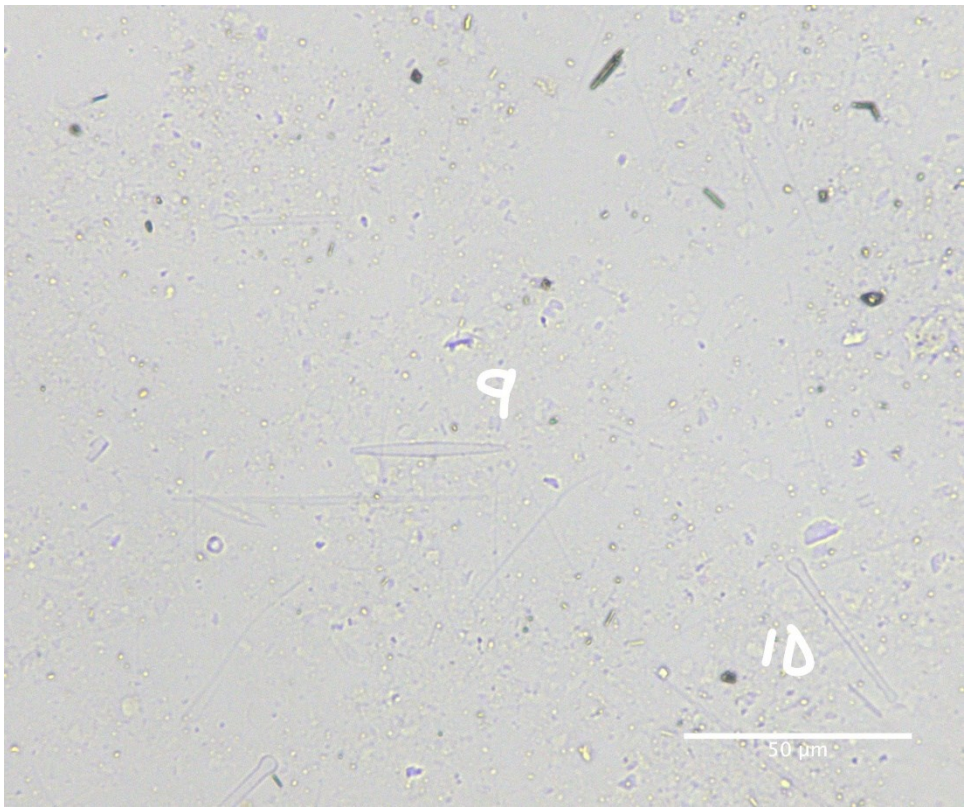


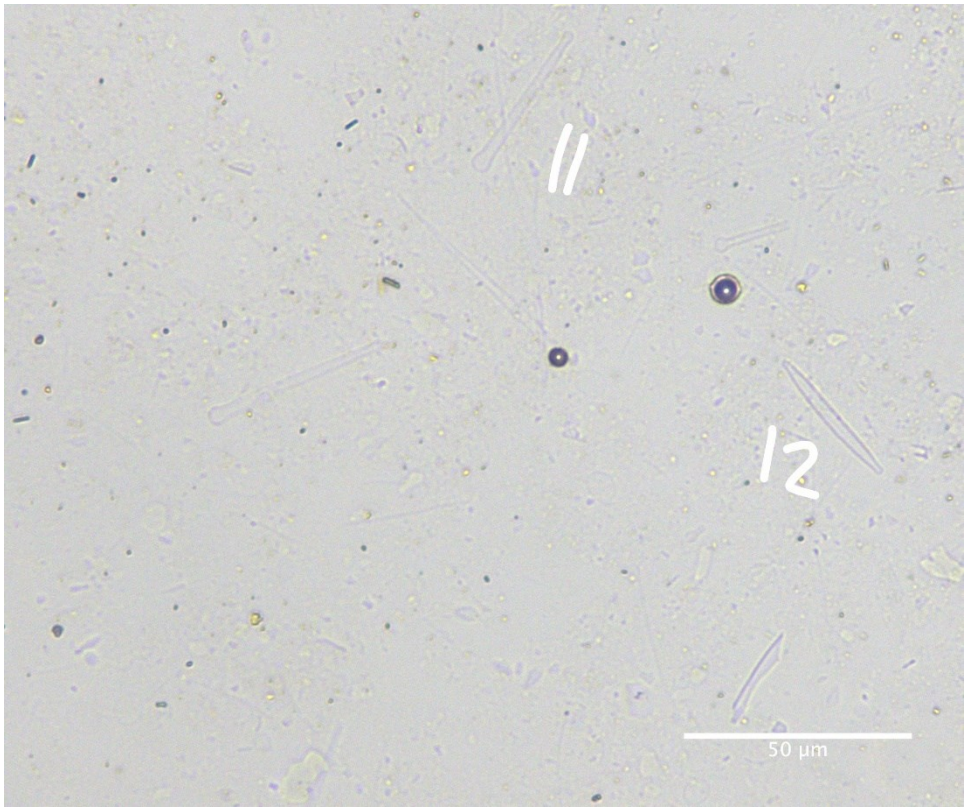

25-30 cm downcore

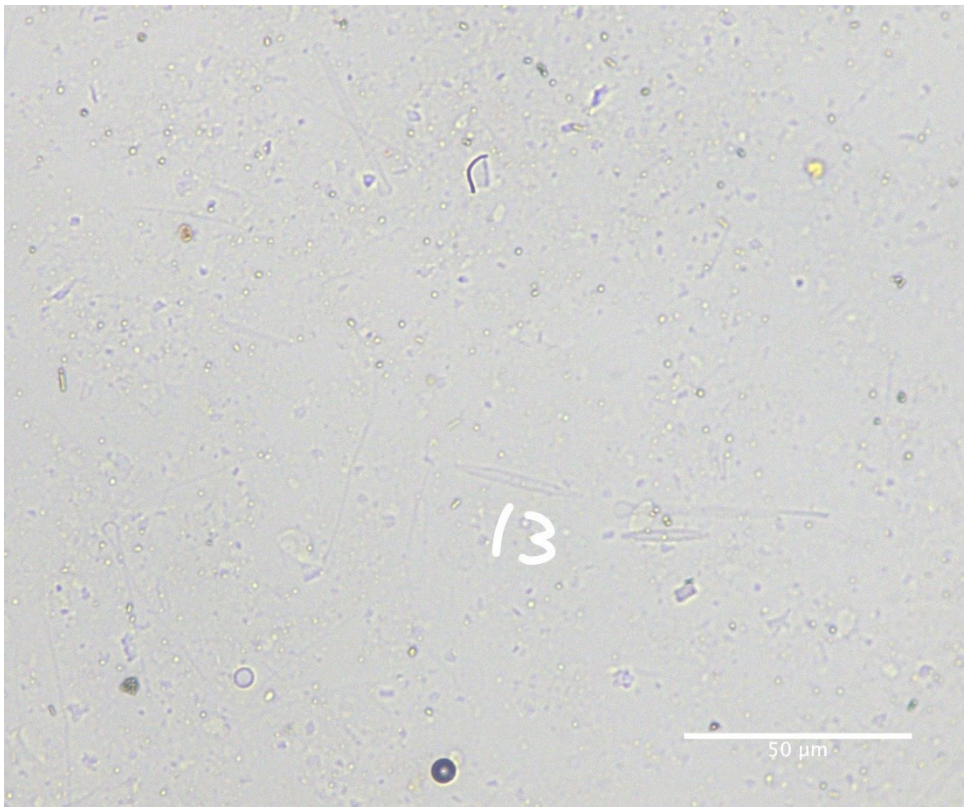


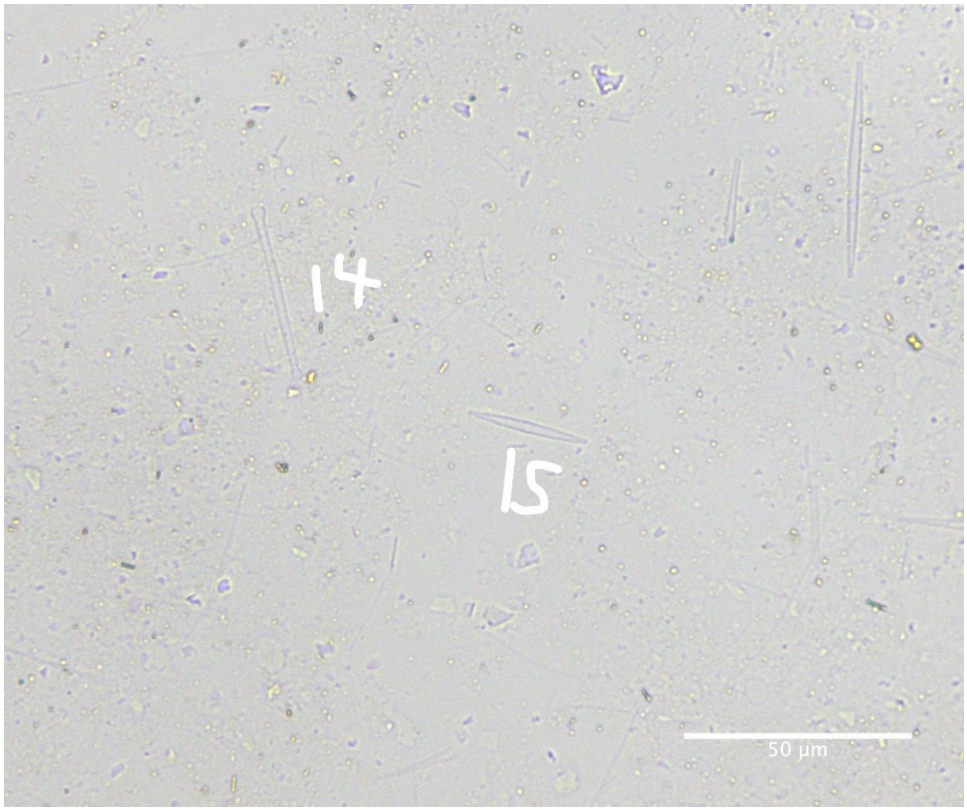

25-30 cm downcore

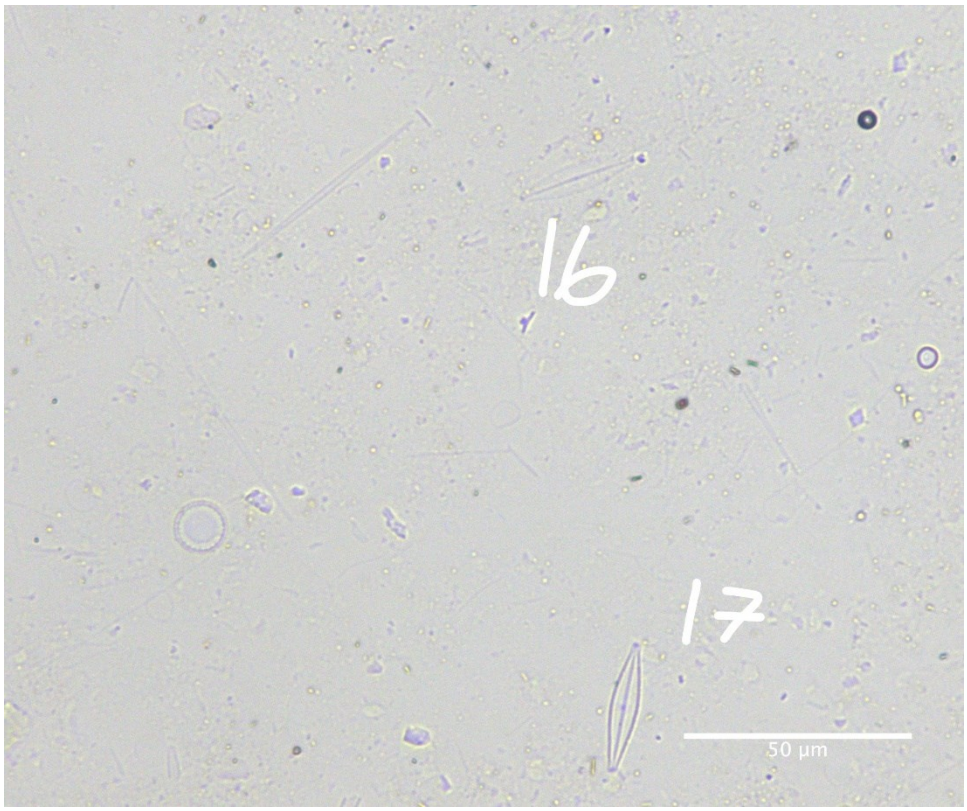


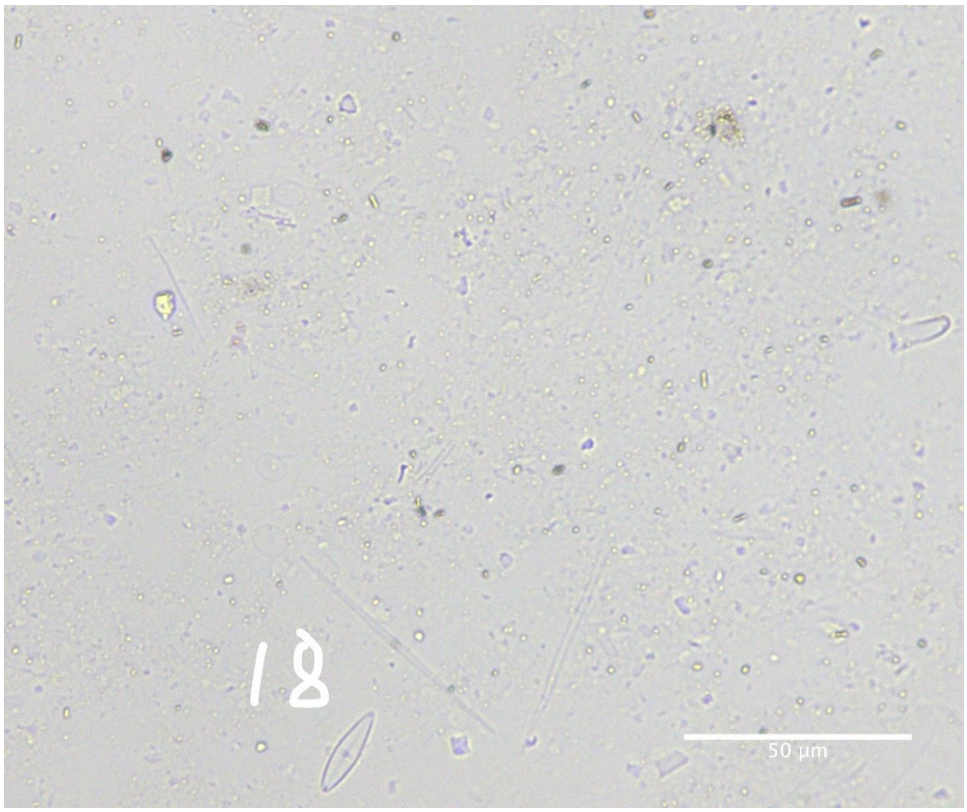

25-30 cm downcore

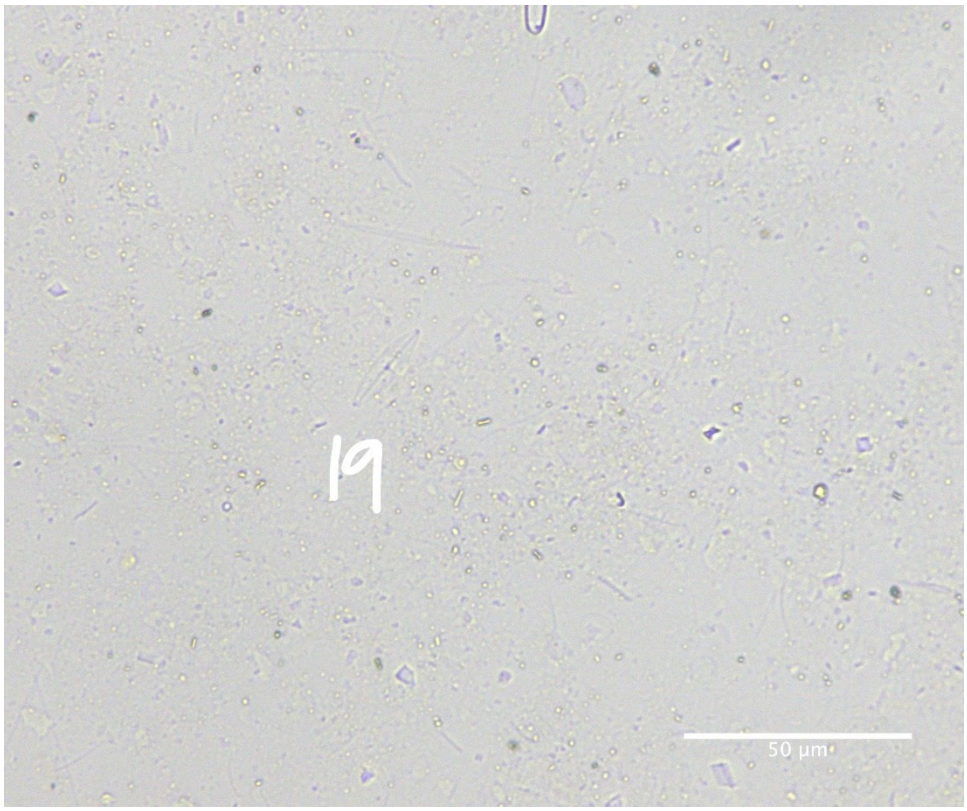


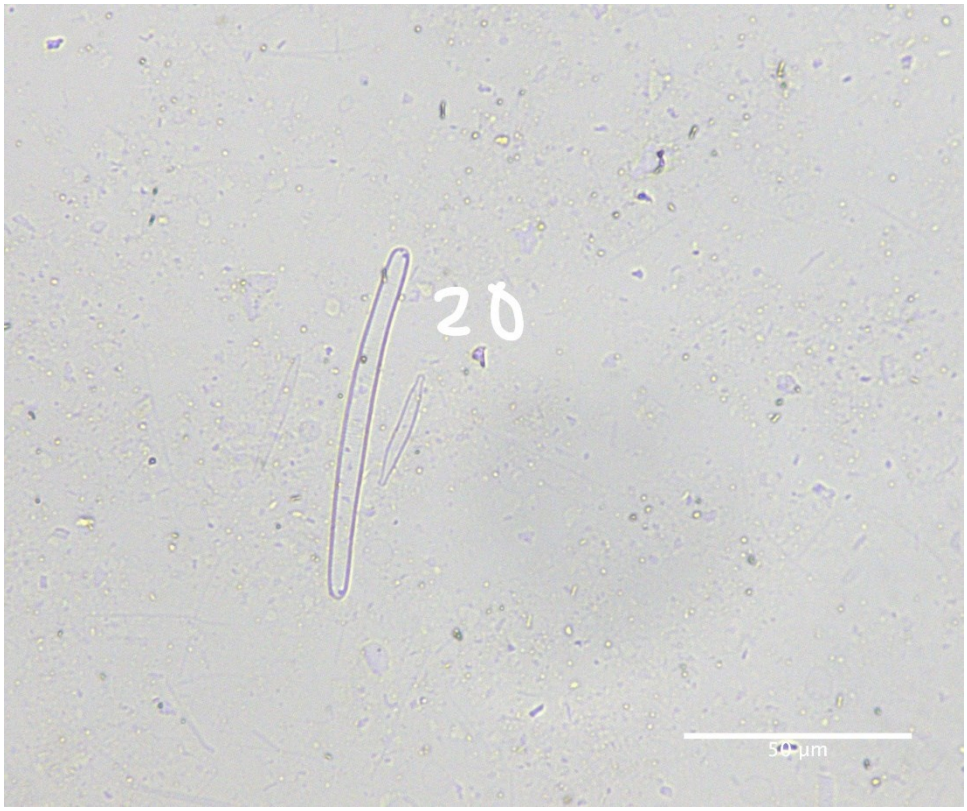

25-30 cm downcore

| Diatom ID | Taxon | Diatom ID | Taxon |
|---|---|---|---|
| 1 | *Fragilaria* sp. | 11 | *Asterionella* sp. |
| 2 | *Gomphonema* sp. | 12 | *Fragilaria* sp. |
| 3 | *Asterionella* sp. | 13 | *Fragilaria* sp. |
| 4 | *Navicula* sp. | 14 | *Asterionella* sp. |
| 5 | *Asterionella* sp. | 15 | *Fragilaria* sp. |
| 6 | *Fragilaria* sp. | 16 | *Navicula* sp. |
| 7 | *Asterionella* sp. | 17 | *Navicula* sp. |
| 8 | *Fragilaria* sp. | 18 | *Gomphonema* sp. |
| 9 | *Fragilaria* sp. | 19 | *Navicula* sp. |
| 10 | *Asterionella* sp. | 20 | *Eunotia* sp. |

30-35 cm downcore

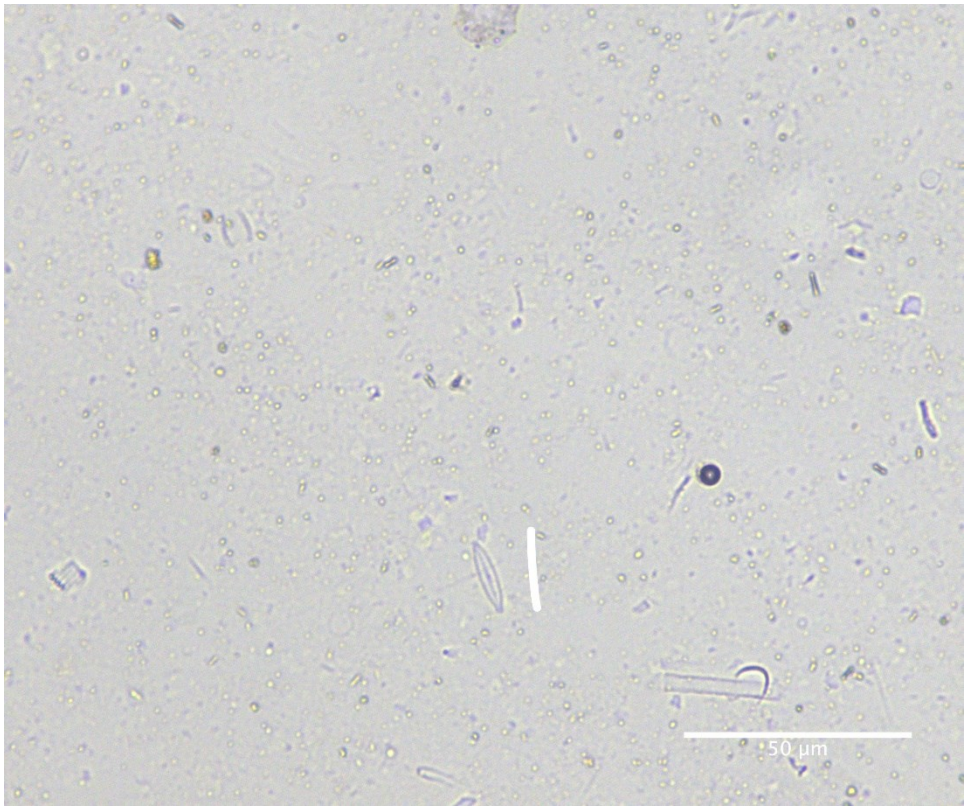


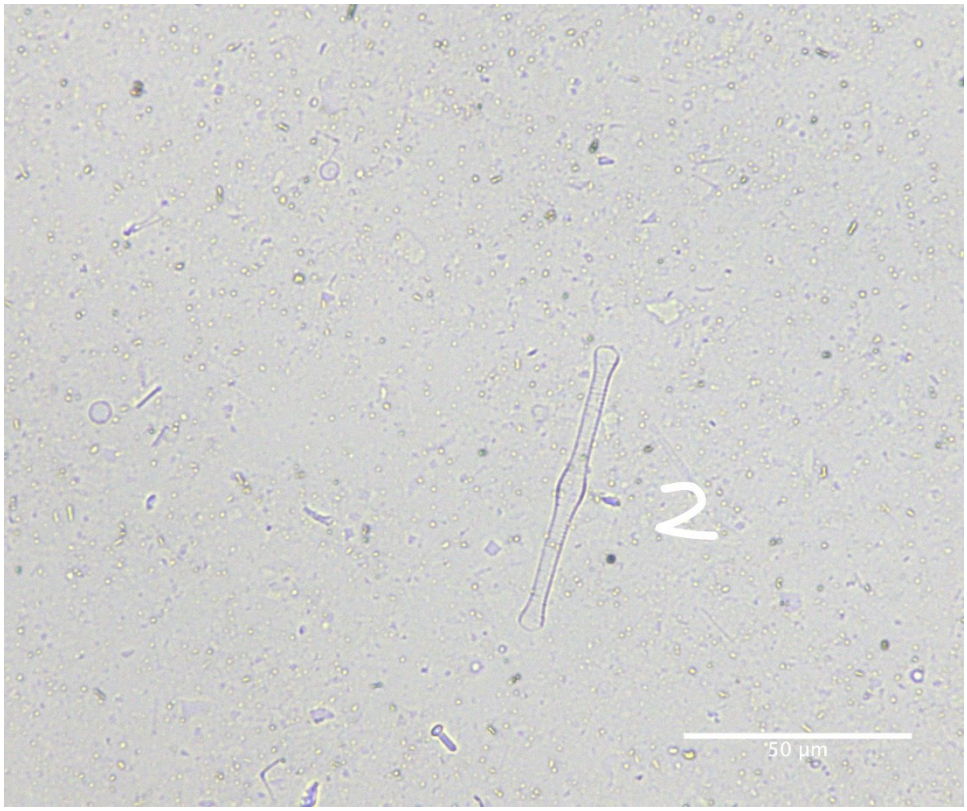

30-35 cm downcore

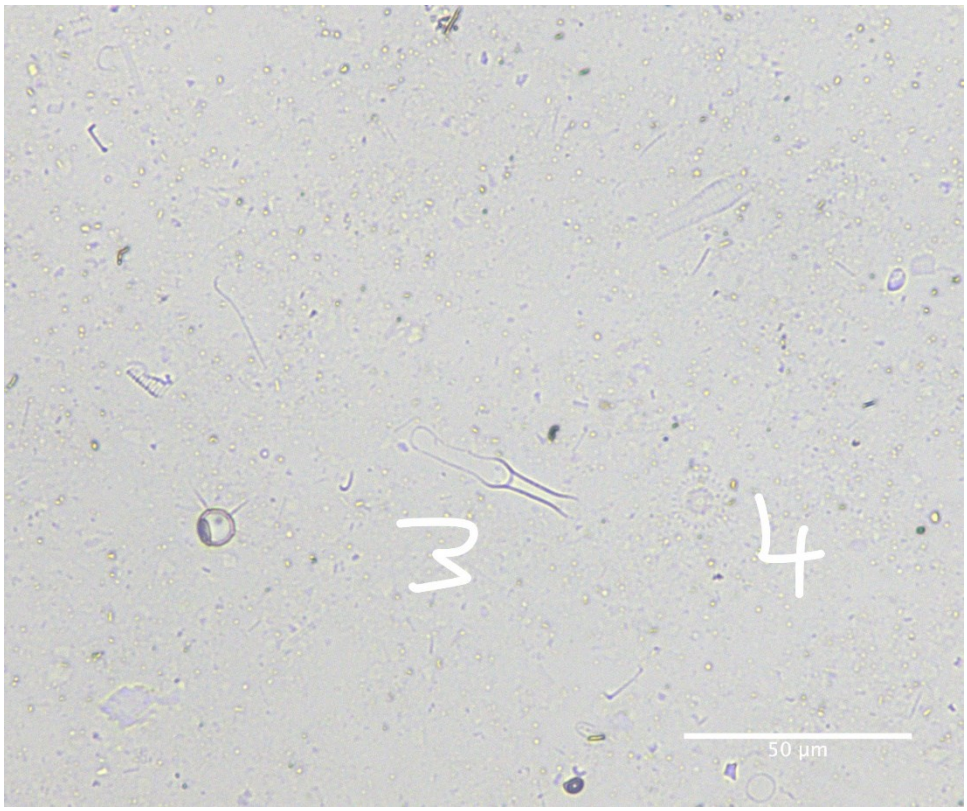


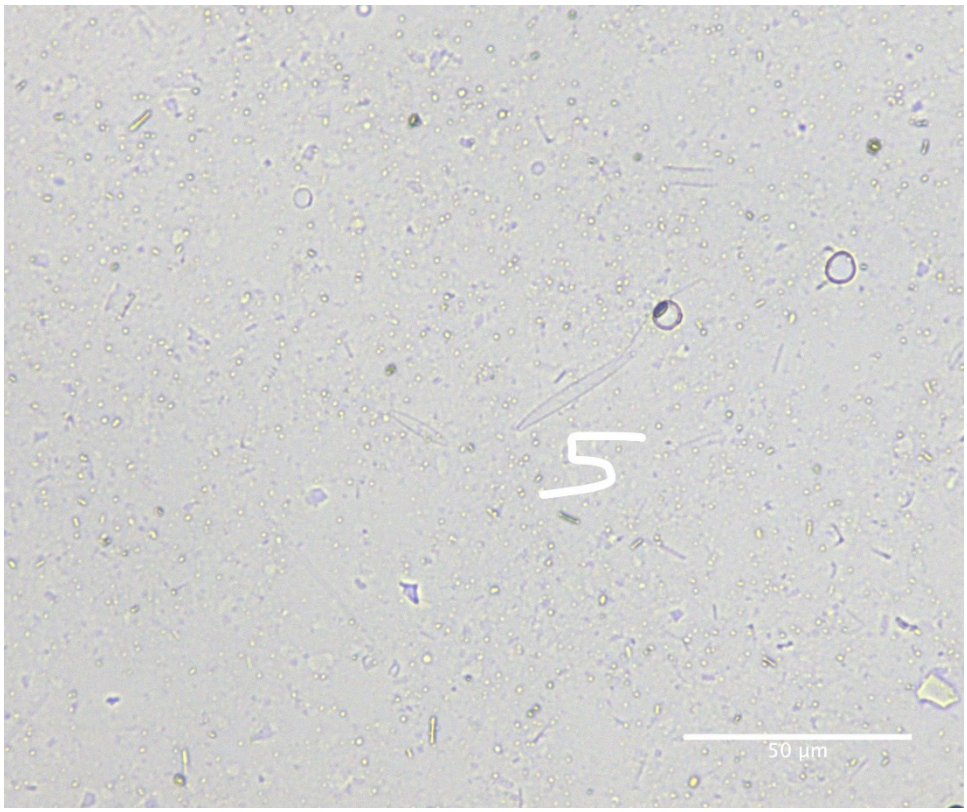

30-35 cm downcore

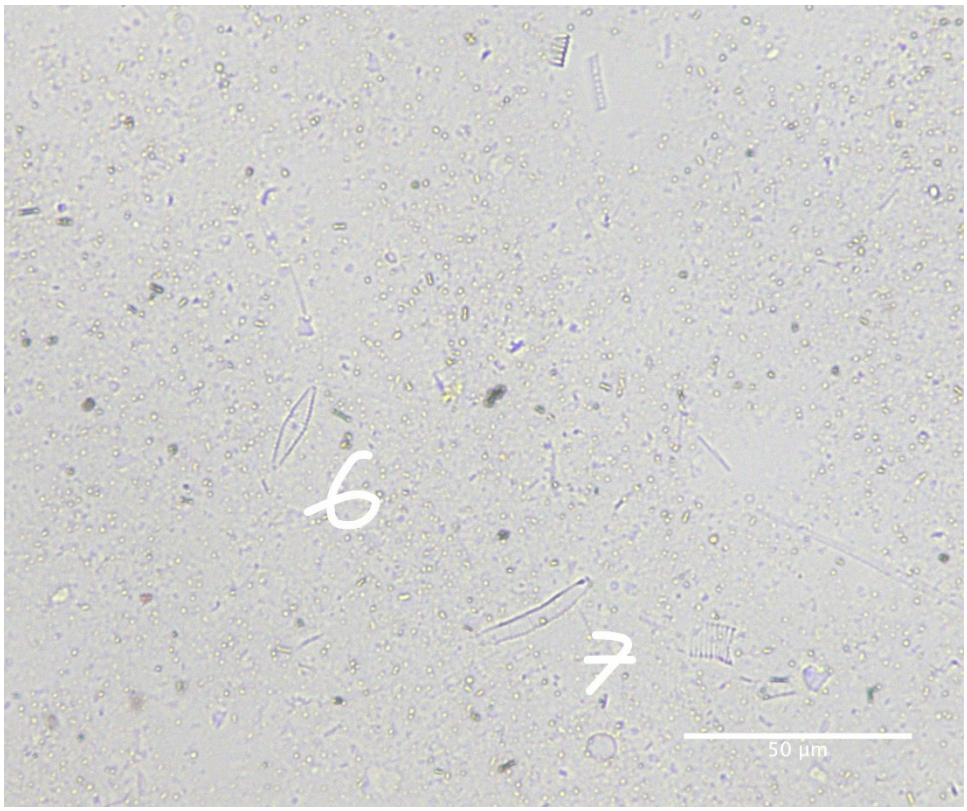


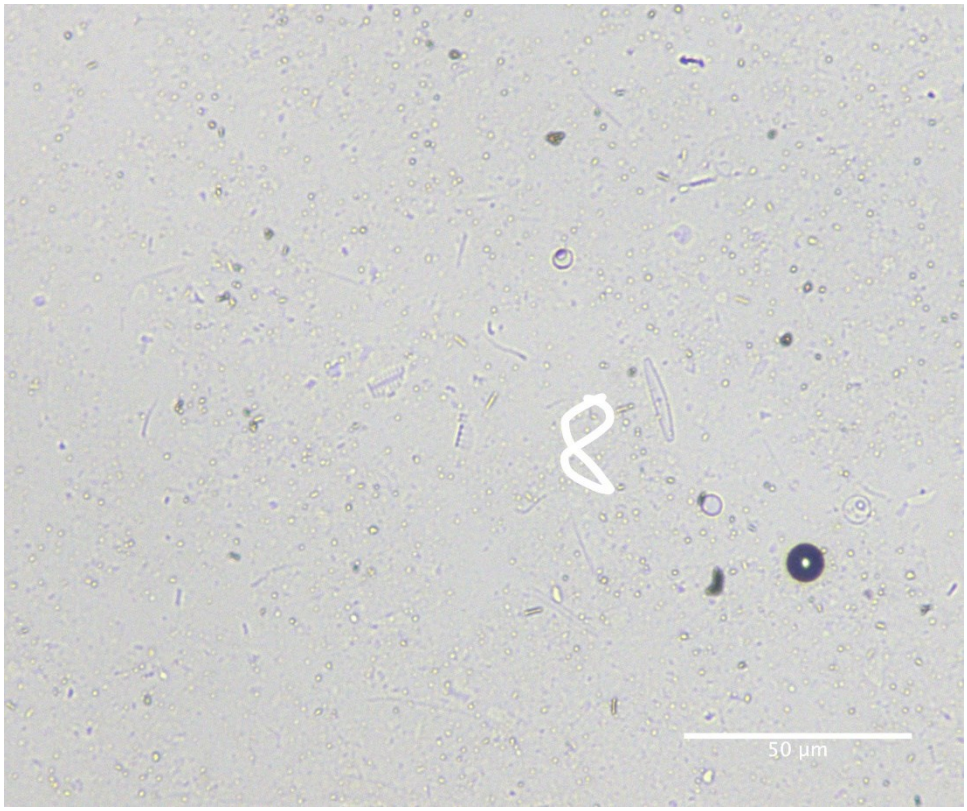

30-35 cm downcore

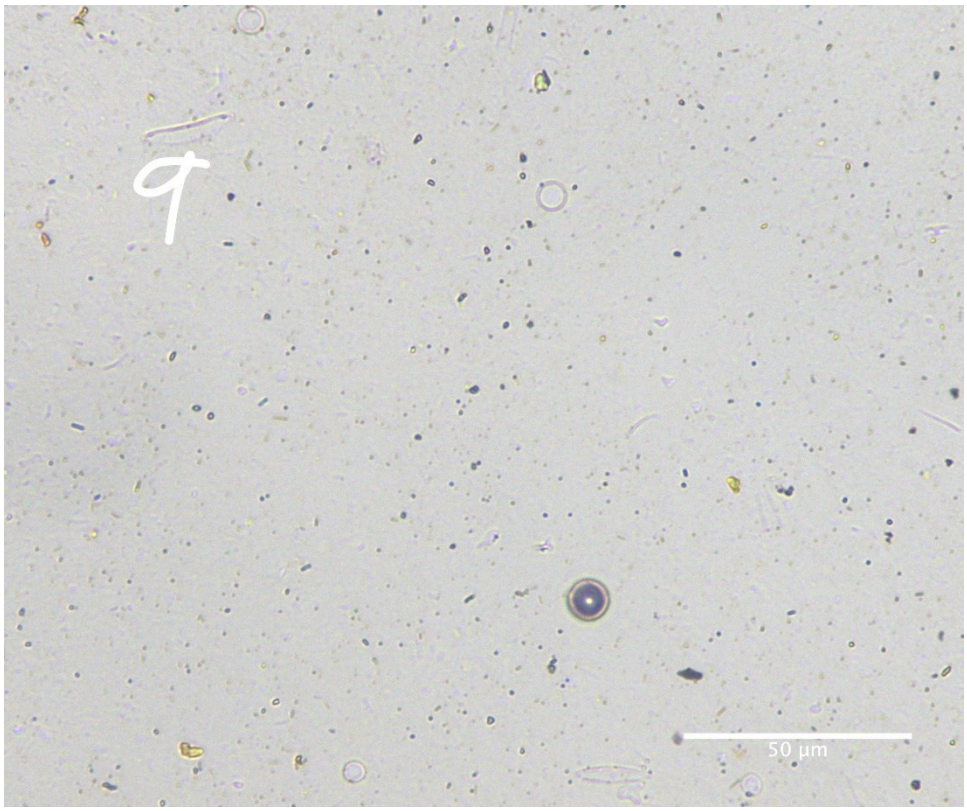


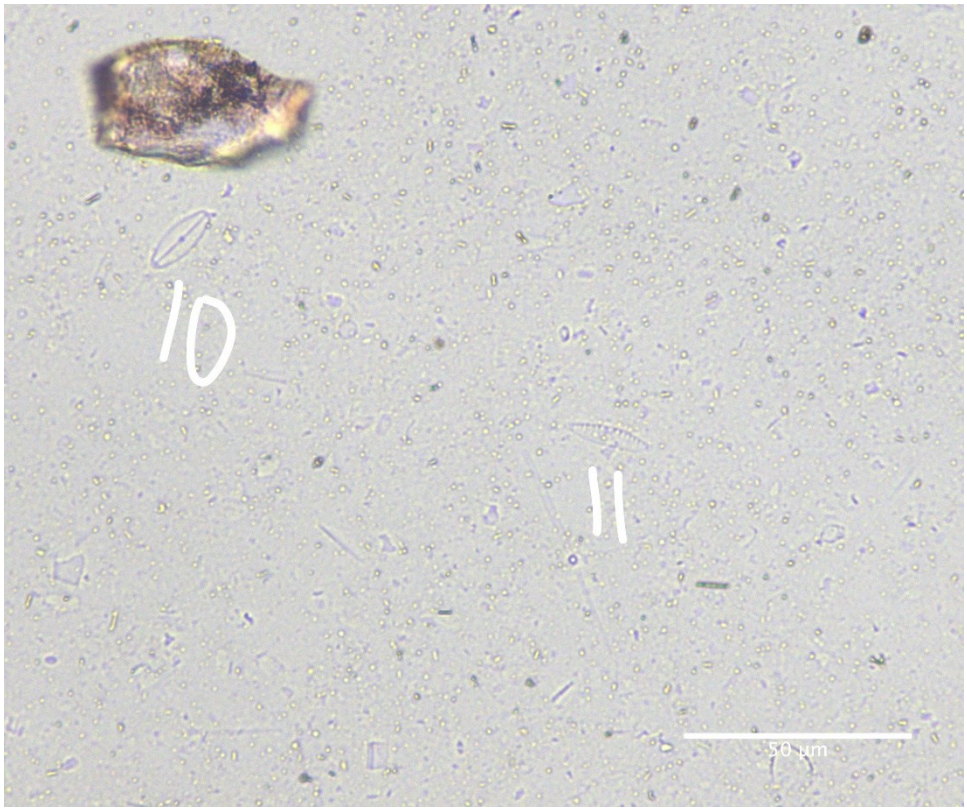

30-35 cm downcore

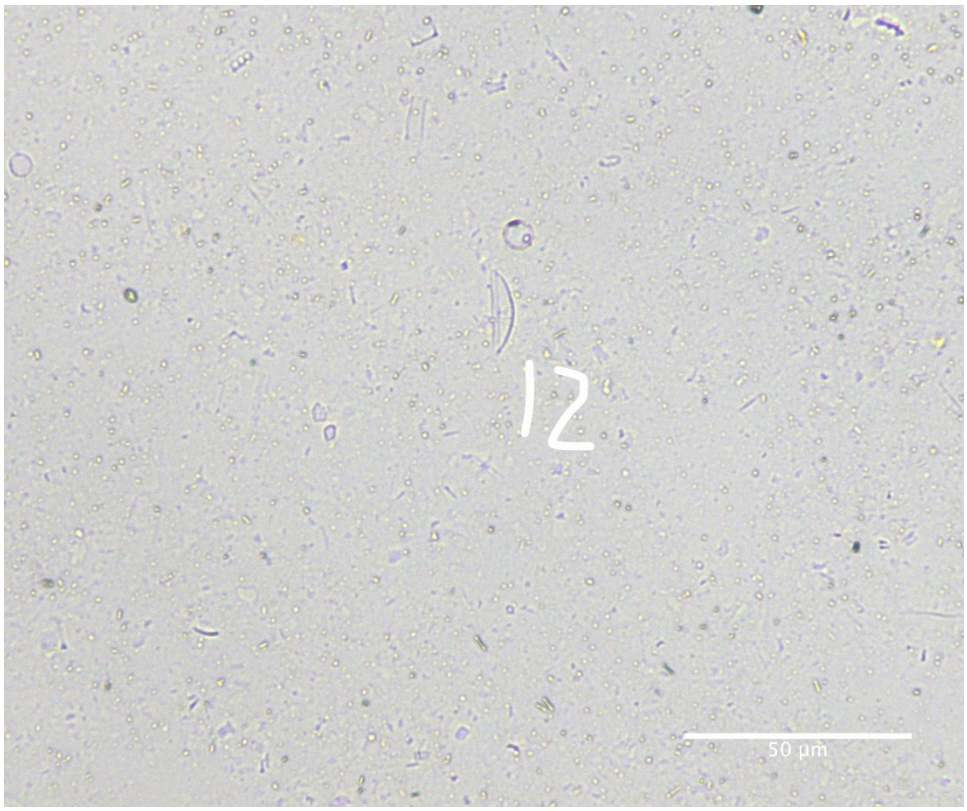


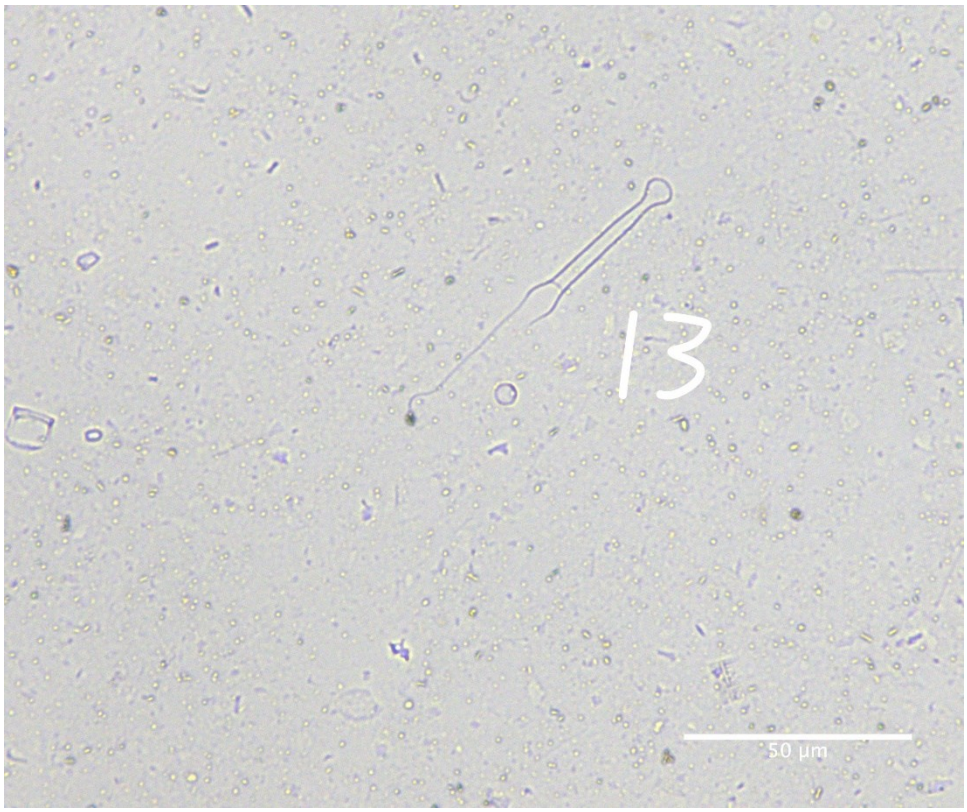

30-35 cm downcore

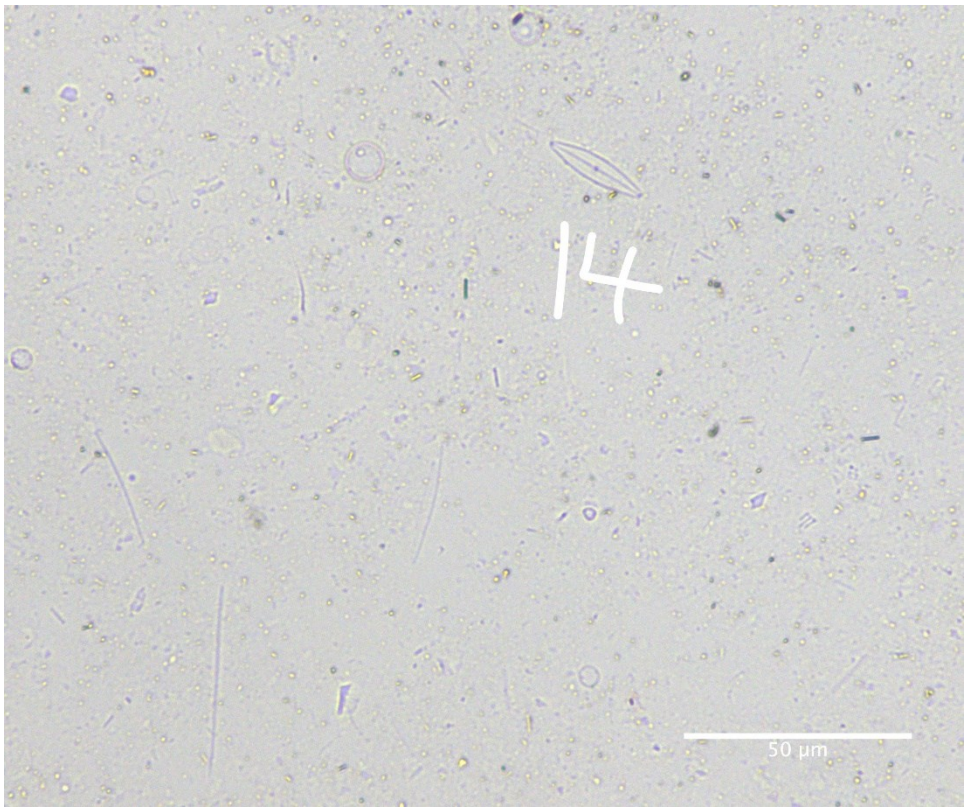


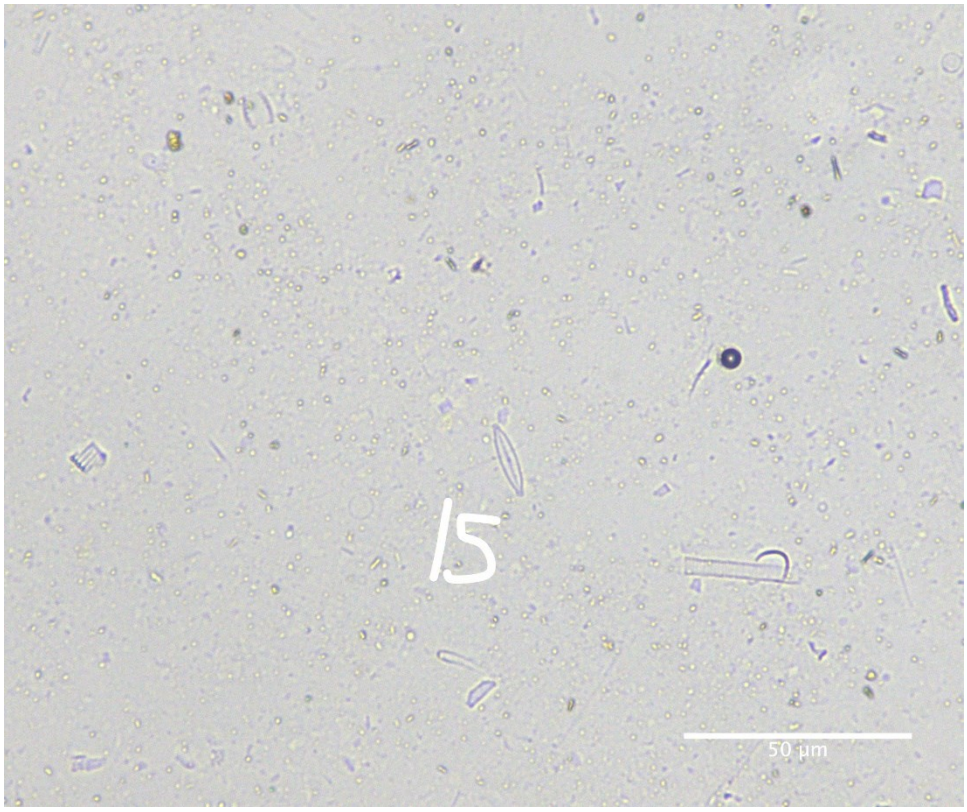

30-35 cm downcore

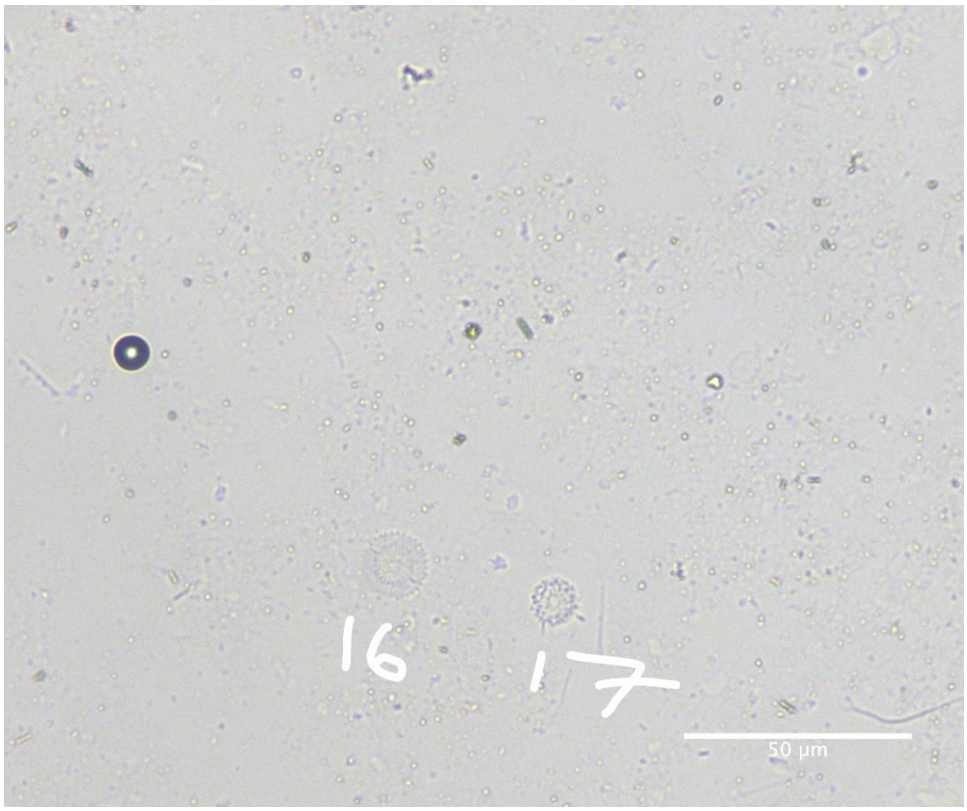


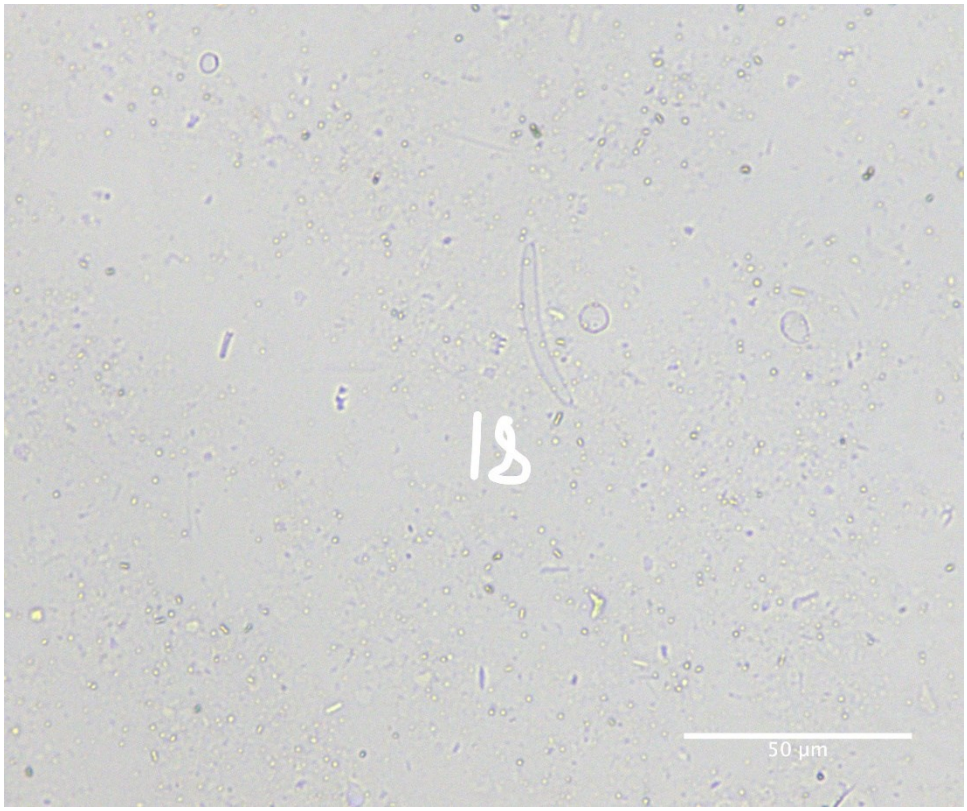

30-35 cm downcore

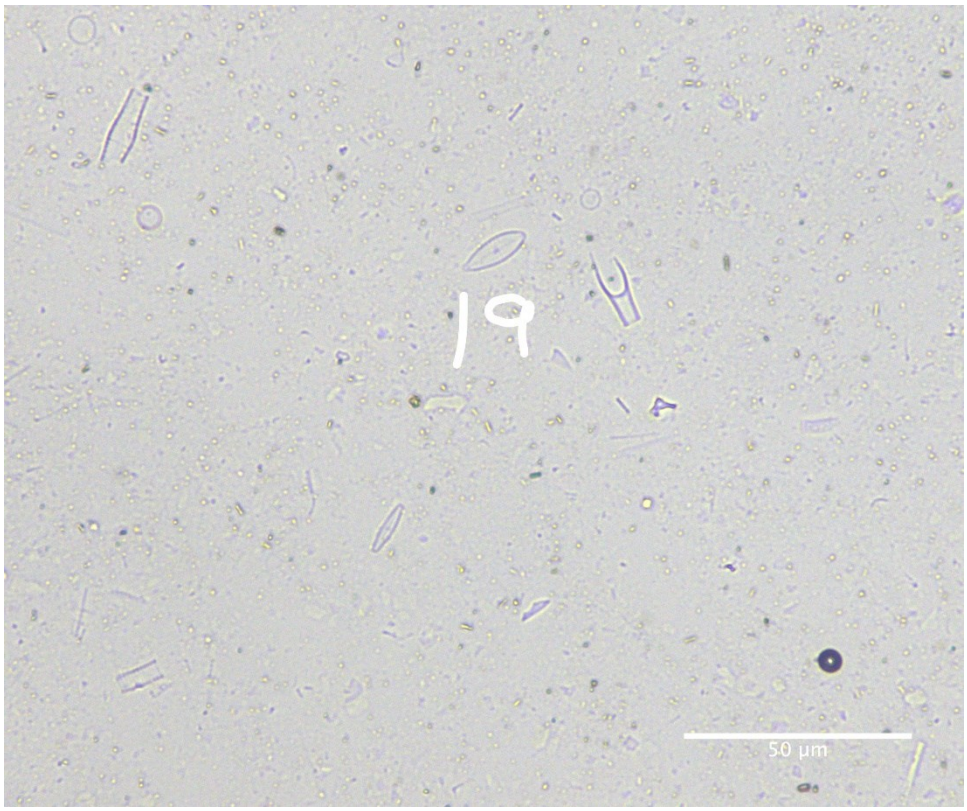


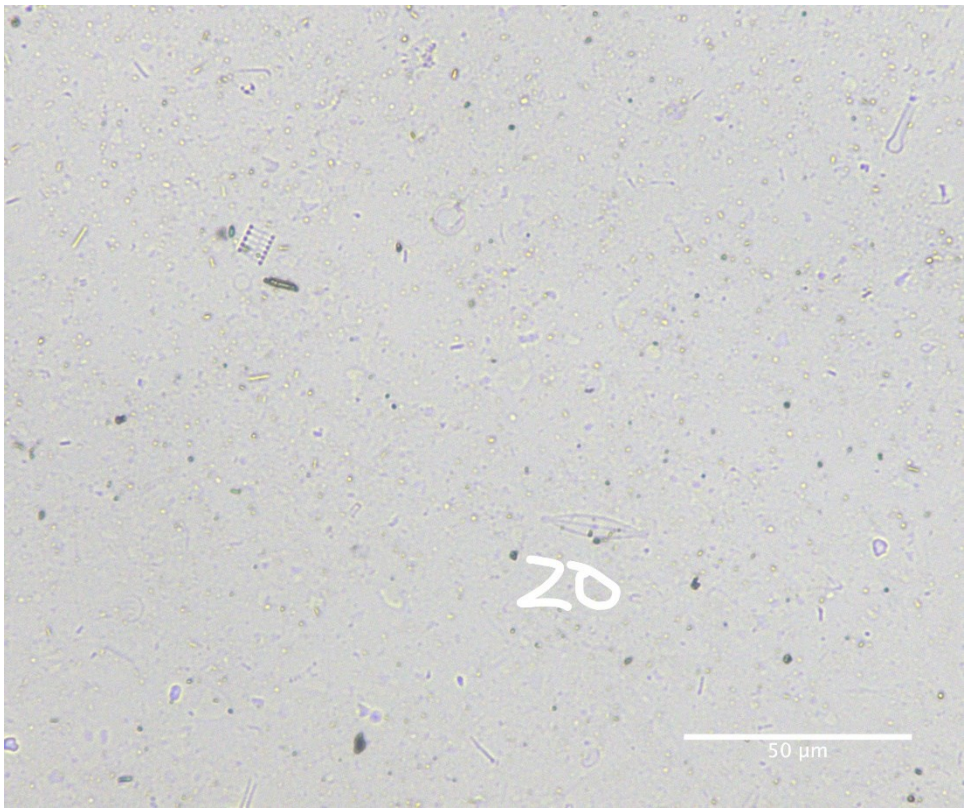

30-35 cm downcore

| Diatom ID | Taxon | Diatom ID | Taxon |
|---|---|---|---|
| 1 | *Achnanthidium* sp. | 11 | *Nitzschia* sp. |
| 2 | *Tabellaria* sp. | 12 | *Cymbella* sp. |
| 3 | *Tabellaria* sp. | 13 | *Tabellaria* sp. |
| 4 | *Cyclotella* sp. | 14 | *Navicula* sp. |
| 5 | *Nitzschia* sp. | 15 | *Achnanthidium* sp. |
| 6 | *Gomphonema* sp. | 16 | *Cyclotella* sp. |
| 7 | *Eunotia* sp. | 17 | *Cyclotella* sp. |
| 8 | *Gomphonema* sp. | 18 | *Eunotia* sp. |
| 9 | *Eunotia* sp. | 19 | *Gomphonema* sp. |
| 10 | *Navicula* sp. | 20 | *Navicula* sp. |

35-40 cm downcore

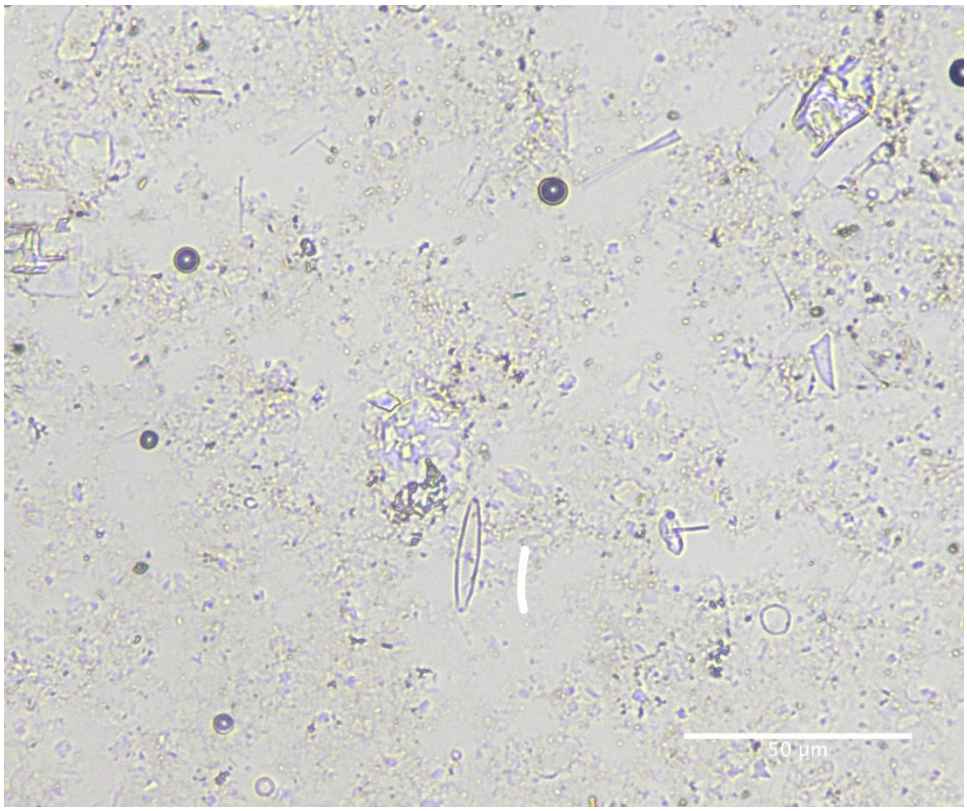


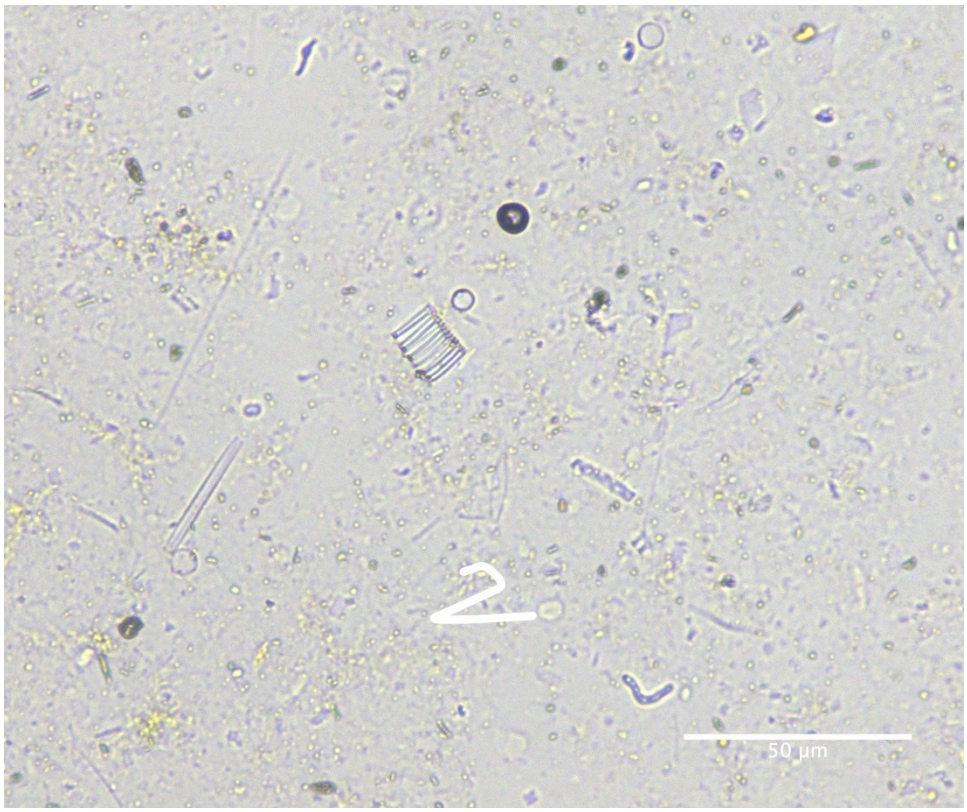

35-40 cm downcore

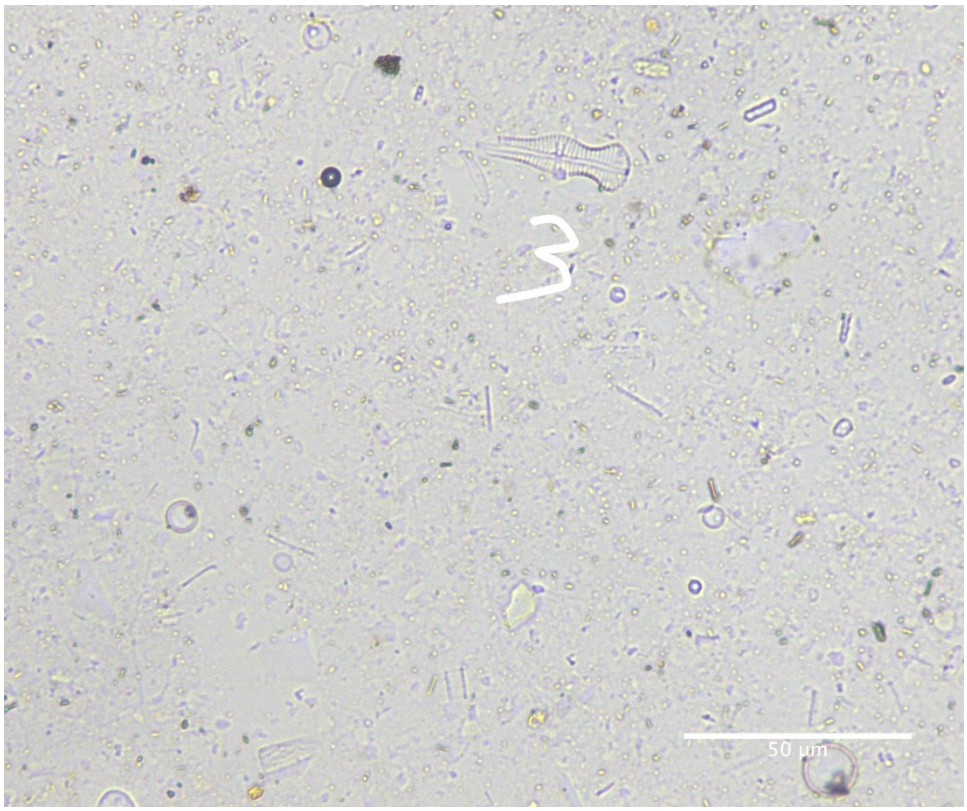


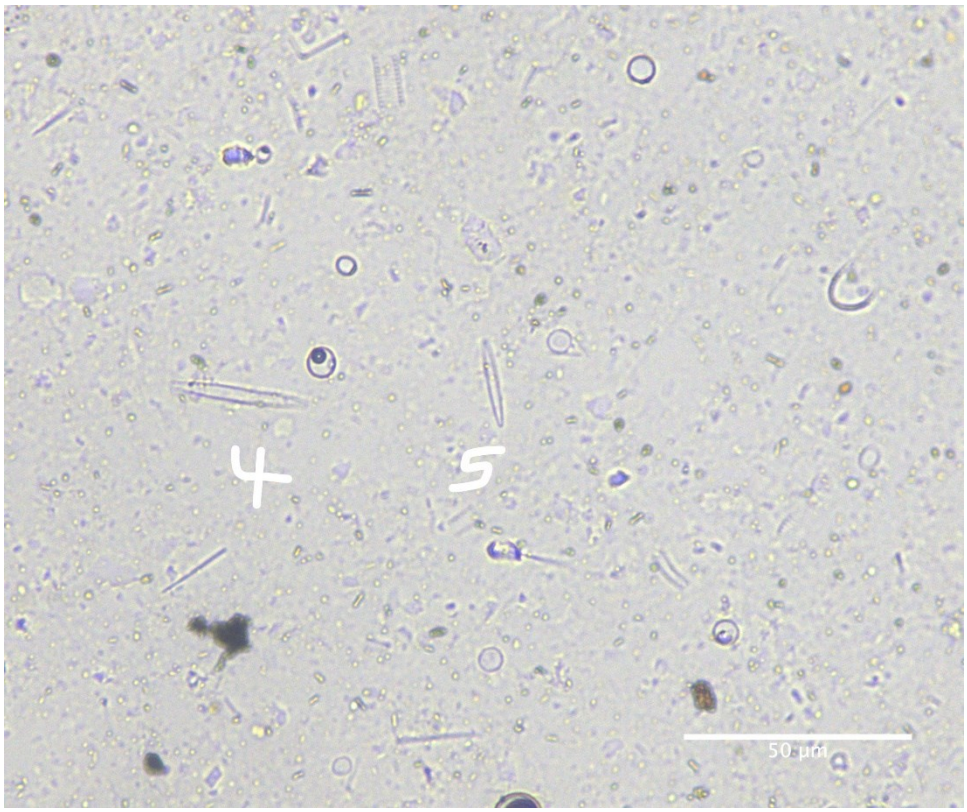

35-40 cm downcore

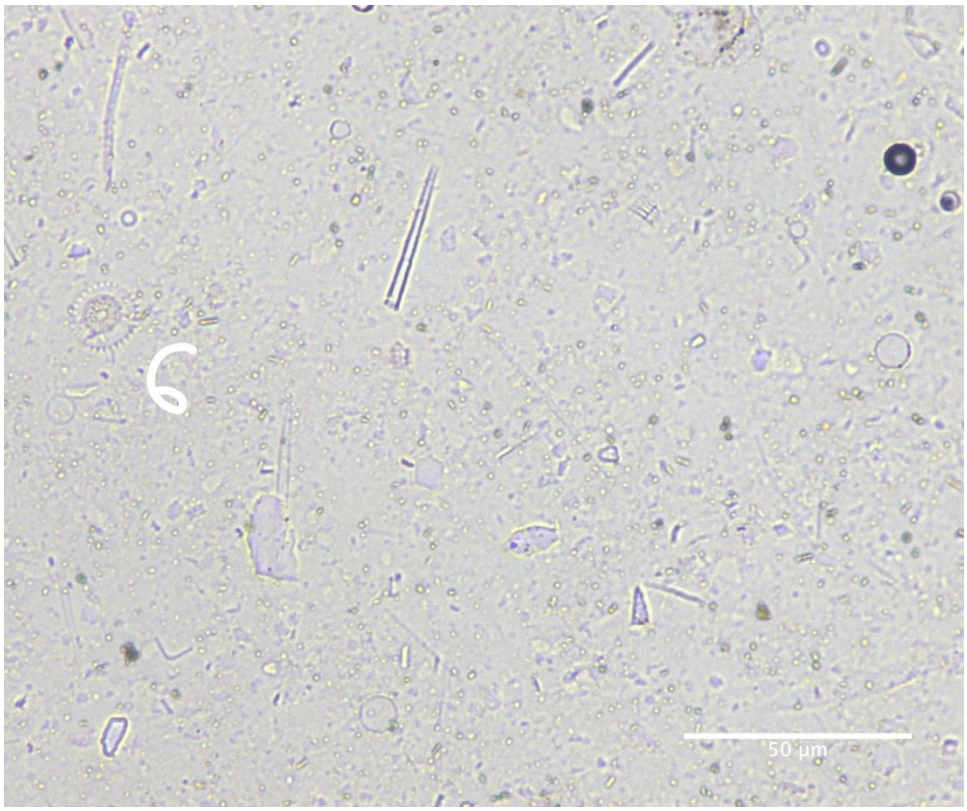


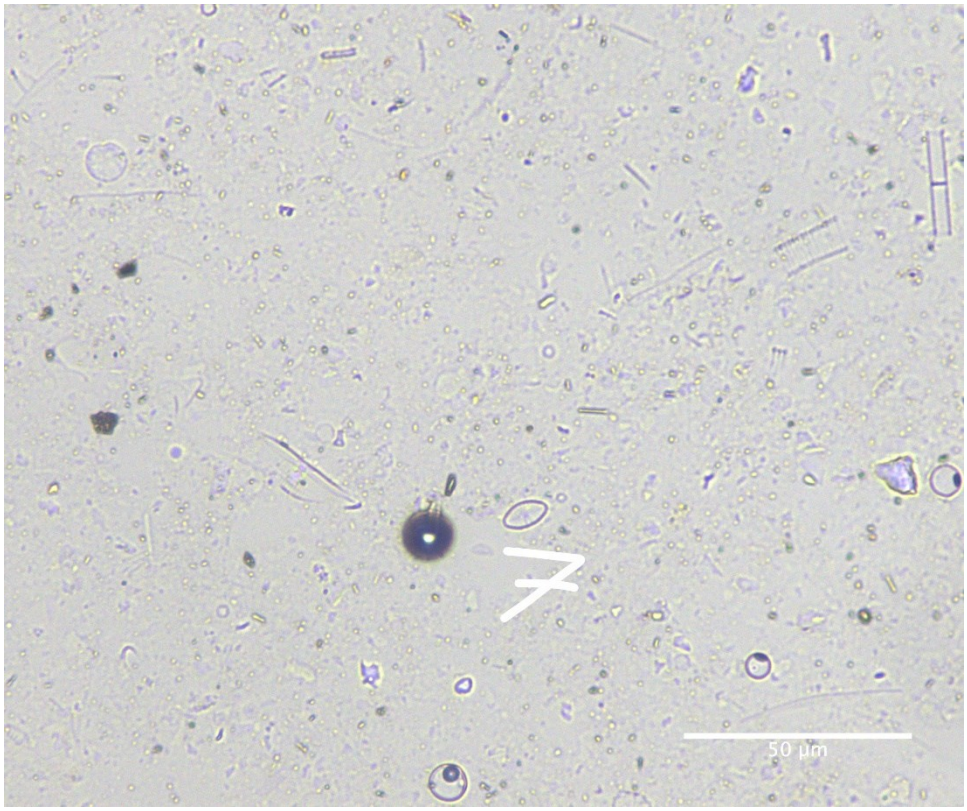

35-40 cm downcore

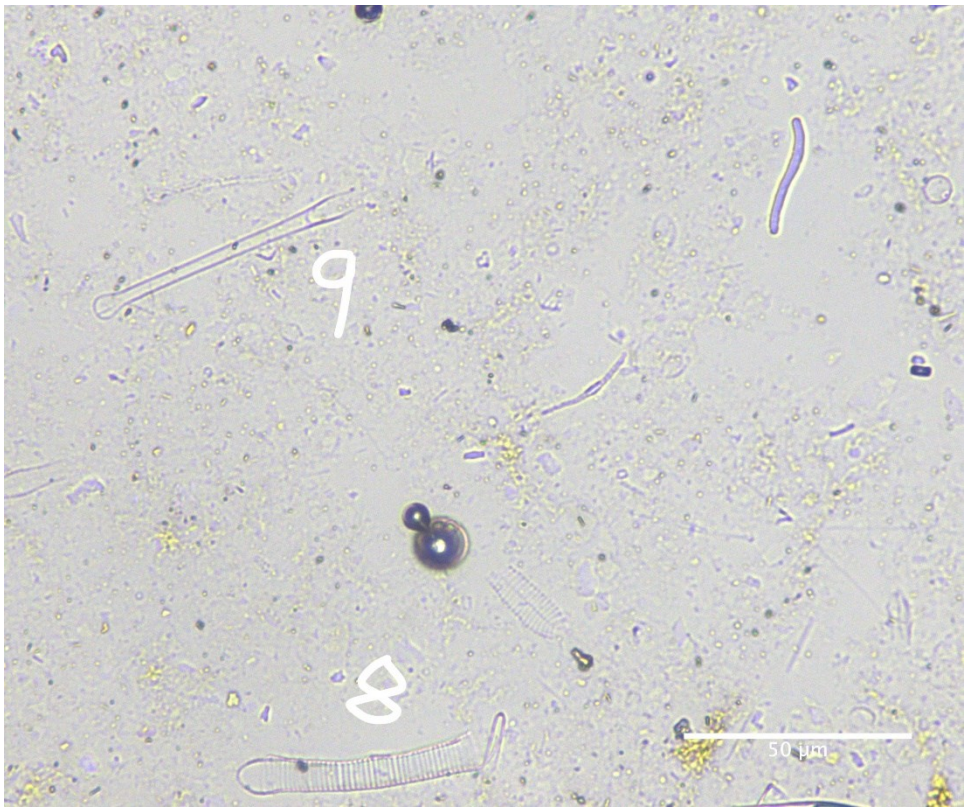


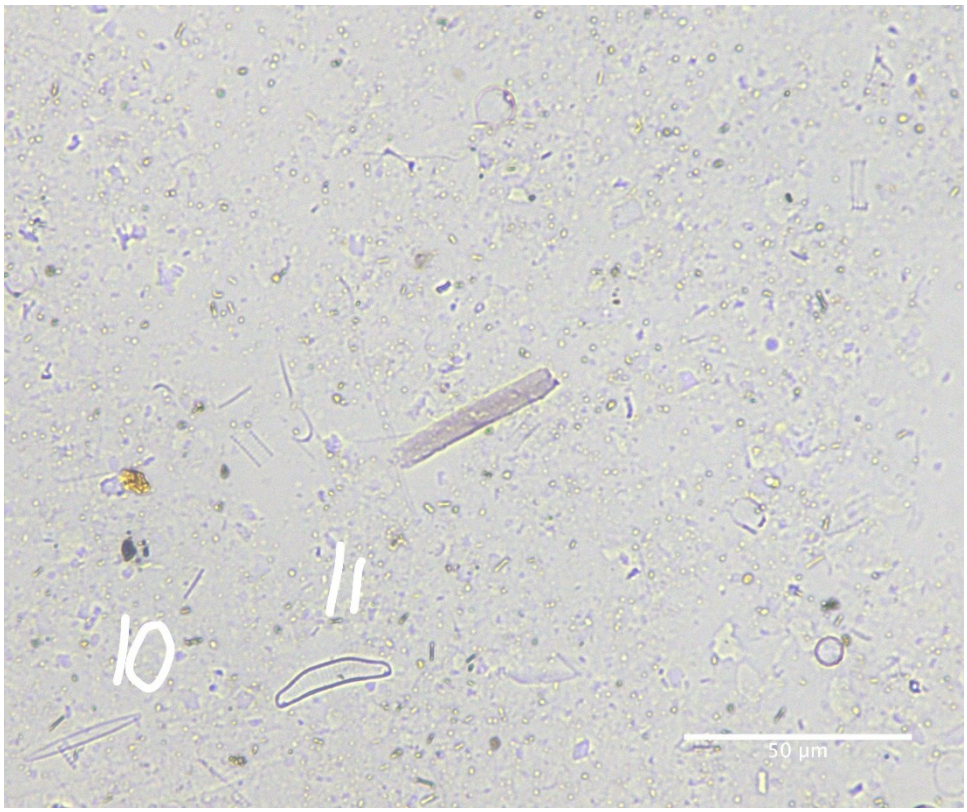

35-40 cm downcore

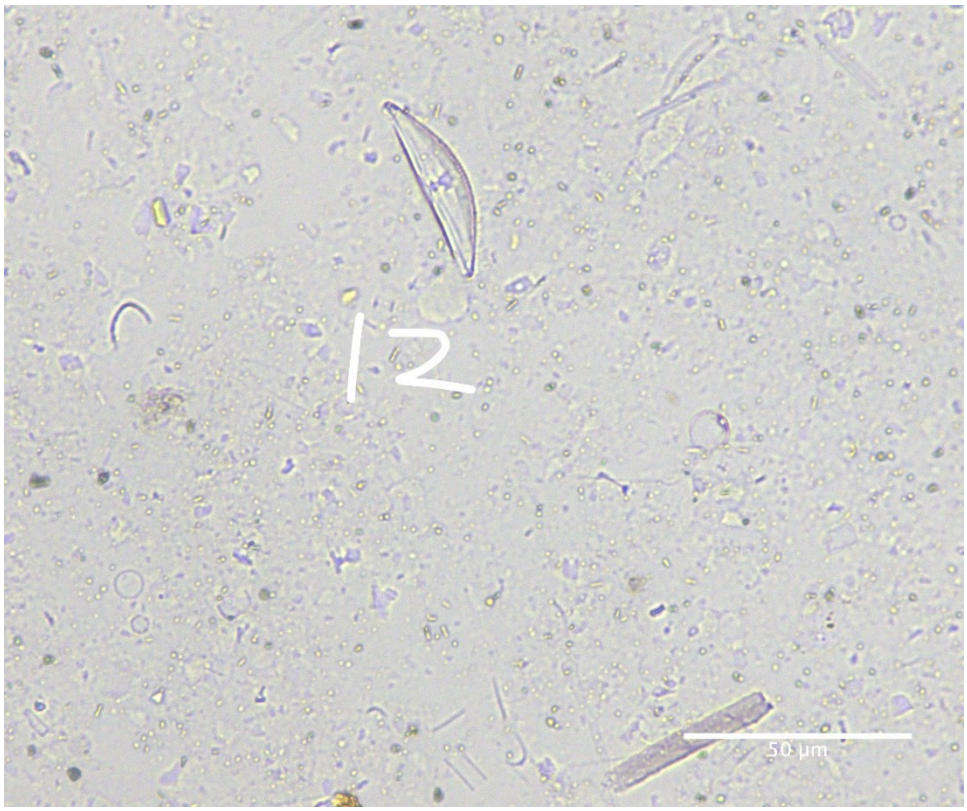


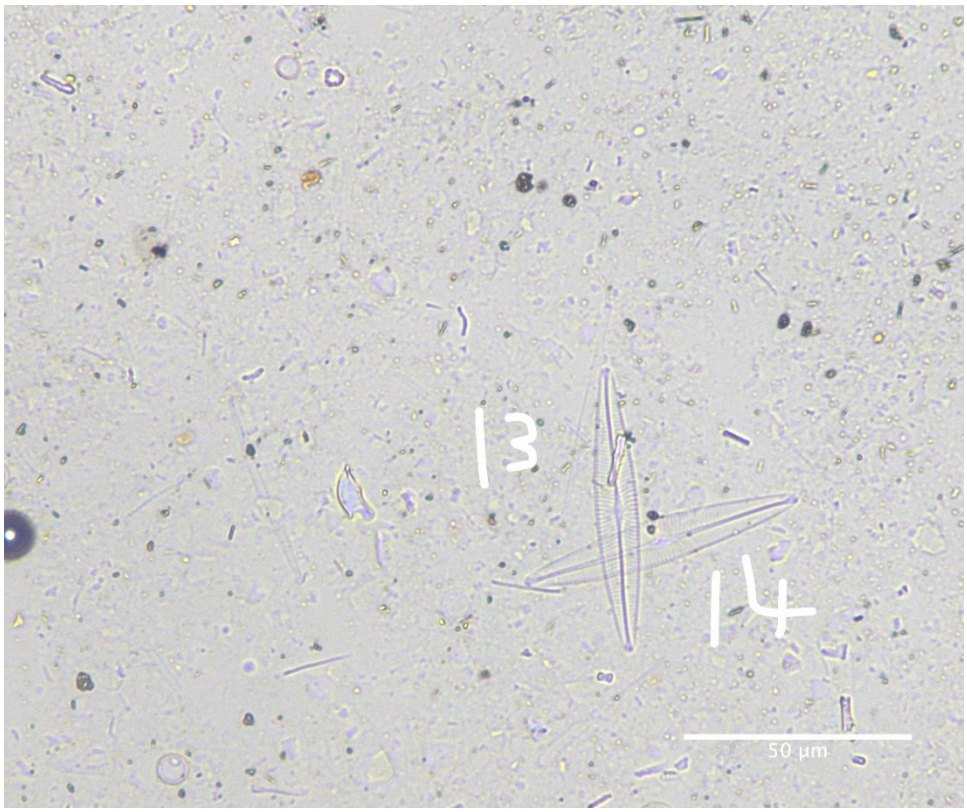

35-40 cm downcore

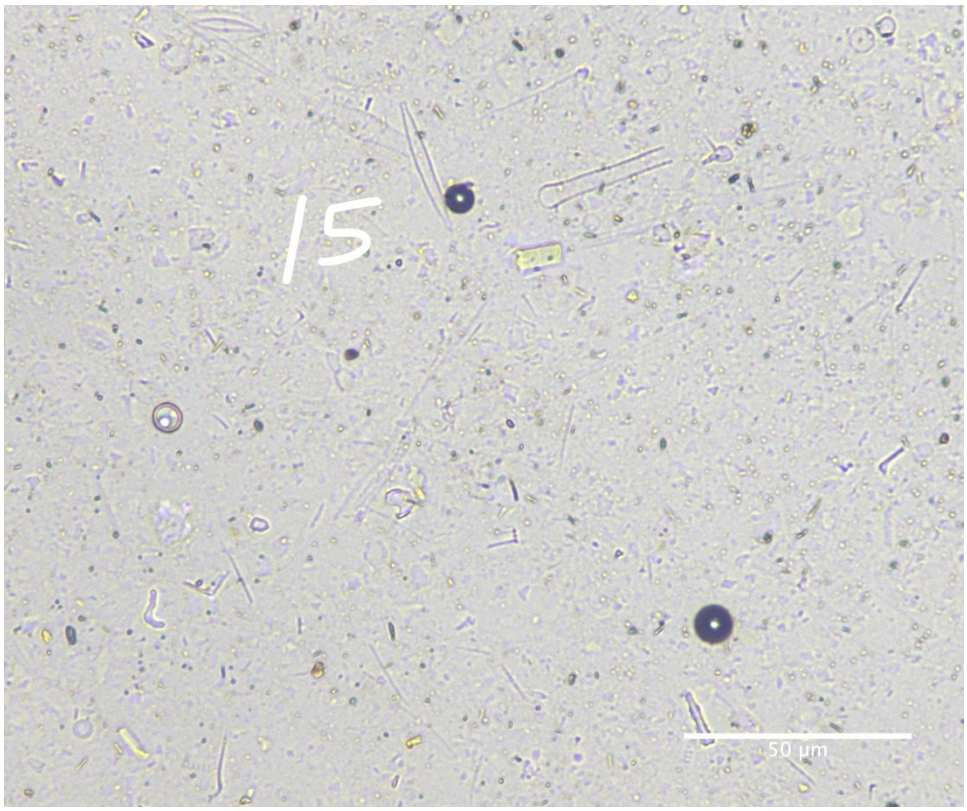


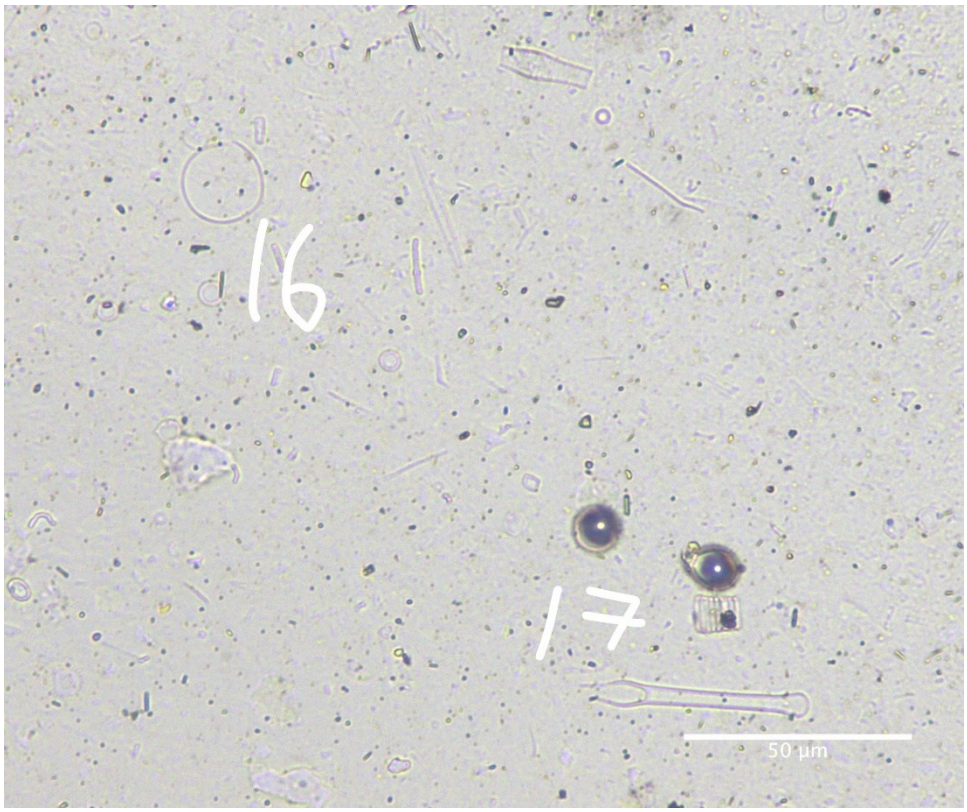

35-40 cm downcore

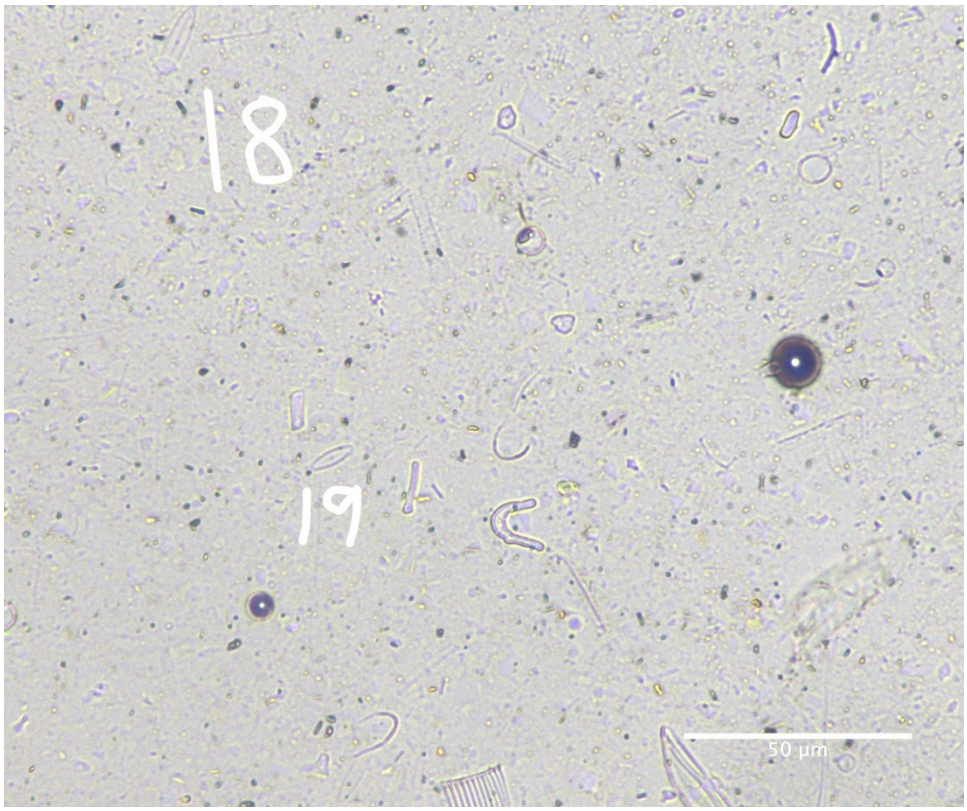


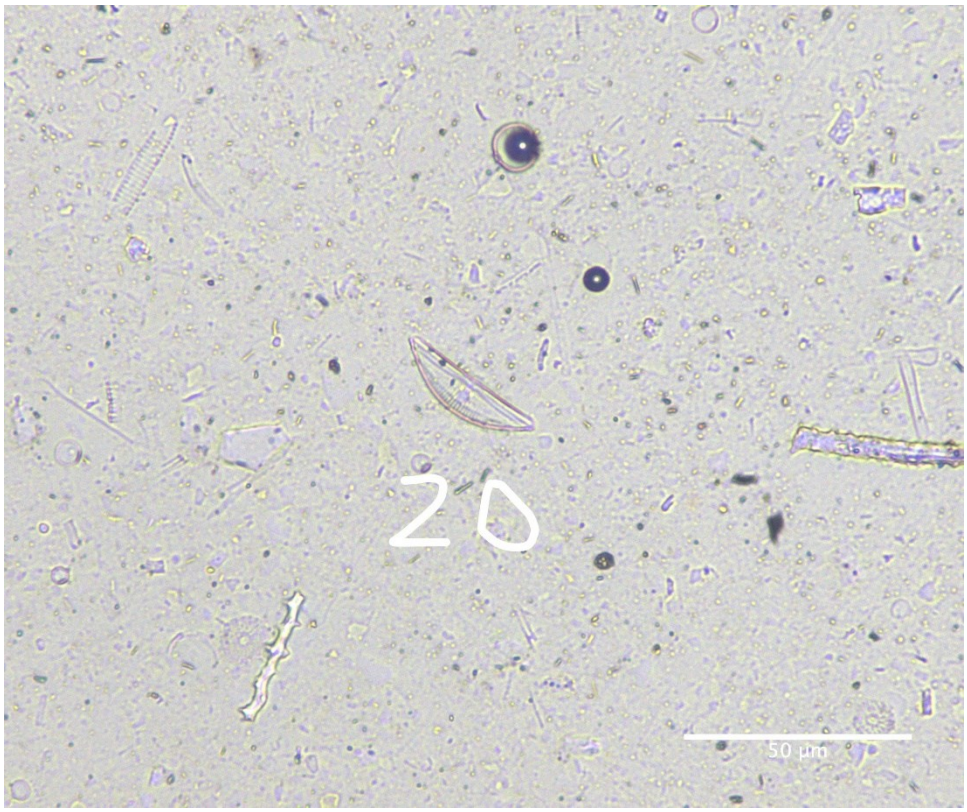

35-40 cm downcore

| Diatom ID | Taxon | Diatom ID | Taxon |
|---|---|---|---|
| 1 | *Gomphonema* sp. | 11 | *Eunotia* sp. |
| 2 | *Gomphonema* sp. | 12 | *Cymbella* sp. |
| 3 | *Gomphonema* sp. | 13 | *Navicula* sp. |
| 4 | *Nitzschia* sp. | 14 | *Navicula* sp. |
| 5 | *Nitzschia* sp. | 15 | *Nitzschia* sp. |
| 6 | *Cyclotella* sp. | 16 | *Thalassiosira* sp. |
| 7 | *Achnanthidium* sp. | 17 | *Tabellaria* sp. |
| 8 | *Eunotia* sp. | 18 | *Navicula* sp. |
| 9 | *Tabellaria* sp. | 19 | *Achnanthidium* sp. |
| 10 | *Nitzschia* sp. | 20 | *Cymbella* sp. |

40-45 cm downcore

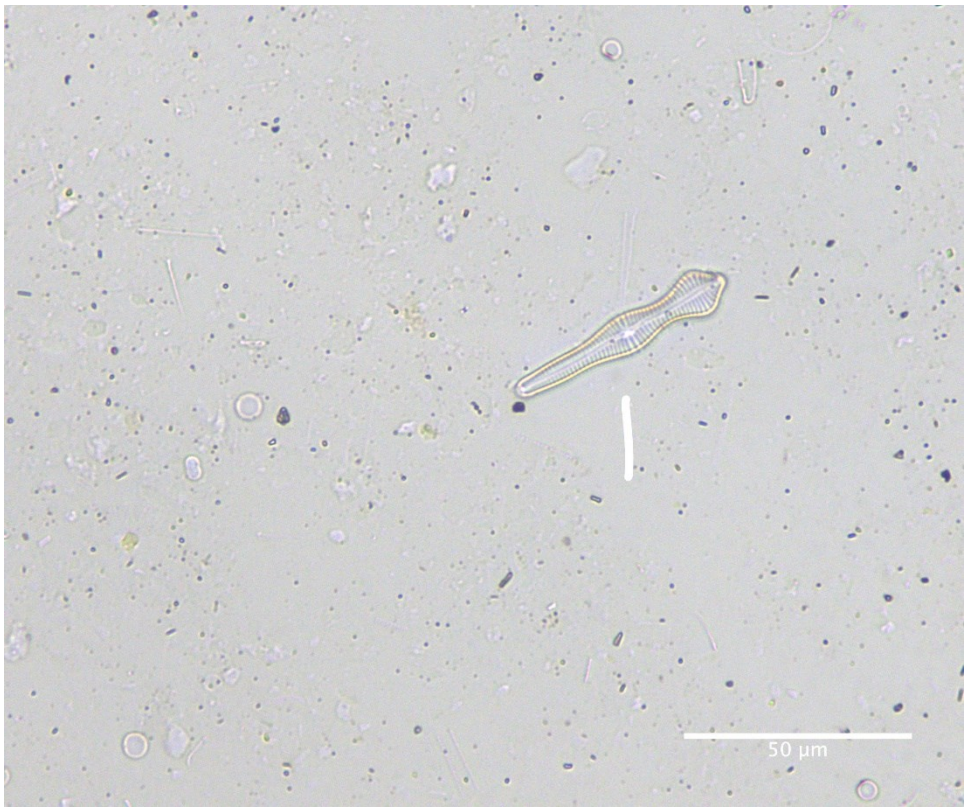


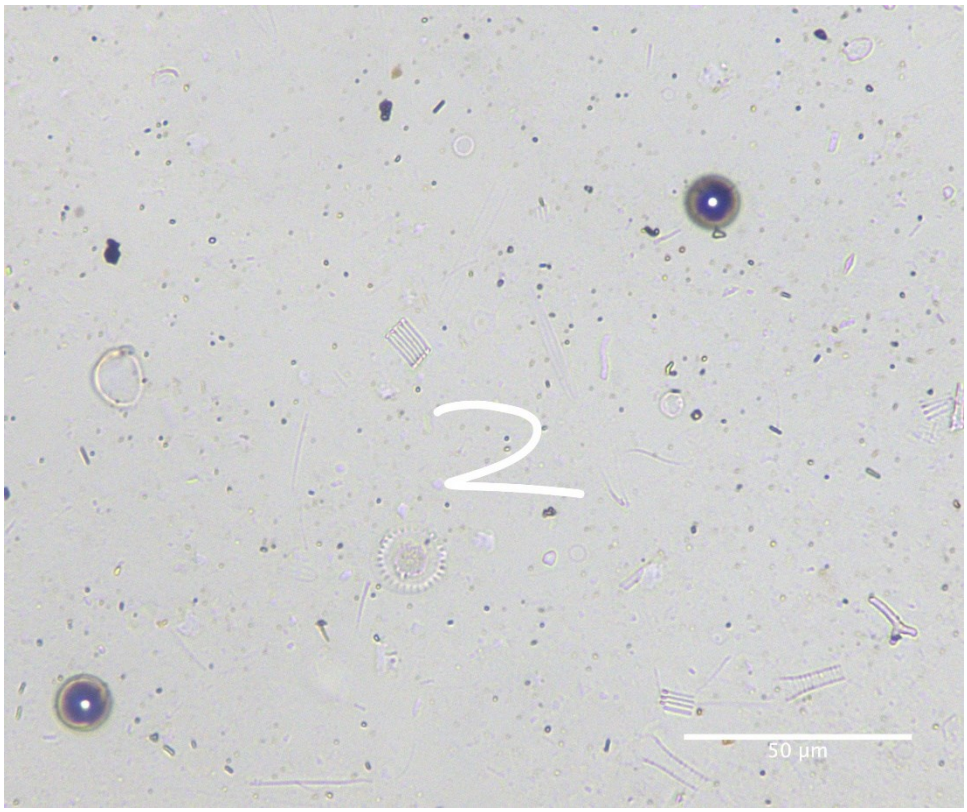

40-45 cm downcore

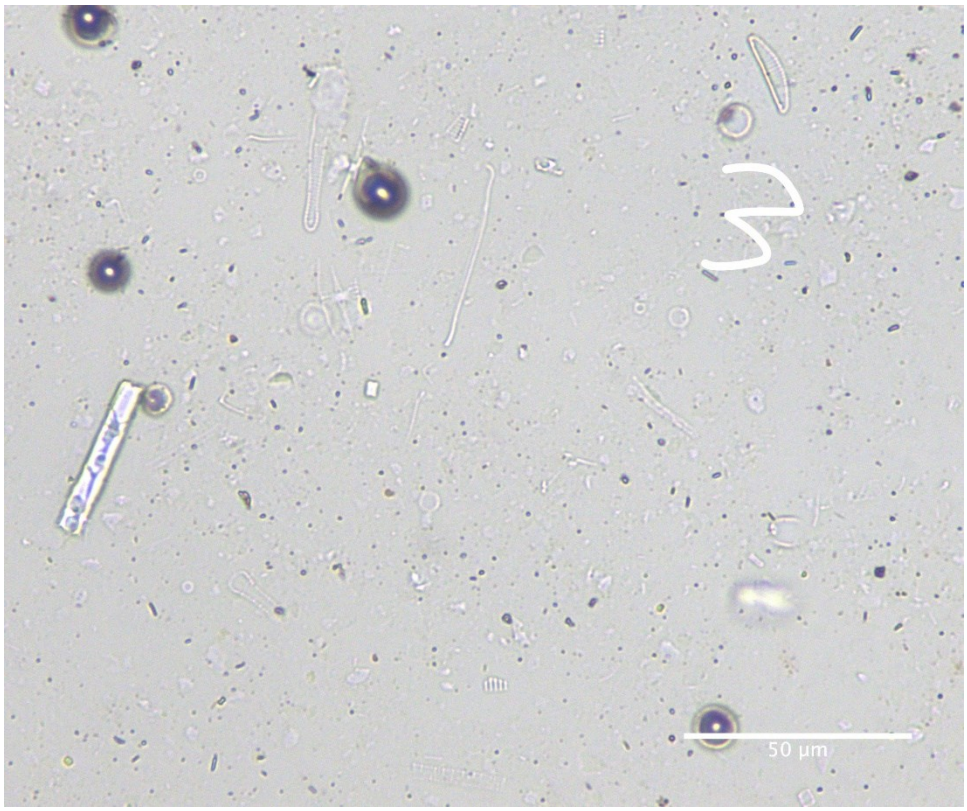


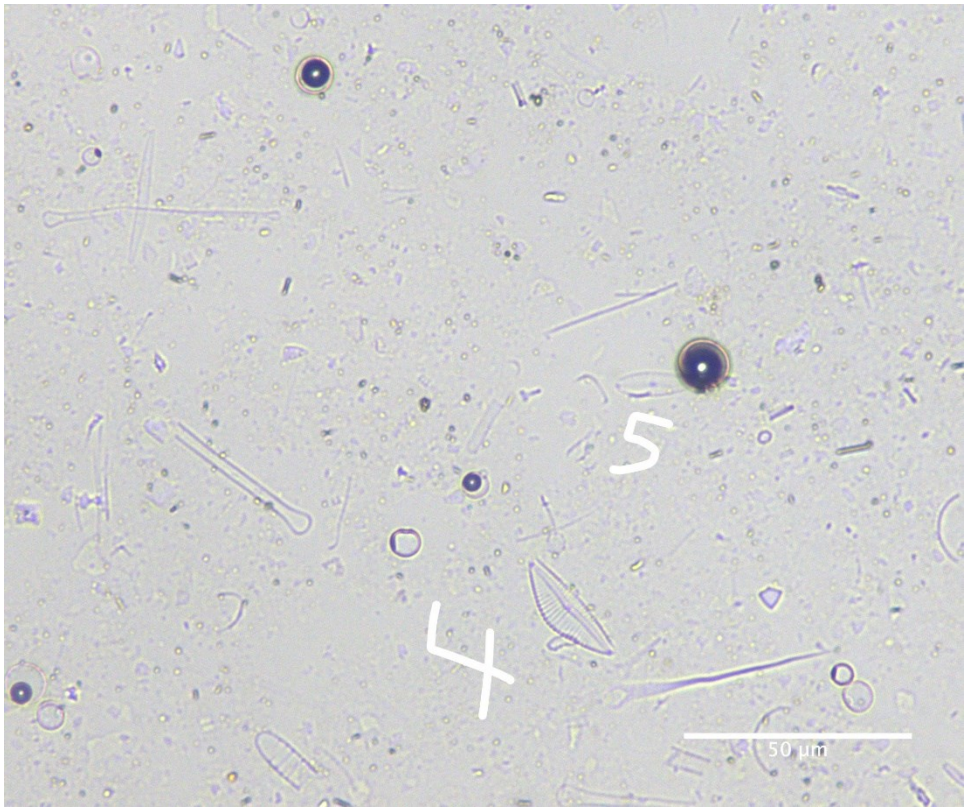

40-45 cm downcore

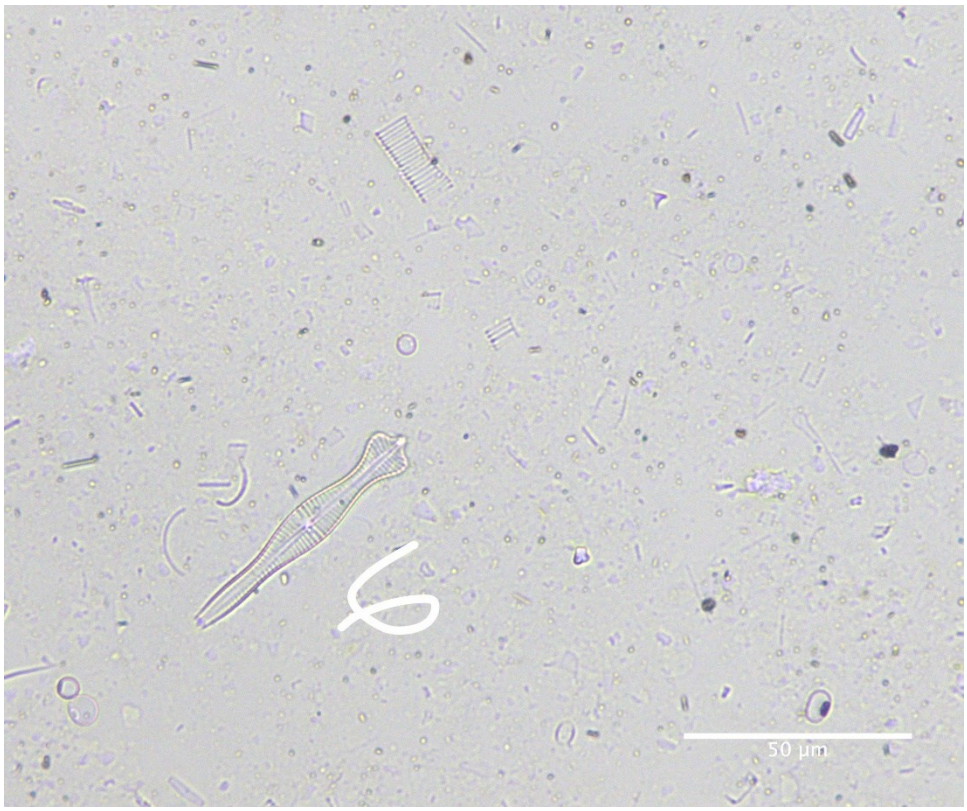


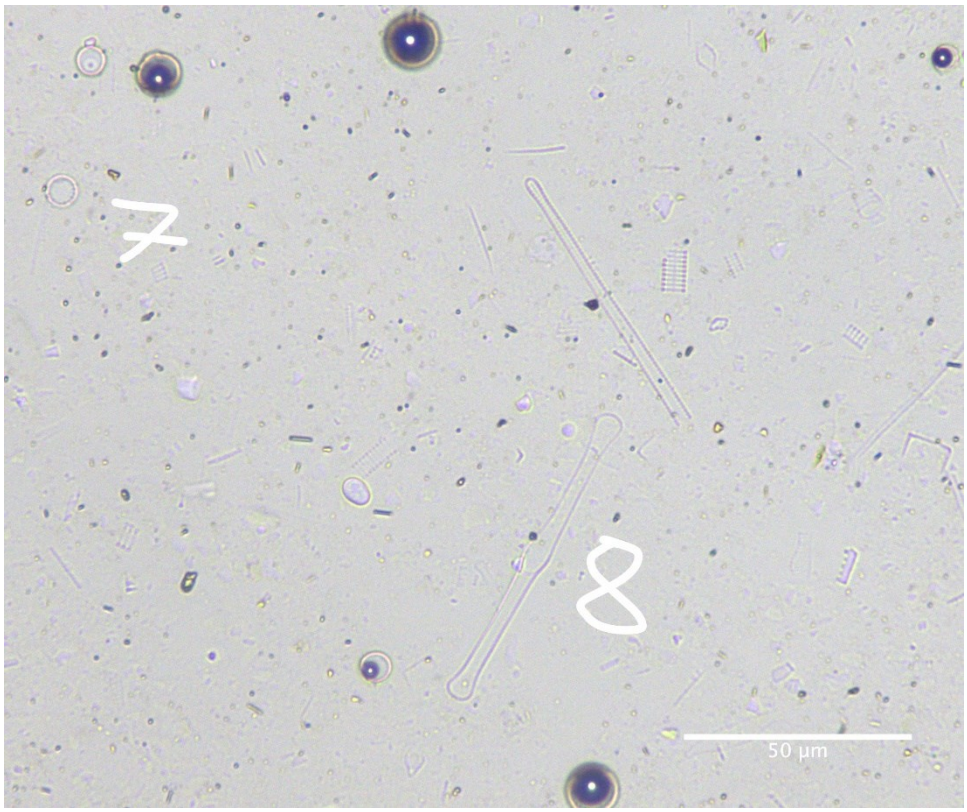

40-45 cm downcore

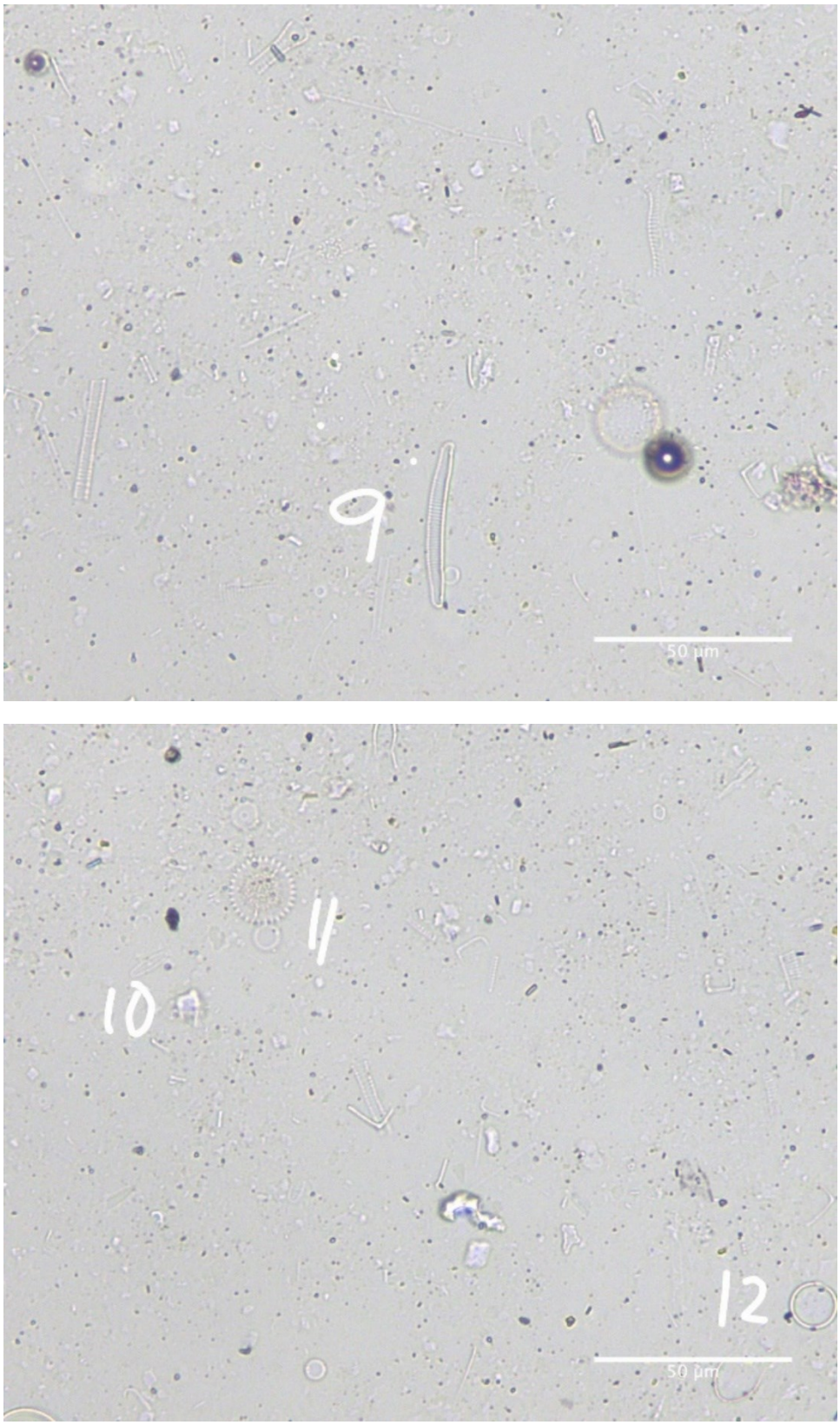

40-45 cm downcore

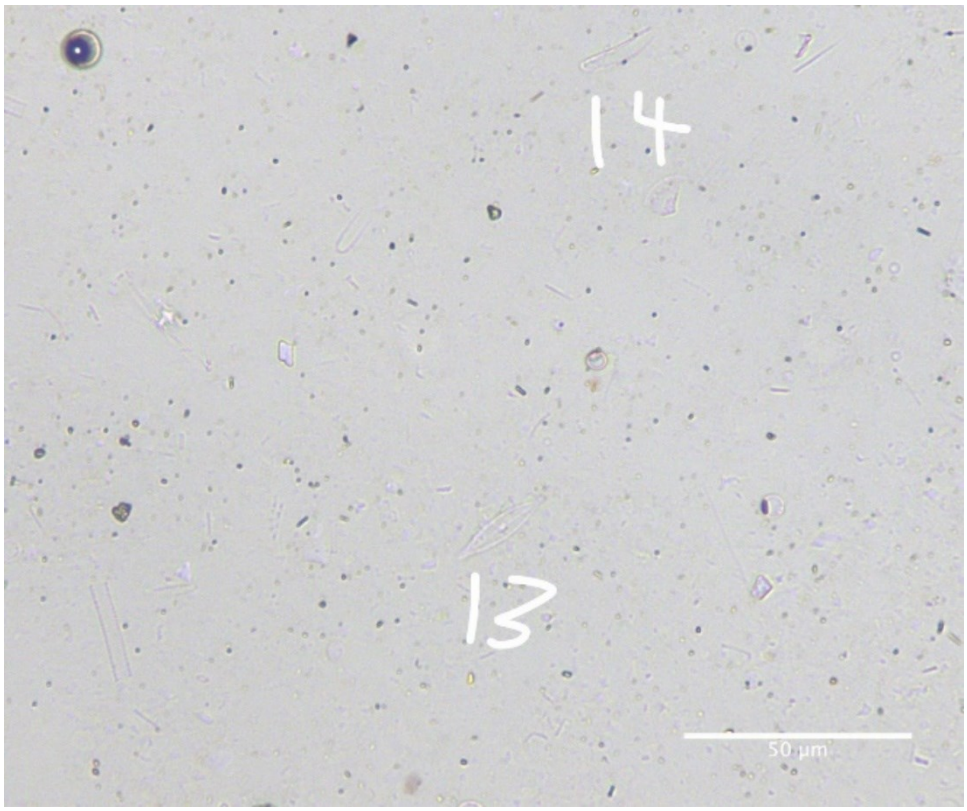


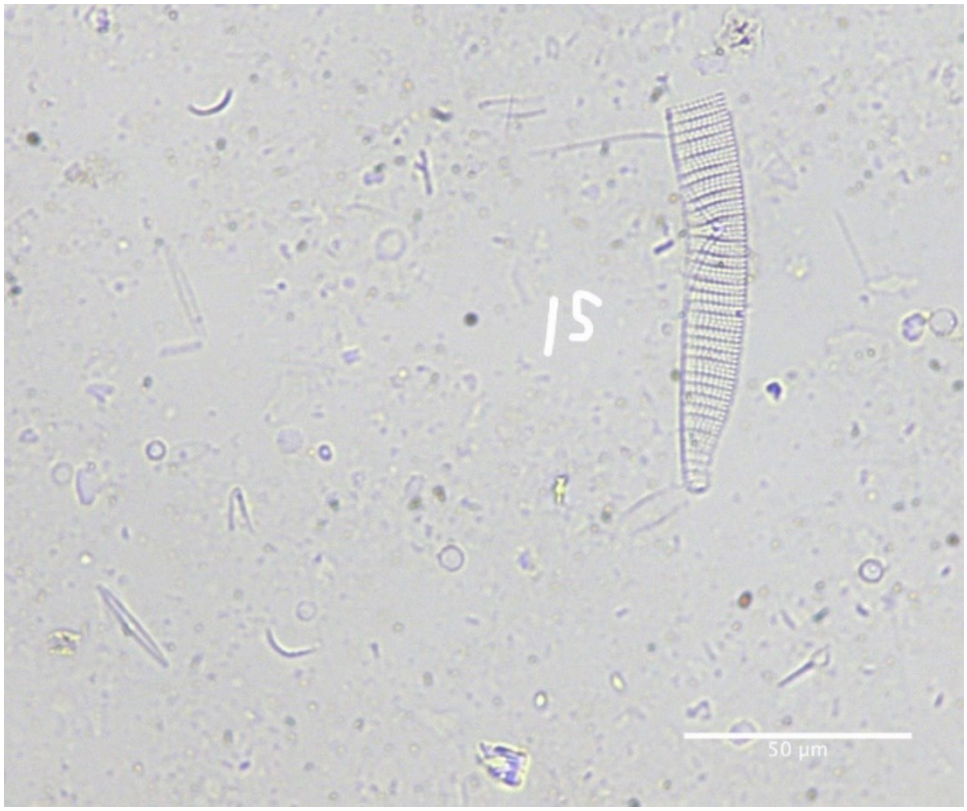

40-45 cm downcore

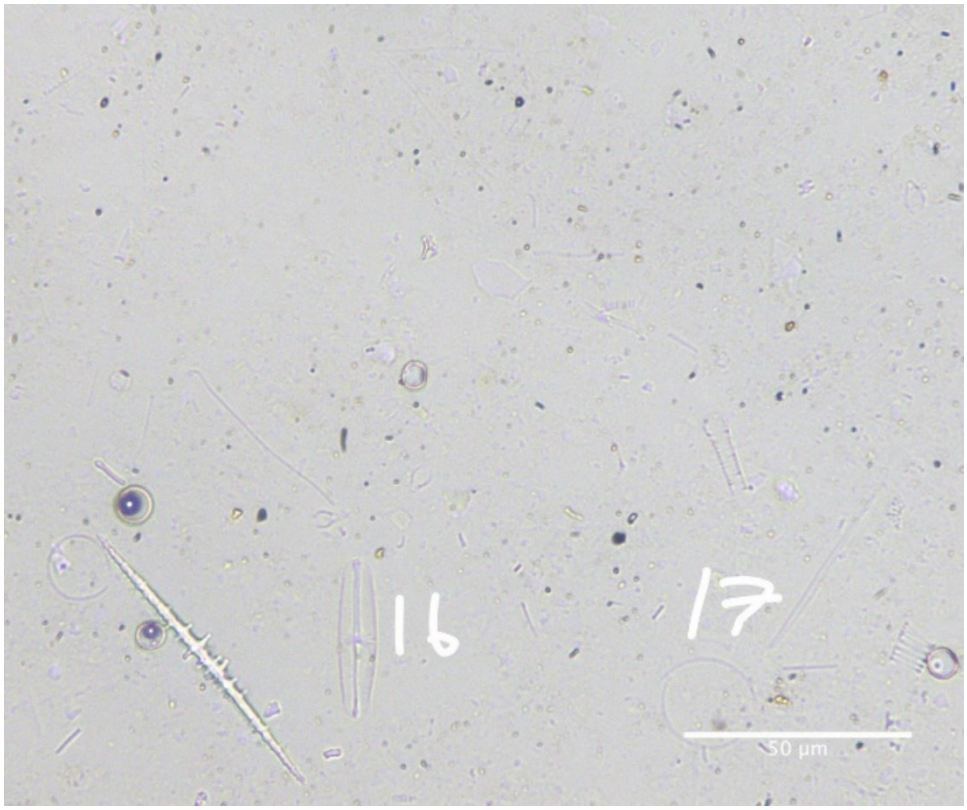


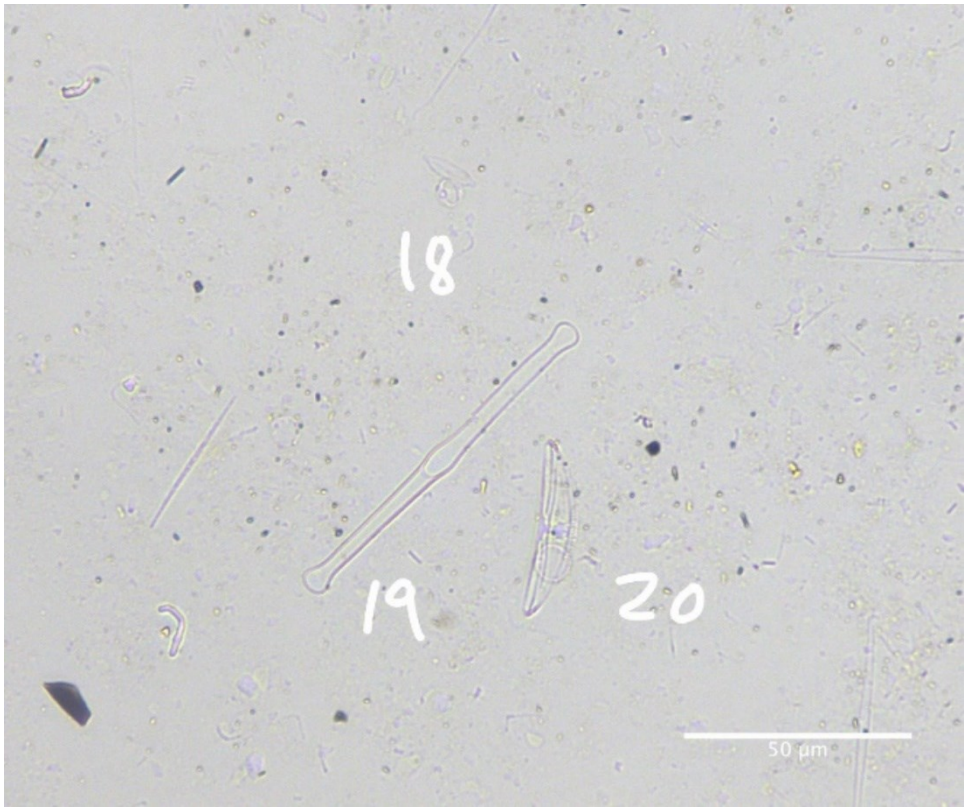

40-45 cm downcore

| Diatom ID | Taxon | Diatom ID | Taxon |
|---|---|---|---|
| 1 | *Gomphonema* sp. | 11 | *Cyclotella* sp. |
| 2 | *Cyclotella* sp. | 12 | *Thalassiosira* sp. |
| 3 | *Thalassiosira* sp. | 13 | *Navicula* sp. |
| 4 | *Cymbella* sp. | 14 | *Eunotia* sp. |
| 5 | *Gomphonema* sp. | 15 | *Epithemia* sp. |
| 6 | *Gomphonema* sp. | 16 | *Navicula* sp. |
| 7 | *Thalassiosira* sp. | 17 | *Thalassiosira* sp. |
| 8 | *Tabellaria* sp. | 18 | *Navicula* sp. |
| 9 | *Eunotia* sp. | 19 | *Tabellaria* sp. |
| 10 | *Achnanthidium* sp. | 20 | *Cymbella* sp. |

45-50 cm downcore

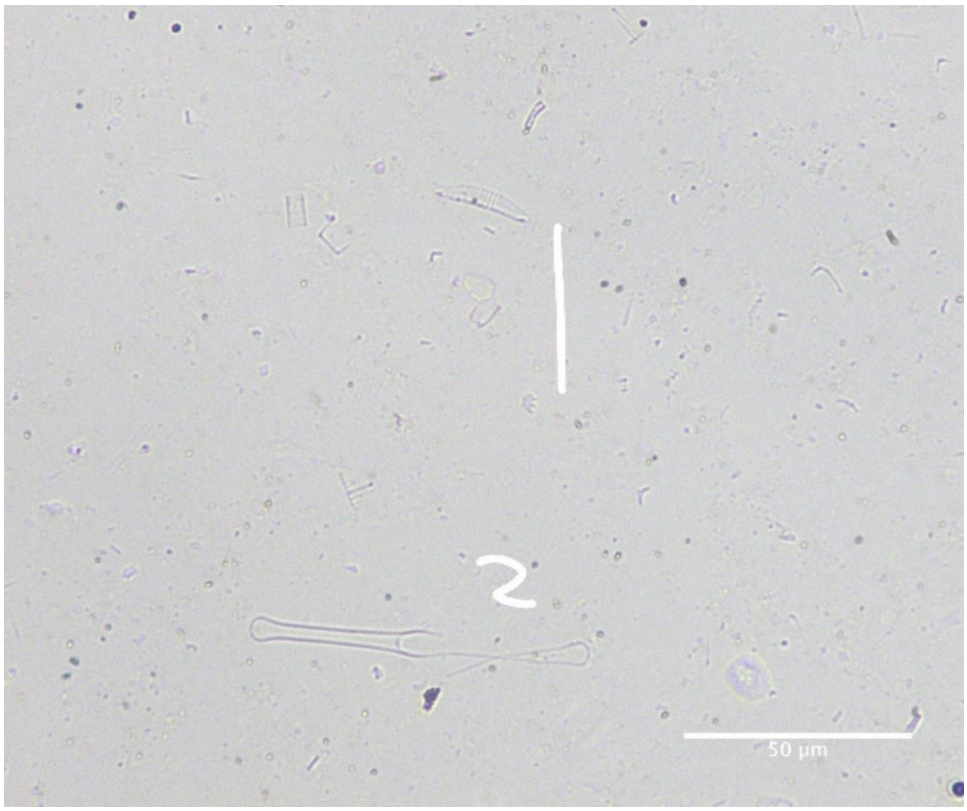


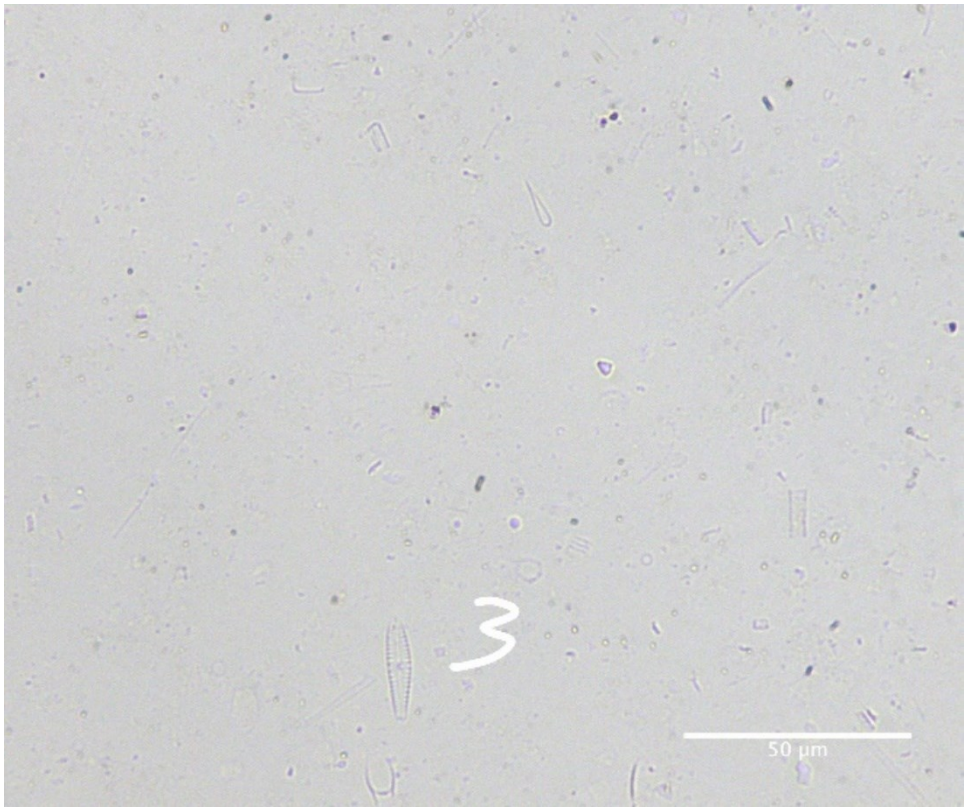

45-50 cm downcore

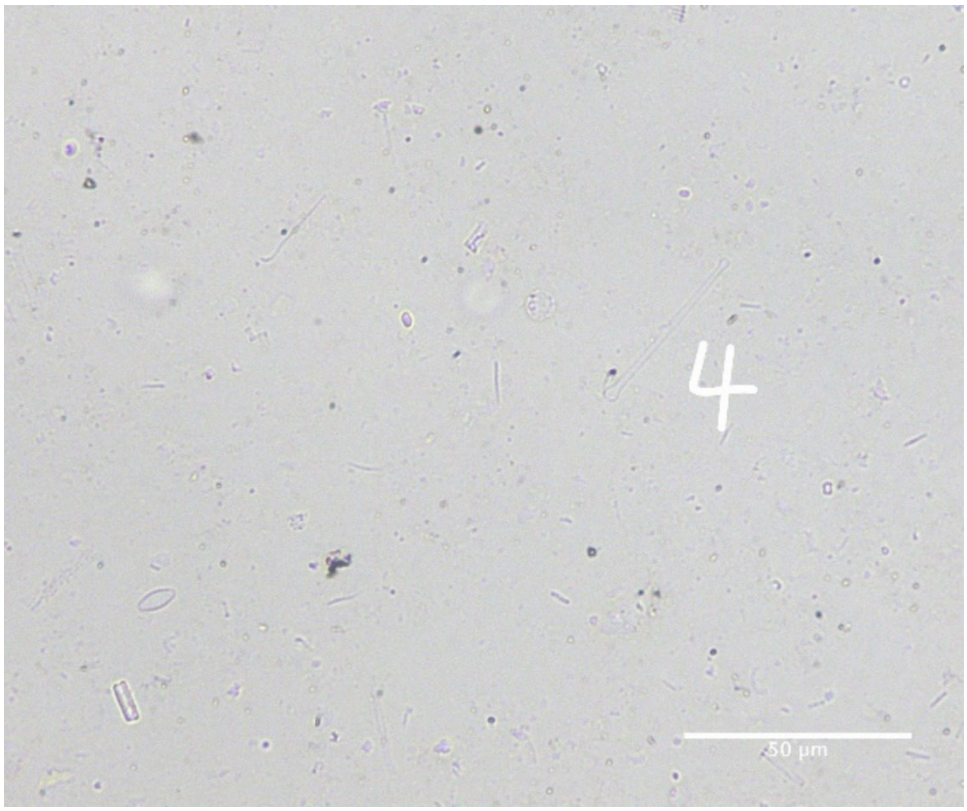


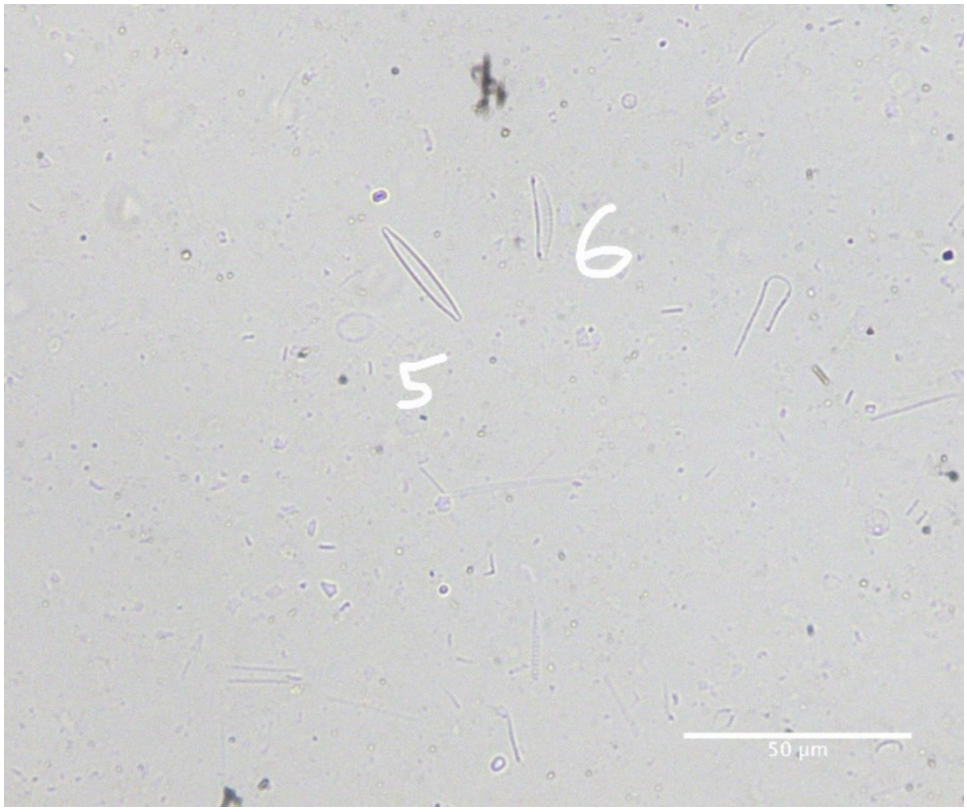

45-50 cm downcore

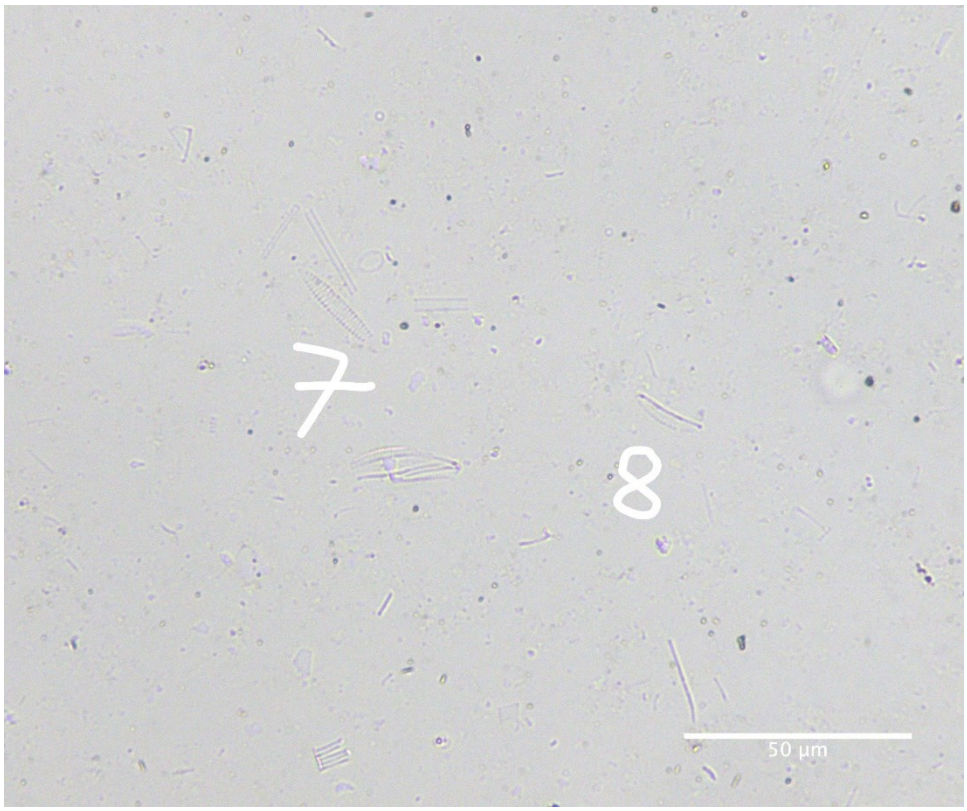


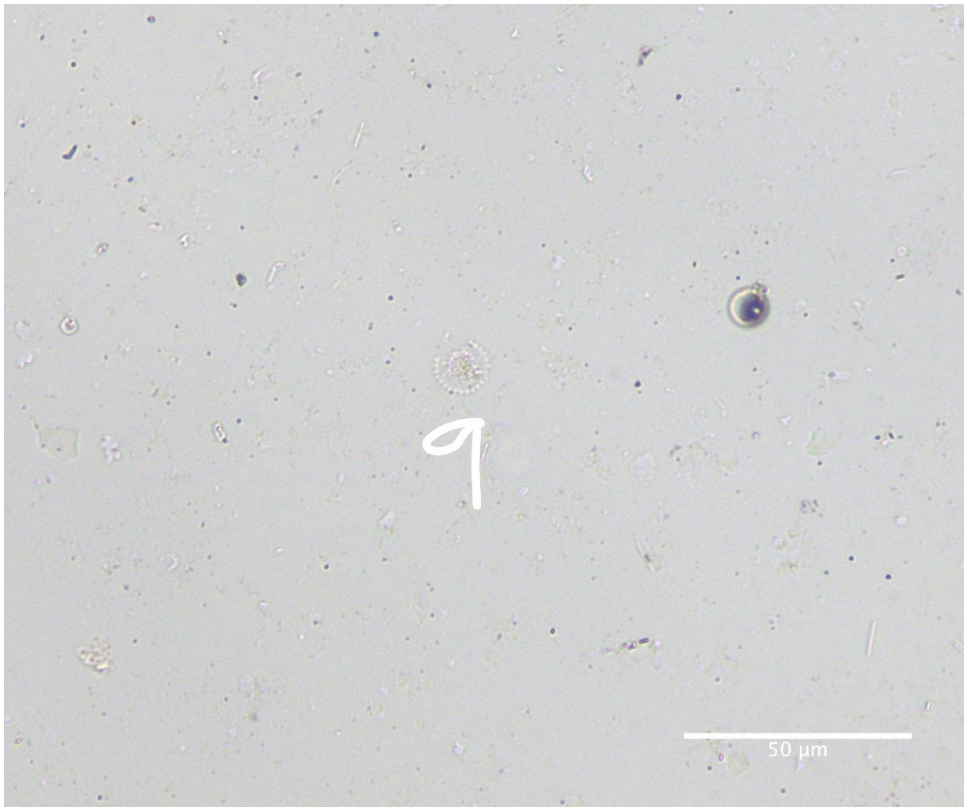

45-50 cm downcore

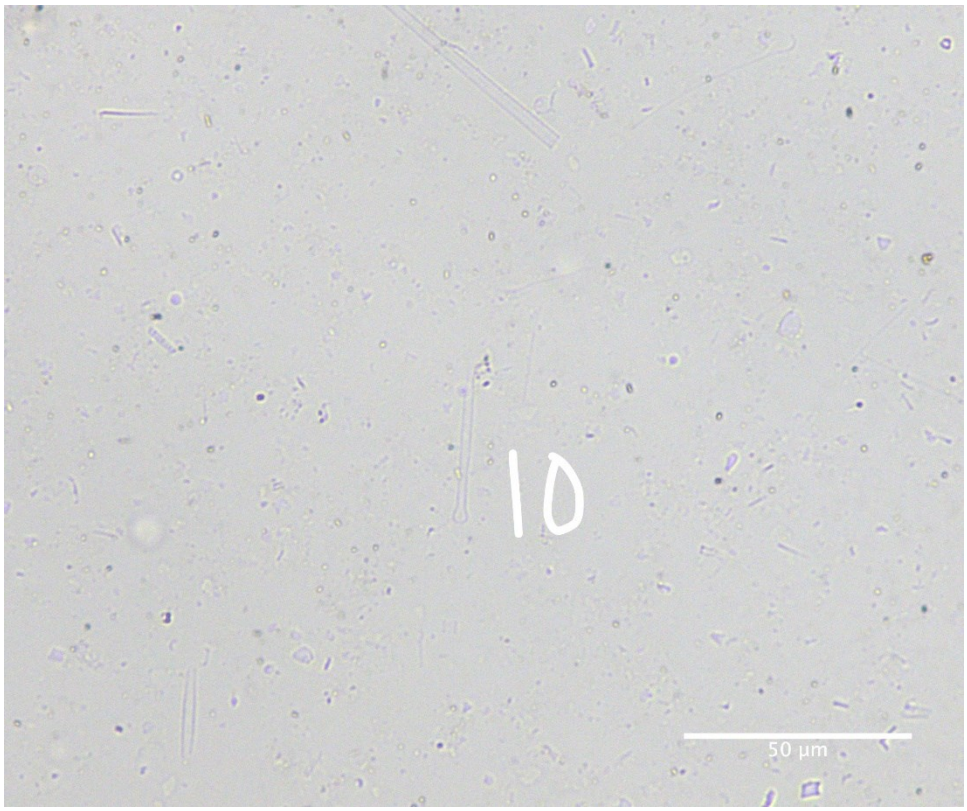


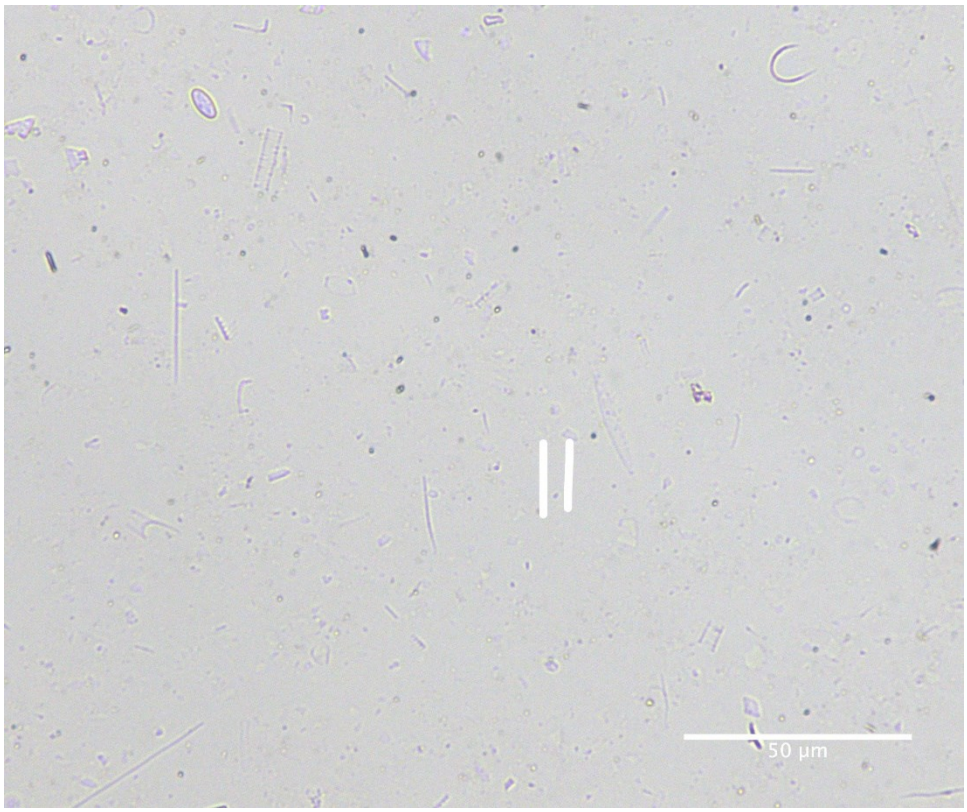

45-50 cm downcore

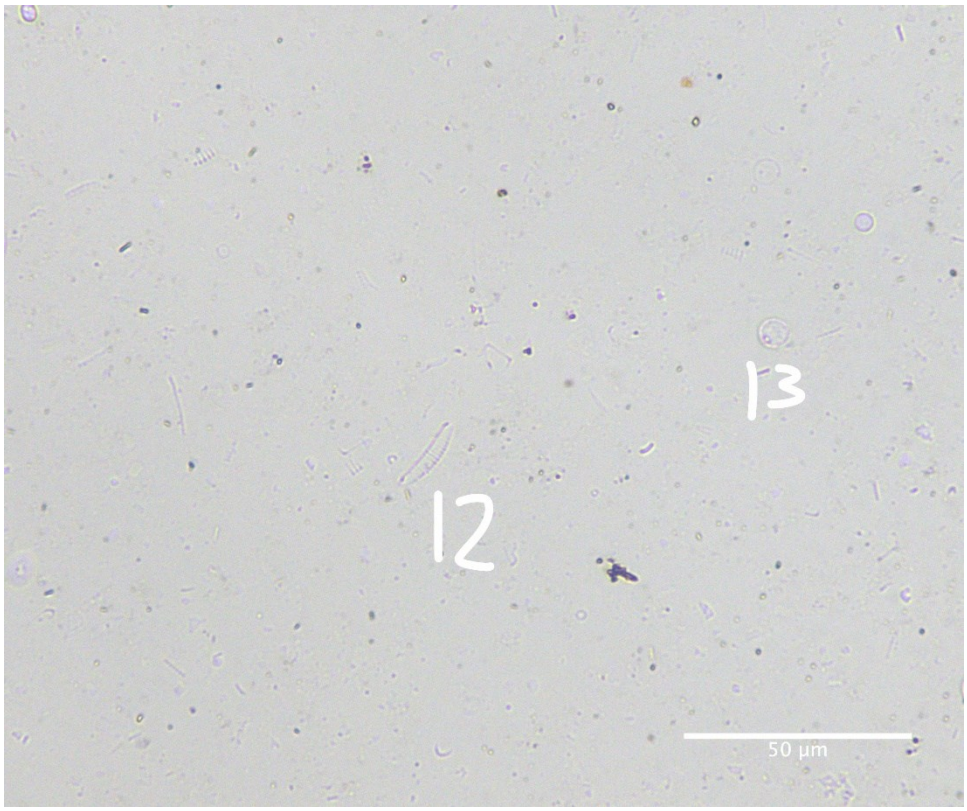


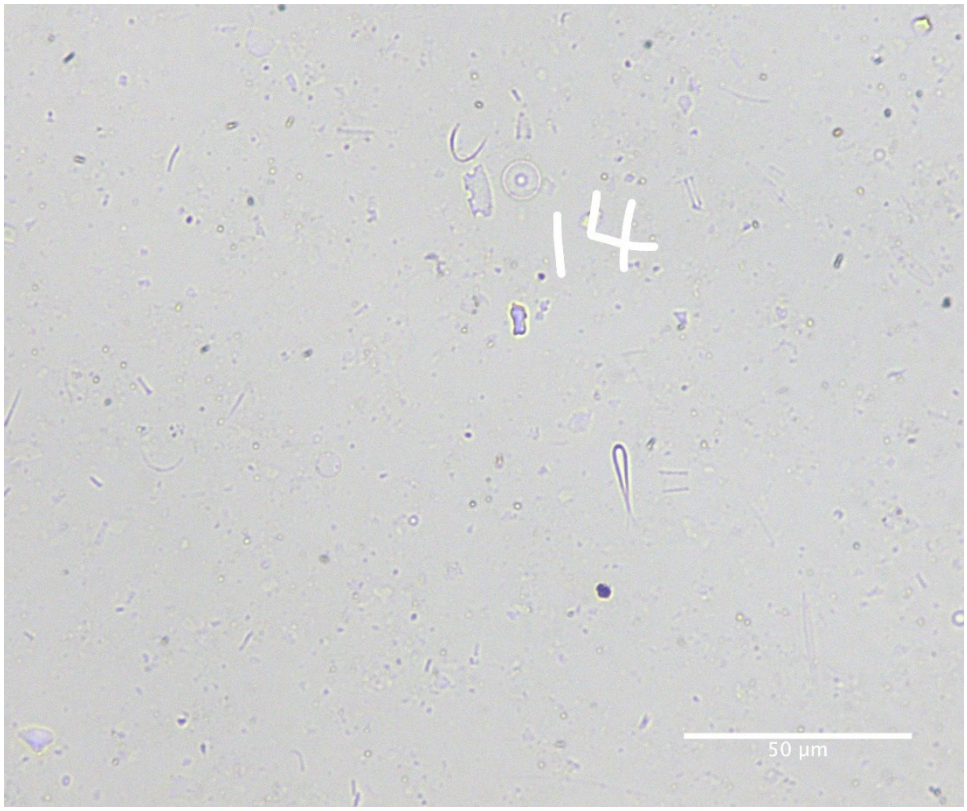

45-50 cm downcore

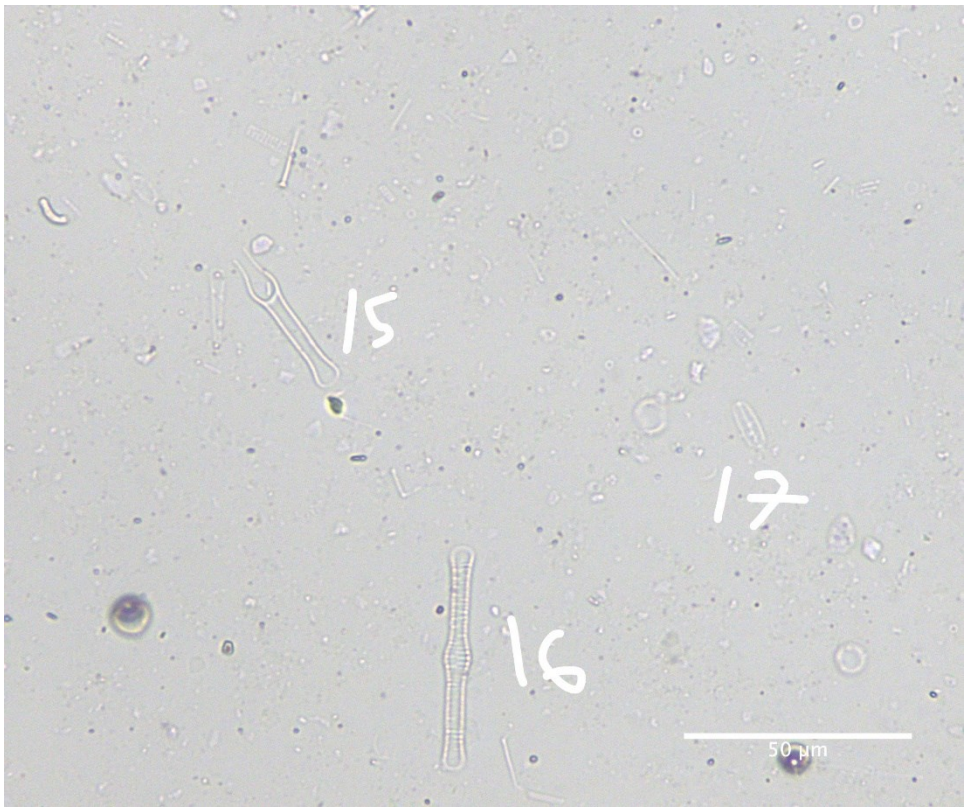


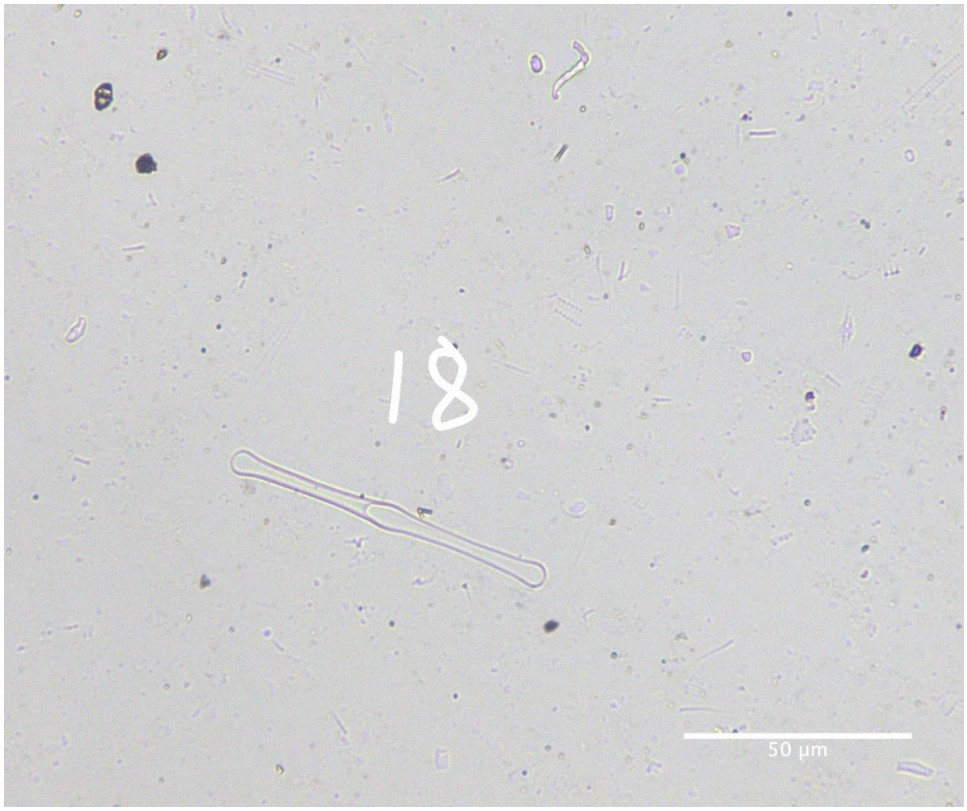

45-50 cm downcore

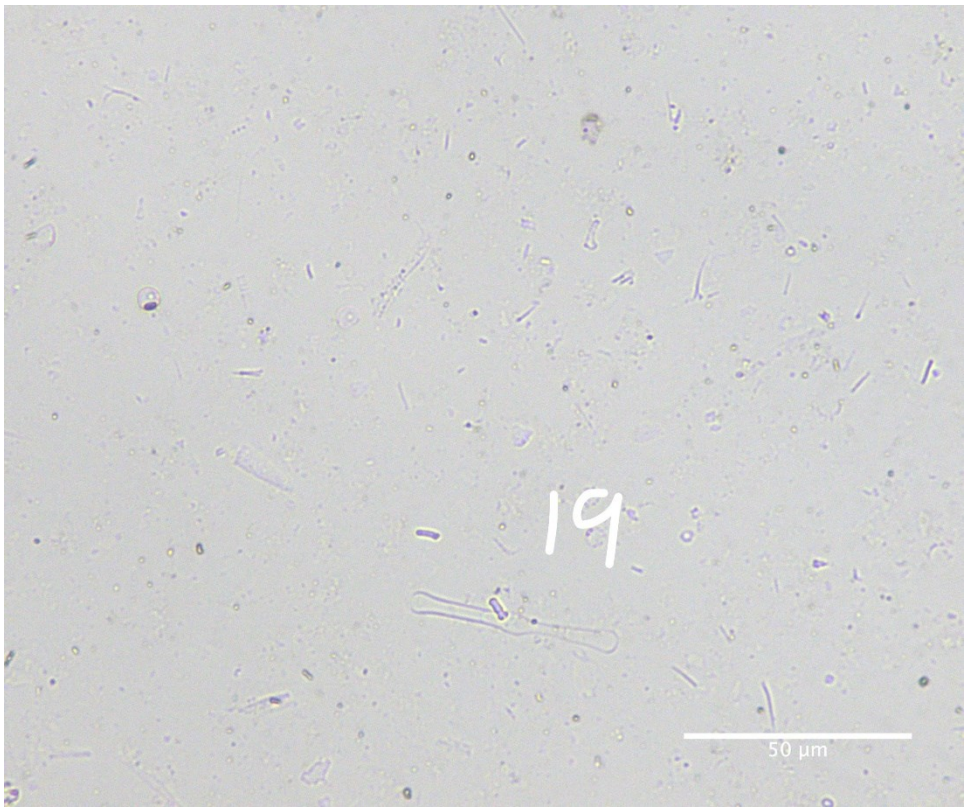


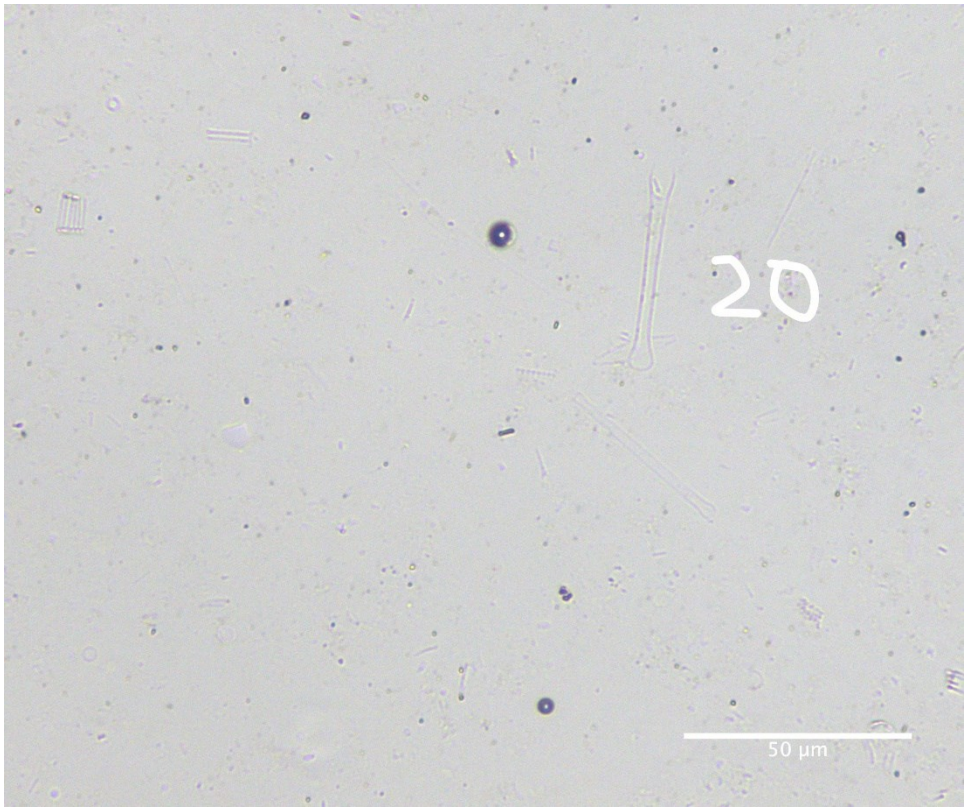

45-50 cm downcore

| Diatom ID | Taxon | Diatom ID | Taxon |
|---|---|---|---|
| 1 | *Eunotia* sp. | 11 | *Nitzschia* sp. |
| 2 | *Tabellaria* sp. | 12 | *Eunotia* sp. |
| 3 | *Gomphonema* sp. | 13 | *Thalassiosira* sp. |
| 4 | *Asterionella* sp. | 14 | *Thalassiosira* sp. |
| 5 | *Nitzschia* sp. | 15 | *Tabellaria* sp. |
| 6 | *Eunotia* sp. | 16 | *Tabellaria* sp. |
| 7 | *Nitzschia* sp. | 17 | *Navicula* sp. |
| 8 | *Eunotia* sp. | 18 | *Tabellaria* sp. |
| 9 | *Cyclotella* sp. | 19 | *Tabellaria* sp. |
| 10 | *Asterionella* sp. | 20 | *Tabellaria* sp. |

50-55 cm downcore

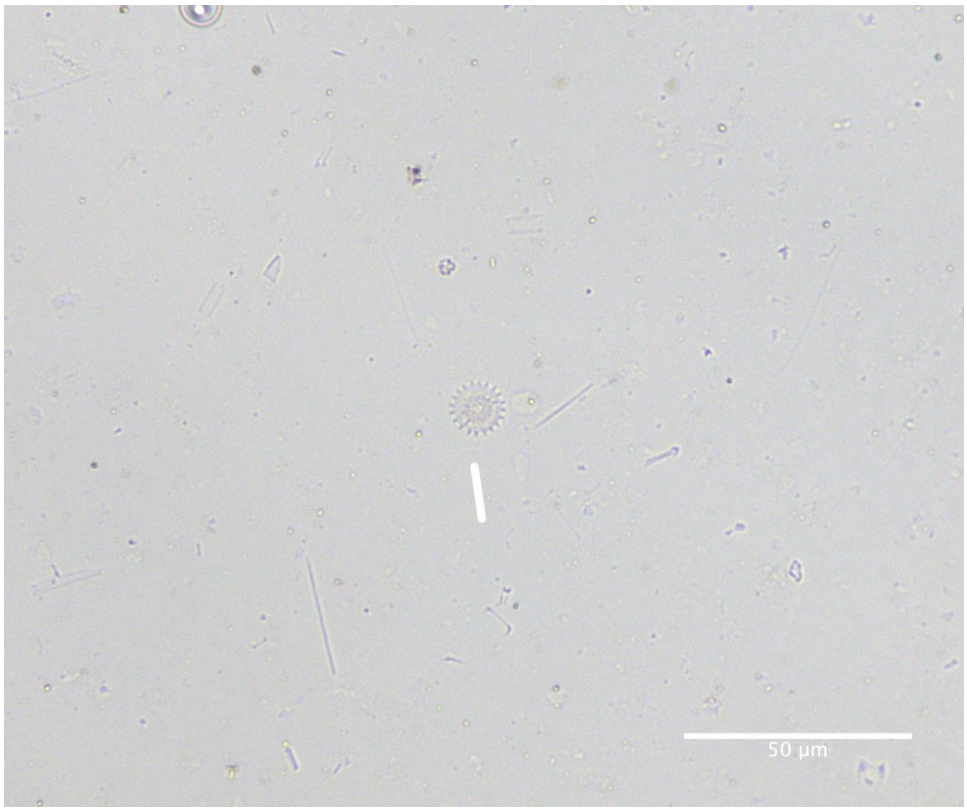


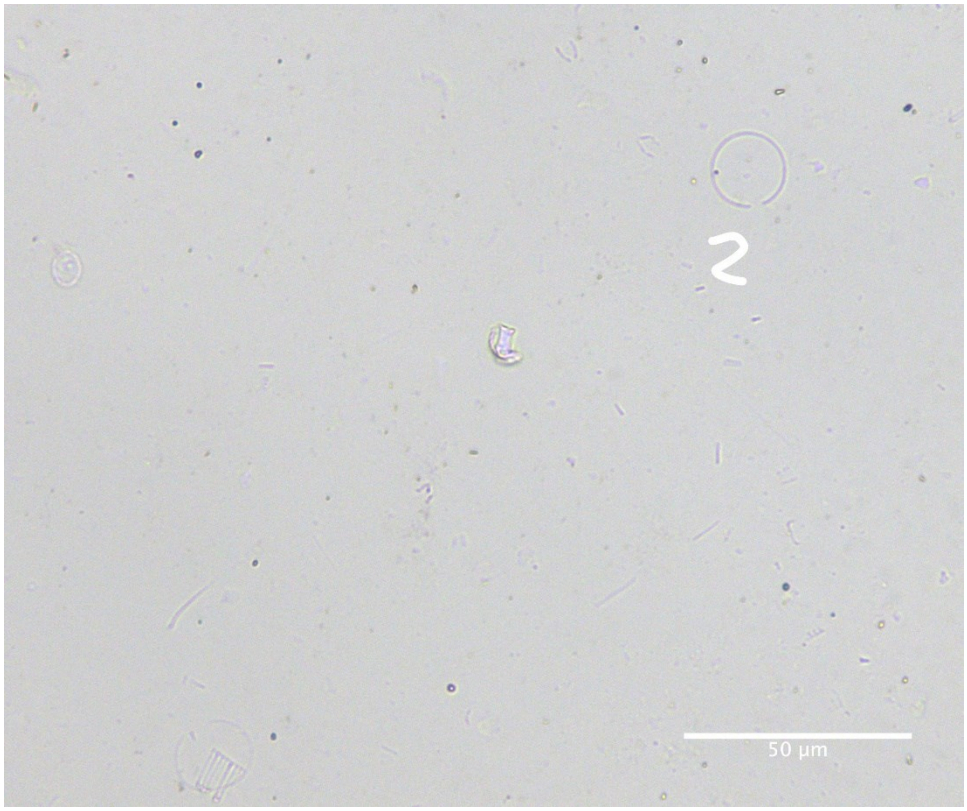

50-55 cm downcore

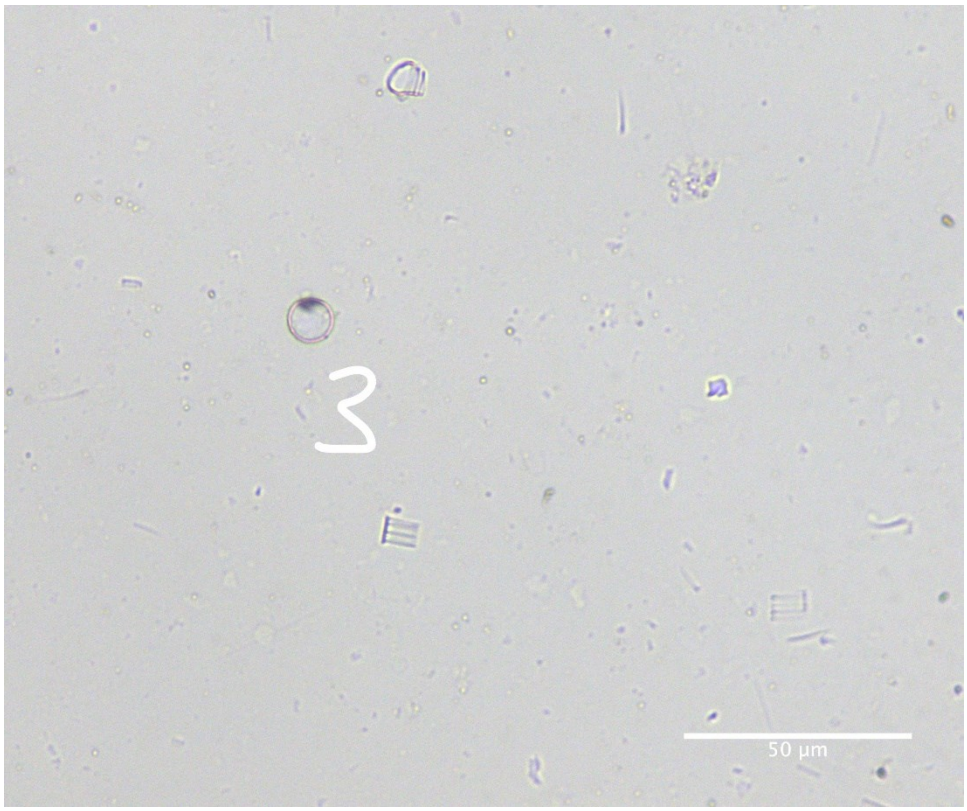


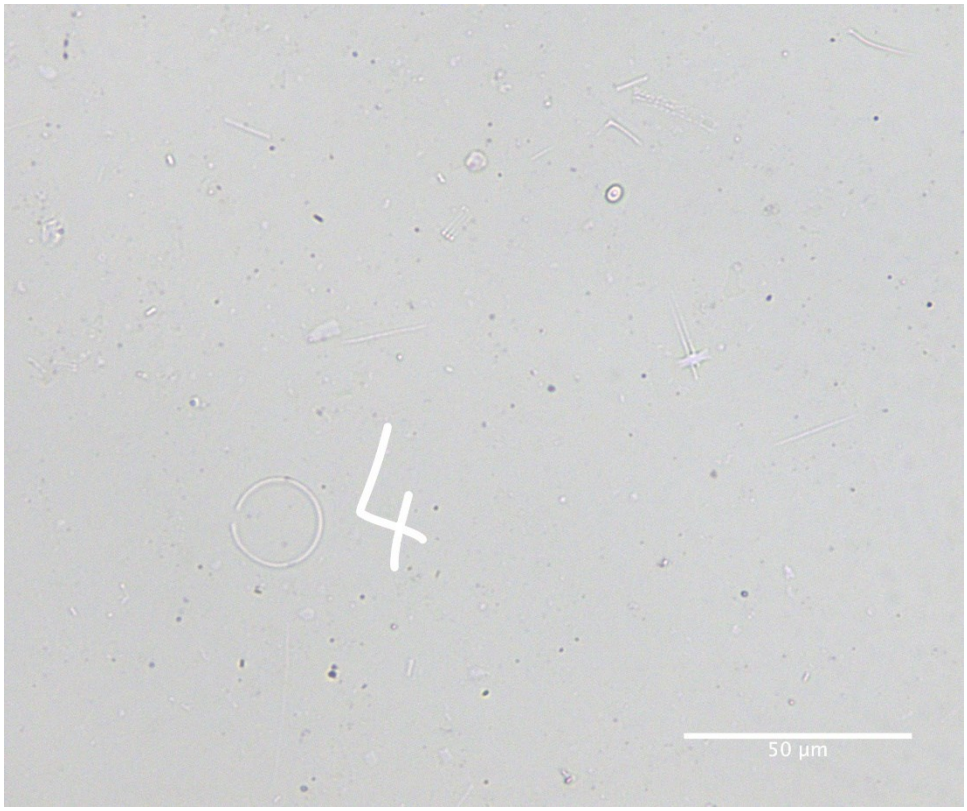

50-55 cm downcore

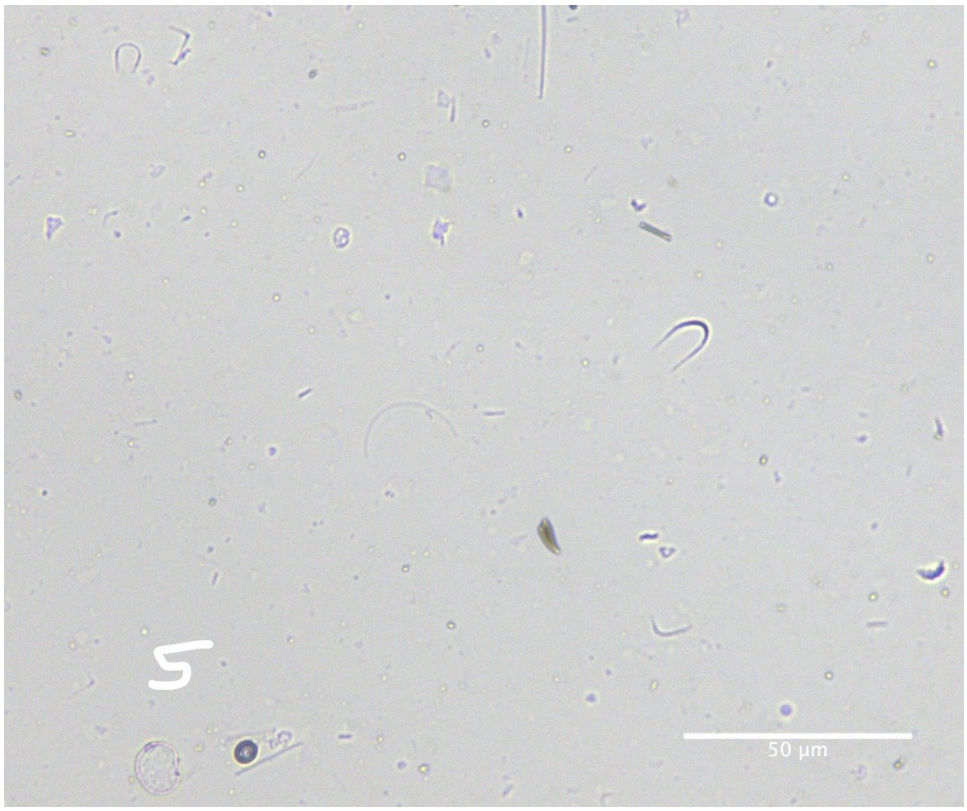


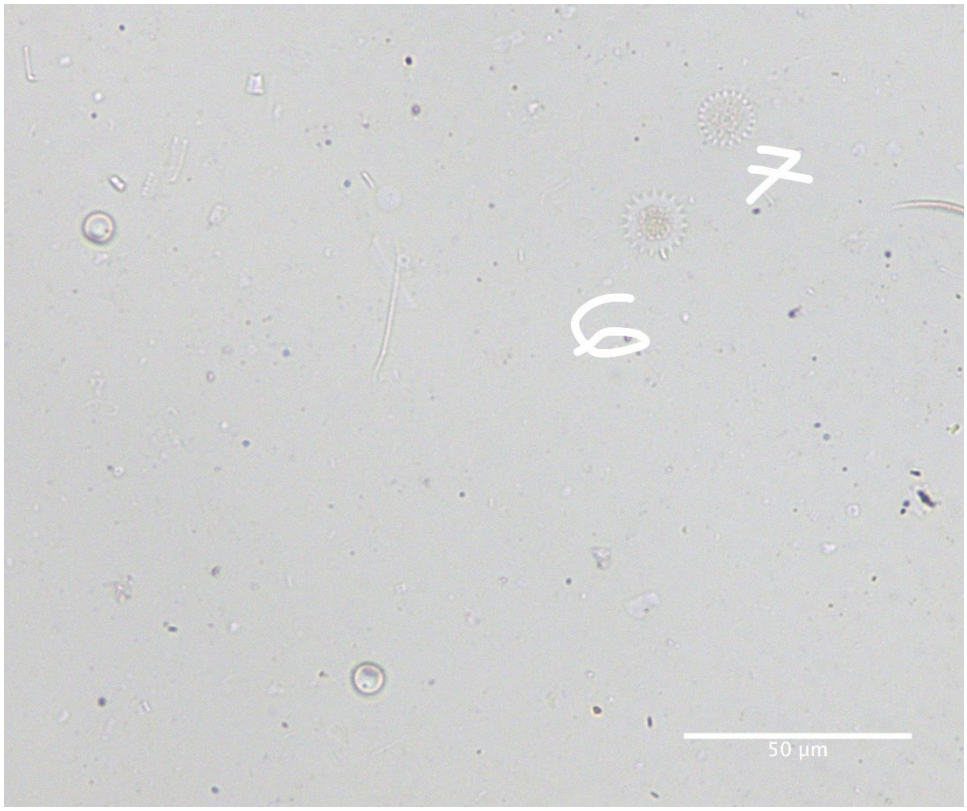

50-55 cm downcore

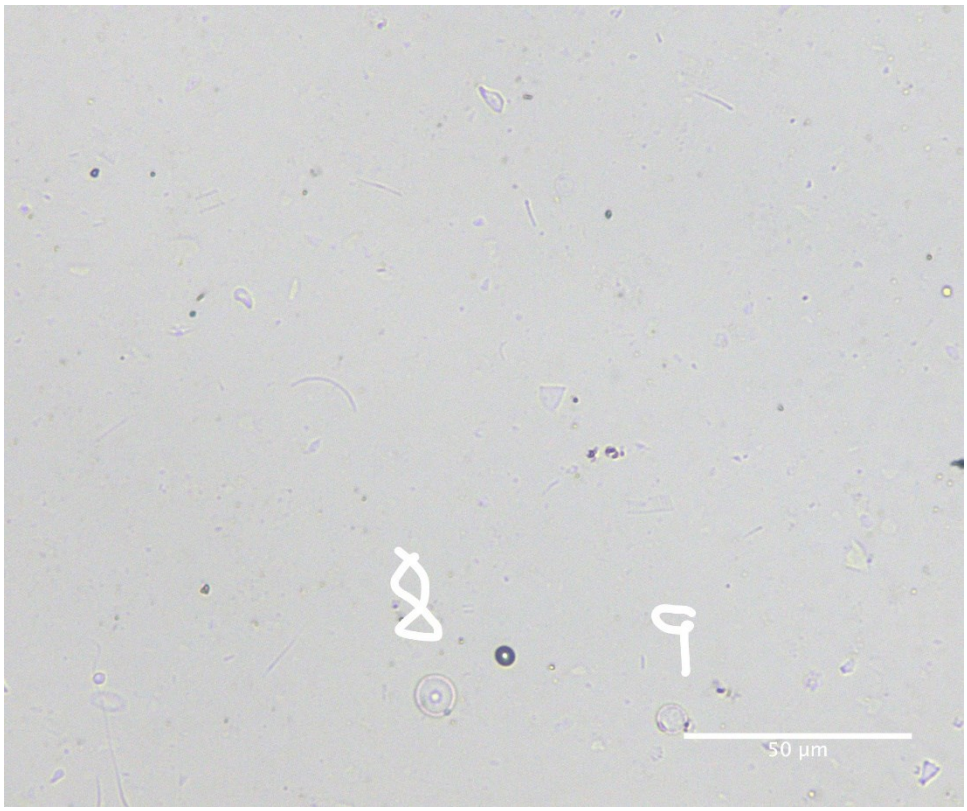


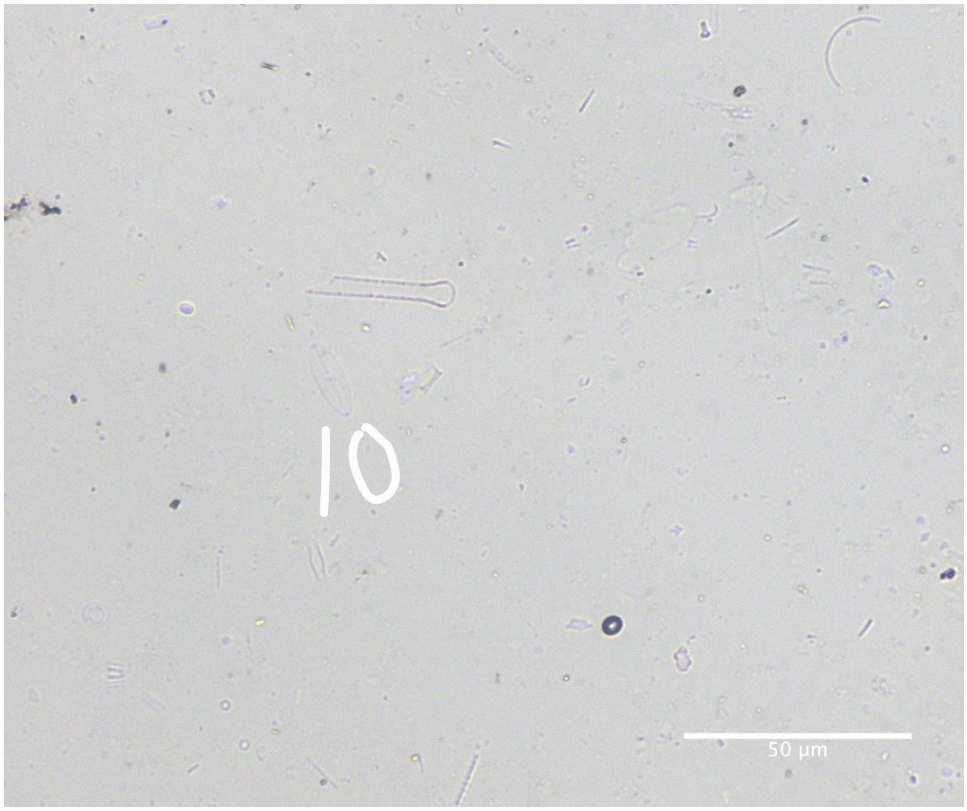

50-55 cm downcore

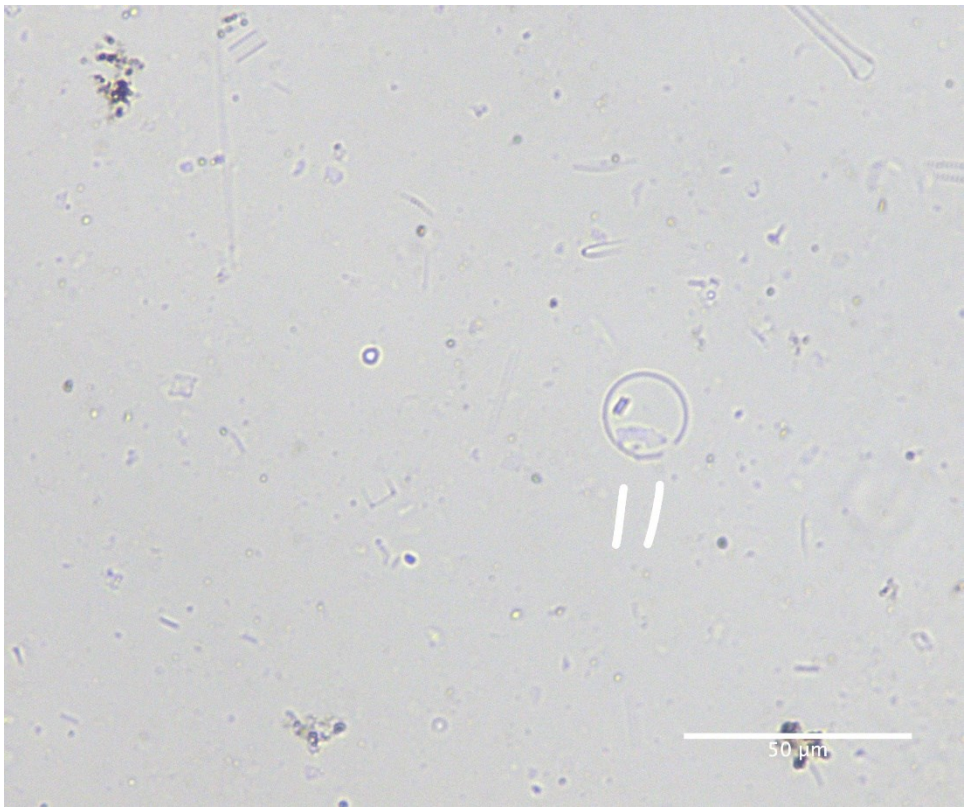


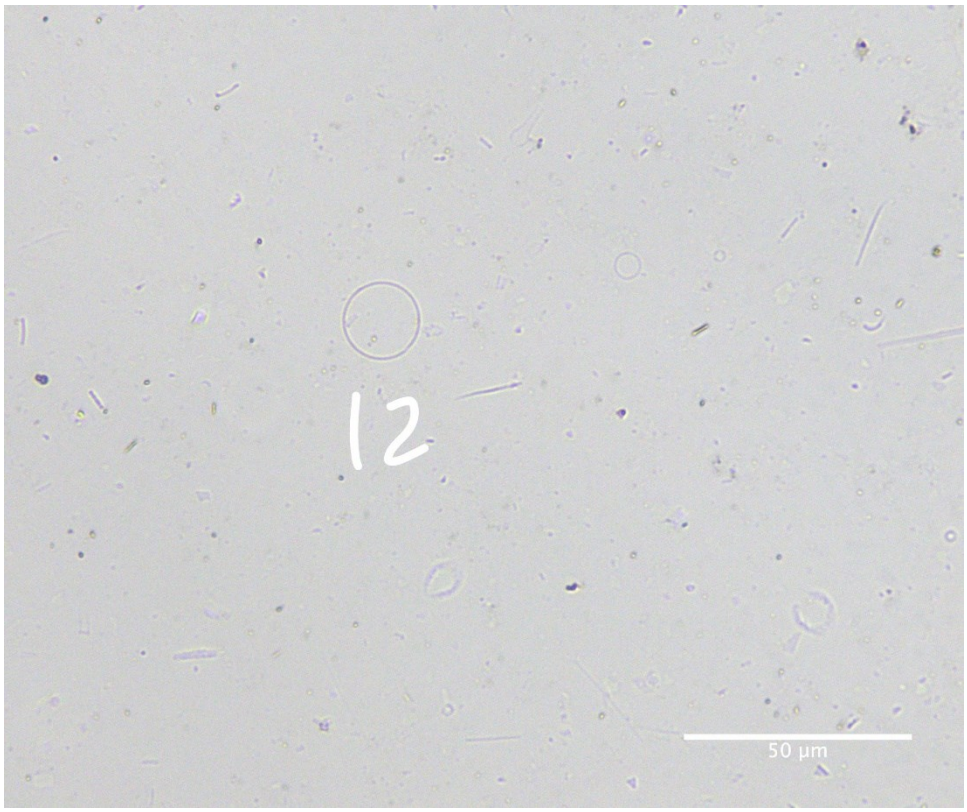

50-55 cm downcore

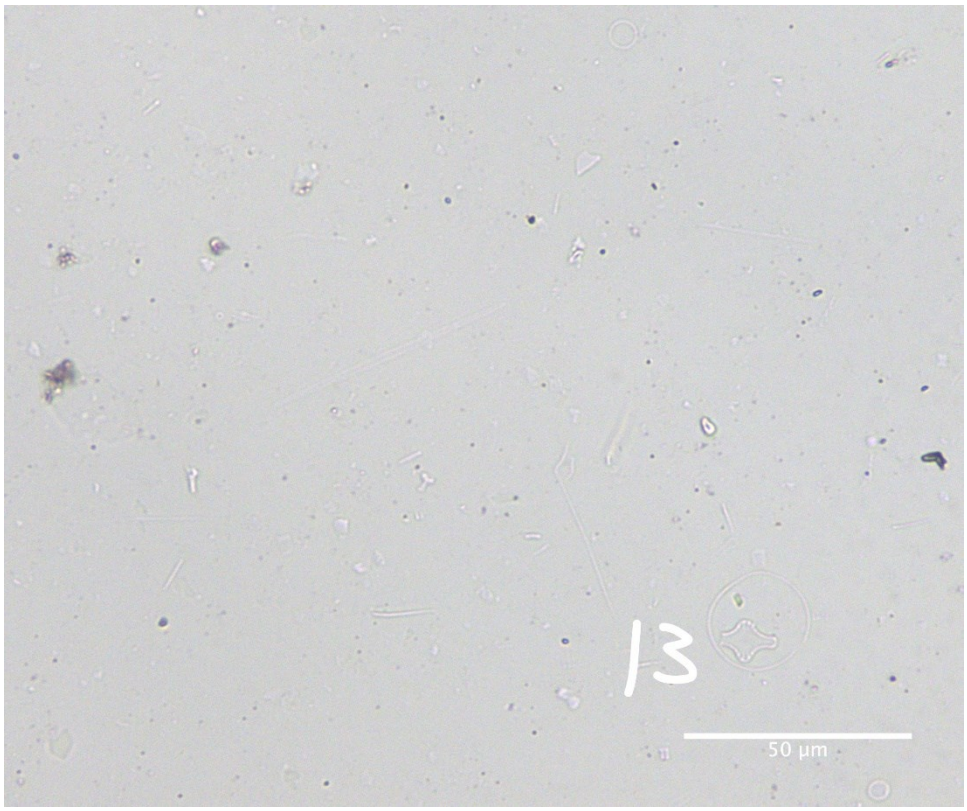


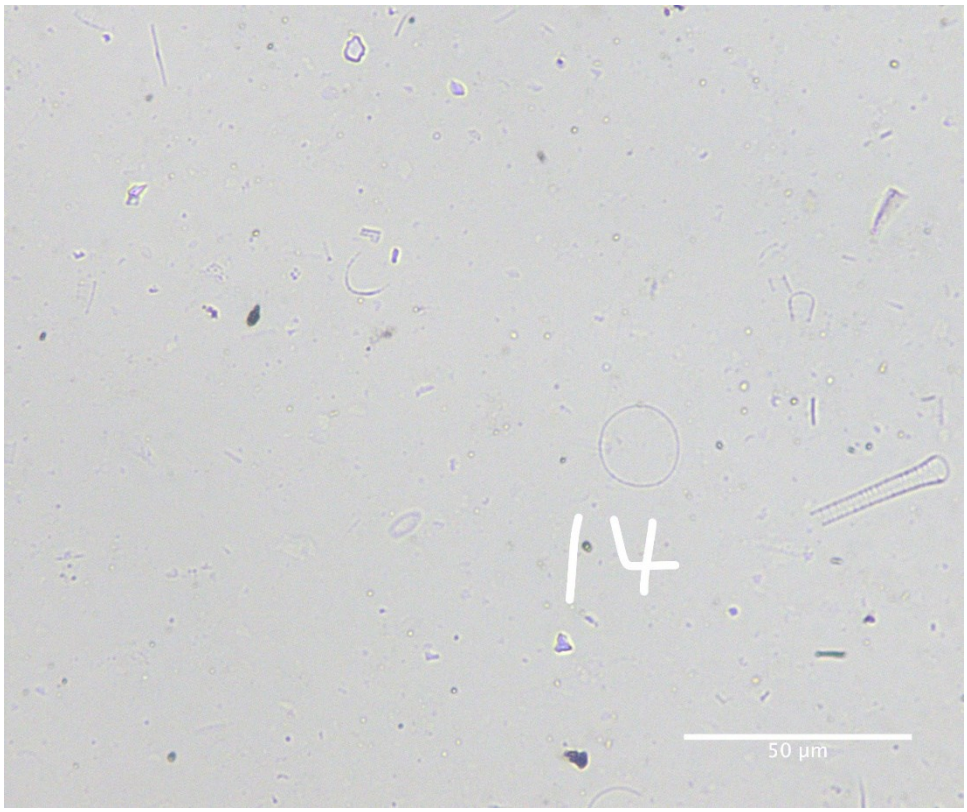

50-55 cm downcore

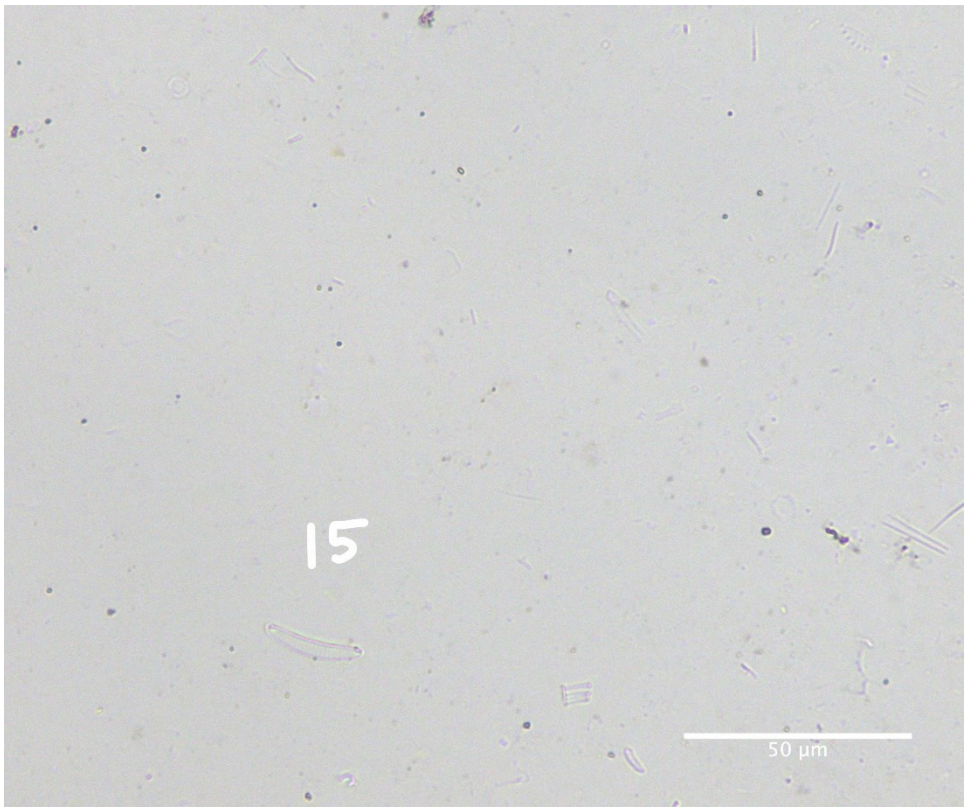


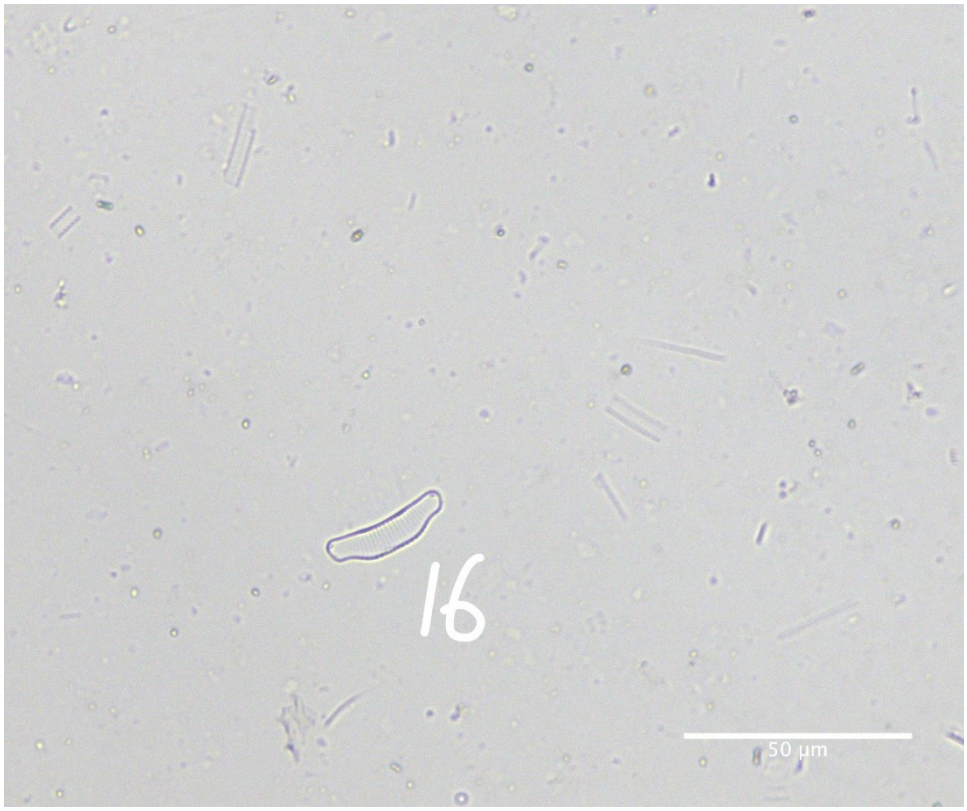

50-55 cm downcore

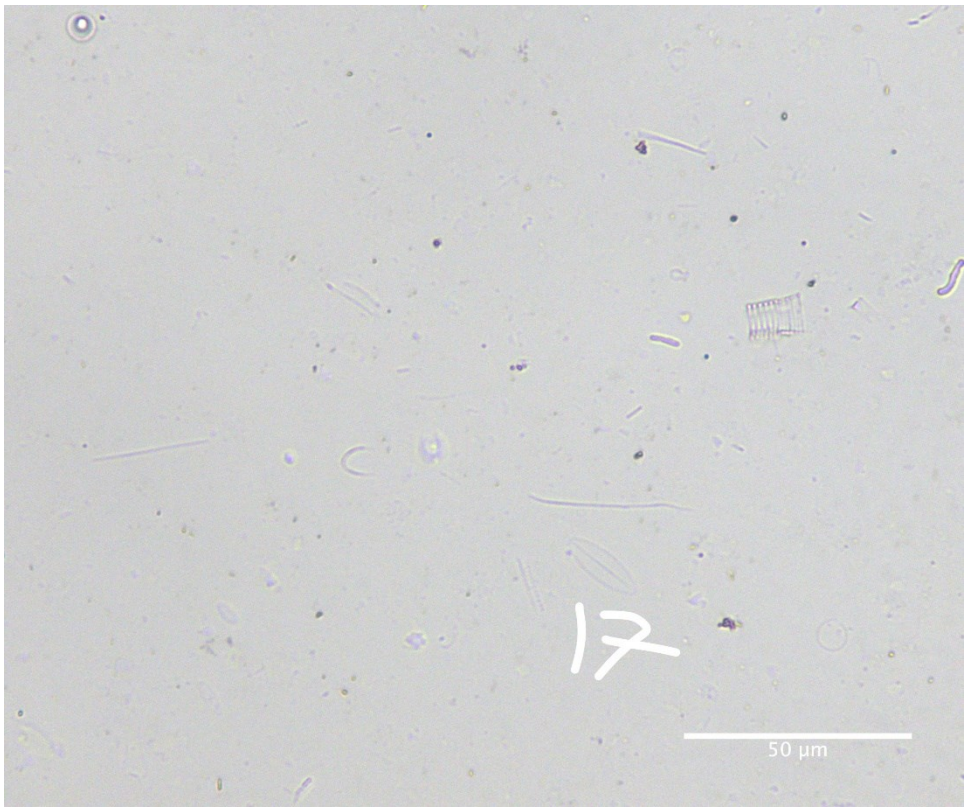


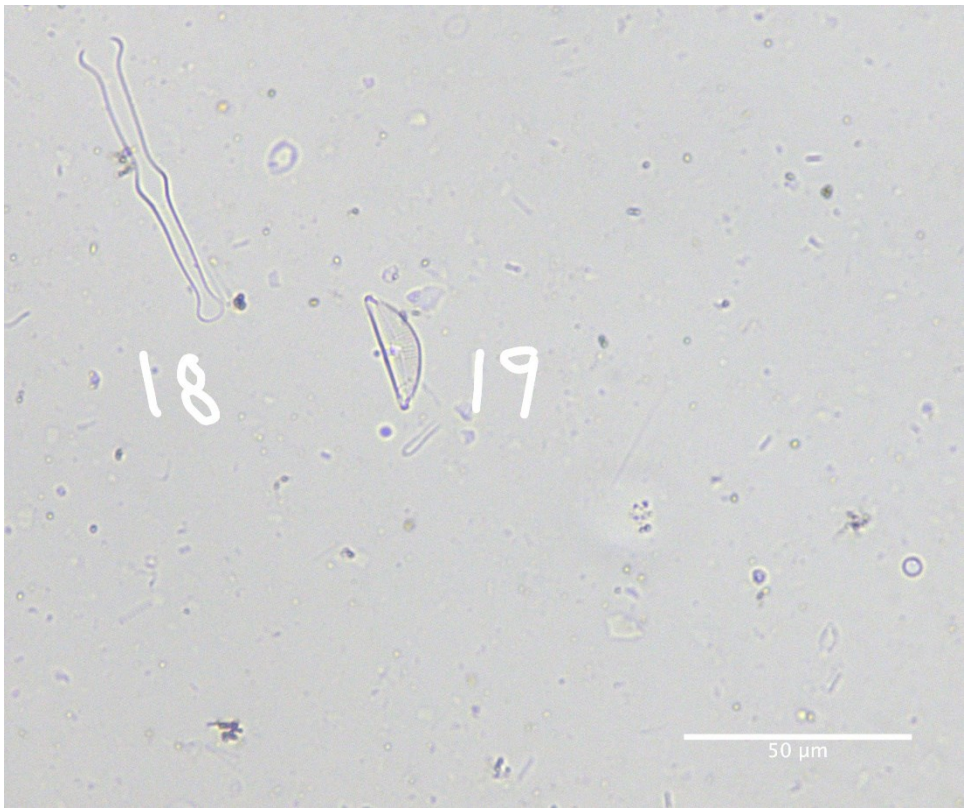

50-55 cm downcore

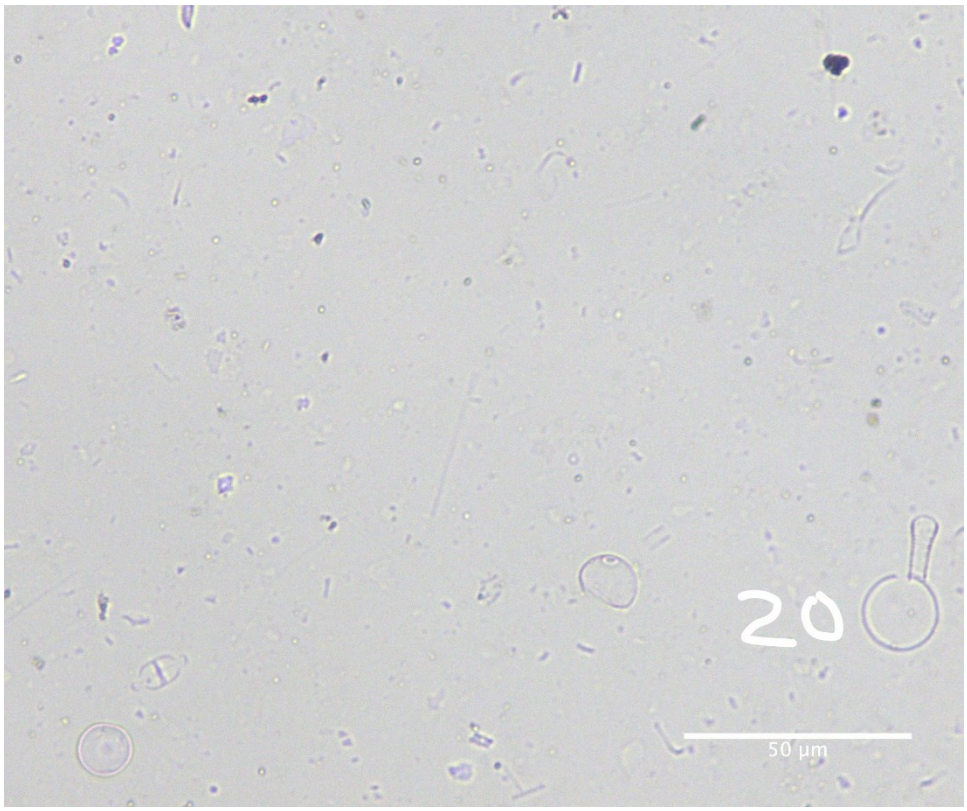


| Diatom ID | Taxon | Diatom ID | Taxon |
|---|---|---|---|
| 1 | *Cyclotella* sp. | 11 | *Thalassiosira* sp. |
| 2 | *Thalassiosira* sp. | 12 | *Thalassiosira* sp. |
| 3 | *Thalassiosira* sp. | 13 | *Thalassiosira* sp. |
| 4 | *Thalassiosira* sp. | 14 | *Thalassiosira* sp. |
| 5 | *Thalassiosira* sp. | 15 | *Eunotia* sp. |
| 6 | *Cyclotella* sp. | 16 | *Eunotia* sp. |
| 7 | *Cyclotella* sp. | 17 | *Navicula* sp. |
| 8 | *Thalassiosira* sp. | 18 | *Tabellaria* sp. |
| 9 | *Thalassiosira* sp. | 19 | *Cymbella* sp. |
| 10 | *Navicula* sp. | 20 | *Thalassiosira* sp. |

55-60 cm downcore

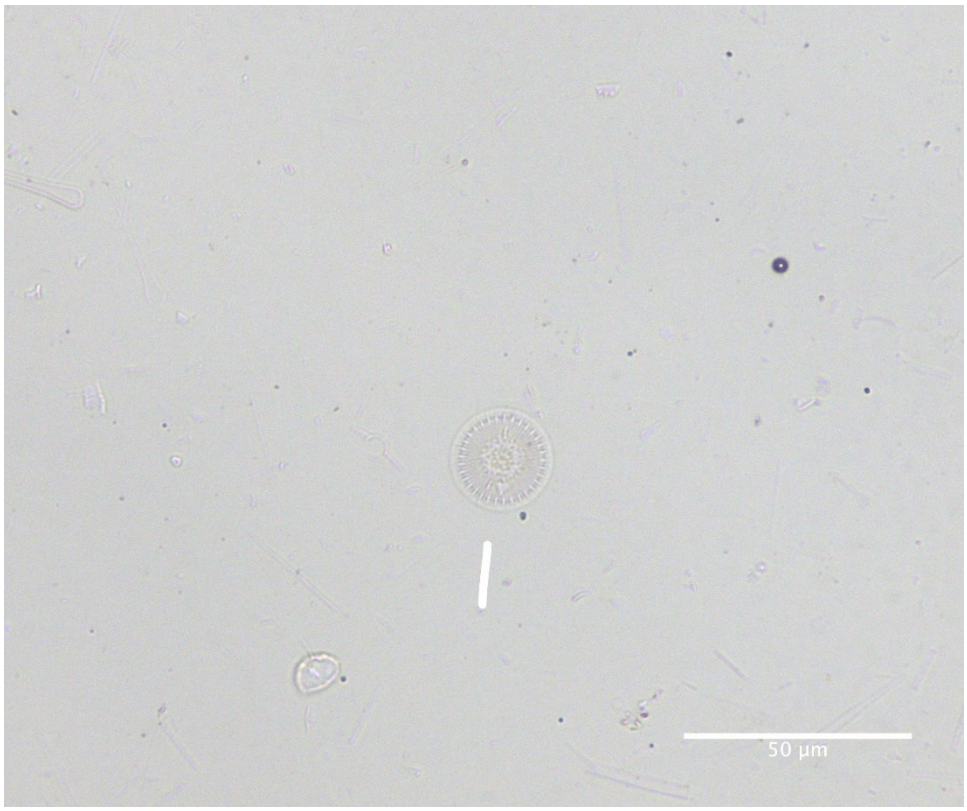


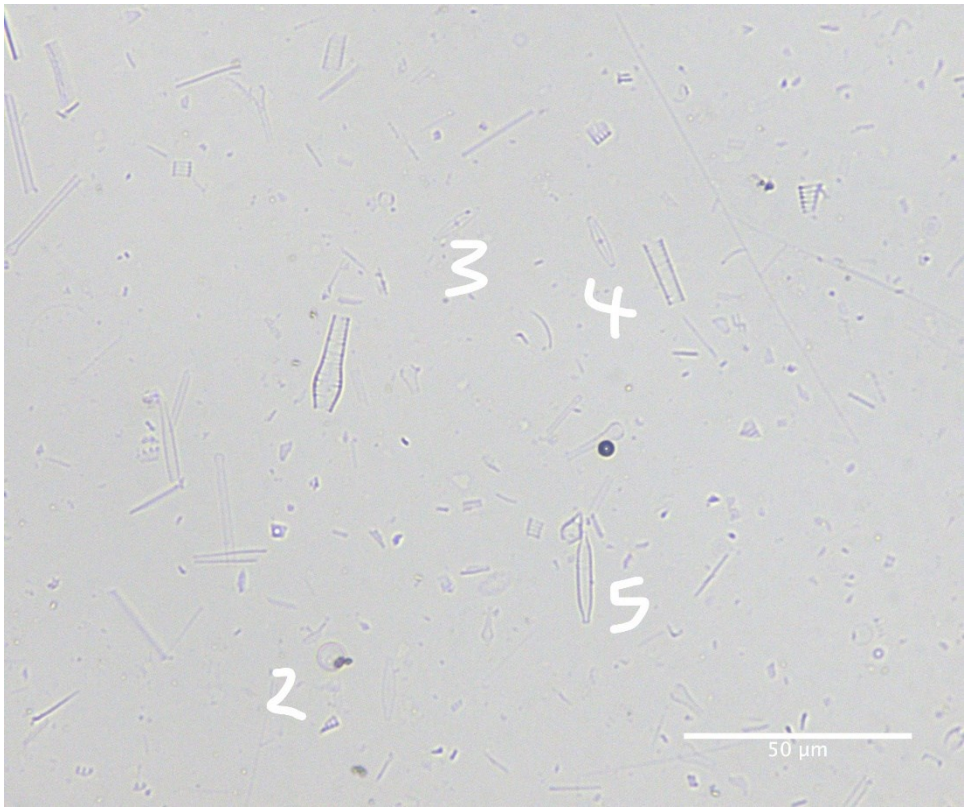

55-60 cm downcore

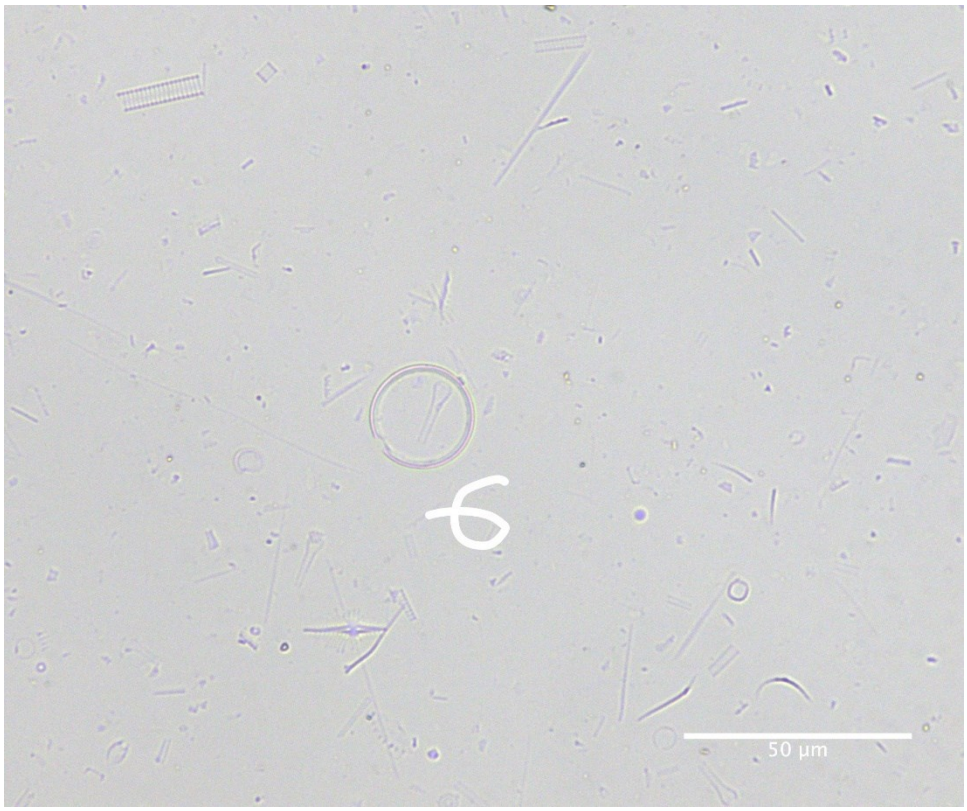


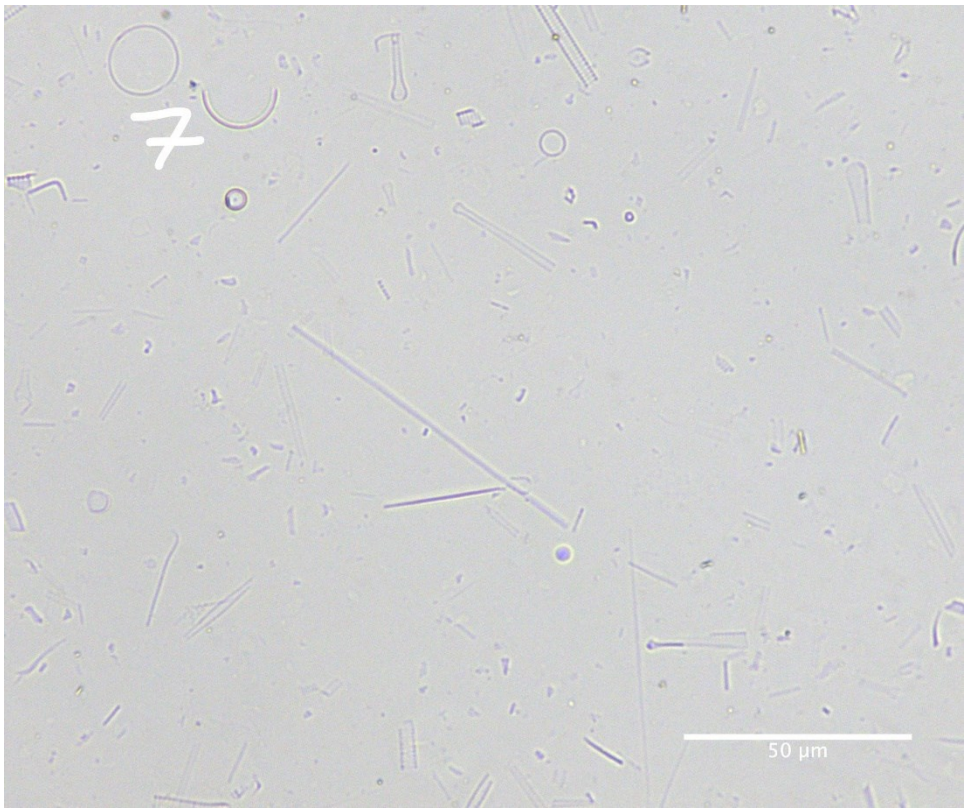

55-60 cm downcore

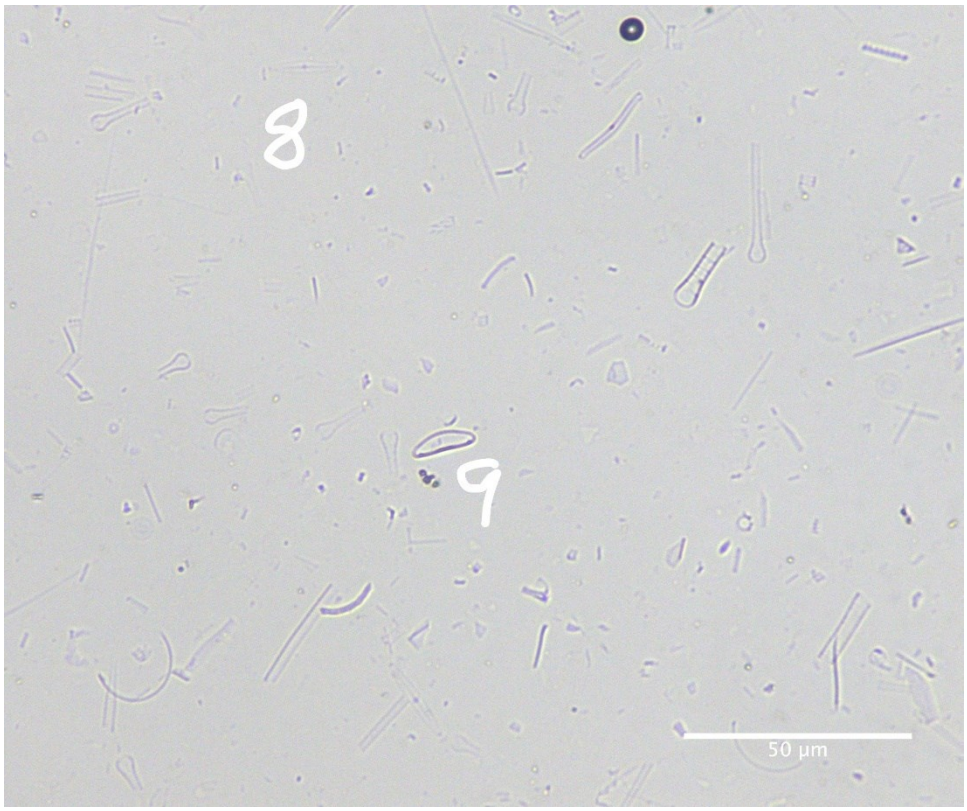


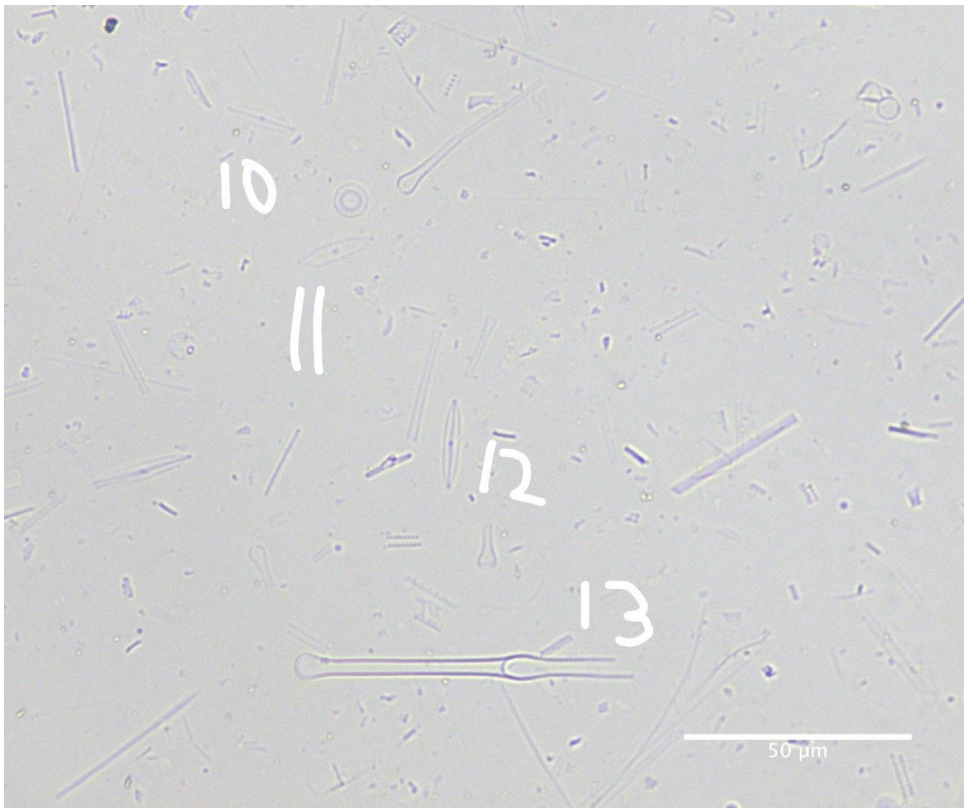

55-60 cm downcore

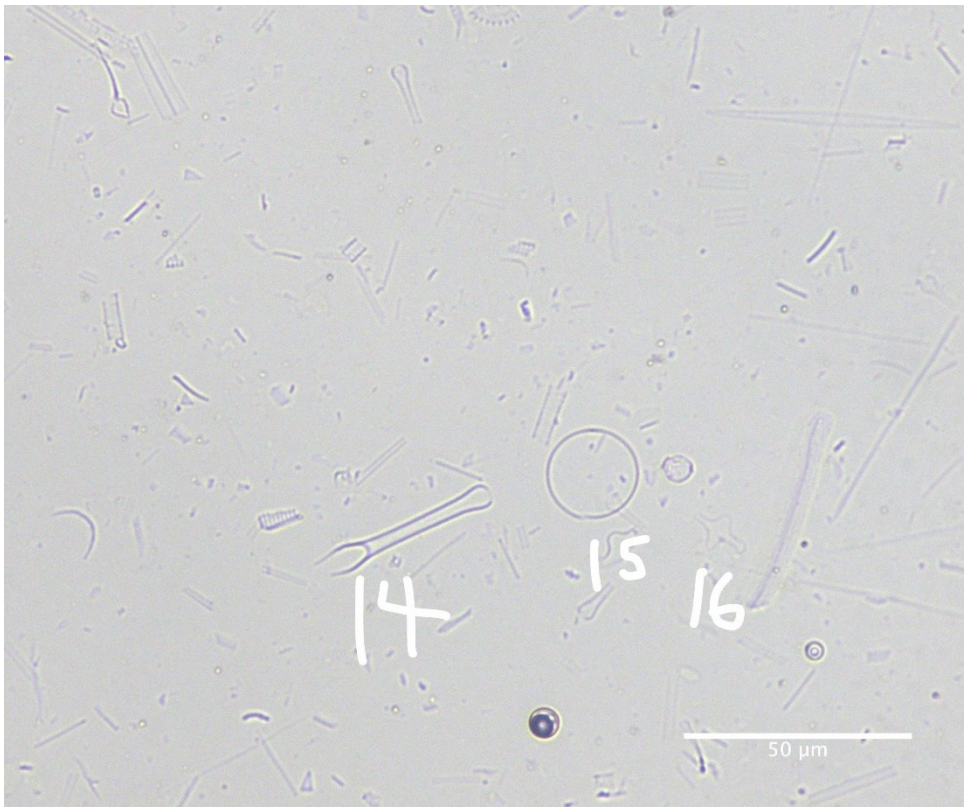


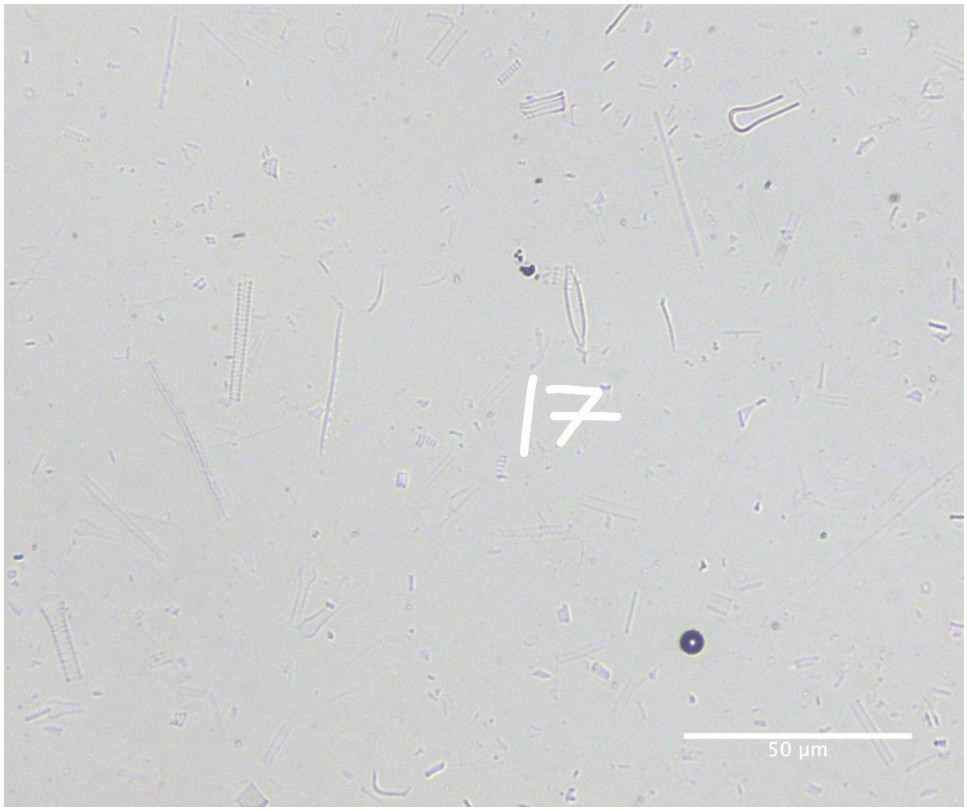

55-60 cm downcore

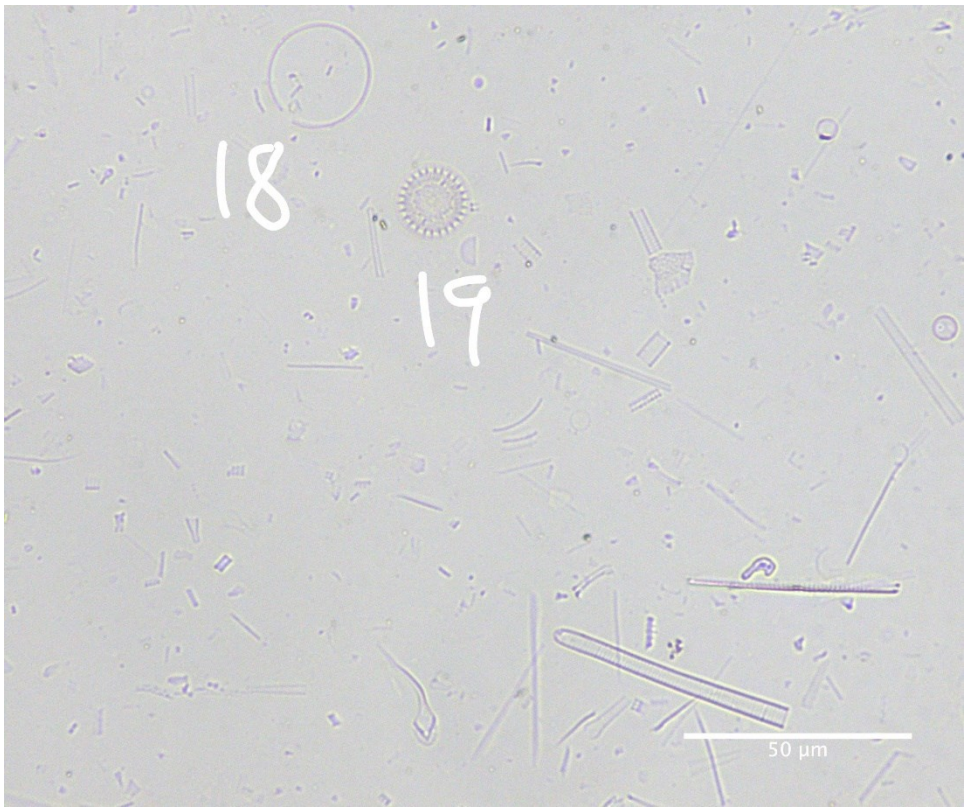


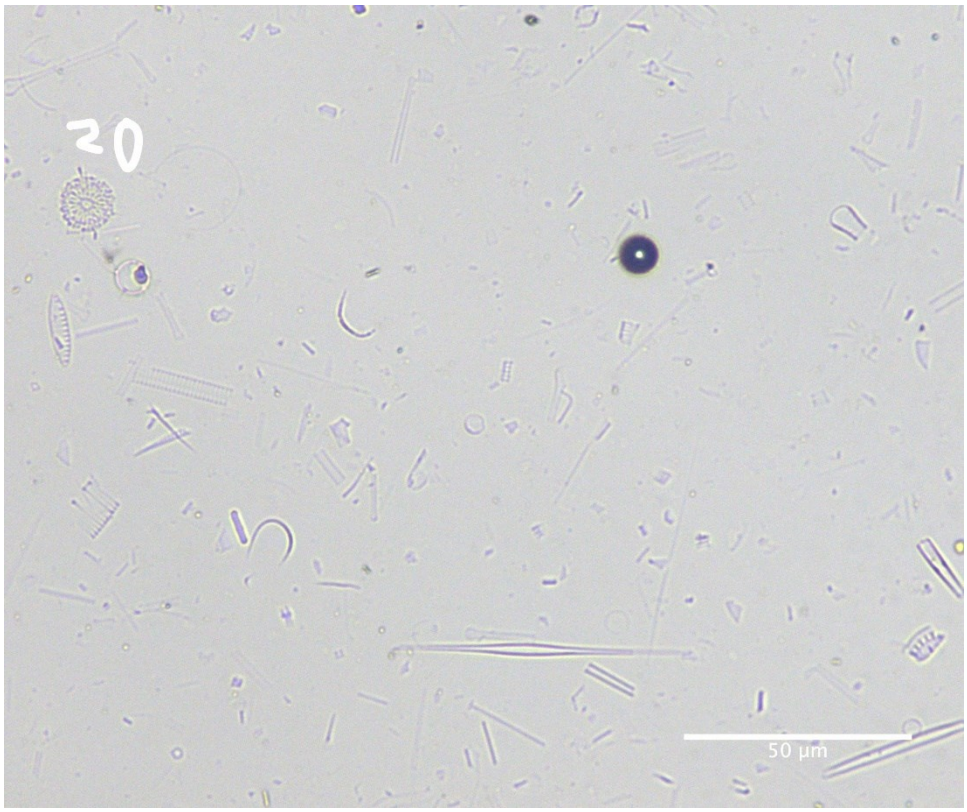

55-60 cm downcore

| Diatom ID | Taxon | Diatom ID | Taxon |
|---|---|---|---|
| 1 | *Cyclotella* sp. | 11 | *Navicula* sp. |
| 2 | *Thalassiosira* sp. | 12 | *Navicula* sp. |
| 3 | *Achnanthidium* sp. | 13 | *Tabellaria* sp. |
| 4 | *Achnanthidium* sp. | 14 | *Tabellaria* sp. |
| 5 | *Nitzschia* sp. | 15 | *Thalassiosira* sp. |
| 6 | *Thalassiosira* sp. | 16 | *Fragilaria* sp. |
| 7 | *Thalassiosira* sp. | 17 | *Nitzschia* sp. |
| 8 | *Navicula* sp. | 18 | *Thalassiosira* sp. |
| 9 | *Eunotia* sp. | 19 | *Cyclotella* sp. |
| 10 | *Navicula* sp. | 20 | *Cyclotella* sp. |

60-65 cm downcore

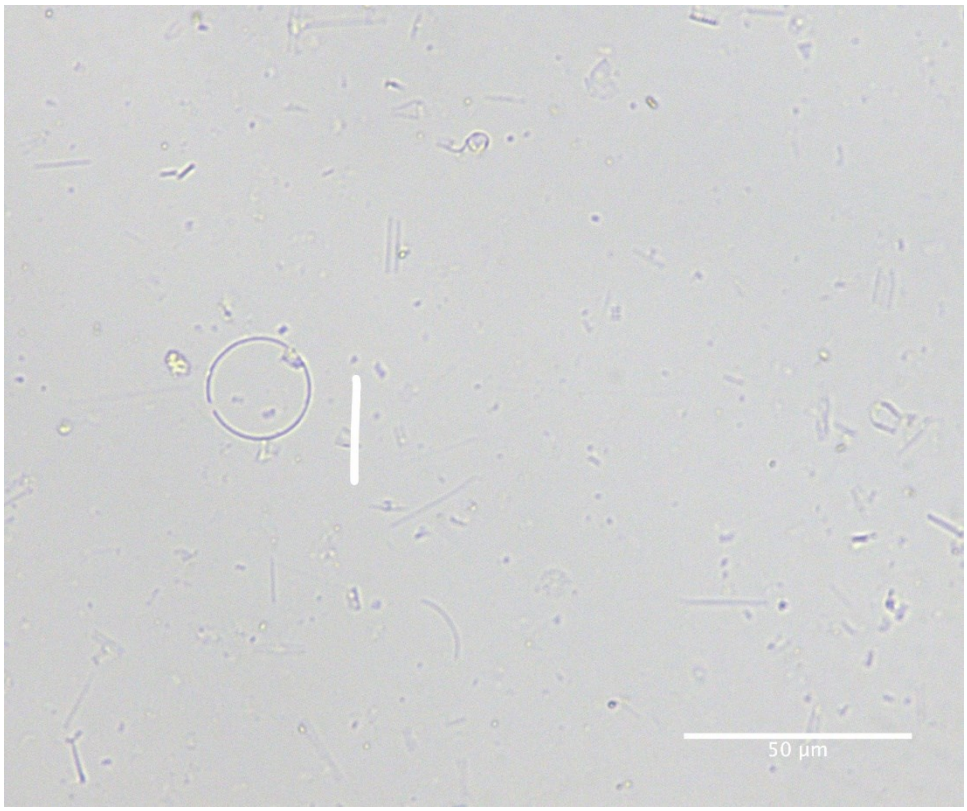


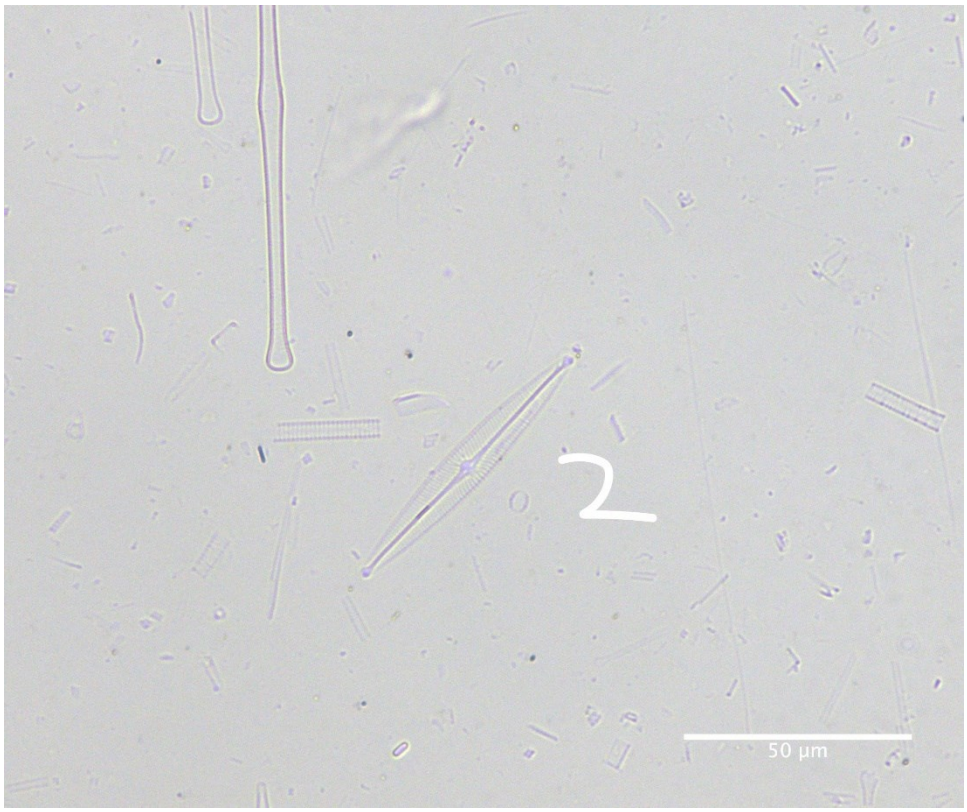

60-65 cm downcore

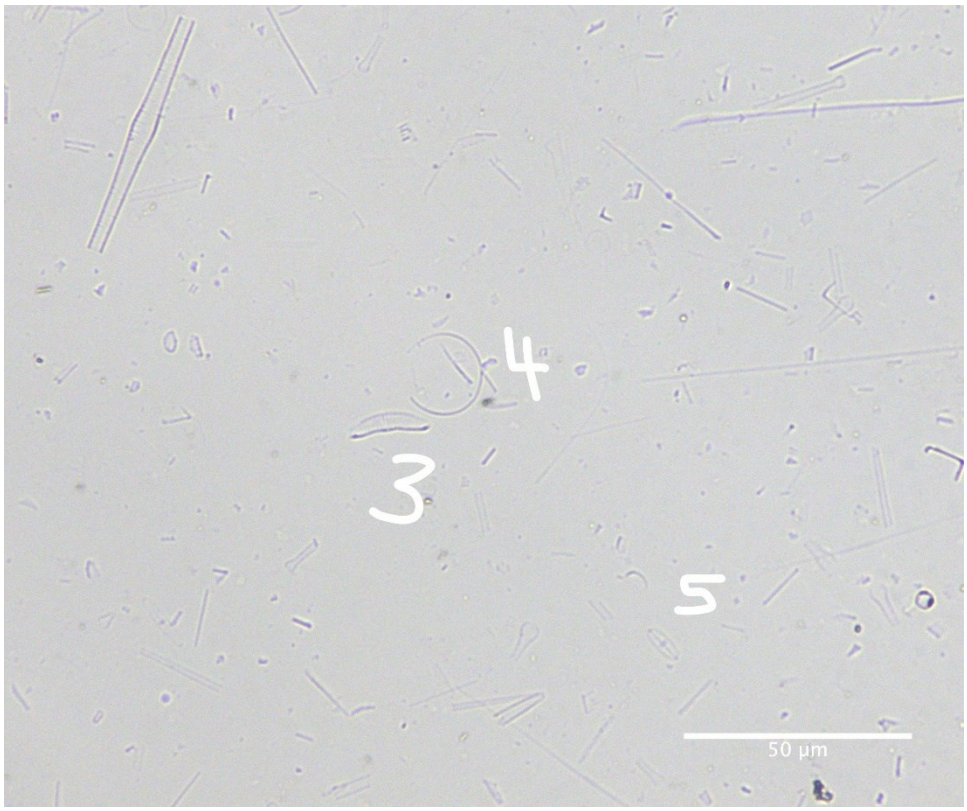


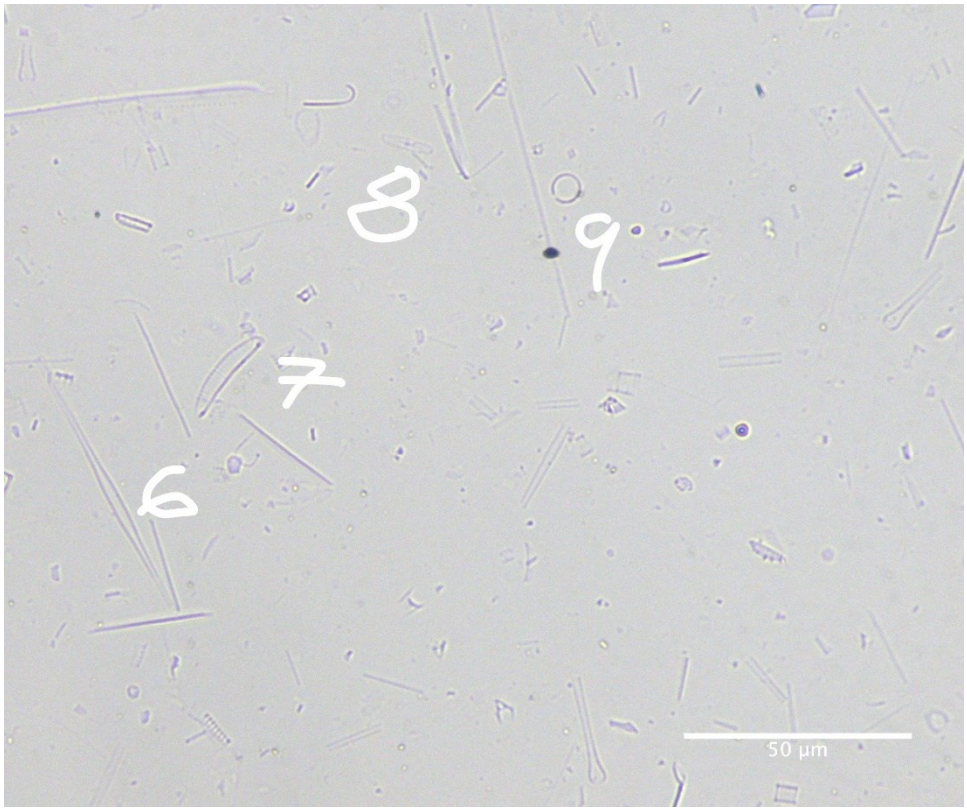

60-65 cm downcore

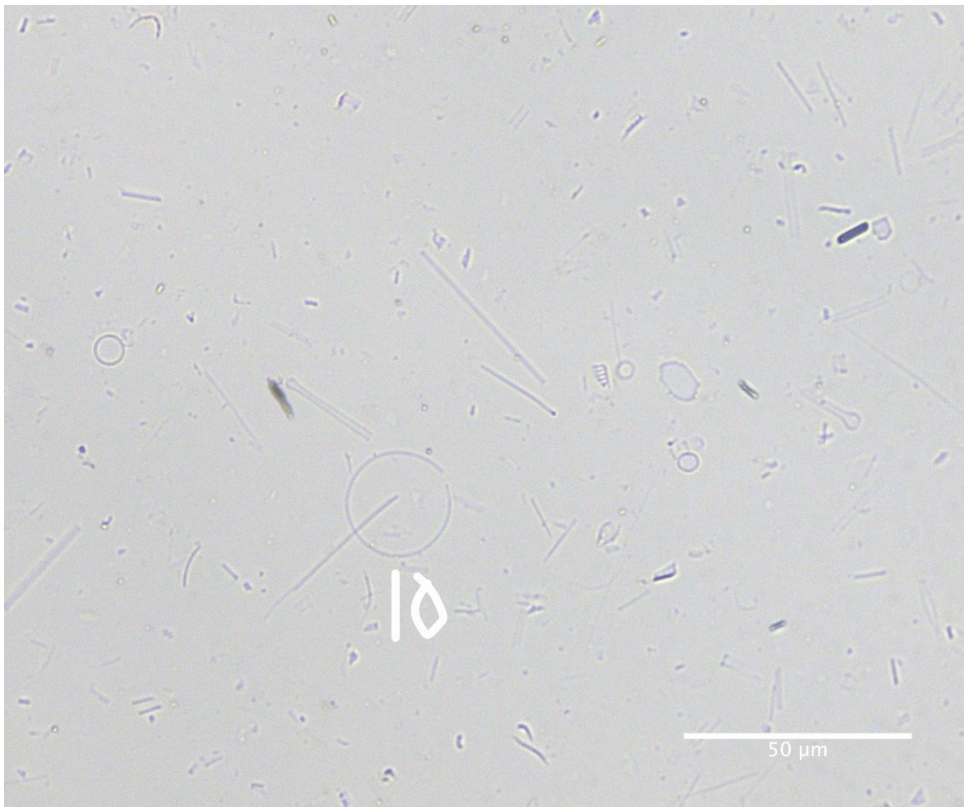


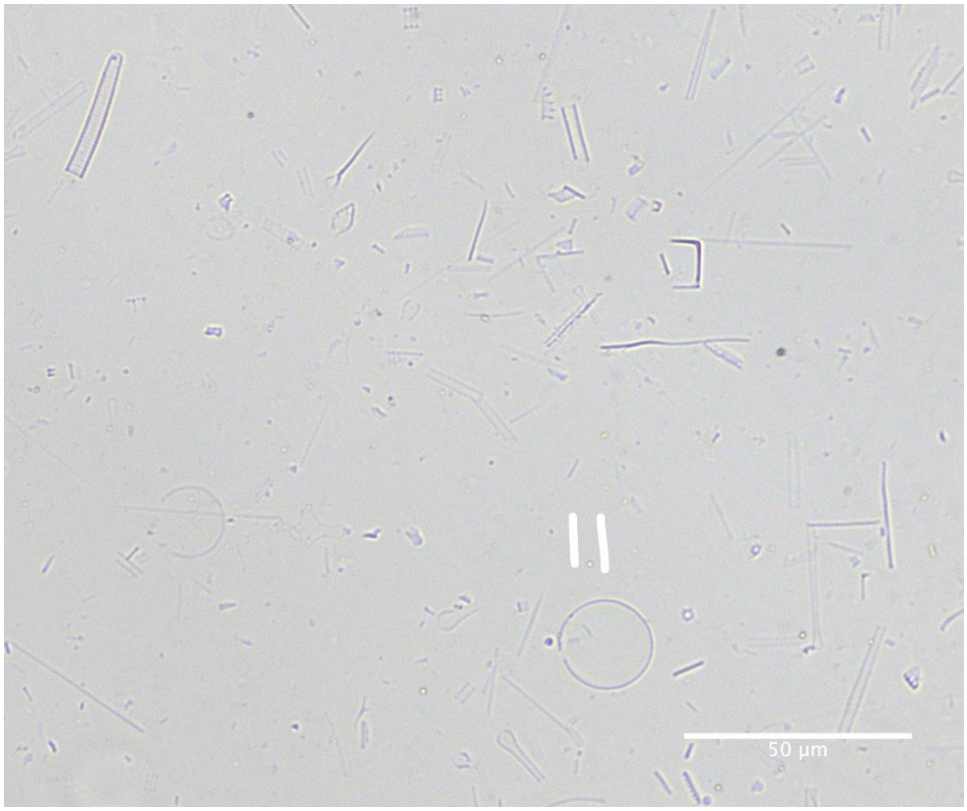

60-65 cm downcore

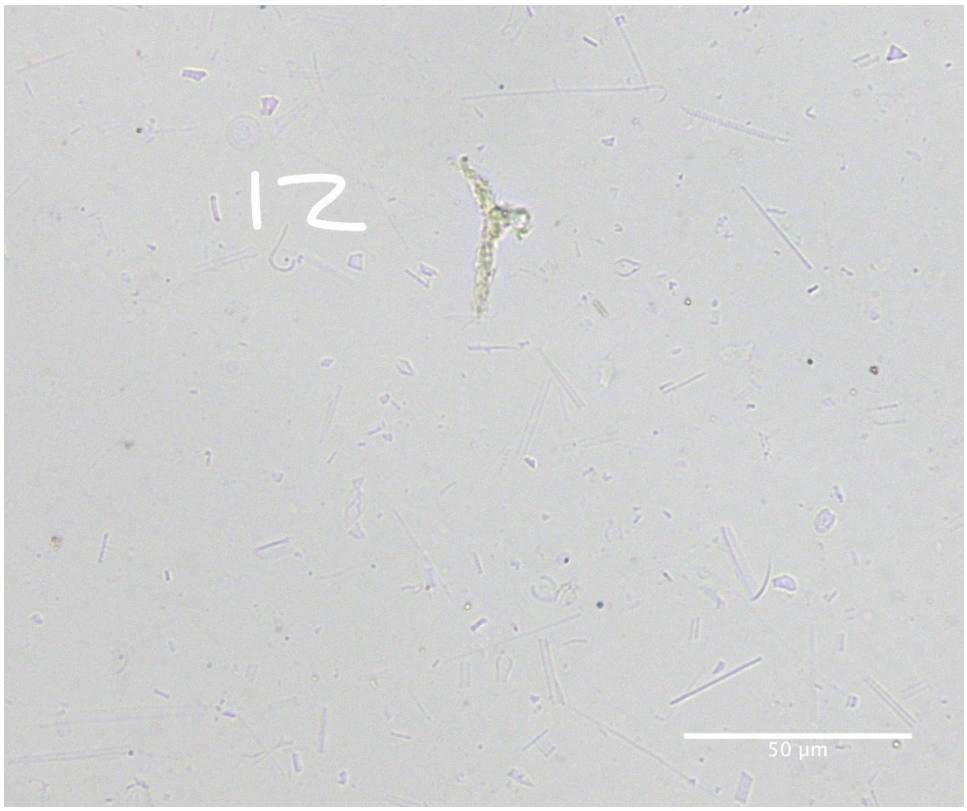


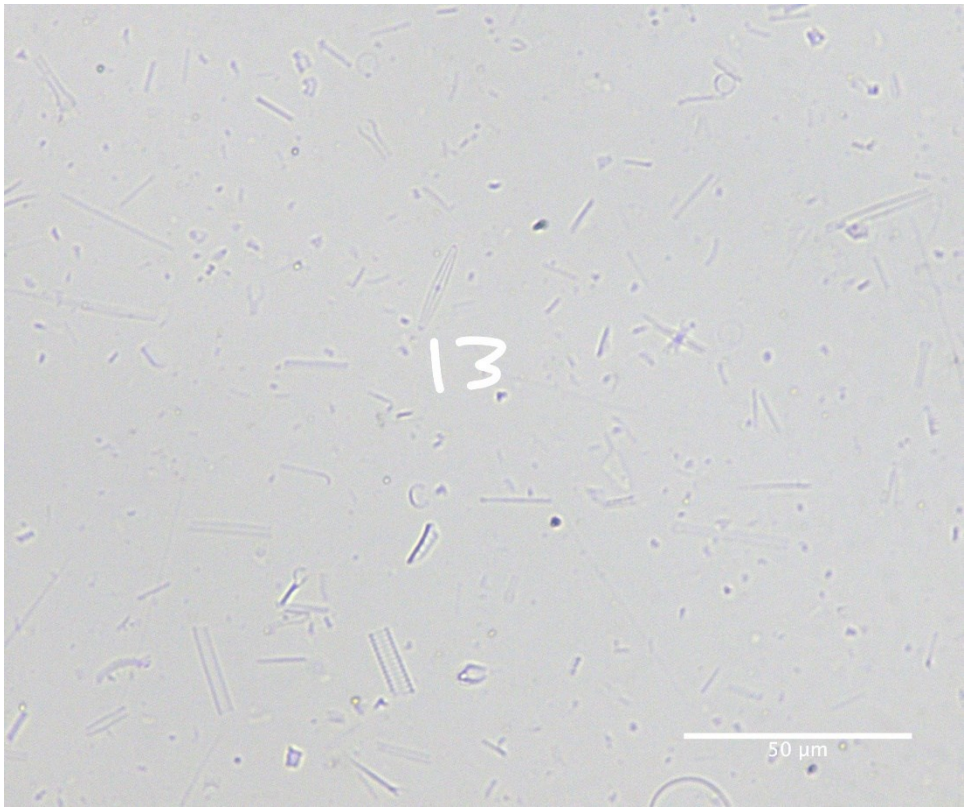

60-65 cm downcore

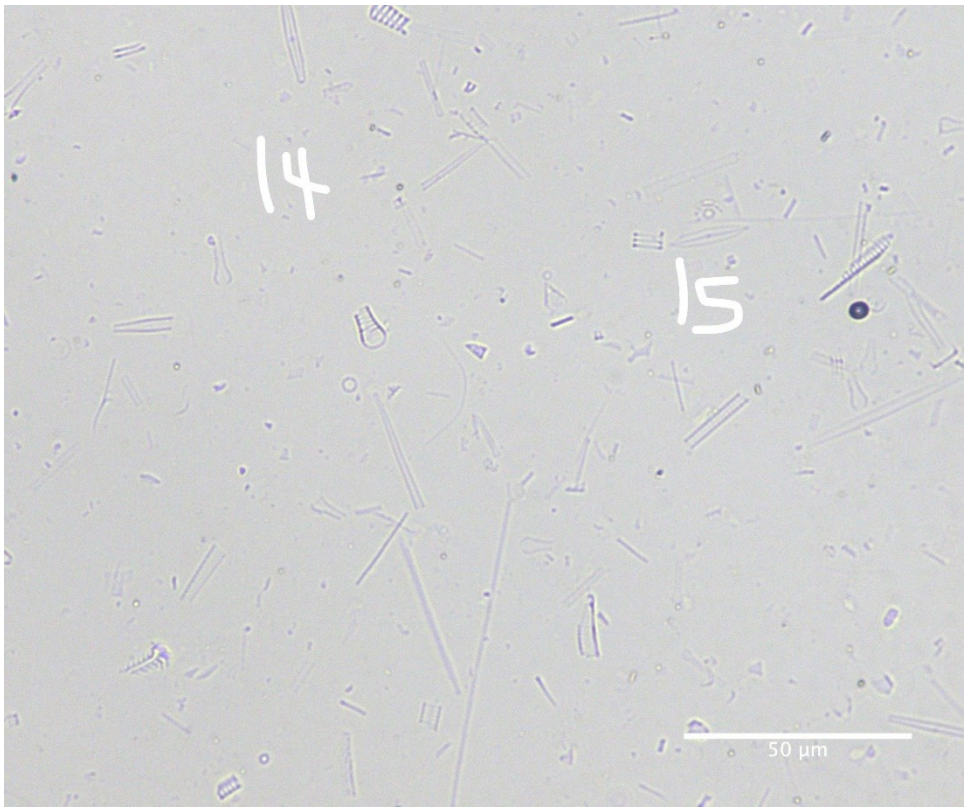


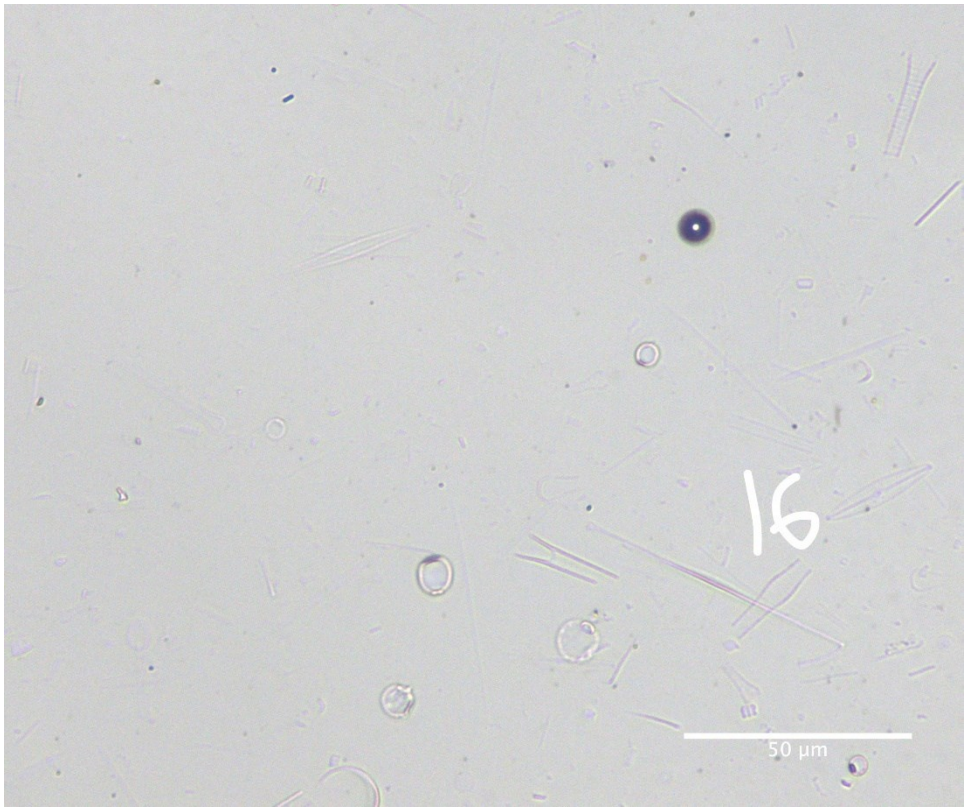

60-65 cm downcore

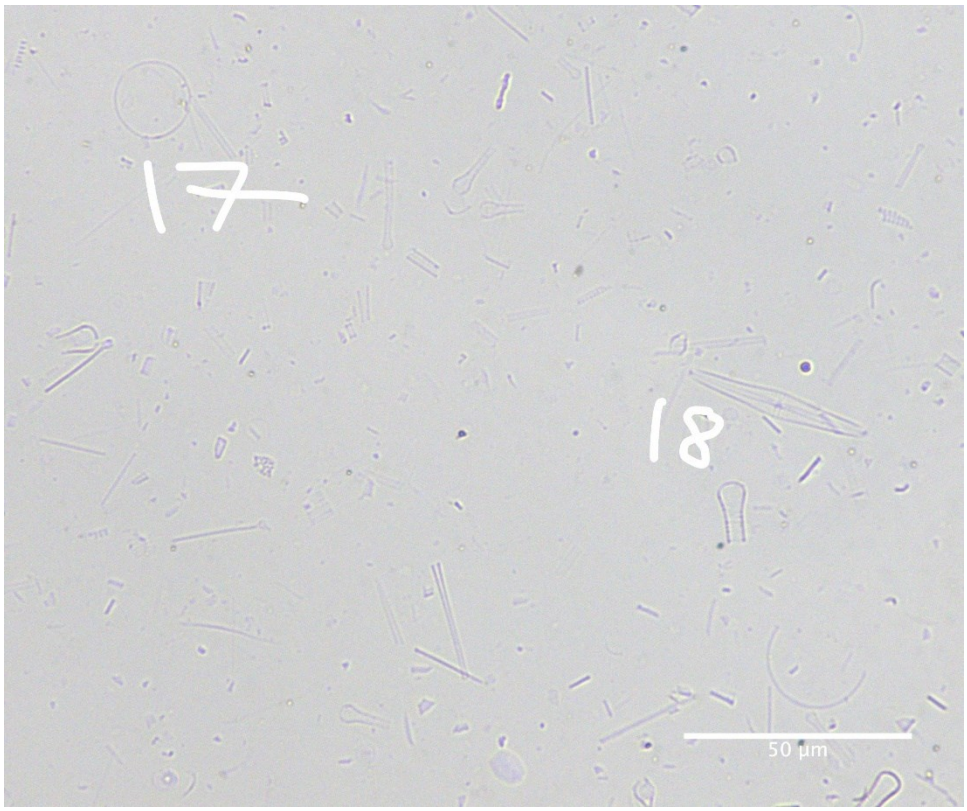


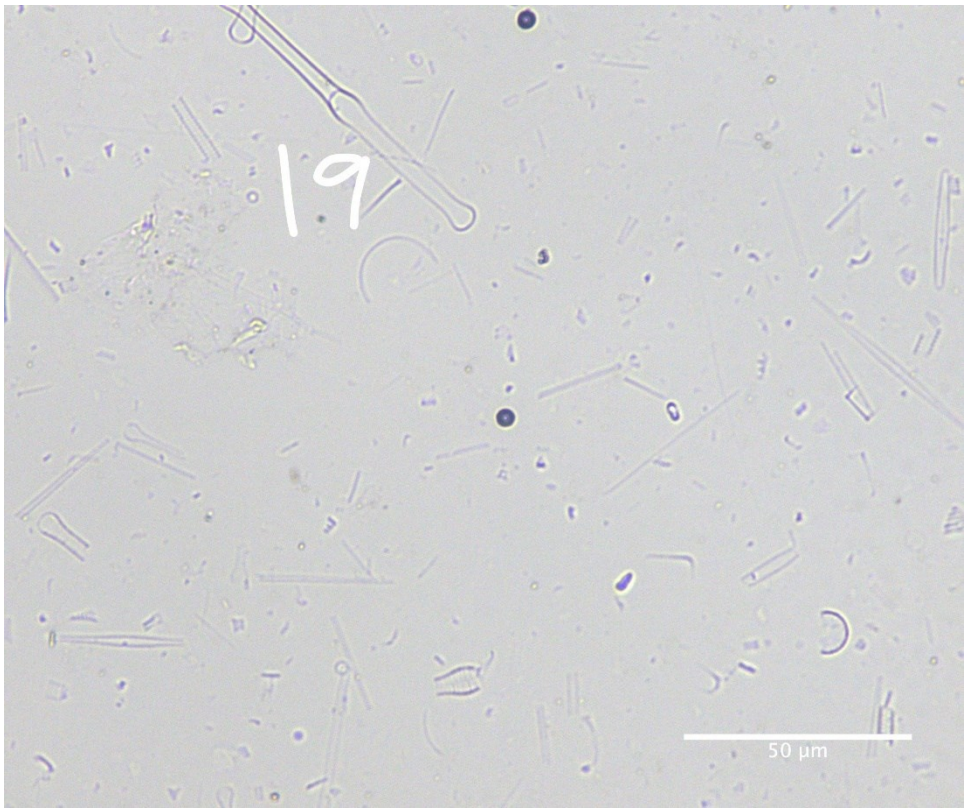

60-65 cm downcore

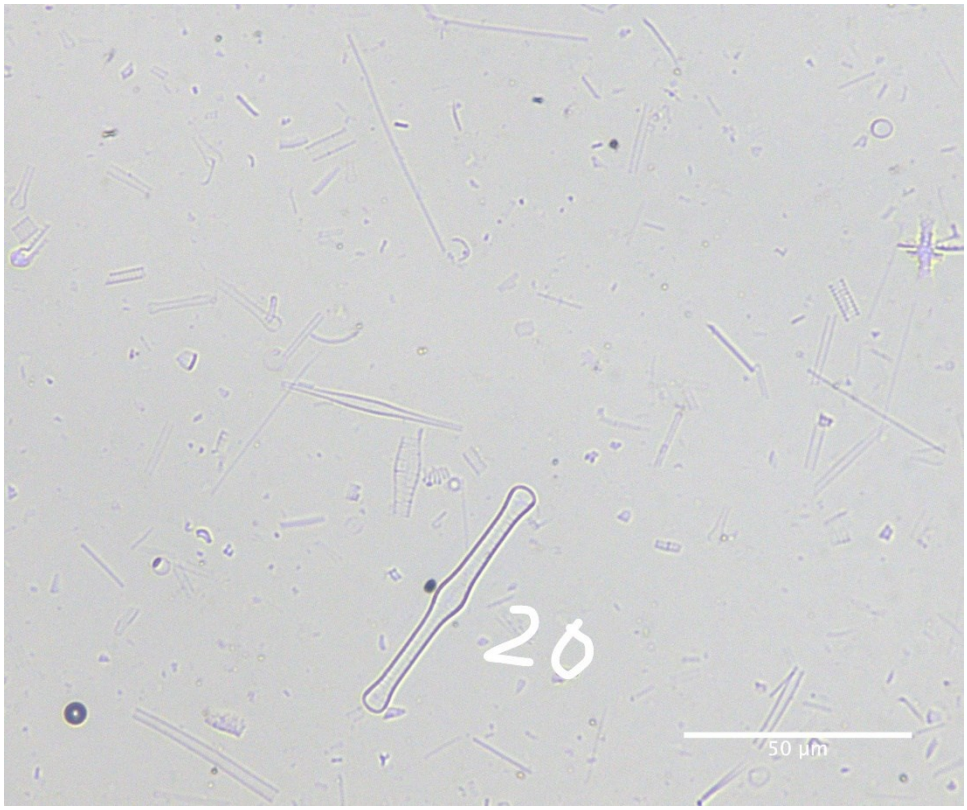


| Diatom ID | Taxon | Diatom ID | Taxon |
|---|---|---|---|
| 1 | *Thalassiosira* sp. | 11 | *Thalassiosira* sp. |
| 2 | *Navicula* sp. | 12 | *Cyclotella* sp. |
| 3 | *Eunotia* sp. | 13 | *Achnanthidium* sp. |
| 4 | *Thalassiosira* sp. | 14 | *Achnanthidium* sp. |
| 5 | *Achnanthidium* sp. | 15 | *Navicula* sp. |
| 6 | *Fragilaria* sp. | 16 | *Navicula* sp. |
| 7 | *Eunotia* sp. | 17 | *Thalassiosira* sp. |
| 8 | *Achnanthidium* sp. | 18 | *Gomphonema* sp. |
| 9 | *Thalassiosira* sp. | 19 | *Tabellaria* sp. |
| 10 | *Thalassiosira* sp. | 20 | *Tabellaria* sp. |

65-70 cm downcore


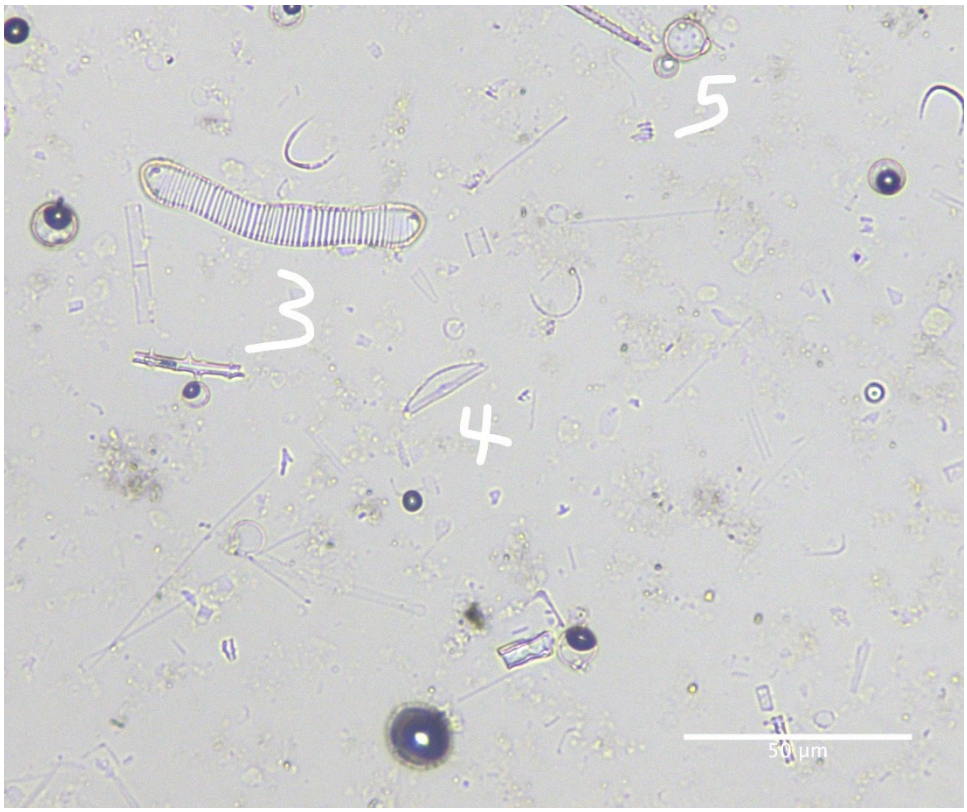

65-70 cm downcore

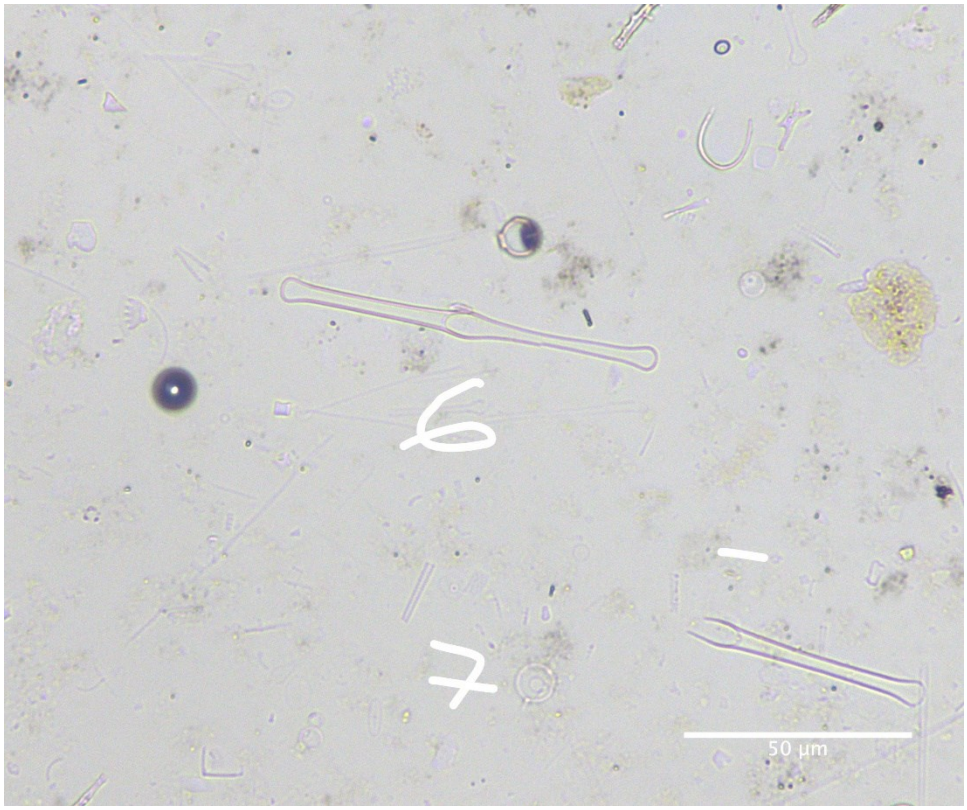


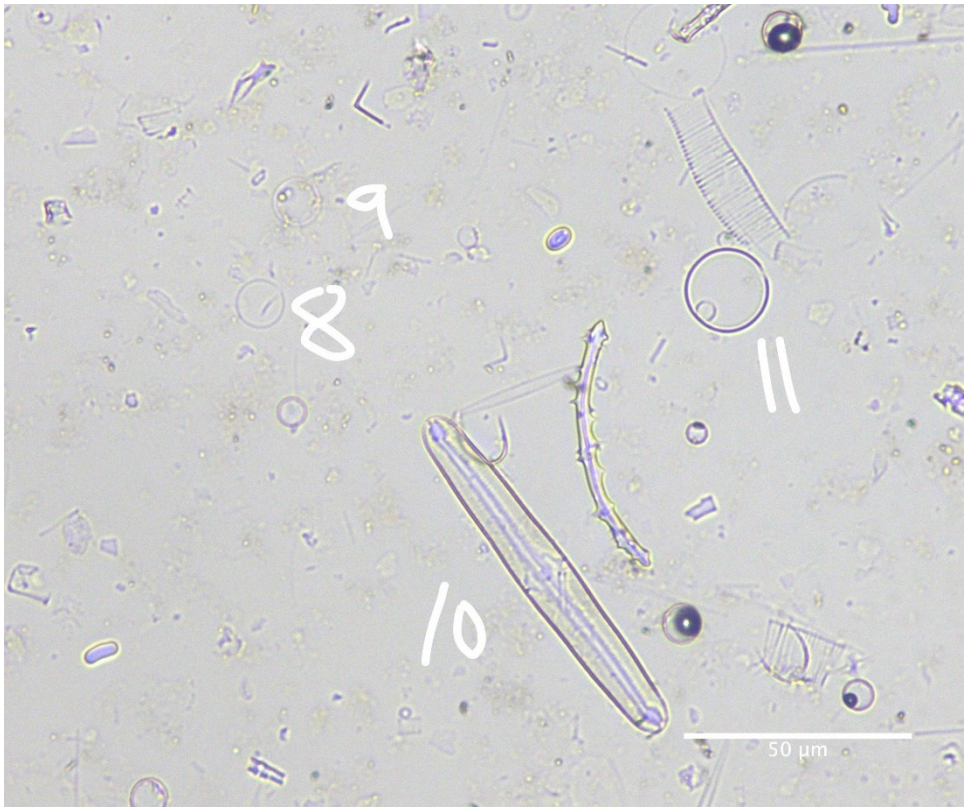

65-70 cm downcore

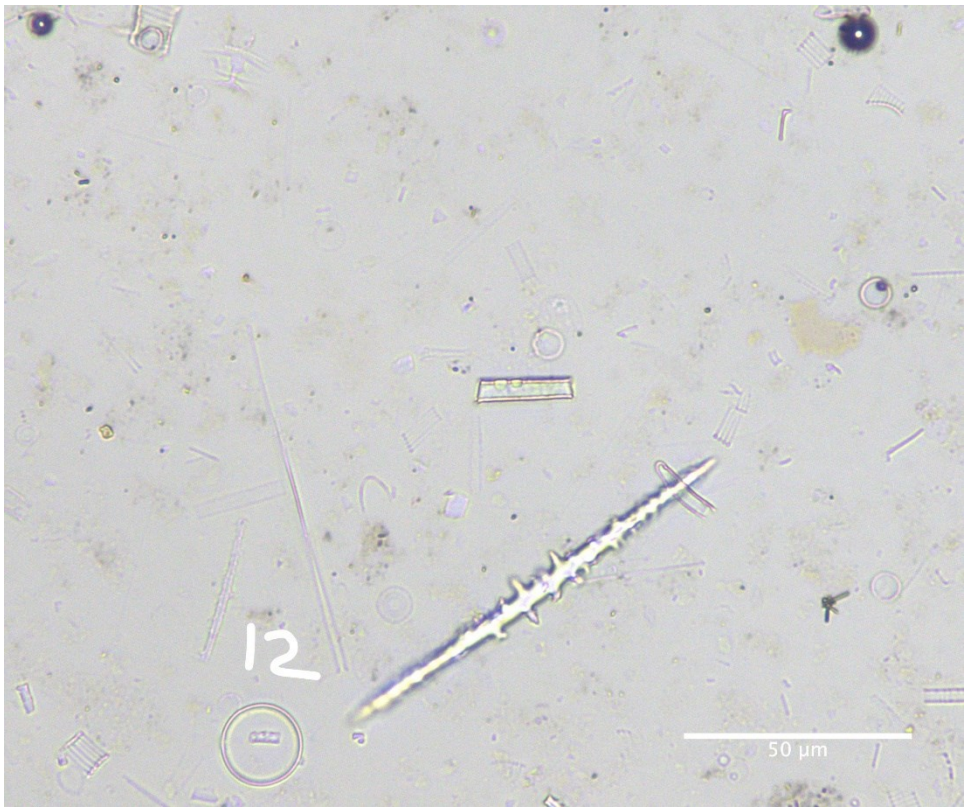


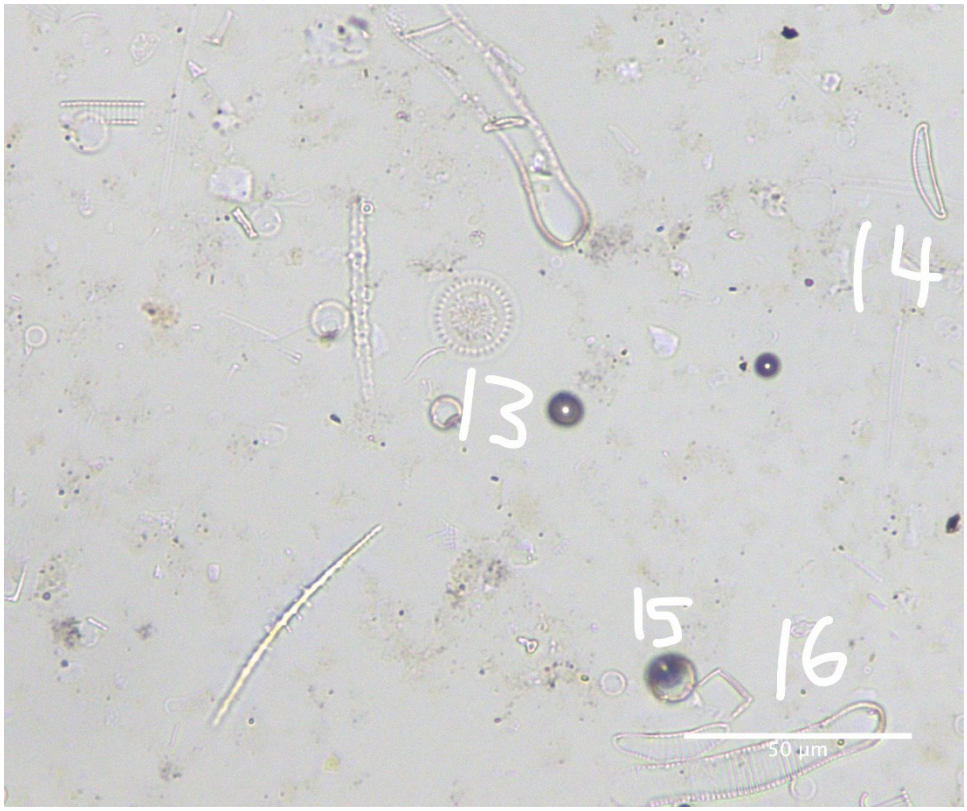

65-70 cm downcore

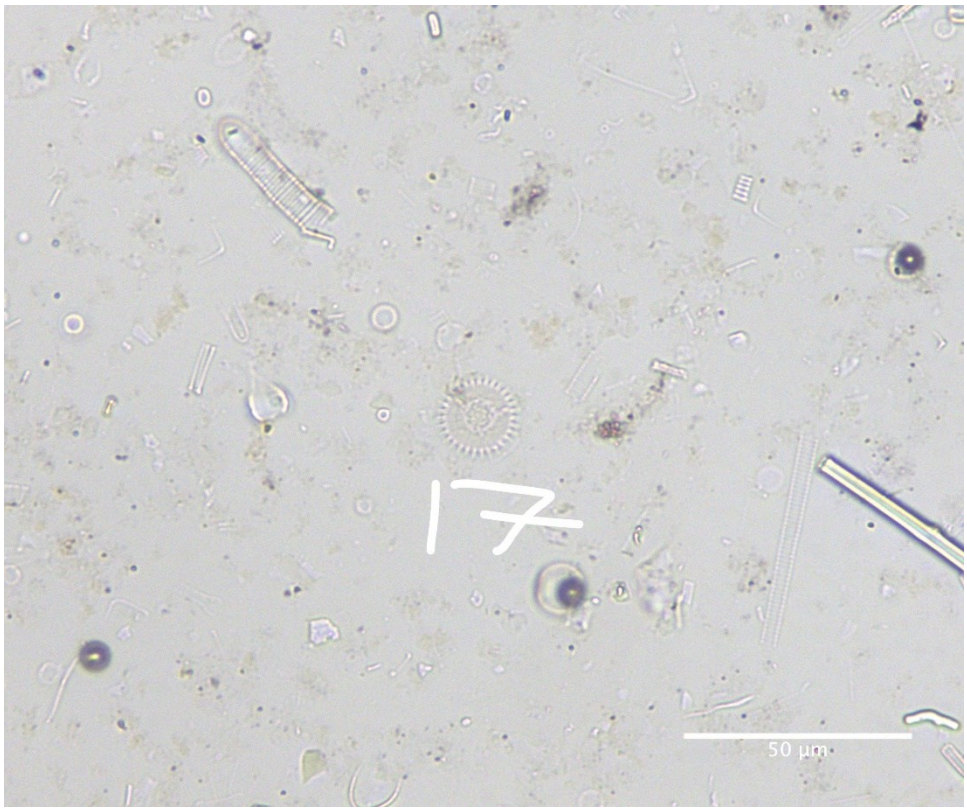


65-70 cm downcore


| Diatom ID | Taxon | Diatom ID | Taxon |
|---|---|---|---|
| 1 | *Eunotia* sp. | 11 | *Thalassiosira* sp. |
| 2 | *Eunotia* sp. | 12 | *Thalassiosira* sp. |
| 3 | *Eunotia* sp. | 13 | *Cyclotella* sp. |
| 4 | *Tabellaria* sp. | 14 | *Eunotia* sp. |
| 5 | *Thalassiosira* sp. | 15 | *Thalassiosira* sp. |
| 6 | *Tabellaria* sp. | 16 | *Eunotia* sp. |
| 7 | *Cyclotella* sp. | 17 | *Cyclotella* sp. |
| 8 | *Thalassiosira* sp. | 18 | *Eunotia* sp. |
| 9 | *Thalassiosira* sp. | 19 | *Navicula* sp. |
| 10 | *Pinnularia* sp. | 20 | *Eunotia* sp. |

70-75 cm downcore

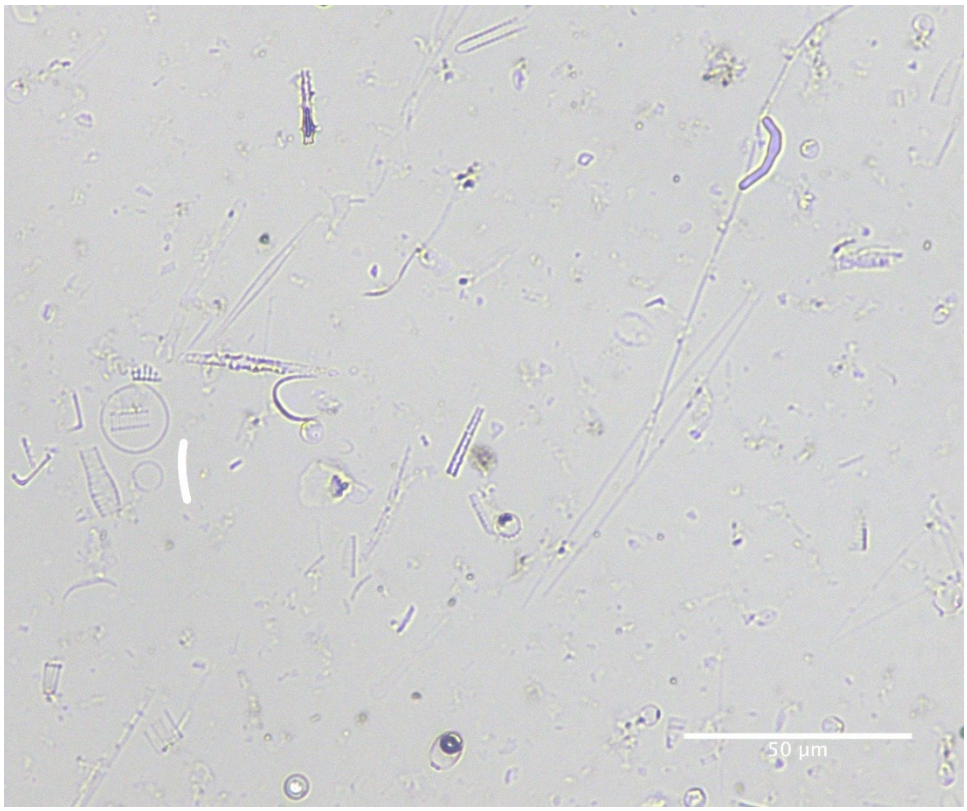


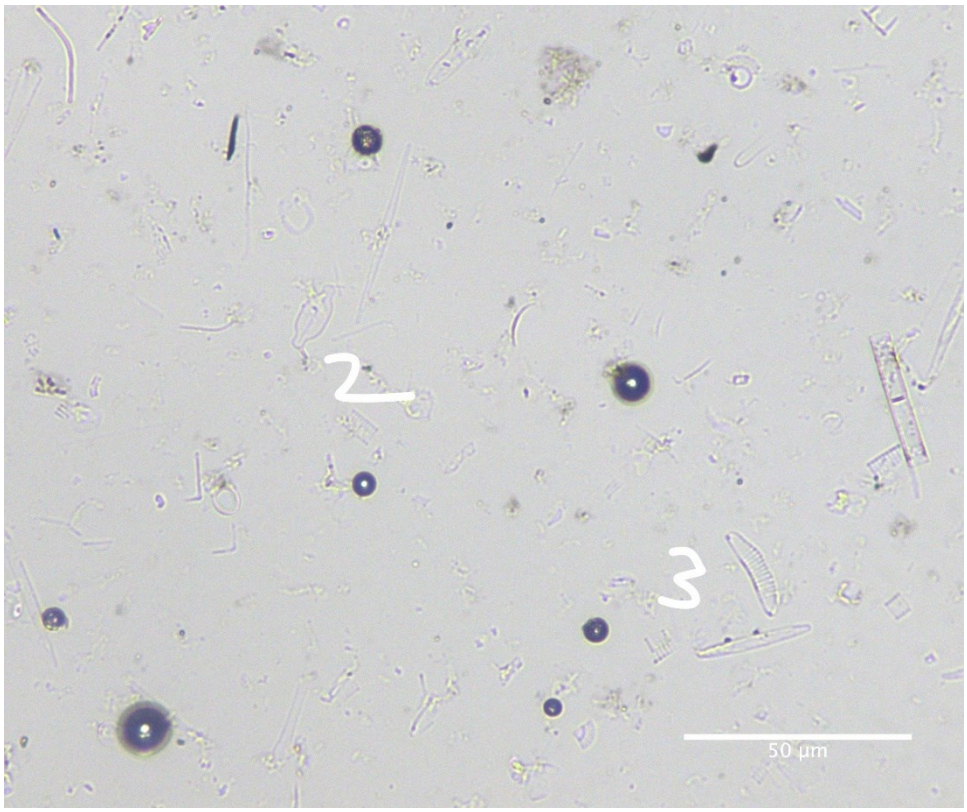

70-75 cm downcore

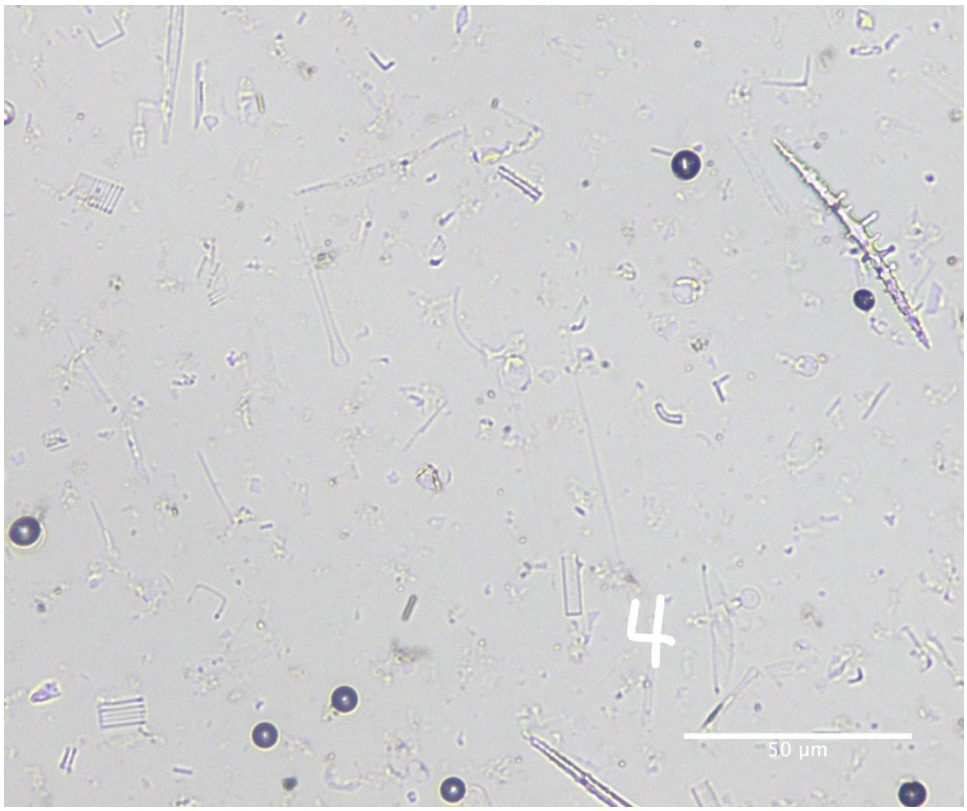


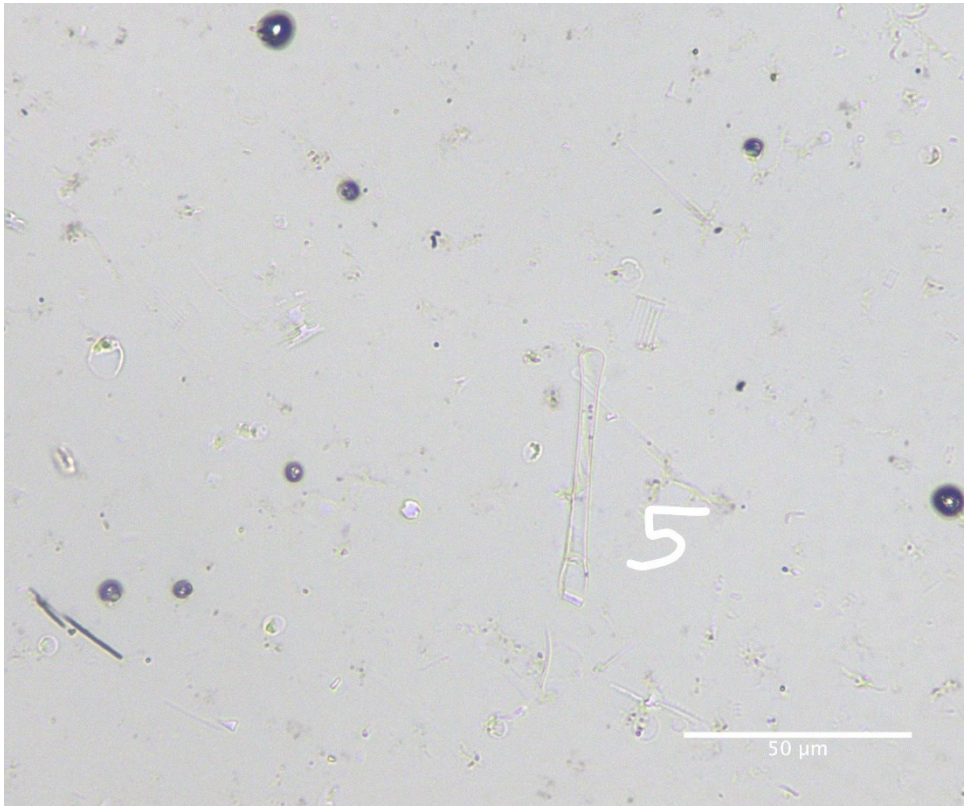

70-75 cm downcore

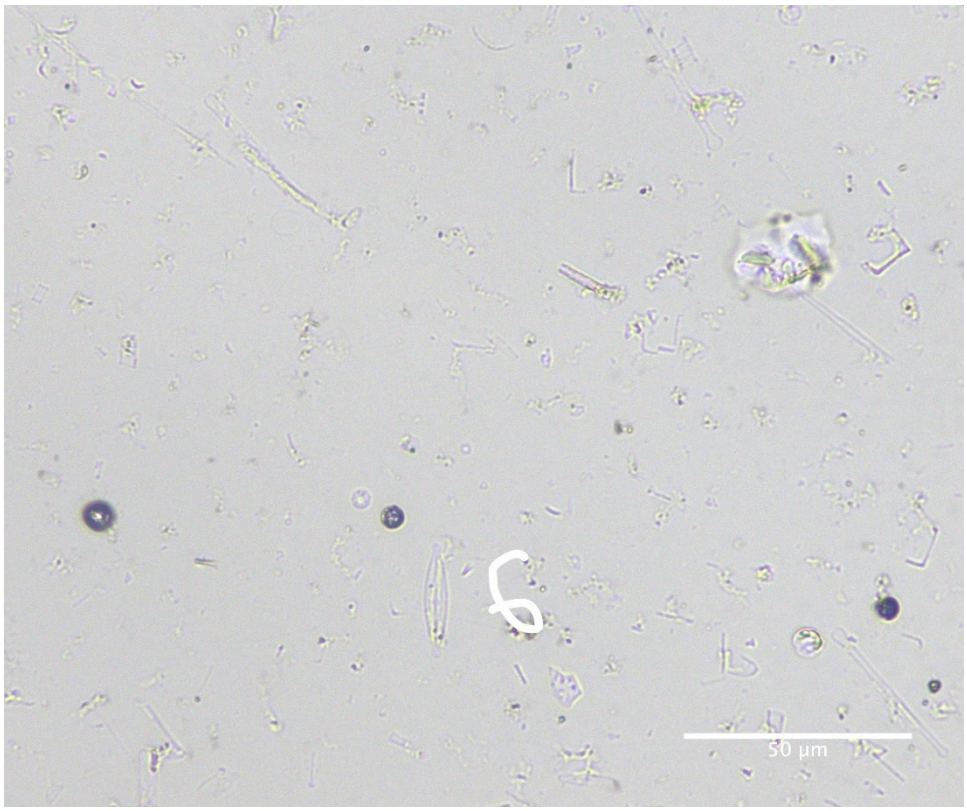


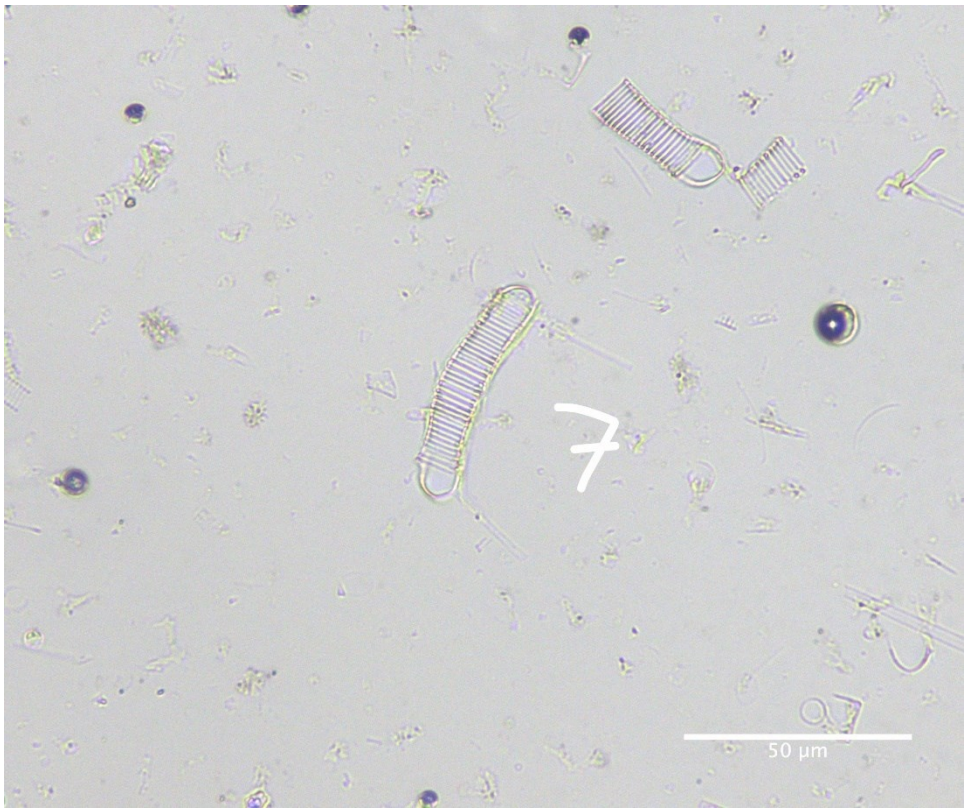

70-75 cm downcore

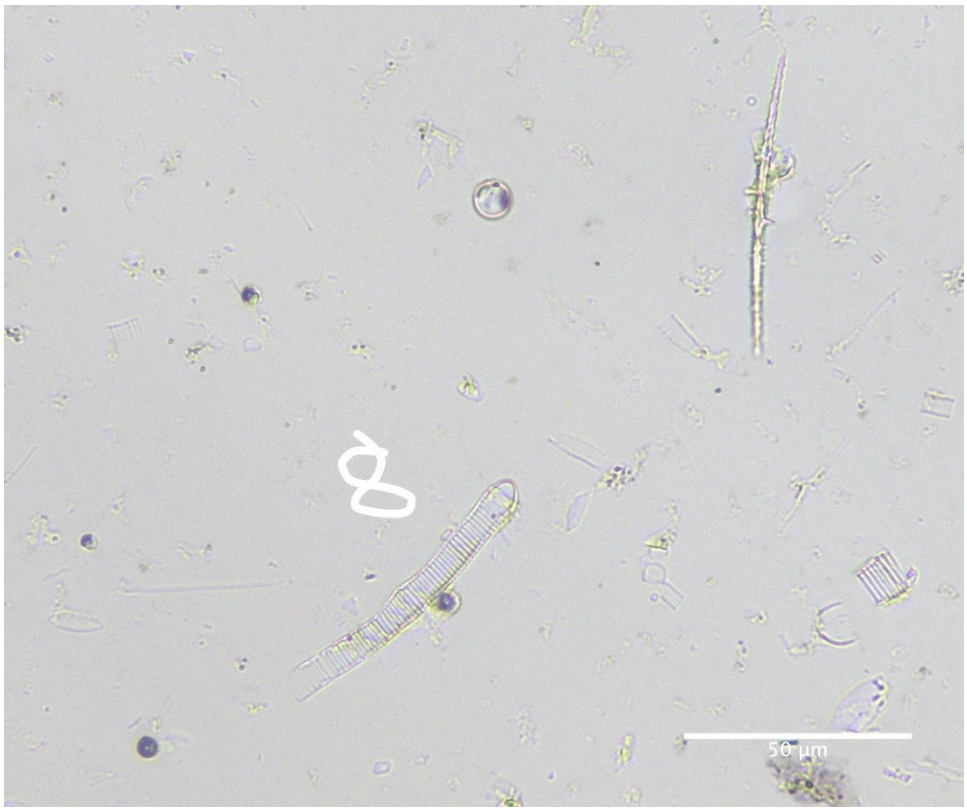


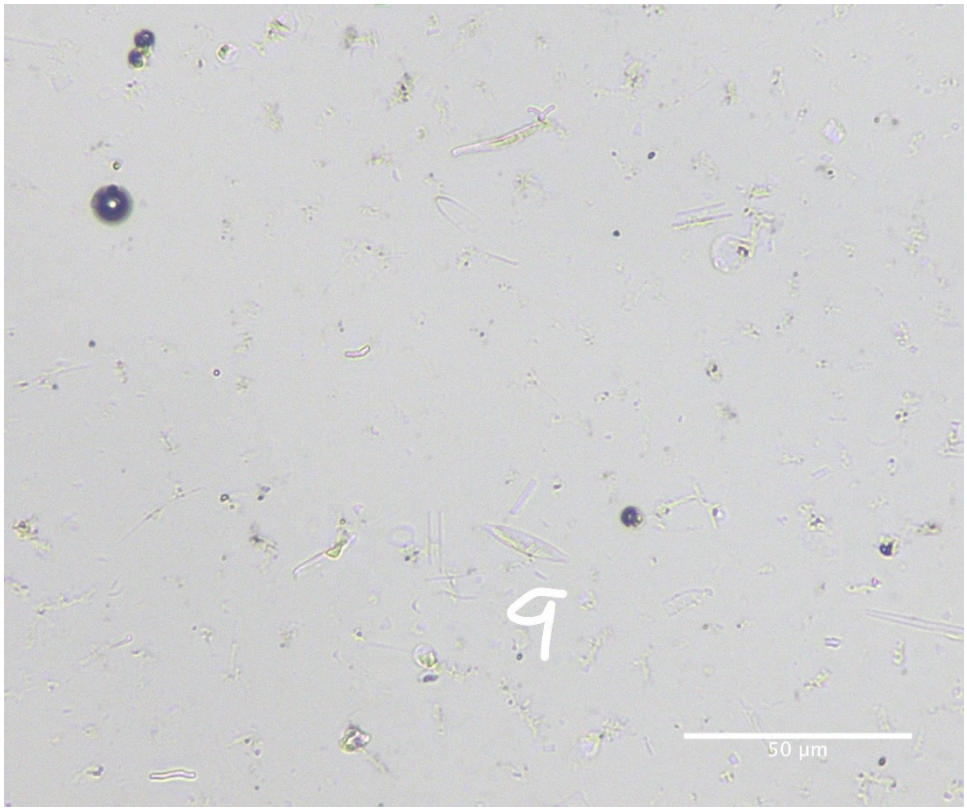

70-75 cm downcore

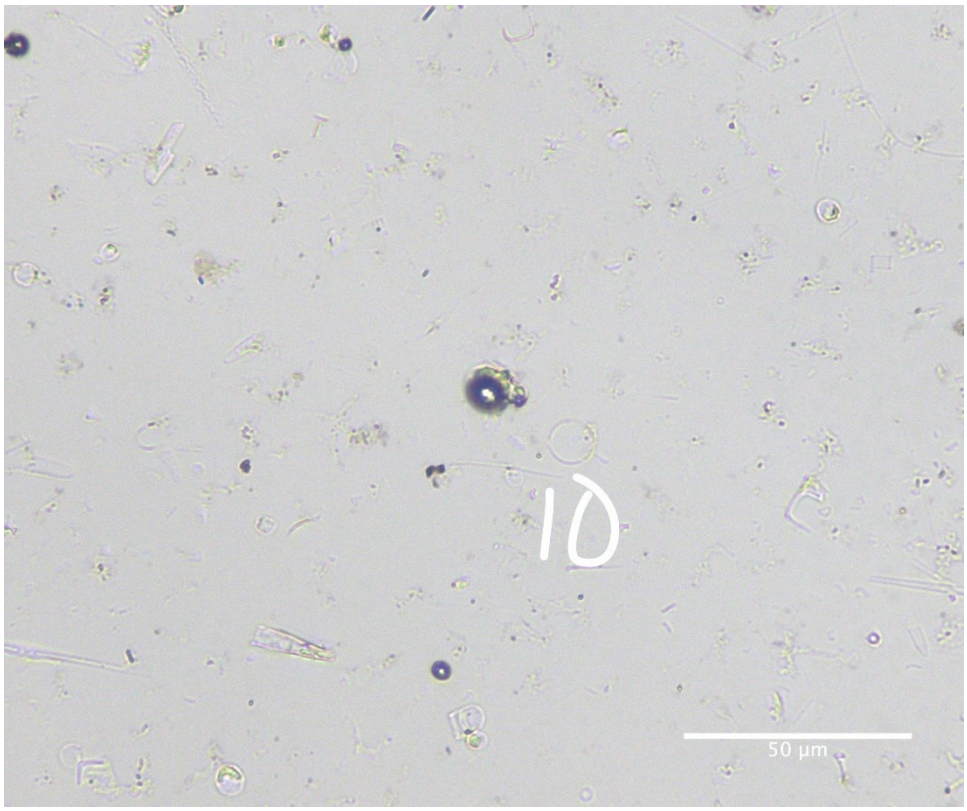


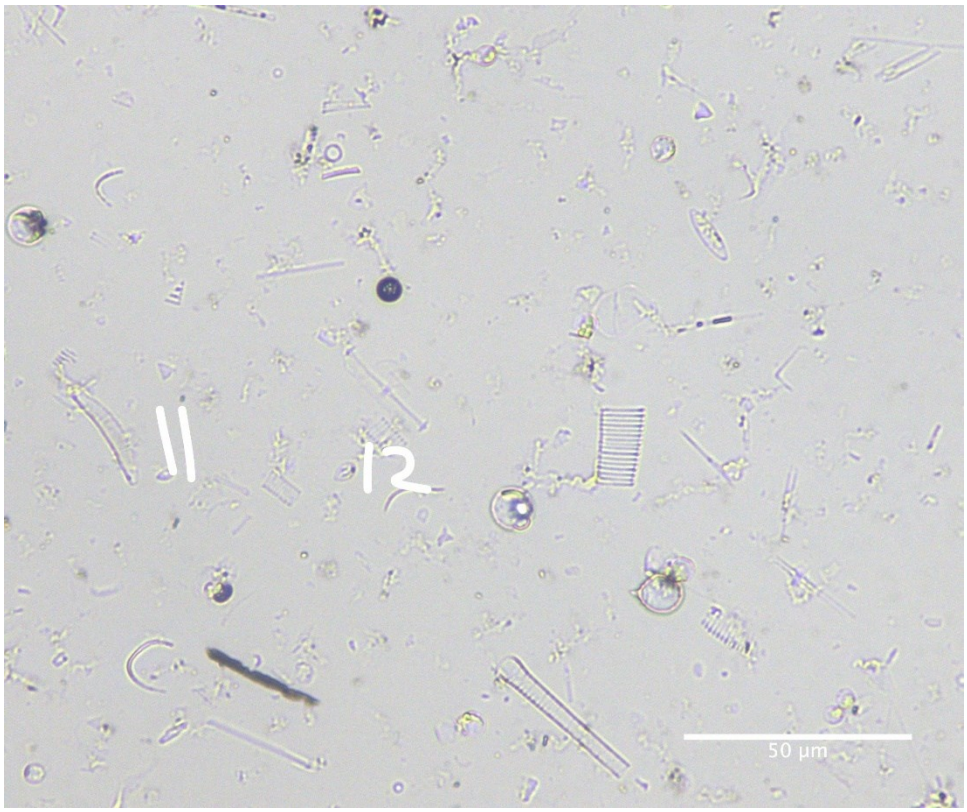

70-75 cm downcore

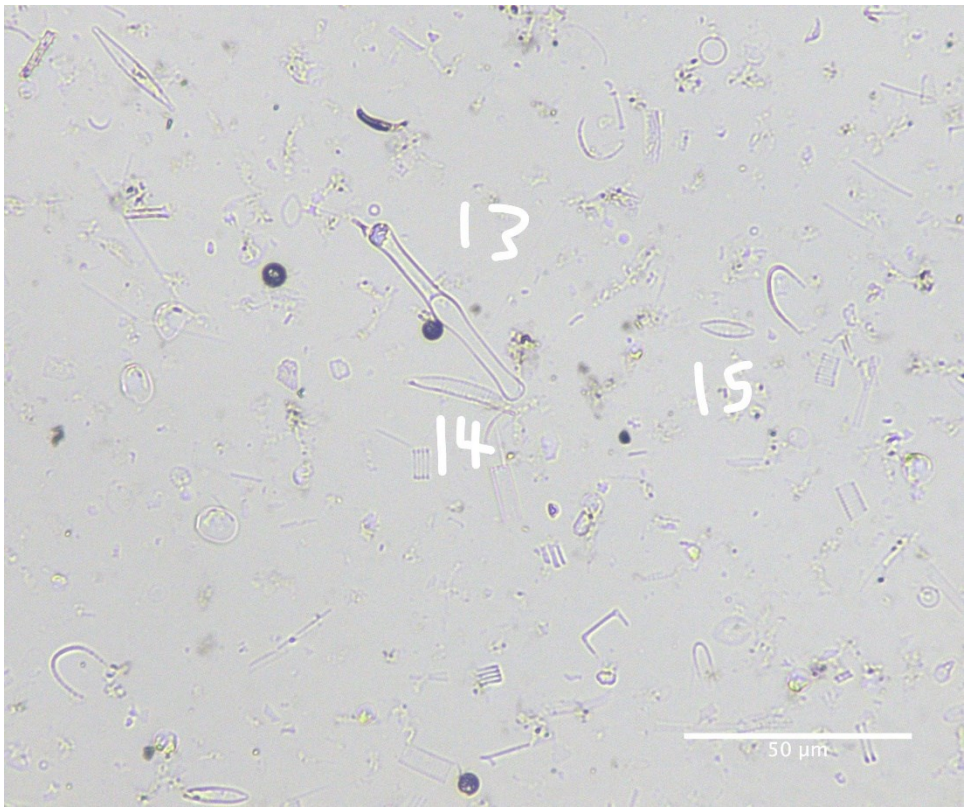


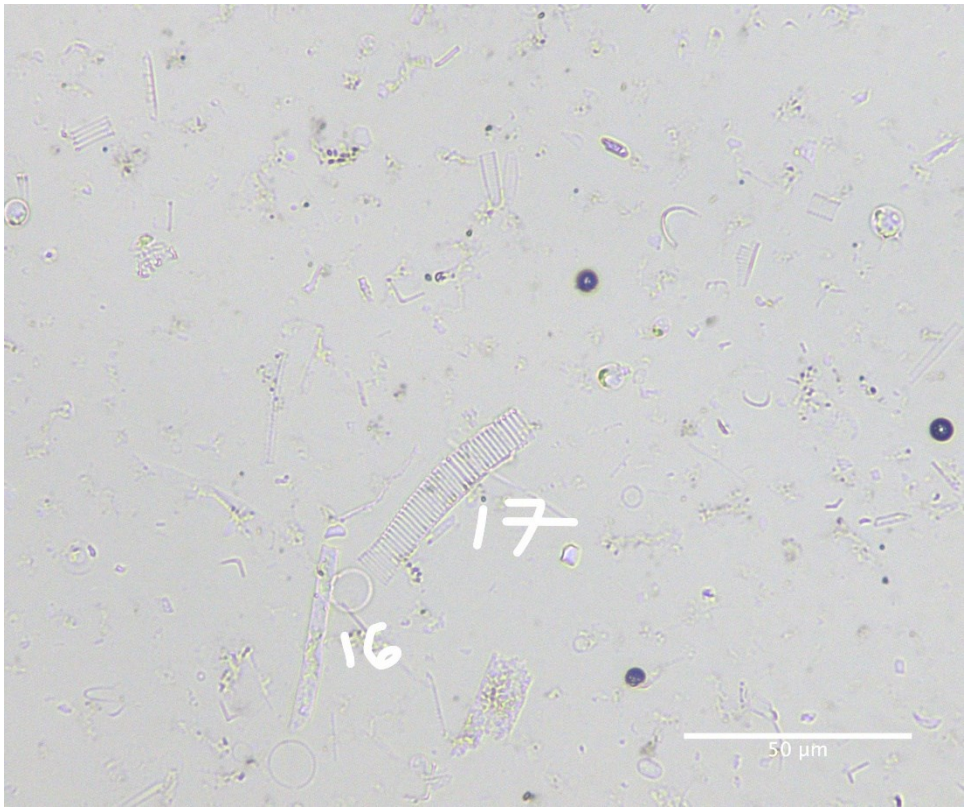

70-75 cm downcore

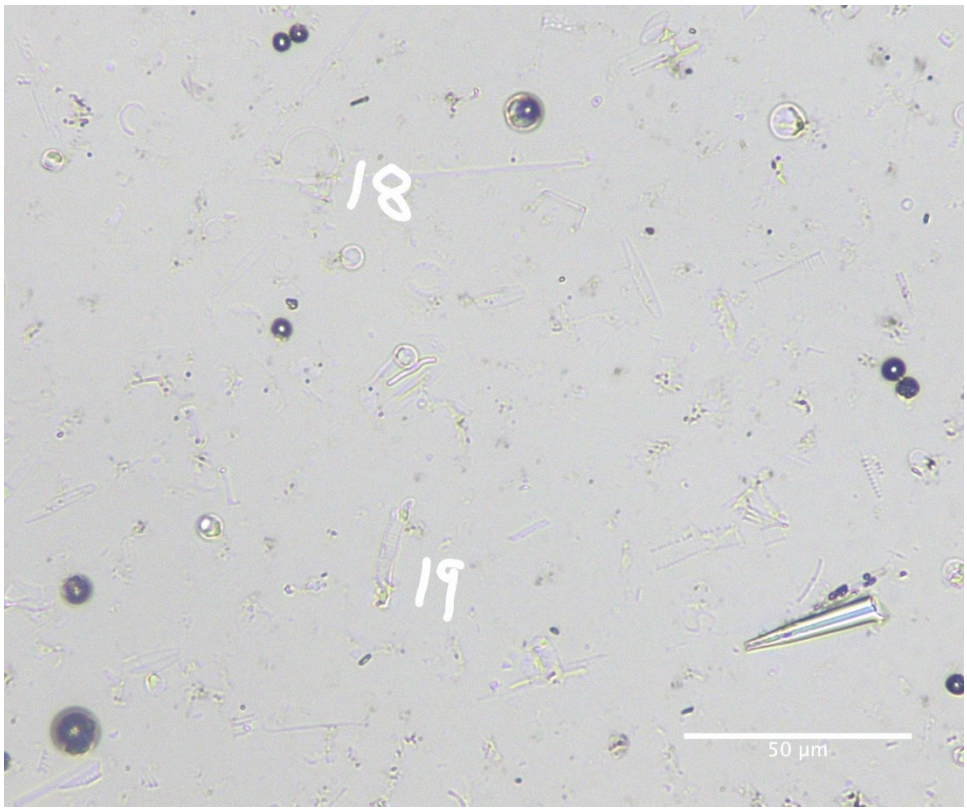


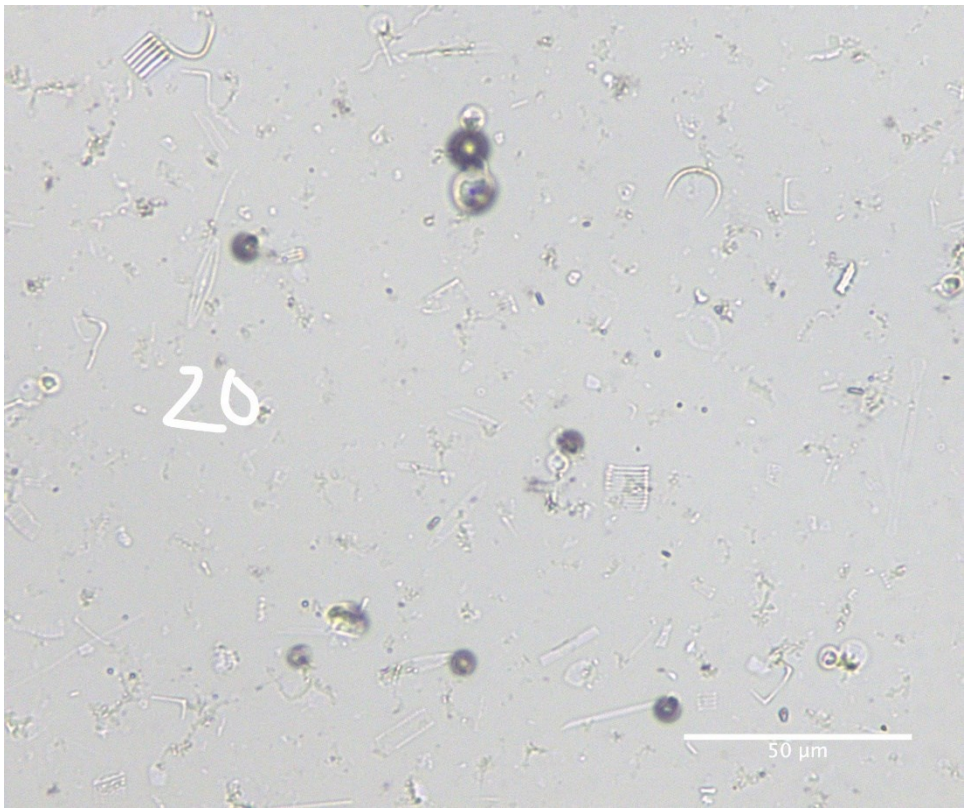

70-75 cm downcore

| Diatom ID | Taxon | Diatom ID | Taxon |
|---|---|---|---|
| 1 | *Thalassiosira* sp. | 11 | *Eunotia* sp. |
| 2 | *Achnanthidium* sp. | 12 | *Navicula* sp. |
| 3 | *Eunotia* sp. | 13 | *Tabellaria* sp. |
| 4 | *Eunotia* sp. | 14 | *Eunotia* sp. |
| 5 | *Asterionella* sp. | 15 | *Nitzschia* sp. |
| 6 | *Navicula* sp. | 16 | *Thalassiosira* sp. |
| 7 | *Eunotia* sp. | 17 | *Eunotia* sp. |
| 8 | *Eunotia* sp. | 18 | *Thalassiosira* sp. |
| 9 | *Navicula* sp. | 19 | *Eunotia* sp. |
| 10 | *Thalassiosira* sp. | 20 | *Gomphonema* sp. |

75-80 cm downcore

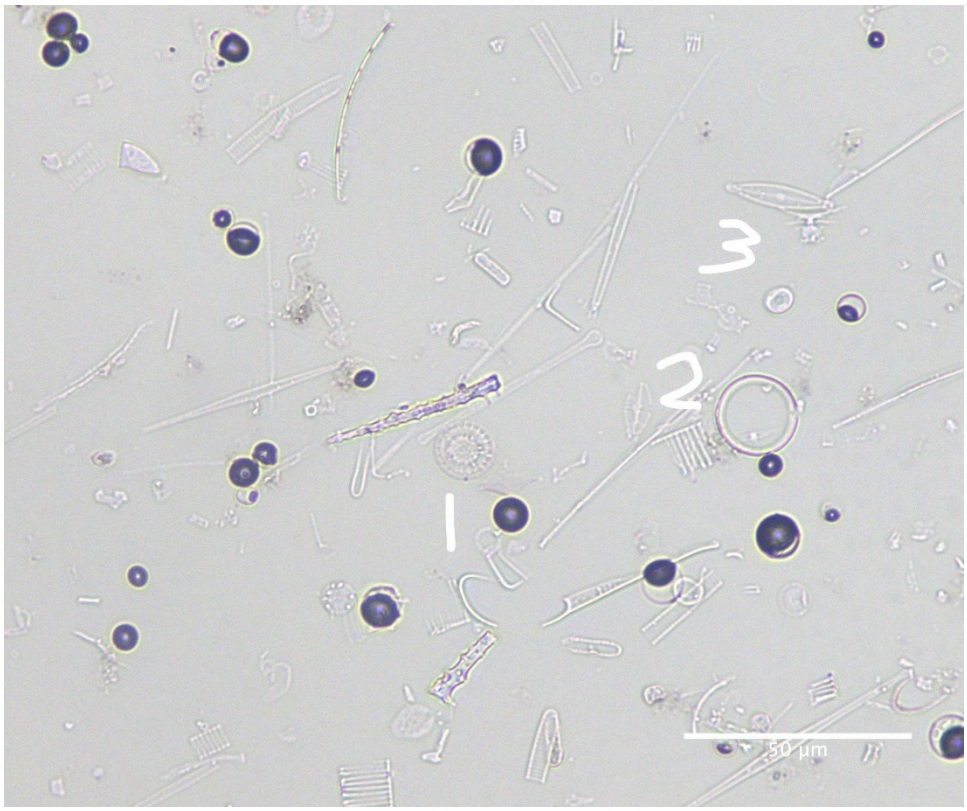


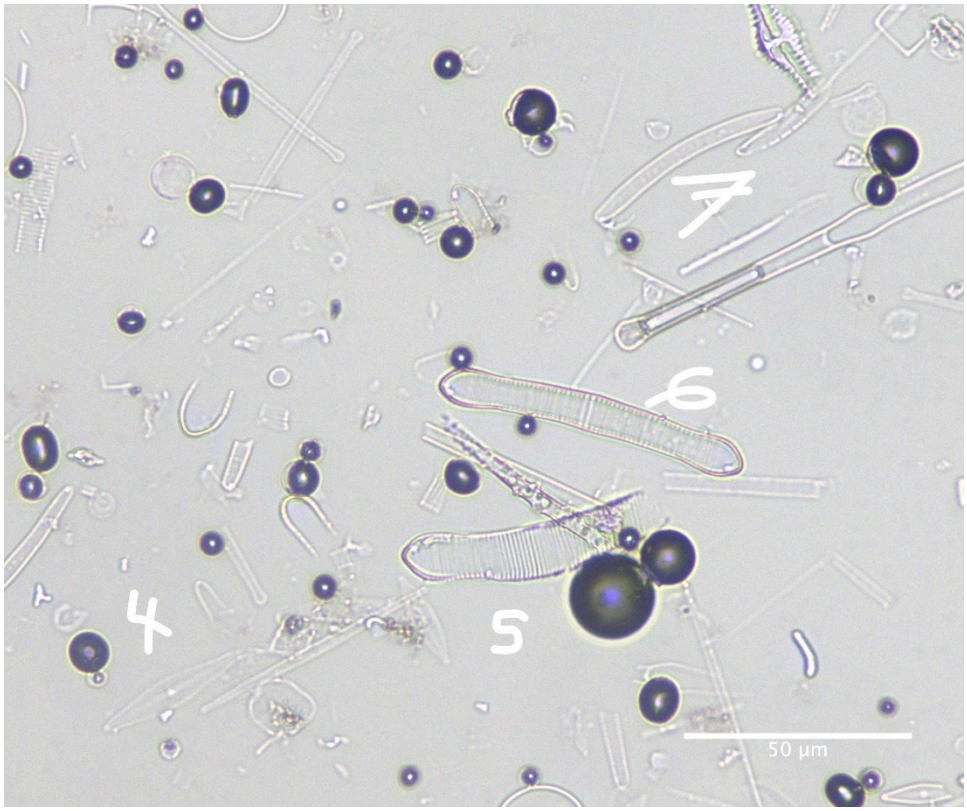

75-80 cm downcore

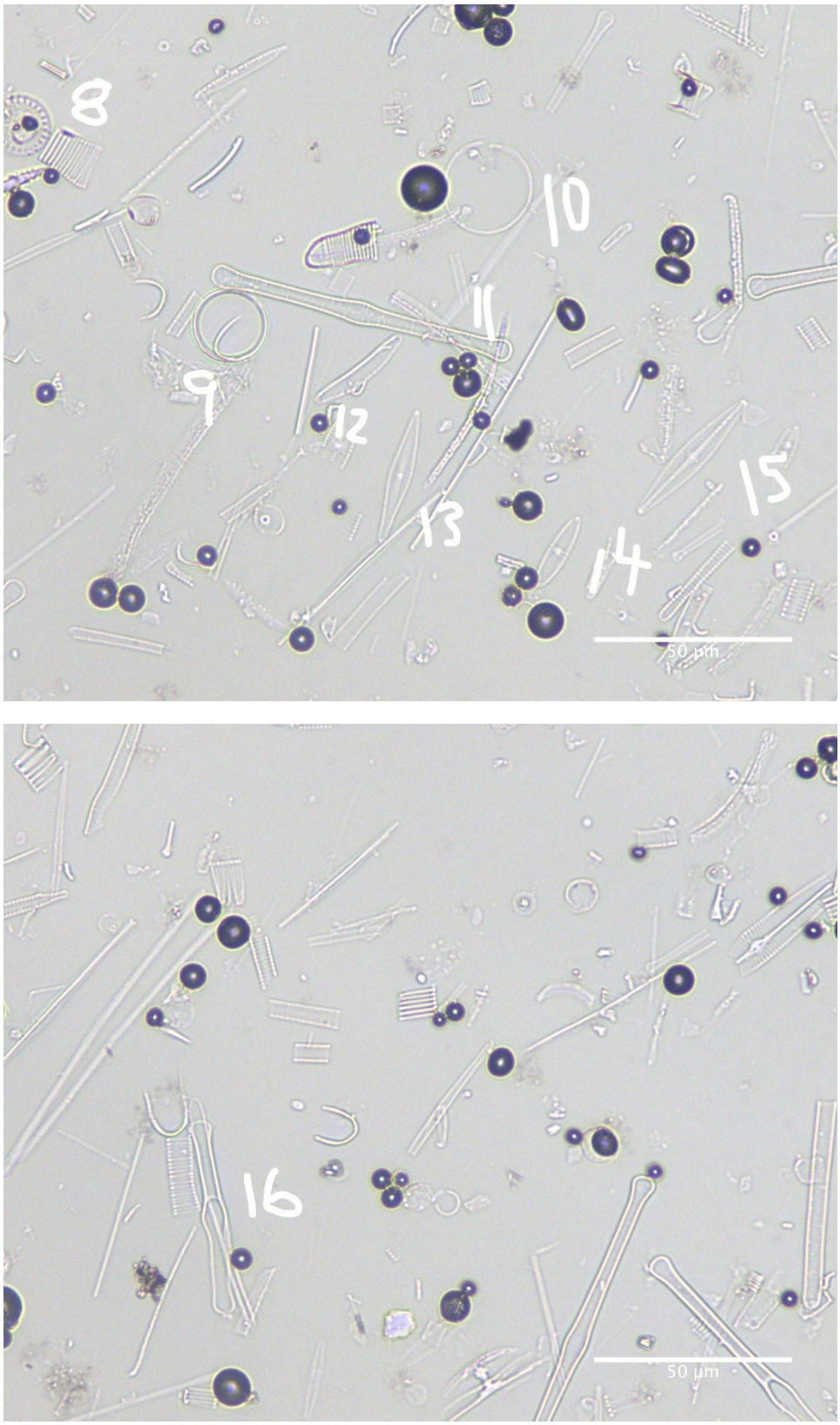

75-80 cm downcore

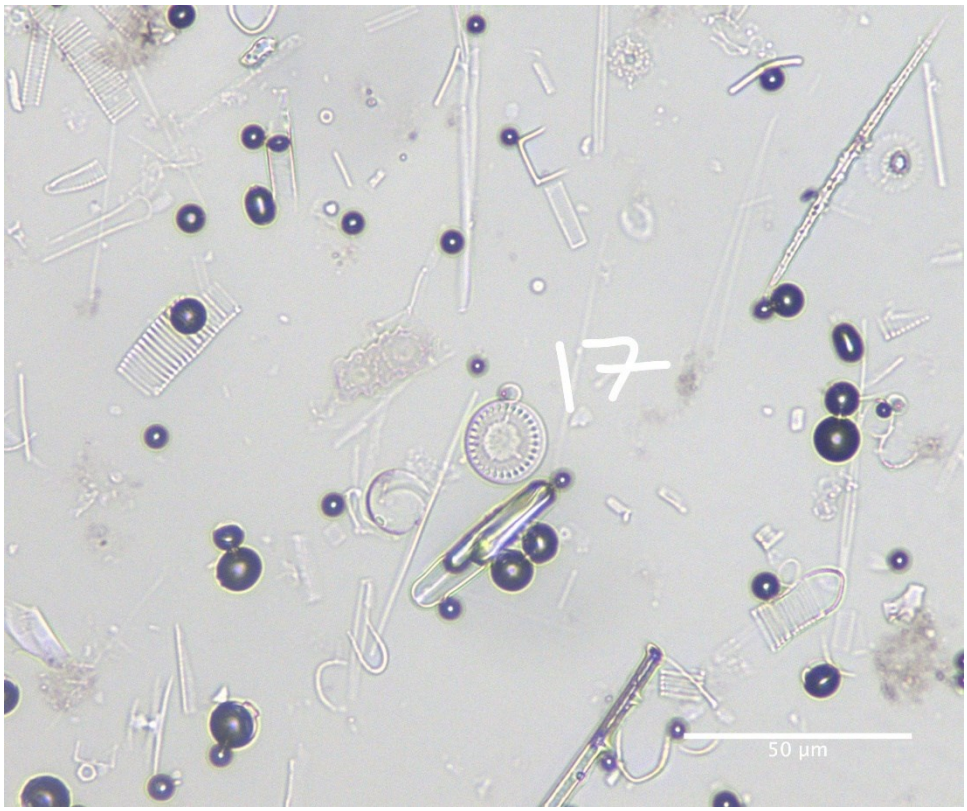


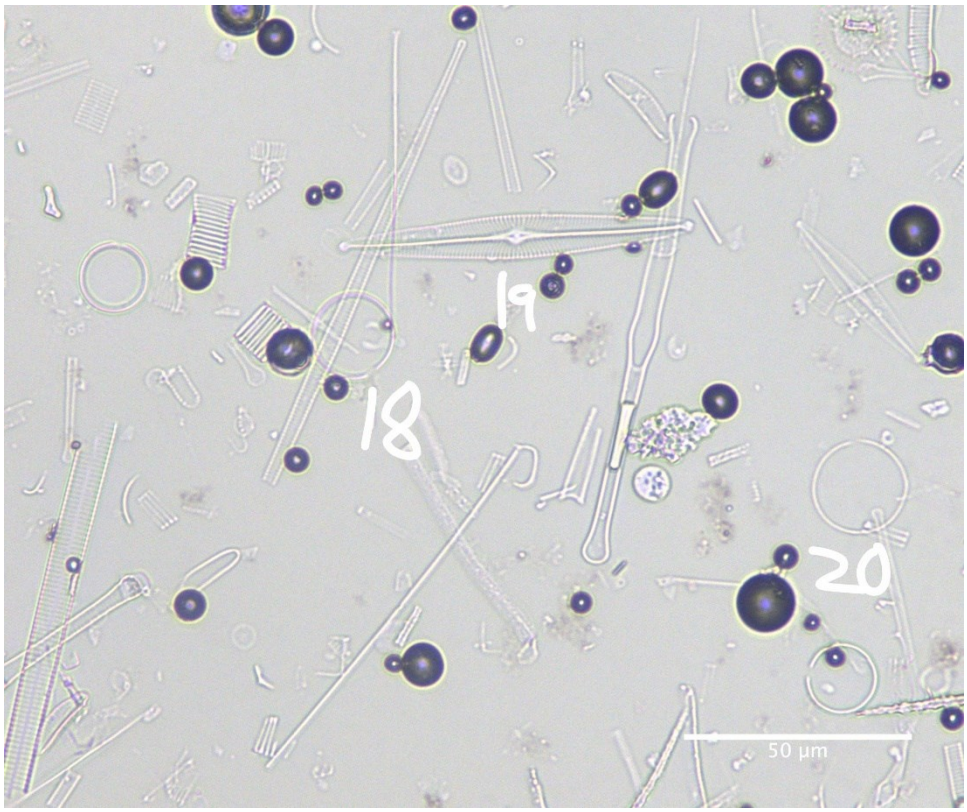

75-80 cm downcore

| Diatom ID | Taxon | Diatom ID | Taxon |
|---|---|---|---|
| 1 | *Cyclotella* sp. | 11 | *Tabellaria* sp. |
| 2 | *Thalassiosira* sp. | 12 | *Eunotia* sp. |
| 3 | *Navicula* sp. | 13 | *Gomphonema* sp. |
| 4 | *Gomphonema* sp. | 14 | *Gomphonema* sp. |
| 5 | *Eunotia* sp. | 15 | *Navicula* sp. |
| 6 | *Eunotia* sp. | 16 | *Tabellaria* sp. |
| 7 | *Eunotia* sp. | 17 | *Cyclotella* sp. |
| 8 | *Cyclotella* sp. | 18 | *Thalassiosira* sp. |
| 9 | *Thalassiosira* sp. | 19 | *Navicula* sp. |
| 10 | *Thalassiosira* sp. | 20 | *Thalassiosira* sp. |

80-85 cm downcore

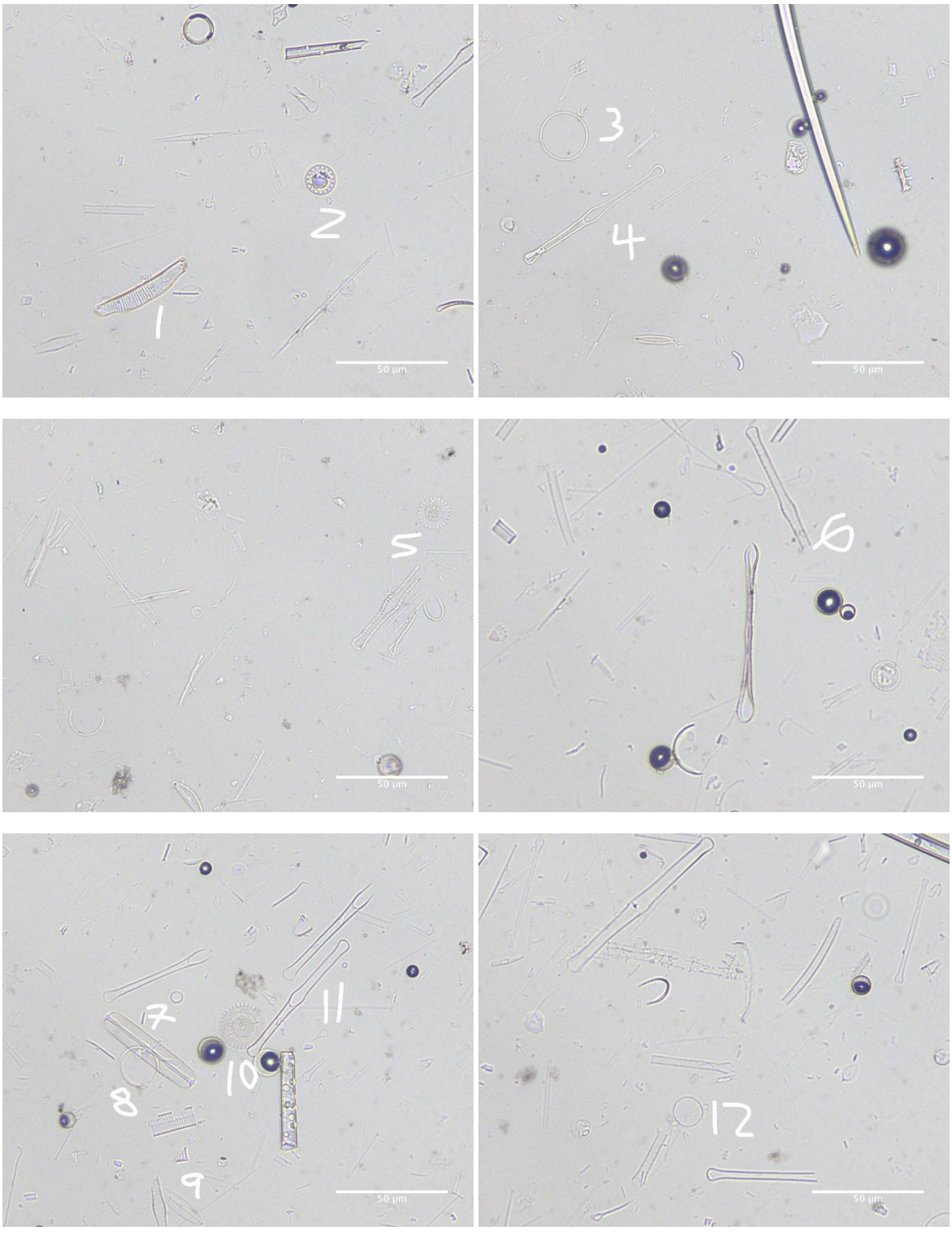

80-85 cm downcore


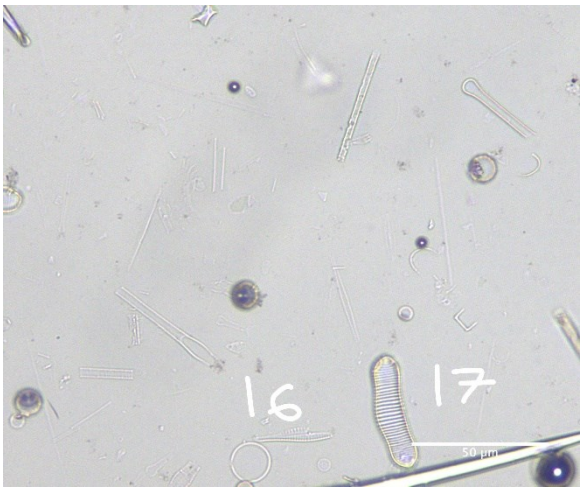



| Diatom ID | Taxon | Diatom ID | Taxon |
|---|---|---|---|
| 1 | *Eunotia* sp. | 11 | *Tabellaria* sp. |
| 2 | *Cyclotella* sp. | 12 | *Thalassiosira* sp. |
| 3 | *Thalassiosira* sp. | 13 | *Tabellaria* sp. |
| 4 | *Tabellaria* sp. | 14 | *Cyclotella* sp. |
| 5 | *Cyclotella* sp. | 15 | *Cyclotella* sp. |
| 6 | *Tabellaria* sp. | 16 | *Thalassiosira* sp. |
| 7 | *Navicula* sp. | 17 | *Eunotia* sp. |
| 8 | *Thalassiosira* sp. | 18 | *Eunotia* sp. |
| 9 | *Navicula* sp. | 19 | *Gomphonema* sp. |
| 10 | *Cyclotella* sp. | 20 | *Thalassiosira* sp. |

85-90 cm downcore

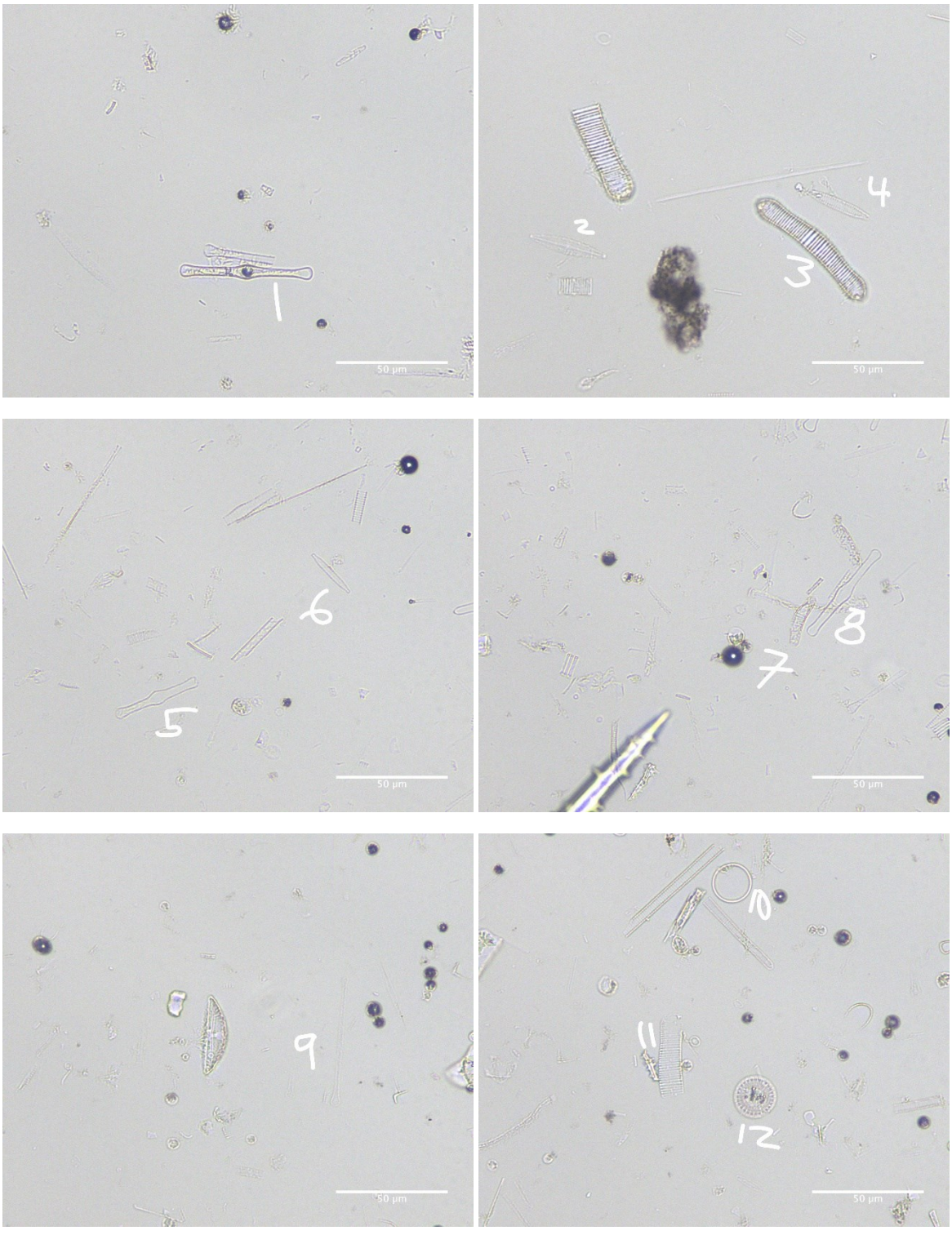

85-90 cm downcore

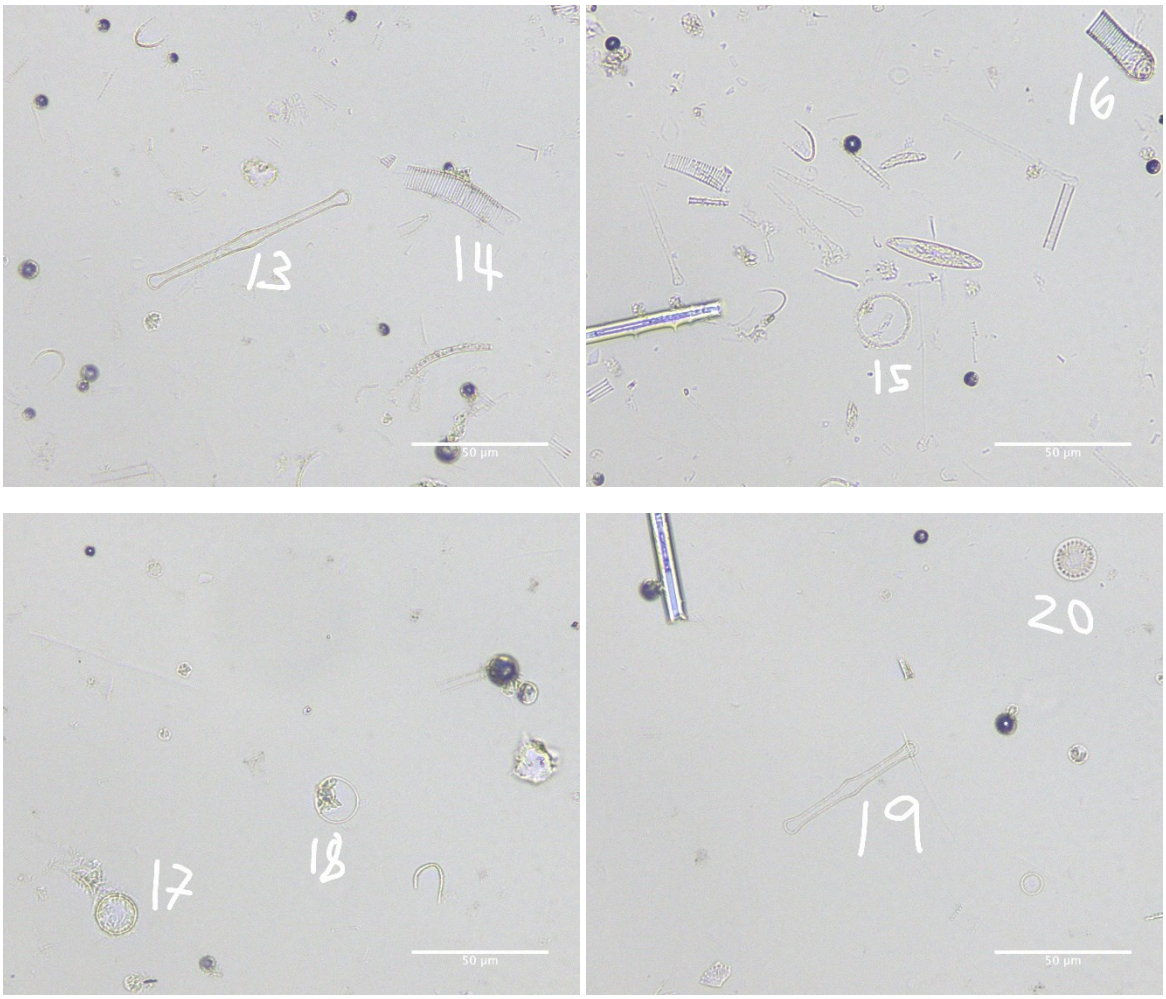


| Diatom ID | Taxon | Diatom ID | Taxon |
|---|---|---|---|
| 1 | *Tabellaria* sp. | 11 | *Eunotia* sp. |
| 2 | *Navicula* sp. | 12 | *Cyclotella* sp. |
| 3 | *Eunotia* sp. | 13 | *Tabellaria* sp. |
| 4 | *Nitzschia* sp. | 14 | *Eunotia* sp. |
| 5 | *Tabellaria* sp. | 15 | *Thalassiosira* sp. |
| 6 | *Nitzschia* sp. | 16 | *Eunotia* sp. |
| 7 | *Eunotia* sp. | 17 | *Thalassiosira* sp. |
| 8 | *Tabellaria* sp. | 18 | *Thalassiosira* sp. |
| 9 | *Cymbella* sp. | 19 | *Tabellaria* sp. |
| 10 | *Thalassiosira* sp. | 20 | *Cyclotella* sp. |

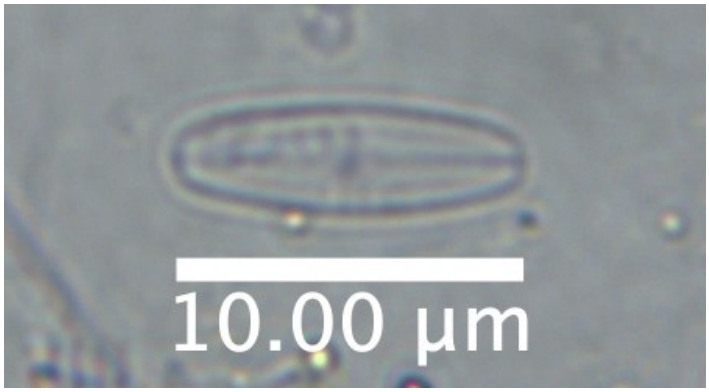


*Achnanthidium* sp.

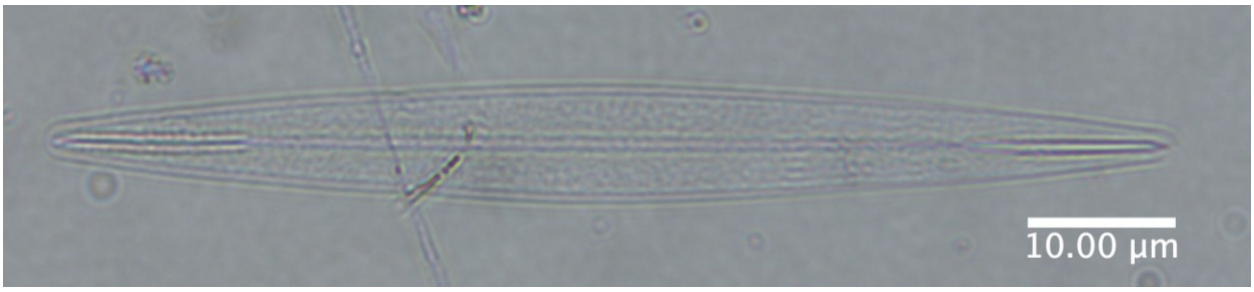


*Amphipleura* sp.

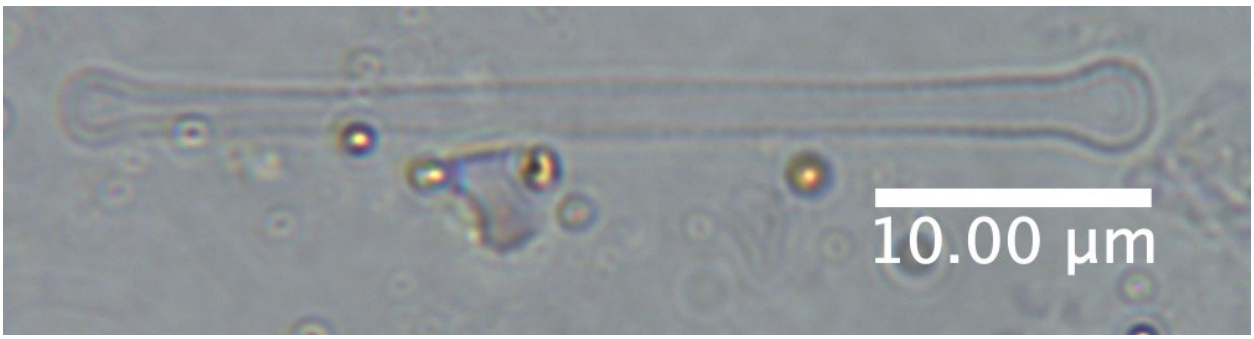


*Asterionella* sp.

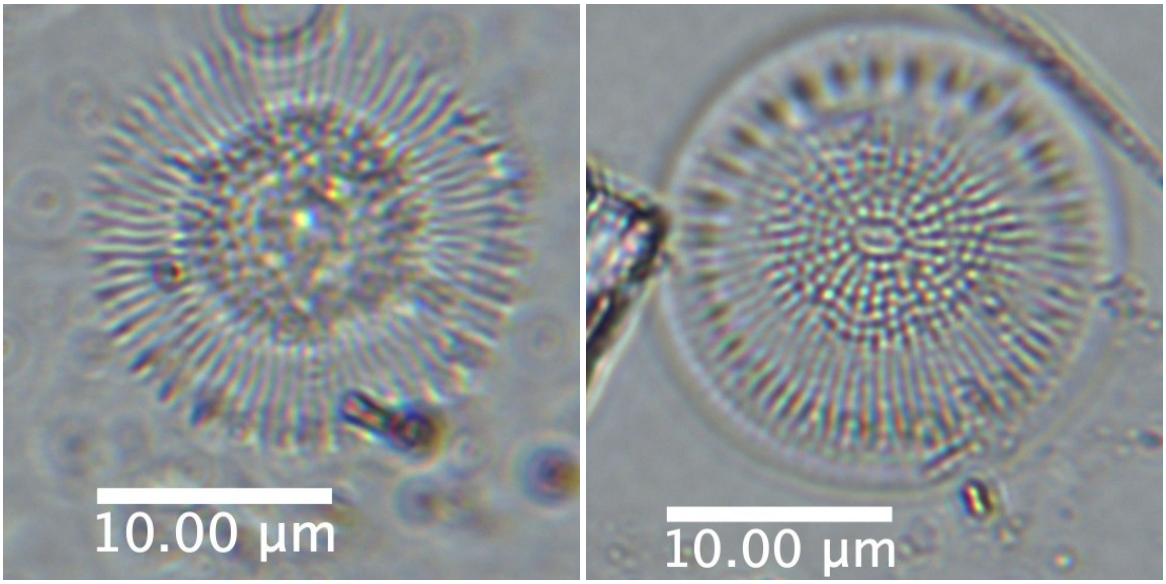


*Cyclotella* spp.

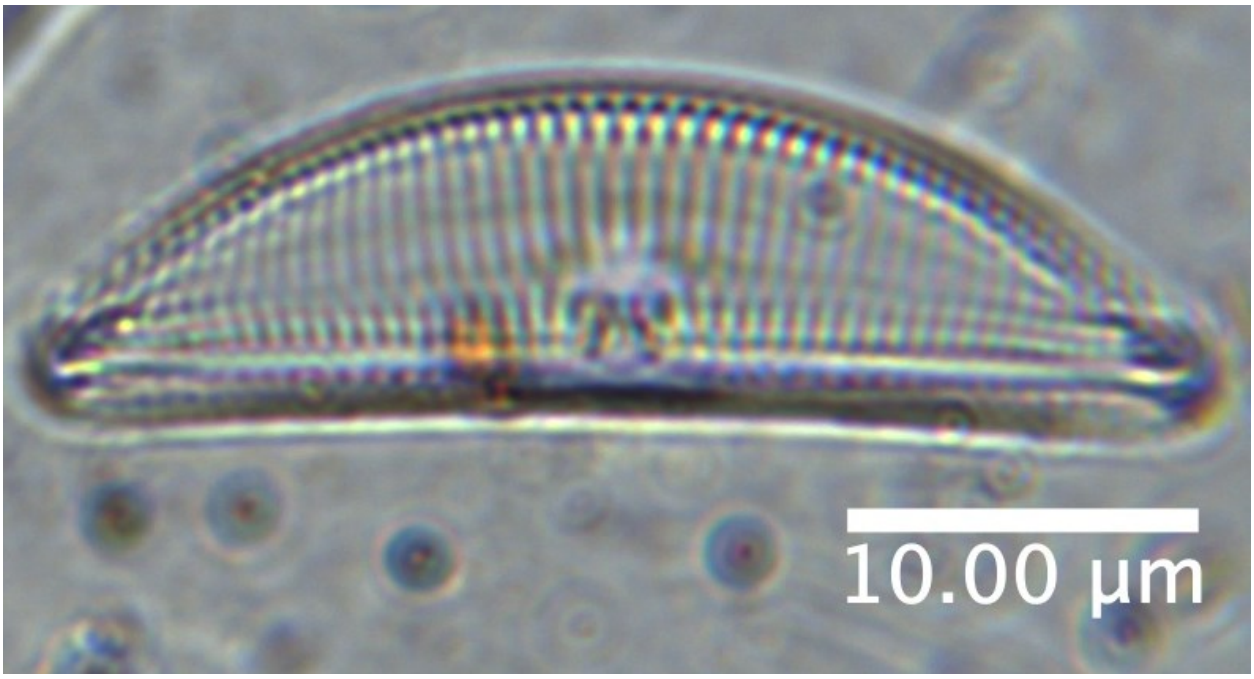


*Cymbella* sp.

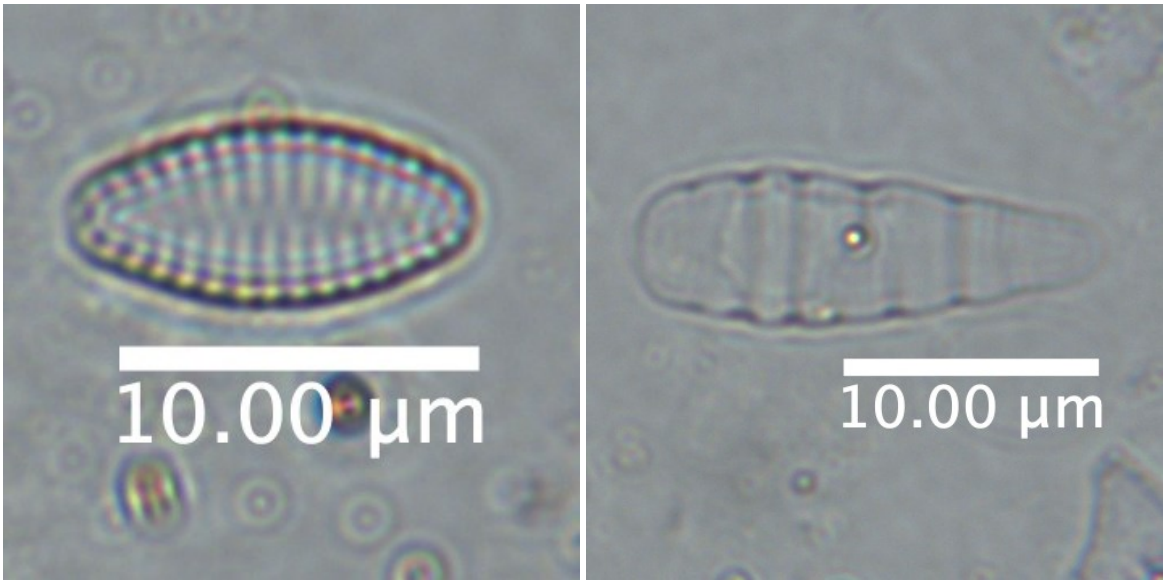


*Diatoma* spp.

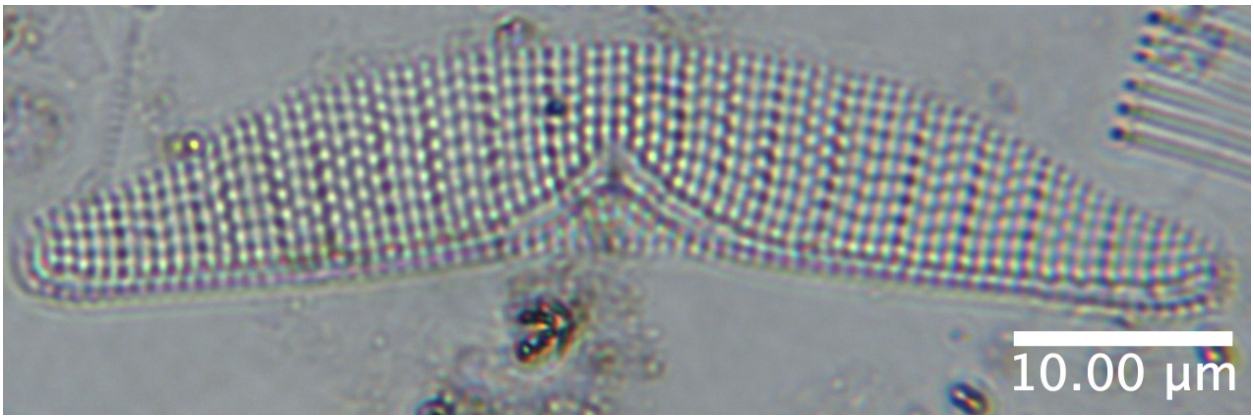


*Epithemia* sp.



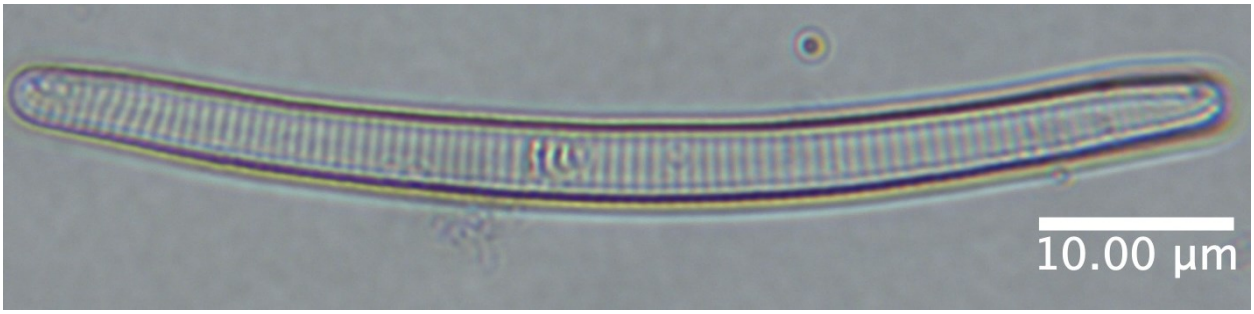


*Eunotia* spp.

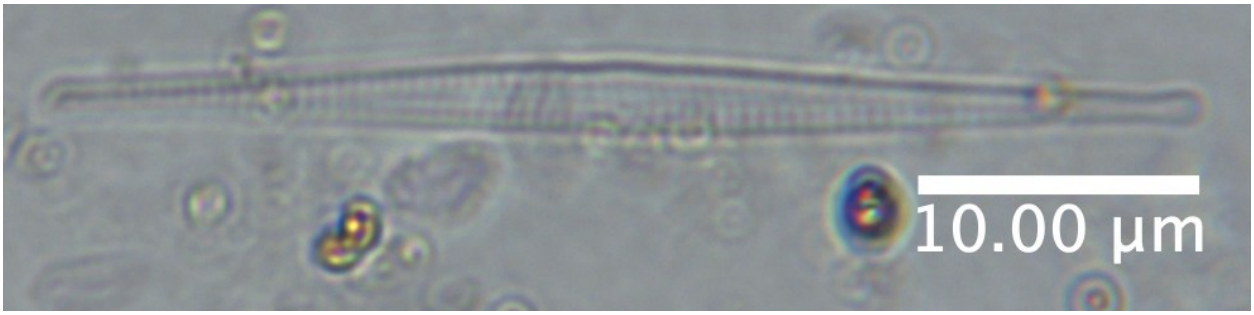


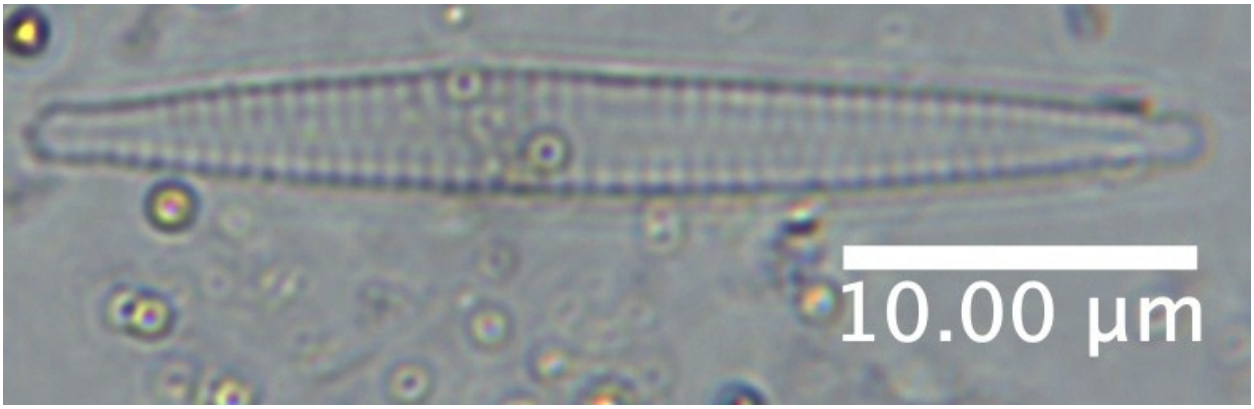


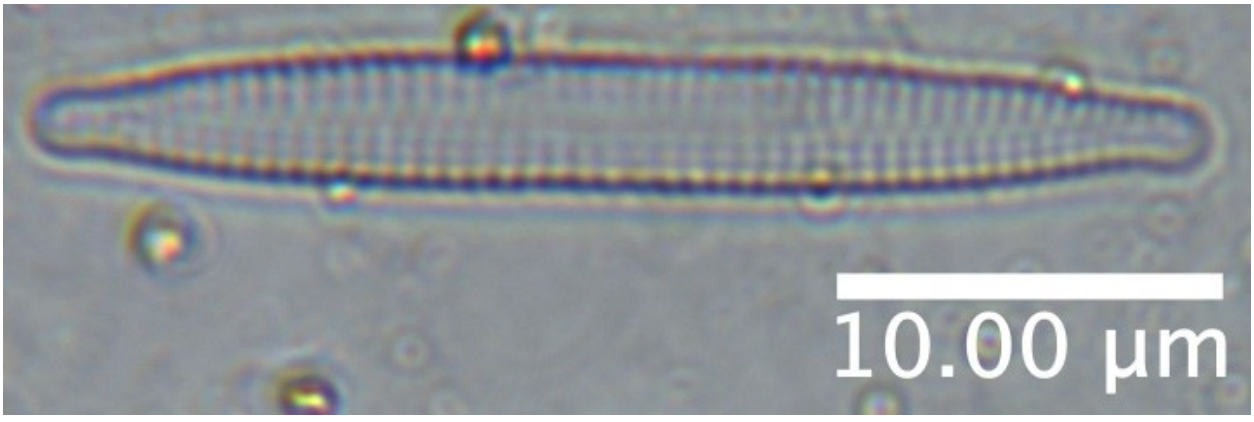


*Fragilaria* spp.

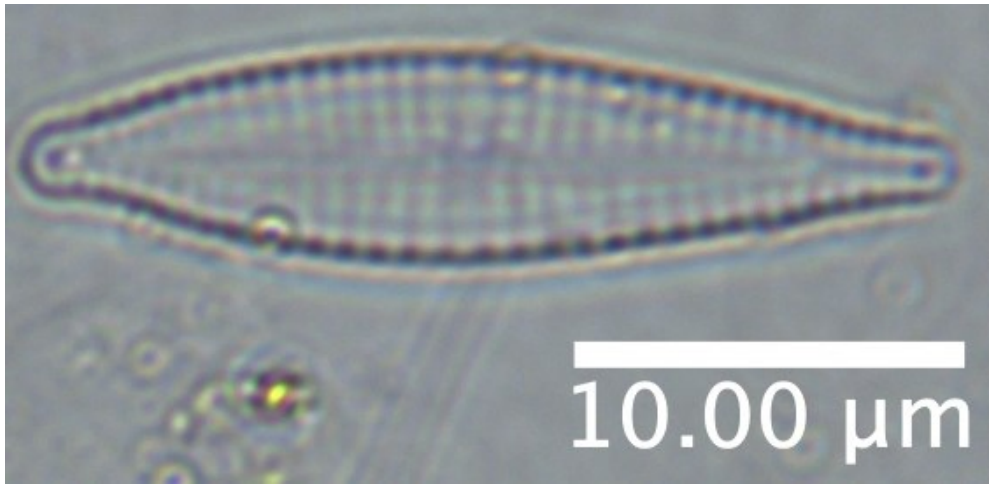


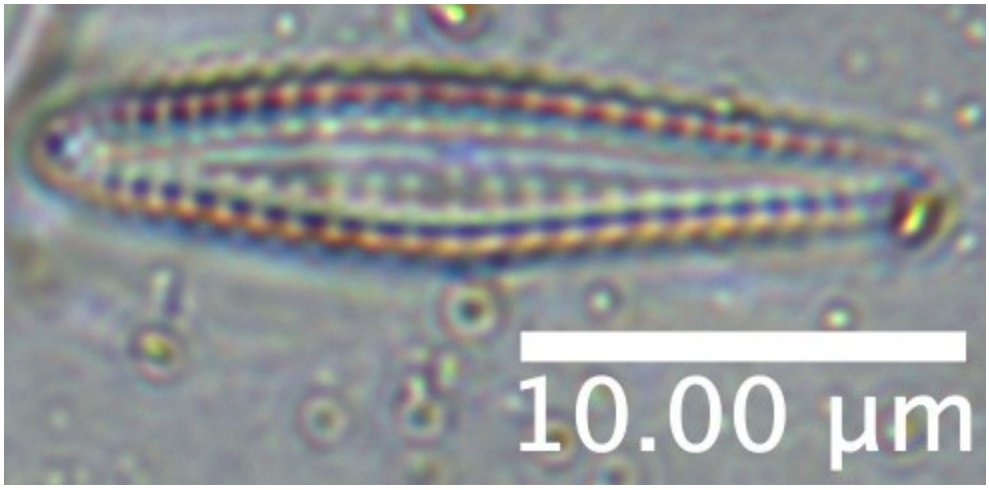


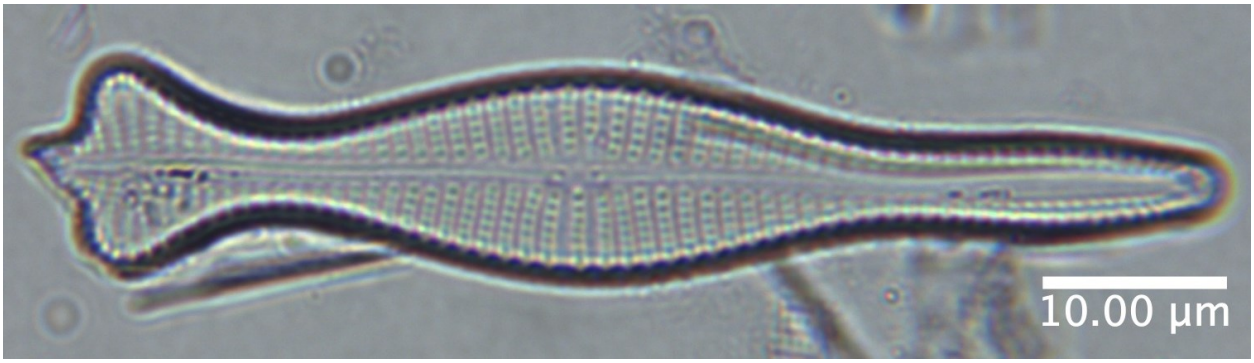


*Gomphonema* spp.

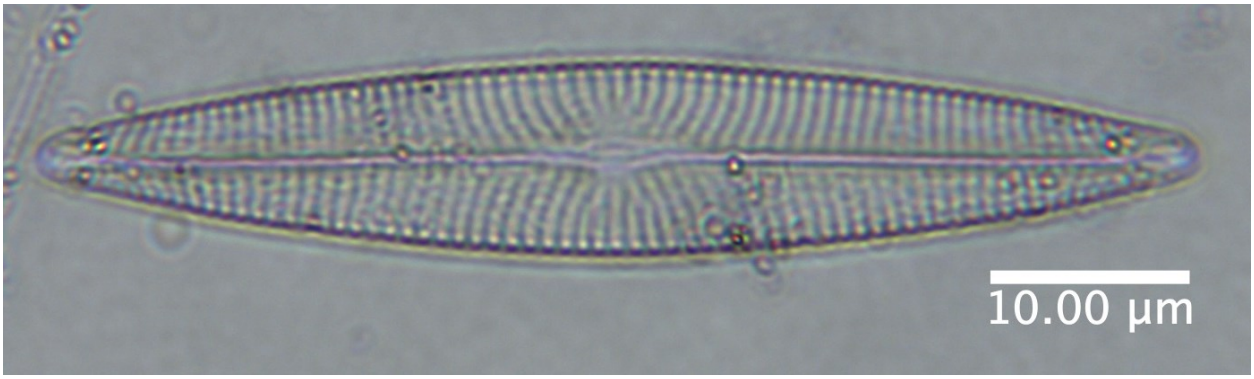


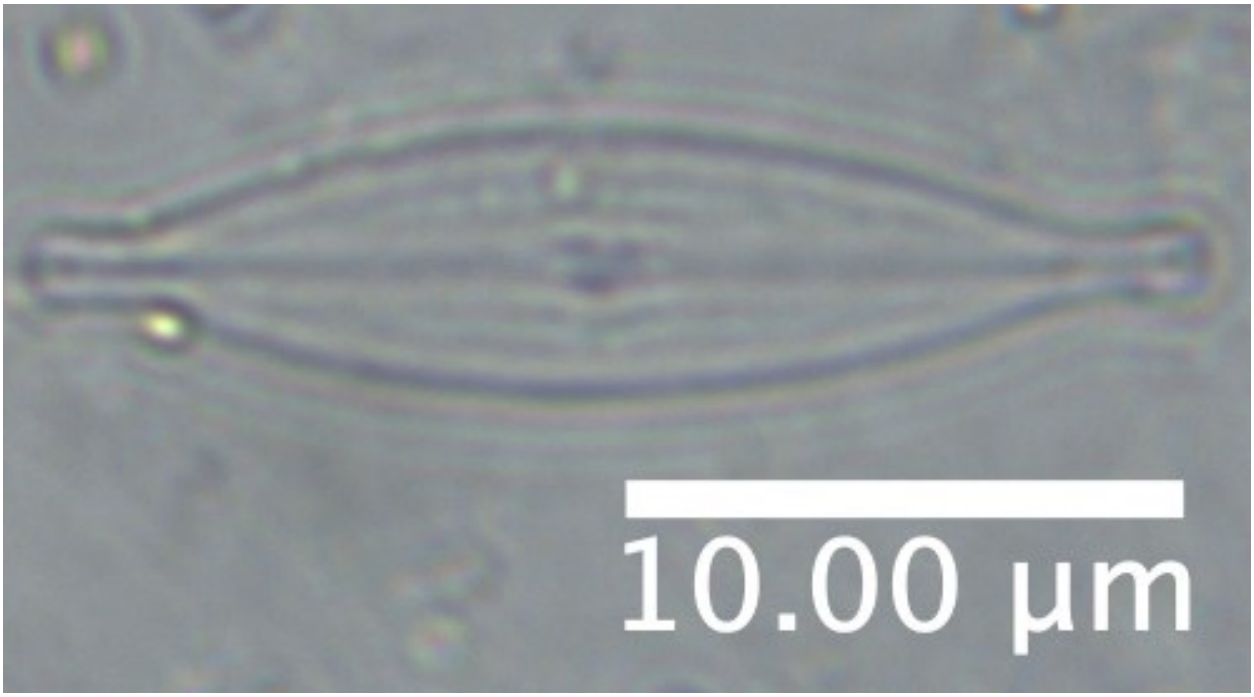


*Navicula* spp.

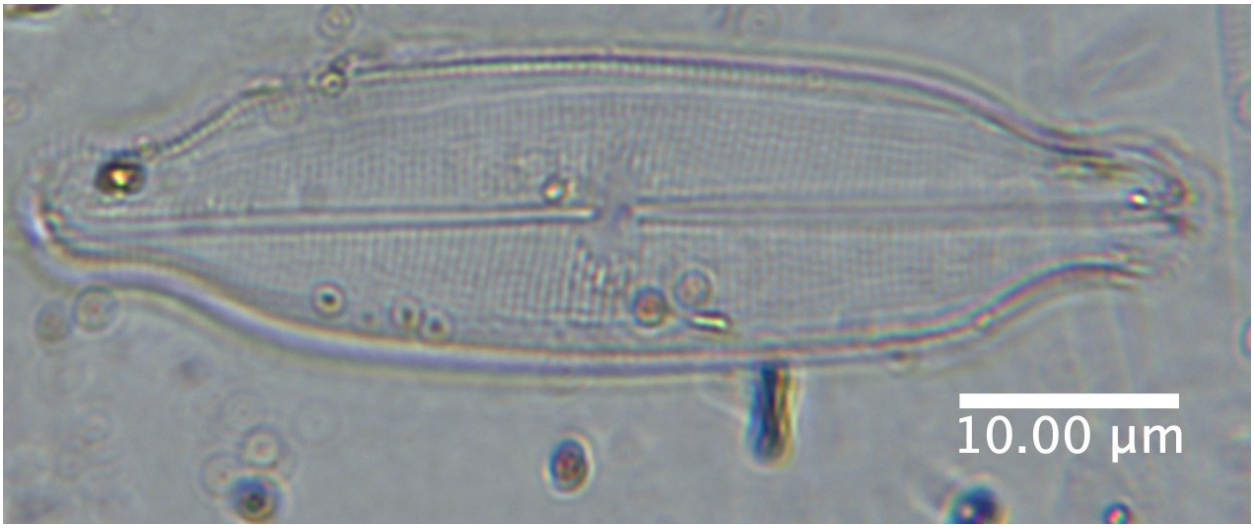



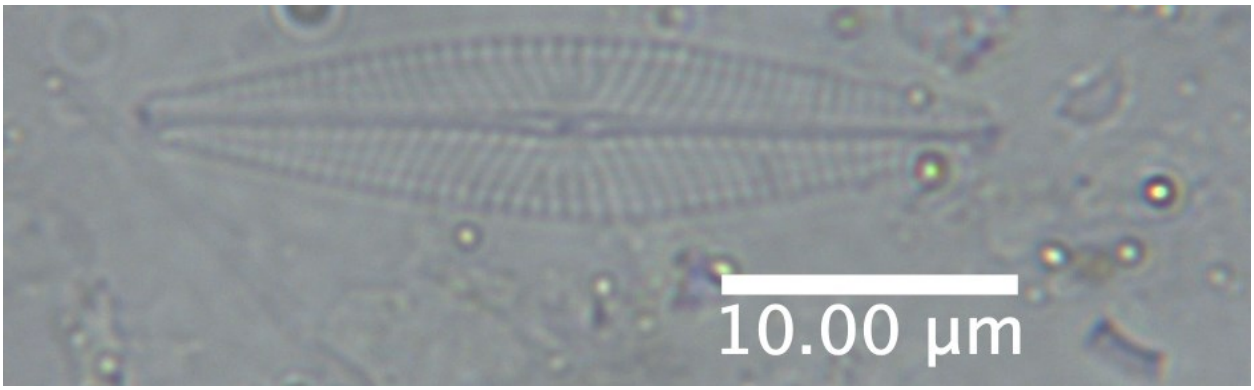


*Navicula* spp.

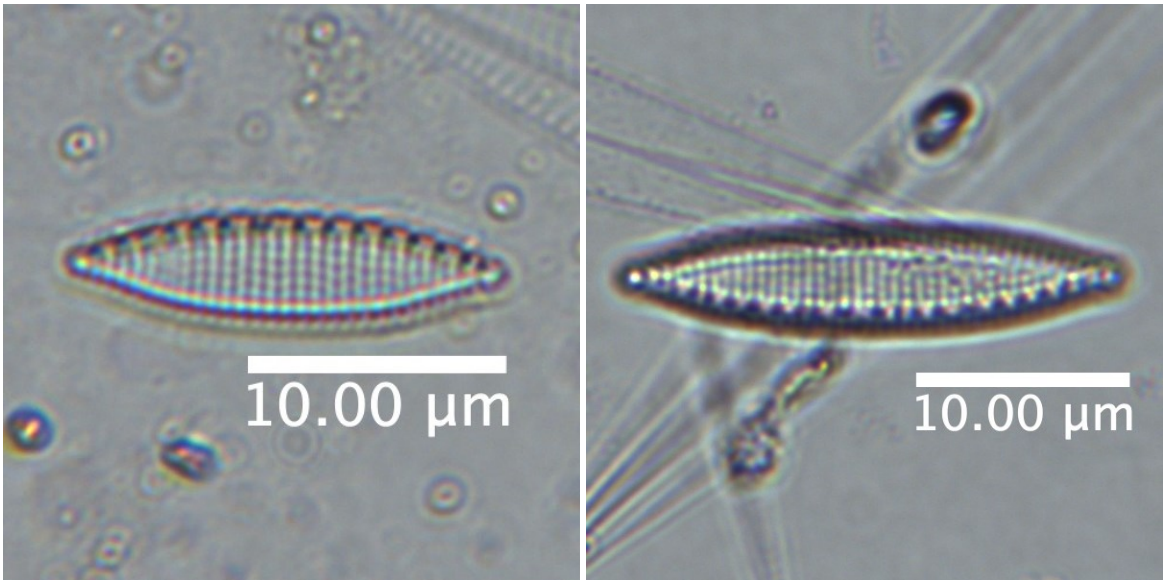


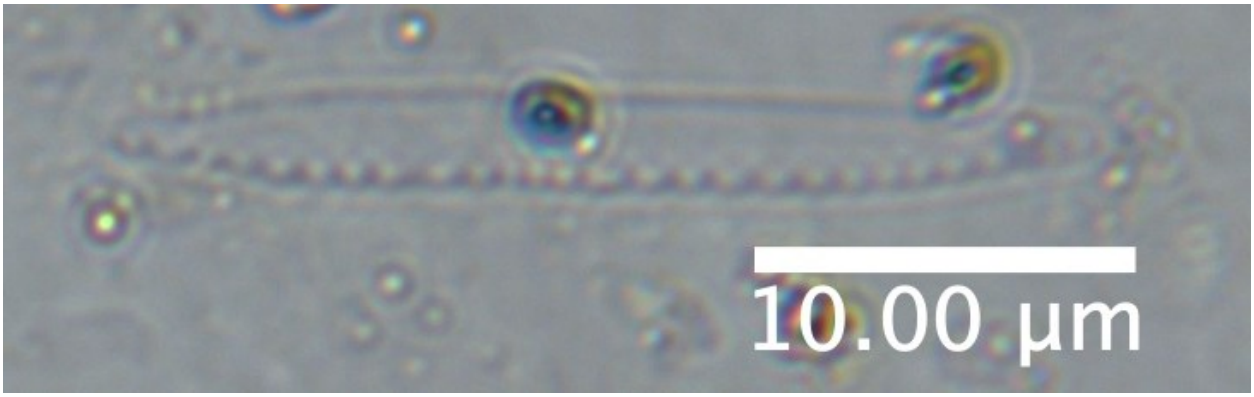


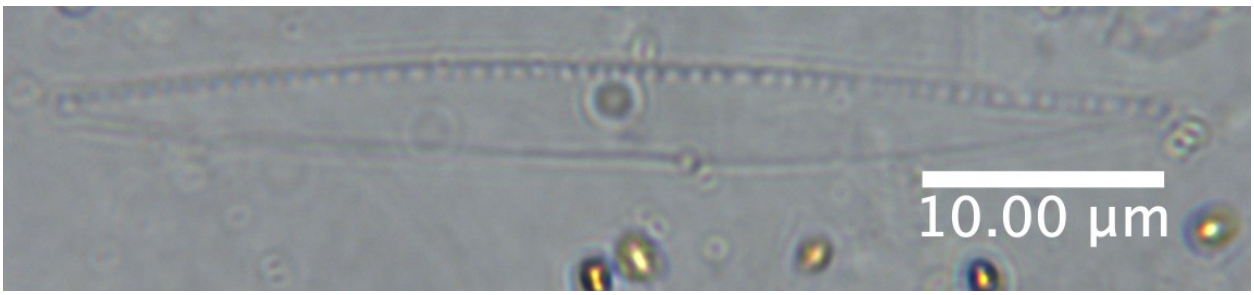


*Nitzschia* sp.

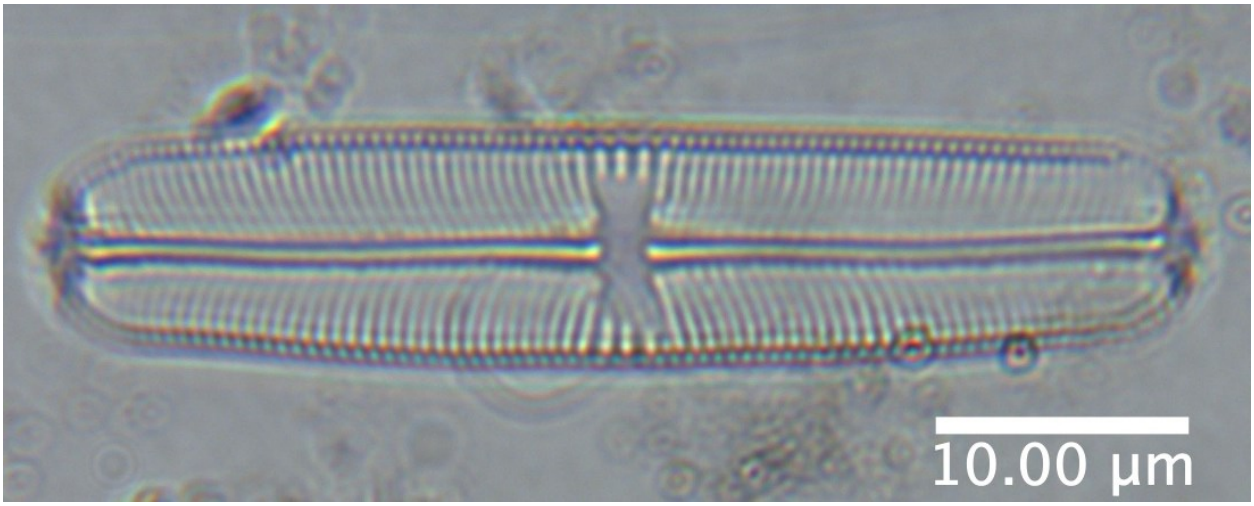


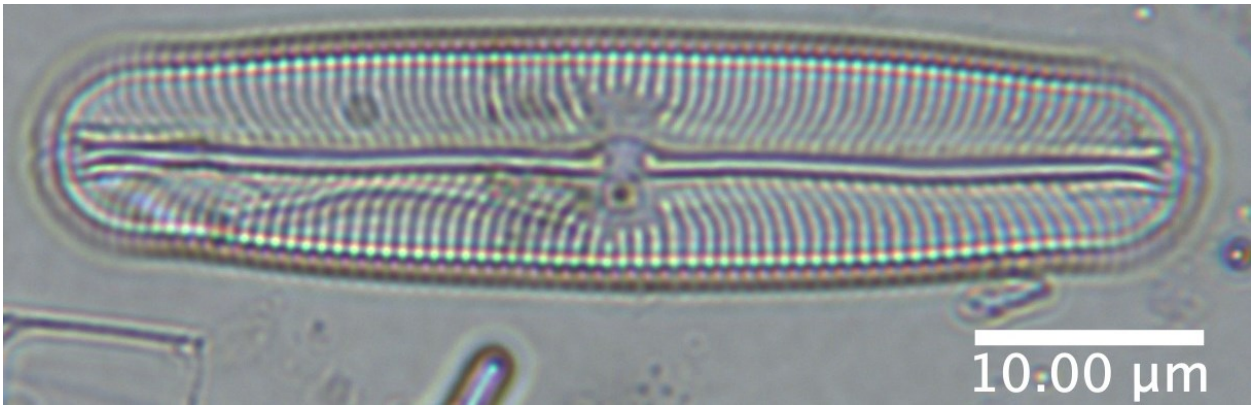


*Pinnularia* spp.

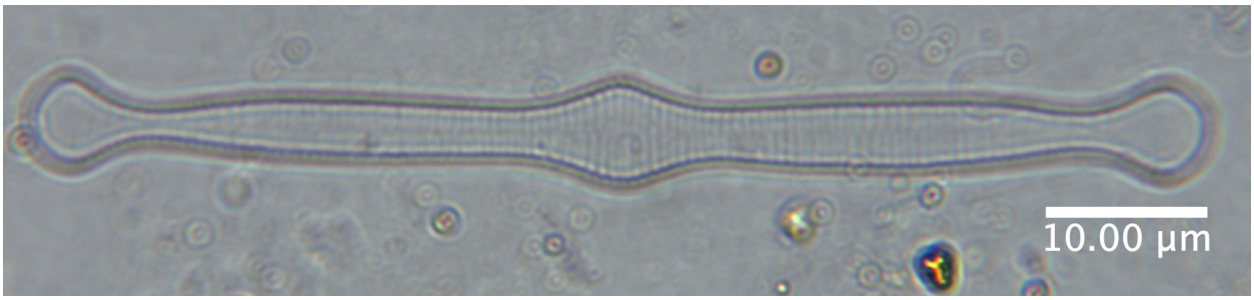


*Tabellaria* sp.

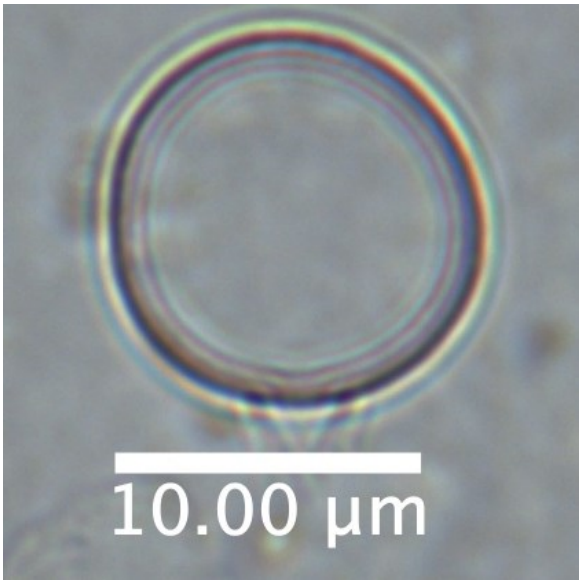


*Thalassiosira* sp.